

EXHIBIT

10/5/13, 7:20

## Proton-Coupled Electron Transfer

My Hang V. Huynh<sup>†</sup> and Thomas J. Meyer<sup>\*‡</sup>

DE-1: High Explosive Sciences and Technology Group, Los Alamos National Laboratory, Los Alamos, New Mexico 87545, and Department of Chemistry, University of North Carolina at Chapel Hill, Chapel Hill, North Carolina 27599-3290

Received April 10, 2006

### Contents

1. Proton-Coupled Electron Transfer (PCET)	5005	3.1. Introduction	5018
1.1. Introduction	5005	3.2. pH-Induced Electron Transfer, Energy Transfer, and Chemical Change	5018
1.2. PCET in Chemistry and Biology	5007	3.2.1. pH-Induced Electron Transfer in Ligand-Bridged Complexes	5018
1.3. Historical Footnote	5007	3.2.2. pH-Induced Energy Transfer	5018
2. Thermodynamics of Proton-Coupled Electron Transfer	5008	3.2.3. pH-Induced Changes in Electronic Coupling	5019
2.1. Introduction	5008	3.2.4. Reversible O <sub>2</sub> Evolution from <i>cis</i> -[Os <sup>IV</sup> (tp)(Cl)(NS(O)-3,5-Me <sub>2</sub> C <sub>6</sub> H <sub>3</sub> )]	5019
2.1.1. Summary of pH-Dependent Thermodynamics	5009	3.3. pH-Induced Redox Effects in Films	5019
2.1.2. Redox Potential Diagrams, Implications for Reactivity	5010	3.3.1. Intra- and Interfilm Electron Transfer	5019
2.1.3. Coverage	5010	3.3.2. pH-“Encapsulation”	5019
2.2. Metal Complexes with Oxygen as the Donor Atom	5011	4. Mechanistic Aspects of Proton-Coupled Electron Transfer	5020
2.2.1. Aqua/Hydroxy/Oxo Couples	5011	4.1. Introduction	5020
2.2.2. Other O-Based Couples	5011	4.2. Electron Transfer	5020
2.2.3. PCET Arising from pH-Dependent Chemical Changes	5012	4.2.1. Reorganization Energies	5020
2.3. pH-Dependent, Metal Complex Couples Based on Donor Atoms Other than Oxygen	5012	4.2.2. Barrier Crossing	5021
2.3.1. Reversible Couples Based on N Donors	5012	4.2.3. Including Quantum Modes	5021
2.3.2. Oxidation of Coordinated Amines	5012	4.2.4. Bimolecular Reactions	5022
2.4. Organic PCET	5013	4.2.5. Cross Reactions	5022
2.4.1. Reduction of Quinones	5013	4.3. PCET: Energies and Mechanisms	5022
2.4.2. Quinhydrones and Intramolecular PCET	5014	4.3.1. Stepwise Mechanisms	5022
2.5. Biological PCET	5014	4.4. Coupled Electron-Proton Transfer (EPT). Competition between Stepwise and E <sup>±</sup> T Mechanisms	5023
2.5.1. Iron-Sulfur Proteins	5014	5. Defining Electron-Proton Transfer	5024
2.5.2. Superoxide Dismutases	5014	5.1. Electron-Proton Transfer (EPT)	5024
2.5.3. PCET in Flavodoxin	5014	5.1.1. Multiple Site Electron-Proton Transfer (MS-EPT)	5024
2.5.4. Membrane Effects on Redox Potentials	5014	5.2. Related Pathways	5024
2.6. PCET on Surfaces	5015	5.2.1. H-Atom Transfer (HAT)	5024
2.6.1. “Tethered” Surface Couples	5015	5.2.2. Hybrid Mechanisms	5025
2.6.2. Directly Adsorbed Couples	5015	5.2.3. Energetics of HAT and “H-Alom Abstraction”	5025
2.6.3. Surface Couples	5015	5.2.4. Related Pathways	5026
2.6.4. Solid State PCET	5015	5.3. Theory of Coupled Electron-Proton Transfer	5026
2.7. PCET in Films	5015	5.3.1. Introduction	5026
2.7.1. Electropolymerized Films	5016	5.3.2. Kinetic Isotope Effects	5028
2.7.2. Ion-Exchanged Films	5016	5.3.3. Temperature-Dependence	5028
2.7.3. Liquid Crystal Films	5016	5.3.4. ΔG-Dependence	5029
2.8. Excited States	5016	5.4. H-Bonding and Distance-Dependence	5029
2.8.1. Excited State Superacids	5016	5.4.1. Precursor H-Bonding	5029
2.8.2. Proton Transfer Quenching of <i>trans</i> -[Re <sup>IV</sup> (py)(O <sub>2</sub> )] <sup>+</sup>	5017	5.4.2. Distance-Dependence	5029
2.8.3. MLCT Excited States	5017	5.5. Solvent	5030
3. pH-Induced Redox Phenomena	5018	5.5.1. Solvent Effects on $\lambda_{\text{a}}$ and $\Delta G$	5030
		5.5.2. Proton Inventory	5030
		5.5.3. The Solvent as Proton Donor or Acceptor: Solvent-Assisted MS-EPT	5030

<sup>†</sup> Los Alamos National Laboratory.  
<sup>‡</sup> University of North Carolina at Chapel Hill.

5.5.4. pH Variations and the Distinction between $\Delta G_c$ and $\Delta G$	5031
6. Coupled Electron-Proton Transfer in Chemistry	5032
6.1. EPT in Metal Complexes	5032
6.1.1. <i>cis</i> [Ru <sup>II</sup> (bpy) <sub>2</sub> (py)(O)] <sup>2+</sup> and Related Complexes	5032
6.1.2. Oxidation of Phenols by <i>trans</i> -[Ru <sup>II</sup> (L)-O] <sup>2+</sup> (L = 1,12-Dimethyl-3,4,9,10-dibenzo-1,2-diaza-5,8-dioxacyclopentadecane)	5033
6.1.3. Two-Electron-Proton Transfer (2e <sup>-</sup> /1H <sup>+</sup> EPT) in the Oxidation of Aniline	5034
6.1.4. "Colossal" Kinetic Isotope Effects in the Oxidation of Os(IV) Hydrazido and Related Complexes by Quinone	5034
6.1.5. Metal Complex Self-Exchange	5035
6.1.6. EPT in Metal Complex PCET	5035
6.2. EPT in Organic PCET	5036
6.2.1. Excited States	5036
6.2.2. Organic Radicals	5037
6.3. PCET through "Salt Bridges"	5038
6.4. Multiple-Site Electron-Proton Transfer (MS-EPT)	5039
6.4.1. Phenol Quenching of $^3[\text{C}_6\text{H}_5]$	5039
6.4.2. An Intramolecular Analogue, <i>Internal</i> MS-EPT	5039
6.4.3. Proton Activation of Bound $\text{HO}_2^-$	5039
6.4.4. Oxidation of DNA Bases	5039
6.4.5. pH-Dependent MS-EPT with Solvent as the Proton Acceptor(?)	5041
6.5. EPT on Surfaces	5042
6.5.1. Adsorbed Molecules	5042
6.5.2. Oxidative Activation of Carbon Electrodes	5043
6.5.3. EPT at Electrodes	5043
7. PCET in Biology	5044
7.1. Introduction	5044
7.2. PCET in Photosystem II	5044
7.2.1. Introduction	5044
7.2.2. Possible Role for MS-EPT in the Oxidation of $\text{Y}_2$ by $\text{P}_{\text{ox}}^+$	5045
7.2.3. Oxidation of the OEC by $\text{Y}_2^+$	5045
7.2.4. Oxidation of the $\text{Y}_2^+$ Mechanism	5047
7.2.5. 8 State Mechanistic Summary	5051
7.2.6. Conclusions	5052
7.3. Reduction of $\text{Q}_8$	5052
7.4. PCET-EPT in Other Biological Reactions	5052
7.4.1. Cytochrome c Oxidase (CcO)	5052
7.4.2. Cytochrome c Peroxidase (Cp)	5053
7.4.3. Dioxygen Binding to Hemerythrin	5053
7.4.4. H-Atom Abstraction by Lipoxigenases (LO)	5053
7.4.5. Long-Range PCET in Class I Ribonucleotide Reductase	5054
8. Summary	5054
8.1. Addenda	5055
9. References	5055

## 1. Proton-Coupled Electron Transfer (PCET)

### 1.1. Introduction

At the core of many important energy conversion processes in chemistry and biology are oxidation-reduction reactions in which both electrons and protons are transferred. An



My Haeng H. Hwang received her B.S. in chemistry and her B.A. in Mathematics at the State University of New York at Geneseo. Her Ph.D. work on the *Stereochemical Ligand Effects of Mono- and Bidentate Ligands in Ruthenium Chemistry* was accomplished at the State University of New York at Buffalo. Her postdoctoral work on the *Redox Chemistry of High Oxidation State Osmium(VI) Nitrido Complexes* was carried out at the University of North Carolina at Chapel Hill and the Los Alamos National Laboratory (LANL) in New Mexico with Professor Thomas J. Meyer. Her current energetic materials research on High-Nitrogen Chemistry at LANL has concentrated on syntheses and applications of new inorganic Green Primary Explosives, secondary explosives, gas generators, and propellants. She recently received the E. O. Lawrence Award in Chemistry and was named a MacArthur fellow in September, 2007.



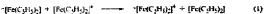
Thomas J. Meyer rejoined the faculty of the University of North Carolina at Chapel Hill as Arey Professor of Chemistry on July 1, 2005. In 2000 he was named Associate Director for Strategic Research at the Los Alamos National Laboratory in New Mexico. From 1994 to 1999, he was Vice-Chancellor for Graduate Studies and Research and Kenan Professor of Chemistry at UNC. He received his undergraduate degree at Ohio University and his graduate degree at Stanford under the direction of the late Henry Taube. After a NATO postdoctoral fellowship at University College, London, in 1997, he joined the chemistry faculty at UNC in 1998. His research interests include inorganic photodissociation, redox mechanisms and catalysis, and artificial photosynthesis. Meyer is a member of the National Academy of Sciences and the American Academy of Arts and Sciences and has been one of the most highly cited chemists in the world.

example is photosynthesis in green plants, in which carbon dioxide and water are converted into glucose and oxygen by the reaction  $6\text{CO}_2 + 6\text{H}_2\text{O} \rightarrow \text{C}_6\text{H}_{12}\text{O}_6 + 6\text{O}_2$ , which is favored by  $\Delta G^\circ = -675$  kcal.

The details of how electrons and protons are transferred in these reactions lie at the heart of successful energy conversion strategies in chemistry and biology. The coupling of electron and proton transfer influences both energetics and mechanism. It allows for the buildup of multiple redox

equivalents needed to carry out multielectron reactions. It also provides reaction pathways in which electrons and protons are transferred simultaneously, thus avoiding high-energy intermediates. Gaining knowledge of these processes is critical in developing our understanding of important biological reactions such as respiration, nitrogen fixation, and photosynthesis as well as energy conversion in artificial photosynthesis or fuel cells.

Oxidation-reduction (redox) reactions occur by a variety of mechanisms. The simplest is *outer-sphere* electron transfer, in which only an electron is transferred in the elementary step. An example is the ferrocene/ferricinium ion self-exchange reaction in eq 1.<sup>1</sup> In other reactions, more complex



pathways or elementary steps are used which take advantage of decreased reaction barriers and/or avoid high-energy intermediates.

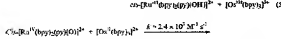
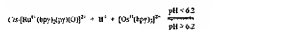
An example is reduction of  $[\text{Co}^{\text{II}}(\text{NH}_3)_6(\text{Cl})_6]^{2+}$  by  $[\text{Cr}^{\text{II}}(\text{H}_2\text{O})_6]^{2+}$ , which occurs by *inner-sphere* electron transfer through  $\text{Cl}^-$  as a bridge. Compared to reduction by  $[\text{Co}(\text{NH}_3)_6]^{2+}$ , this pathway offers a rate enhancement of  $\sim 10^{11}$ .<sup>2,3</sup>

A second example is oxidation of formate anion by the  $\text{Ru}^{\text{IV}}$ -oxo complex  $cis\text{-}[\text{Ru}^{\text{IV}}(\text{bpy})(\text{py})(\text{O})]^{2+}$  ( $\text{bpy}$  is 2,2'-bipyridine,  $\text{py}$  is pyridine),  $cis\text{-}[\text{Ru}^{\text{IV}}(\text{bpy})(\text{py})(\text{O})]^{2+} + \text{HCOO}^- + \text{H}^+ \rightarrow cis\text{-}[\text{Ru}^{\text{IV}}(\text{bpy})(\text{py})(\text{H}_2\text{O})]^{2+} + \text{CO}_2$ . Electron transfer in eq 2 has an associated energy penalty



of  $\Delta G^\circ > 1.9$  eV ( $> 44$  kcal/mol) compared to hydride transfer in eq 4. Similarly, the energy penalty for H-atom transfer in eq 3 is 1.21 eV (27.9 kcal/mol) compared to hydride transfer. Hydride transfer avoids  $1\text{e}^-$  intermediates and dominates reactivity at room temperature in solution.<sup>4</sup>

Significant energy penalties can also exist for reactions in which both electrons and protons are transferred.  $\Delta G$  for electron transfer between  $cis\text{-}[\text{Ru}^{\text{IV}}(\text{bpy})(\text{py})(\text{O})]^{2+}$  and  $[\text{Ox}^{\text{II}}(\text{bpy})]^{2+}$  in eq 5 is pH-dependent. Below pH = 6.2, the



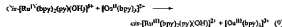
reaction occurs to the right, and above pH = 6.2, it occurs to the left. The pH-dependence arises from the proton added to Ru(II) to give  $cis\text{-}[\text{Ru}^{\text{IV}}(\text{bpy})(\text{py})(\text{OH})]^{2+}$ . There is an increase in  $\text{pK}_a$  of  $> 18$  between  $cis\text{-}[\text{Ru}^{\text{IV}}(\text{bpy})(\text{py})(\text{O})]^{2+}$  and  $cis\text{-}[\text{Ru}^{\text{IV}}(\text{bpy})(\text{py})(\text{OH})]^{2+}$ .<sup>5</sup>

As shown in eqs 5 and 7, below pH = 6.2, the reaction occurs by a stepwise mechanism in which electron transfer (ET) is followed by proton transfer (PT). Even though a

proton is transferred in the net reaction, the Os complex is substitutionally inert, and there is no orbital basis for more complex, low-energy pathways in which electrons and protons are transferred simultaneously.<sup>5</sup>

The electron transfer step in eq 6 is slow because the initial Ru product is  $cis\text{-}[\text{Ru}^{\text{IV}}(\text{bpy})(\text{py})(\text{O})]^{2+}$  and  $\Delta G^\circ > 0.33$  eV.  $\Delta G^\circ$  is the standard free energy change in the prevailing medium. The proton transfer that follows is highly favored with  $\Delta G^\circ = -0.059$  ( $\text{pK}_a[\text{Ru}^{\text{IV}}\text{-OH}]^{2+} - \text{pH}] < -0.40$  eV ( $< -9.2$  kcal/mol) at pH = 6.2 at 25 °C.<sup>6</sup>

Another possible mechanism is PT followed by ET in eq 8—  
 $cis\text{-}[\text{Ru}^{\text{IV}}(\text{bpy})(\text{py})(\text{OH})]^{2+} + \text{H}^+ \longrightarrow cis\text{-}[\text{Ru}^{\text{IV}}(\text{bpy})(\text{py})(\text{OH})]^{2+}$

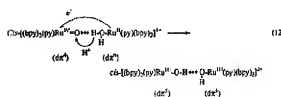
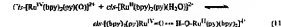


intermediate under the prevailing conditions with  $\Delta G^\circ \geq 0.72$  eV (17 kcal/mol) for its formation at pH = 6.2.<sup>6,7</sup>

By contrast, in the comproportionation reaction in eq 10,  
 $cis\text{-}[\text{Ru}^{\text{IV}}(\text{bpy})(\text{py})(\text{O})]^{2+} + cis\text{-}[\text{Ru}^{\text{IV}}(\text{bpy})(\text{py})(\text{H}_2\text{O})]^{2+} \longrightarrow 2 cis\text{-}[\text{Ru}^{\text{IV}}(\text{bpy})(\text{py})(\text{OH})]^{2+} \quad (10)$

the oxo complex avoids the high-energy intermediates  $cis\text{-}[\text{Ru}^{\text{IV}}(\text{bpy})(\text{py})(\text{O})]^{2+}$  and  $cis\text{-}[\text{Ru}^{\text{IV}}(\text{bpy})(\text{py})(\text{OH})]^{2+}$  by undergoing simultaneous  $e^-/\text{H}^+$  transfer to give  $cis\text{-}[\text{Ru}^{\text{III}}(\text{bpy})(\text{py})(\text{OH})]^{2+}$ . Comproportionation occurs with  $\Delta G^\circ = -0.11$  eV ( $-2.5$  kcal/mol) and a rate enhancement of  $\sim 100$  compared to electron transfer in eq 6 even though it is less favored by 0.21 eV. The  $k(\text{H}_2\text{O})/k(\text{D}_2\text{O})$  kinetic isotope effect is 16.1 at 25 °C, and based on the dependence of  $k$  on the mole fraction of  $\text{D}_2\text{O}$ , a single proton is involved (section 5.5). The proton lost by  $cis\text{-}[\text{Ru}^{\text{IV}}(\text{bpy})(\text{py})(\text{O})]^{2+}$  is gained by  $cis\text{-}[\text{Ru}^{\text{IV}}(\text{bpy})(\text{py})(\text{OH})]^{2+}$ , as shown by the mole fraction dependence study and similar results in acetonitrile.<sup>7-9</sup>

In the stepwise comproportionation mechanism in eqs 11 and 12, the initial step is preassociation, with a H-bond



interaction between the transferring proton and a lone pair on the oxo group, followed by concerted  $e^-/\text{H}^+$  transfer. The experimental kinetic isotope effect is the product of the equilibrium isotope effect for eq 11 and the kinetic isotope effect for the concerted electron-proton transfer in eq 12 (section 5.4). In the concerted step, the electron is transferred from a dx orbital at  $\text{d}^{\text{v}}(\text{Ru}^{\text{IV}})$  to a dx orbital at  $\text{d}^{\text{a}}(\text{Ru}^{\text{IV}})$ . The proton is transferred from a  $\sigma_{\text{ON}}$  orbital on the O-atom of  $\text{Ru}^{\text{IV}}\text{-OH}_2^{2+}$  to a lone pair on the oxo group. The magnitude of the isotope effect is due largely to the concerted reaction and a long proton transfer distance due to unsymmetrical hydrogen bonding in the association complex (section 5.4.1).

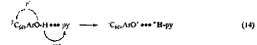
The elementary step in eq 12 was initially described as proton-coupled electron transfer (PCET) to distinguish it from H-atom transfer (HAT), in which the transferring electron and proton come from the same bond.<sup>7,8,10</sup> An

ambiguity has arisen in the use of this term. It has been used to describe both elementary steps in reactions such as the one in eq 12 and the class of reactions in which electron transfer is accompanied by proton transfer. To distinguish between the two, it has been proposed that the concerted pathway be described as electron transfer-proton transfer (ETPT),<sup>10</sup> or electron proton transfer (EPT),<sup>12</sup> or even concerted proton-electron transfer (CPET).<sup>13</sup>

The term **electron-proton transfer (EPT)** will be used in this account to describe concerted electron-proton transfer. This is both for its simplicity and to avoid a potential ambiguity with mechanisms in which electron transfer is followed by proton transfer, ET-PT. The term **proton-coupled electron transfer** will be used to describe the general class of reactions. A more detailed discussion of the limitations of this terminology and of distinctions between HAT and EPT as elementary steps is presented in sections 5.1-5.2.

There is a second type of EPT pathway in which concerted electron-proton transfer also occurs but involving more than one site. In multiple site-electron proton transfer (MS-EPT), an electron-proton donor simultaneously transfers electrons and protons to different acceptors, or an electron-proton acceptor simultaneously accepts electrons and protons from different donors. An example occurs in the electron transfer quenching of the triplet excited state of  $C_{60}$ ,  $C_{60}^{\bullet}$ , by phenols in the presence of added N bases:  $C_{60}^{\bullet} + ArOH + py \rightarrow [C_{60}^{\bullet} + ArO^{\bullet-} + H^{\bullet-} (py is pyridine)]^{14,15}$

In the stepwise mechanism for this reaction shown in eqs 13-15, preassociation occurs between the excited state and



a H-bonded,  $\text{ArOH}^{\cdots\bullet}\text{py}$  pair. Association is followed by concerted electron transfer from phenol to  ${}^3\text{C}_{60}$  with proton transfer to the H-bonded pyridine (section 4.4). MS-EPT avoids the high-energy phenol radical cation,  $\text{ArOH}^{\bullet+}$ , which would be the initial ET product,  ${}^3\text{C}_{60} + \text{ArOH} \rightarrow {}^3\text{C}_{60} + \text{ArOH}^{\bullet+}$ .

A closely related pathway appears to operate in the activation of Photosystem II toward water oxidation. Oxidative quenching of a chlorophyll excited state,  $P_{680}^*$ , gives  $P_{800}^+$ . It is subsequently reduced by long-range, ~10 Å, electron transfer from tyrosine  $Y_2$  with simultaneous proton transfer probably occurring in H-bonded histidine 190,  $P_{680}^+$ — $Tyro\text{-}OH\cdots His190\cdots P_{680}^+ + His190\cdots P_{680}^+$  (section 7.2). In fact, MS-EPT appears to be a biological pathway of choice for PCET in which long-range electron transfer<sup>16</sup> is coupled to short-range proton transfer (sections 5.3 and 7.2; also note ref. 17).

The orbitally separated, yet concerted, nature of EPT places specific orbital requirements on both donor and acceptor. The electron-proton donor, or donor for MS-EPT, must have energetically accessible orbitals at different sites for donating electrons and protons. Similarly, the acceptor, or acceptors, must have spatially separated orbitals for accepting electrons and protons. These requirements will be

discussed more fully in section 4 as will hybrid mechanisms with EPT for one participating couple and HAT for another.

EPT joins electron transfer (ET), H-atom transfer (HAT), hydride transfer, O-atom transfer, and others as fundamental pathways in which a net transfer of electrons occurs between molecules. It is related to PCET in that EPT provides a pathway by which PCET can occur in addition to sequential ET-PT or ET-PT.

## 1.2. PCET in Chemistry and Biology

Changes in electron content and oxidation state can profoundly affect acid-base and other thermodynamic properties. Thermodynamic coupling between electrons and protons allows pH changes to be used to induce electron transfer through films or over long distances in molecules. Thermodynamic coupling also allows electron transfer to induce long-range proton transfer through proton channels in biological membranes. In transition metal chemistry, oxidation and proton loss stabilize high oxidation states by electron donation and multiple bond formation as in  $\text{RuO}_4$  or  $\text{MnO}_4^-$ . The metal-ligand multiple bonds that result cause large changes in  $pK_a$  between oxidation states, favoring mechanisms more complex than simple electron transfer.

As knowledge of enzymes and biological processes is elucidated at the molecular level, it is becoming apparent that biology uses EPT and MS-EPT extensively and to great advantage. Over the time span of evolution, complex structures have evolved which provide oriented spatial arrays that integrate electron and proton transfer. These structures are critical in enabling MS-EPT and PCET in that they avoid high-energy intermediates, and electrostatic charge builds up in nonaqueous membrane environments. In turn, this leads to a *redox potential leveling* and decrease in potential for sequential redox couples where there is no increase in charge. This phenomenon provides access to higher oxidation states and to multiple electron transfer pathways such as hydride transfer or  $\text{O}$ -atom transfer. Integration of PCET with proton transfer over long distances by use of sequential proton transfers provides a basis for trans-membrane proton equilibration, thus avoiding local pH gradients. The coupling of electron and proton transfer is at the heart of water oxidation, respiration, nitrogen fixation, and other key reactions in biocenergetics.<sup>20-28</sup>

The goal of this account is to describe PCET reactions and phenomena and EPT mechanisms. Both areas will be covered with as much breadth as possible. A goal is to illustrate the scope of acid–base effects coupled to electron transfer. This can only be accomplished by sacrificing depth in particular areas, and we apologize for not including many relevant examples of particular phenomena.

The thermodynamic aspects of PCET and related pH-induced phenomena will be dealt with in sections 2 and 3. Sections 4 and 5 will review electron transfer theory, introduce EPT and mechanisms in which it plays a role, summarize the theory of EPT, and discuss its applications. Section 6 will review EPT in chemistry, and section 7 will review EPT in selected biological examples with a focus on oxygen evolution at the oxygen evolving complex of Photosystem II.

### 1.3. Historical Footnote

The first documented suggestion of PCET as a mechanism appears to have come from the appearance of a pH-dependent term in the rate law for the  $[\text{Fe}(\text{H}_2\text{O})_6]^{3+}/^{2+}$  self-exchange reaction studied by isotopic labeling. A rate increase with



Figure 1. The peptide tyrosine (TyrOH).

increasing pH was attributed to a pathway involving  $[\text{Fe}^{\text{II}}(\text{H}_2\text{O})_6]^{2+}$  and  $[\text{Fe}^{\text{II}}(\text{H}_2\text{O})_6(\text{OH})]^{2+}$  which occurred with  $k(\text{H}_2\text{O})/k(\text{D}_2\text{O})$  = 2 and was attributed to "H-atom transfer" from  $[\text{Fe}^{\text{II}}(\text{H}_2\text{O})_6]^{2+}$  to  $[\text{Fe}^{\text{II}}(\text{H}_2\text{O})_6(\text{OH})]^{2+}$ .<sup>20-21</sup>

A pH-dependent study revealed that, in the oxidation of  $[\text{Ru}^{\text{II}}(\text{H}_2\text{O})_6]^{2+}$  and  $[\text{Ru}^{\text{II}}(\text{NH}_3)_6(\text{H}_2\text{O})]^{2+}$  by  $\text{Fe}(\text{II})$  in water, e.g.,  $\text{Fe}(\text{II}) + [\text{Ru}^{\text{II}}(\text{NH}_3)_6(\text{H}_2\text{O})]^{2+} \rightarrow \text{Fe}(\text{II}) + [\text{Ru}^{\text{IV}}(\text{NH}_3)_6]^{2+}$ ,  $[\text{Fe}^{\text{II}}(\text{H}_2\text{O})_6(\text{OH})]^{2+}$  is less reactive toward  $[\text{Ru}^{\text{II}}(\text{NH}_3)_6]^{2+}$  than  $[\text{Fe}^{\text{II}}(\text{H}_2\text{O})_6]^{2+}$  by a factor of 6 and more reactive toward  $[\text{Ru}^{\text{II}}(\text{NH}_3)_6(\text{H}_2\text{O})]^{2+}$  by 6 even though the driving forces are comparable.<sup>10</sup> In unpublished data, a  $k(\text{H}_2\text{O})/k(\text{D}_2\text{O})$  kinetic isotope effect of  $\sim 36$  was found for the latter.<sup>12</sup> Based on the rate acceleration with  $\text{H}_2\text{O}$  in the inner coordination sphere, it was suggested that "proton transfer from  $[\text{Ru}^{\text{II}}(\text{NH}_3)_6(\text{H}_2\text{O})]^{2+}$  to  $[\text{Fe}^{\text{II}}(\text{H}_2\text{O})_6]^{2+}$ " accompanies electron transfer.<sup>19</sup> In 1981, the term PCET was coined and applied to the compartmentalization reaction in eq 10,<sup>7</sup> and in 1992, it was applied to the oxidation of hydroquinone by  $cis$ - $[\text{Ru}^{\text{IV}}(\text{bpy})_2(\text{py})(\text{OH})]^{2+}$ , which occurs with  $k(\text{H}_2\text{O})/k(\text{D}_2\text{O}) = 29 \pm 1$ .<sup>23</sup>

Brief reviews by Thorp of PCET in metal complexes and in excited states appeared in 1991<sup>24</sup> and 1996,<sup>25</sup> respectively. In the mid 1990s, a series of theoretical papers began appearing from the groups of Cukier<sup>26-29</sup> and Hammes-Schiffer.<sup>30,41</sup> In 1998, a review of PCET by Cukier and Nocera appeared,<sup>11</sup> and in the mid-to-late 1990s, a series of ground breaking papers by Babcock and co-workers on the coupling of electron and proton transfer in Photocytin II and other enzymes appeared.<sup>24-28</sup> Saneau and others have published papers on the role of PCET in electrochemical reactions.<sup>32,33</sup> Recent short reviews have appeared on the theoretical<sup>44-47</sup> and experimental aspects of PCET.<sup>48-50</sup> A colossal  $k(\text{H}_2\text{O})/k(\text{D}_2\text{O})$  kinetic isotope effects have been observed in the oxidation of Os(IV) complexes by quinone,<sup>51</sup> and reviews on the application of density functional theory to redox enzymes including PCET have also appeared.<sup>52,53</sup>

## 2. Thermodynamics of Proton-Coupled Electron Transfer

### 2.1. Introduction

Electron transfer accompanied by a change in proton content is a ubiquitous phenomenon for reactants with dissociable protons.<sup>54-56</sup> The origin of this effect is an increase in acidity with electron loss, with an example being  $\text{pK}_{\text{a},1} = 9.5$  for  $[\text{Fe}(\text{H}_2\text{O})_6]^{2+}$  and 2.2 for  $[\text{Fe}(\text{H}_2\text{O})_6]^{3+}$ .<sup>57</sup> Similarly,  $\text{pK}_{\text{a},1} = 10$  for the phenolic proton of tyrosine in peptides and  $\text{pK}_{\text{a},1} = -2$  for its radical cation, TyrOH<sup>+</sup> (Figure 1).<sup>58,59</sup>

Oxidation of either  $[\text{Fe}(\text{H}_2\text{O})_6]^{2+}$  or TyrOH over a broad pH range is accompanied by loss of a proton.<sup>57-59</sup> This can lead to complex, pH dependent redox potentials. Variations in  $E_{1/2}$  with pH for the Ru(IV/III) and Ru(III/II) couples of  $cis$ - $[\text{Ru}^{\text{IV}}(\text{bpy})_2(\text{py})(\text{H}_2\text{O})]^{2+}$  are illustrated in Figure 2.<sup>56,61</sup> The  $E_{1/2}$  values are half wave potentials measured by voltammetry which are directly related to the formal,  $E^{\circ}$ , and standard potentials,  $E^{\circ\circ}$ .<sup>62-65</sup>

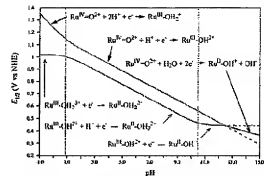


Figure 2.  $E_{1/2}$  vs pH diagrams for the Ru(IV/III) and Ru(III/II) couples of  $cis$ - $[\text{Ru}^{\text{IV}}(\text{bpy})_2(\text{py})(\text{H}_2\text{O})]^{2+}$  ( $\text{Ru}^{\text{IV}}-\text{OH}_2^{2+}$ ) at 25 °C,  $I = 1$  M, vs NHE. The vertical dotted lines correspond to  $\text{pK}_{\text{a},1}$  for  $cis$ - $[\text{Ru}^{\text{IV}}(\text{bpy})_2(\text{py})(\text{H}_2\text{O})]^{2+}$  ( $\text{Ru}^{\text{IV}}-\text{OH}_2^{2+}$ ),  $\text{pK}_{\text{a},2}$  = 10.6, and  $\text{pK}_{\text{a},3}$  for  $cis$ - $[\text{Ru}^{\text{IV}}(\text{bpy})_2(\text{py})(\text{OH})]^{2+}$  ( $\text{Ru}^{\text{IV}}-\text{OH}_2^{+}$ ),  $K_{\text{a},3} = 0.85$ . The remaining abbreviations are as follows:  $cis$ - $[\text{Ru}^{\text{IV}}(\text{bpy})_2(\text{py})(\text{O})]^{2+}$  ( $\text{Ru}^{\text{IV}}-\text{O}_2^{2+}$ ) and  $cis$ - $[\text{Ru}^{\text{IV}}(\text{bpy})_2(\text{py})(\text{OH})]^{2+}$  ( $\text{Ru}^{\text{IV}}-\text{OH}_2^{2+}$ ). The half-cell reactions for the individual couples in the various pH regions are indicated, as are the sixth ligands and whether they are  $\text{O}^{2-}$ ,  $\text{OH}^-$ , or  $\text{H}_2\text{O}$ . The  $E_{1/2}$ -pH curves were calculated from the Nernst equation by using the  $\text{pK}_{\text{a},1}$  values and  $E_{1/2}(cis$ - $[\text{Ru}^{\text{IV}}(\text{bpy})_2(\text{py})(\text{H}_2\text{O})]^{2+}) = 0.62$  V,  $E_{1/2}(cis$ - $[\text{Ru}^{\text{IV}}(\text{bpy})_2(\text{py})(\text{OH})]^{2+}) = 0.46$  V.<sup>56,61,62,64</sup>

There is a significant amount of information in  $E_{1/2}$ -pH diagrams such as Figure 2. Variations in  $E_{1/2}$  with pH are predicted by the Nernst equation. For example, for the Ru(IV/III) couple in Figure 2, in the pH region from 2 to 9 where  $cis$ - $[\text{Ru}^{\text{IV}}(\text{bpy})_2(\text{py})(\text{H}_2\text{O})]^{2+}$  and  $cis$ - $[\text{Ru}^{\text{IV}}(\text{bpy})_2(\text{py})(\text{OH})]^{2+}$  dominate,  $E_{1/2} - E^{\circ}(\text{Ru}^{\text{IV/III}})$  decreases with pH by 0.05916 V/pH unit at 25 °C, as predicted by eq 16.<sup>66</sup> In eq 16,  $K_{\text{II}}^{10}$

$$E_{1/2} - E^{\circ}(\text{Ru}^{\text{IV/III}}) = E^{\circ}(\text{Ru}-\text{OH}_2^{3+2+}) - 0.05916 (\text{pH} - \text{pK}_{\text{a},1}^{10}) \quad (16)$$

is the first acid dissociation constant for the Ru(III) complex. For the Ru(IV/III) couple in strongly acidic solutions at pH  $< 0.85$ , the dominant forms are  $cis$ - $[\text{Ru}^{\text{IV}}(\text{bpy})_2(\text{py})(\text{O})]^{2+}$  and  $cis$ - $[\text{Ru}^{\text{IV}}(\text{bpy})_2(\text{py})(\text{OH})]^{2+}$ .  $E_{1/2}$  decreases by 118 mV/pH unit as the pH is decreased, consistent with the loss of two protons upon reduction. More generally, for a couple,  $\text{Ox} + m\text{e}^- + m\text{H}^+ \rightarrow \text{Red}-\text{H}_m^{(n-m)}$ , with  $\text{Ox}$  and  $\text{Red}-\text{H}_m^{(n-m)}$  the dominant forms,  $E_{1/2}$  decreases with pH as  $0.05916(m/n)$ , with  $m$  being the number of protons transferred and  $n$  being the number of electrons; however, note ref 66.

The vertical dashed lines in Figure 2 are  $\text{pK}_{\text{a},1}$  values for  $cis$ - $[\text{Ru}^{\text{IV}}(\text{bpy})_2(\text{py})(\text{H}_2\text{O})]^{2+}$  (10.6) and  $cis$ - $[\text{Ru}^{\text{IV}}(\text{bpy})_2(\text{py})(\text{H}_2\text{O})]^{3+}$  (0.85). The half-cell reactions for the individual couples in the various pH regions are indicated, as are the sixth ligands and whether they are  $\text{O}^{2-}$ ,  $\text{OH}^-$ , or  $\text{H}_2\text{O}$ .

For the Ru(III/II) Couple: (1) Below pH = 0.8, the Ru(III/II) couple is  $cis$ - $[\text{Ru}^{\text{IV}}(\text{bpy})_2(\text{py})(\text{H}_2\text{O})]^{3+2+}$ , which is independent of pH. (2) From pH = 0.9 to 10.6, the couple changes to  $cis$ - $[\text{Ru}^{\text{IV}}(\text{bpy})_2(\text{py})(\text{OH})]^{2+}/cis$ - $[\text{Ru}^{\text{IV}}(\text{bpy})_2(\text{py})(\text{H}_2\text{O})]^{2+}$ . Consistent with the Nernst equation,  $E_{1/2}$  decreases by 59 mV/pH unit. (3) Above pH = 10.6, the couple becomes  $cis$ - $[\text{Ru}^{\text{IV}}(\text{bpy})_2(\text{py})(\text{OH})]^{2+2+}$  and, once again, is pH-independent.

For the Ru(IV/III) Couple: (1) Below pH = 0.8, the couple is  $cis$ - $[\text{Ru}^{\text{IV}}(\text{bpy})_2(\text{py})(\text{O})]^{2+}/cis$ - $[\text{Ru}^{\text{IV}}(\text{bpy})_2(\text{py})(\text{H}_2\text{O})]^{3+}$ .  $E_{1/2}$  decreases with pH by 118 mV/pH unit,

consistent with the expected  $0.05916(m/n)$  decrease per pH unit with  $m = 2$  and  $n = 1$ .

(2) As the pH is increased above 0.85, the couple becomes  $cis\text{-}[Ru^{IV}(bpy)_3(py)(OH)]^{2+}/cis\text{-}[Ru^{IV}(bpy)_3(py)(OH)]^{2+}$ , and  $E_{1/2}$  decreases by 59 mV/pH unit.

(3) At pH = 12.8, the pH-dependent  $Ru^{VIII}$  and pH-independent  $Ru^{VII}$  couples intersect. As the pH is increased further,  $E_{1/2}(\text{Ru}^{VIII}) > E_{1/2}(\text{Ru}^{VII})$  and  $cis\text{-}[Ru^{IV}(bpy)_3(py)(OH)]^{2+}$  is unstable toward disproportionation (eq 17). In this pH region,  $cis\text{-}[Ru^{IV}(bpy)_3(py)(OH)]^{2+}$  is a stronger oxidant than  $cis\text{-}[Ru^{IV}(bpy)_3(py)(OH)]^{2+}$  because of the pH-dependence of the  $\text{Ru}(\text{VII}/\text{II})$  couple.



(4) At pH > 12.8,  $E_{1/2}$  decreases by 29 mV/pH unit, consistent with the  $1\text{I}^{1+}/cis\text{-}[Ru^{IV}(bpy)_3(py)(OH)]^{2+}/cis\text{-}[Ru^{IV}(bpy)_3(py)(OH)]^{2+}$  couple.<sup>7,60,61</sup>

### 2.1.1. Summary of pH-Dependent Thermodynamics

A number of important conclusions concerning the impact of pH effects on redox potentials can be reached based on analysis of data like those in Figure 2.

• **Effect of Charge Type:** The potential of the  $\text{Ru}(\text{III}/\text{II})$  couple increases from 0.46 V (vs NHE) for the  $cis\text{-}[Ru^{IV}(bpy)_3(py)(OH)]^{2+}/[Ru^{IV}(bpy)_3(py)(OH)]^{2+}$  couple to 1.04 V for the  $cis\text{-}[Ru^{IV}(bpy)_3(py)(H_2\text{O})]^{2+}/[Ru^{IV}(bpy)_3(py)(H_2\text{O})]^{2+}$  couple as charge type increases from  $2+/-1$  to  $3+/-2$ . This is a general phenomenon arising largely from the effect of electrostatics on  $E^\circ$ .

Based on a thermodynamic cycle, the reduction potential,  $E^\circ$ , for the generalized couple  $\text{Ox}^{(n+1)+} + e^- \rightarrow \text{Red}^{n+}$  can be expressed as shown in eq 18.<sup>1,67,68</sup> In this equation,  $\Delta G_{\text{olv}}$

$$E^\circ = \Delta G_{\text{olv}}(\text{Ox}^{(n+1)+}) - \Delta G_{\text{olv}}(\text{Red}^{n+}) + I_n + C \quad (18)$$

$$C = -1/2\Delta G^\circ(\text{H}_2) - I_{\text{H}} - \Delta G^\circ_{\text{aq}}(\text{H}^+) \quad (19)$$

( $\text{Ox}^{(n+1)+}$  and  $\Delta G_{\text{olv}}(\text{Red}^{n+})$  are solvation free energies (hydration free energies in water) for  $\text{Ox}^{(n+1)+}$  and  $\text{Red}^{n+}$  in the prevailing medium, and  $I_n$  is the gas-phase ionization energy for  $\text{Red}^n$ . The constant  $C$  is defined in eq 19 and includes  $\Delta G^\circ(\text{H}_2)$ , the bond dissociation free energy for  $\text{H}_2$ ,  $I_{\text{H}}$ , the H-atom ionization energy, and  $\Delta G^\circ_{\text{aq}}(\text{H}^+)$ , the standard free energy of proton hydration).

Assuming spherical ions of radius  $r$ ,  $\Delta G_{\text{olv}} = -(n^2e^2/2r)(1 - 1/D_s)$  from the Born equation for ion solvation. In this equation,  $n$  is the charge on Red,  $e$  is the unit electron charge, and  $D_s$  is the static dielectric constant of the solvent. This is only an approximation since it assumes spherical ions and treats the solvent as a dielectric continuum. Partitioning  $I_n$  into a promotion energy term,  $I'_n$ , the energy required to transfer the electron to the surface of a sphere enclosing Red, and a charging term,  $ne^2/r$ , the energy required to remove the surface electron to infinity in the gas phase, gives the expression for  $E^\circ$  in eq 20. In eq 20,  $E_e^\circ$  is the electrostatic contribution to  $E^\circ$ .

$$E_e^\circ = -\left((2n+1)\frac{e^2}{2r}\right)\left[1 - \left(\frac{1}{D_s}\right)\right] + \left(\frac{ne^2}{rD_s}\right) + I'_n + C = \\ E_e^\circ + I'_n + C \quad (20)$$

The first term in eq 20 arises from the difference in solvation free energies between  $\text{Ox}^{(n+1)+}$  and  $\text{Red}^{n+}$ . For **cationic couples**, it increases  $E^\circ$  as charge type increases. This term is counterbalanced by the ion charging ( $ne^2/rD_s$ ) and promotion energy ( $I'_n$ ) terms. The net effect is to increase  $E^\circ$  as positive charge accumulates, and this is the primary origin of the 0.58 V increase in  $E_{1/2}$  between  $cis\text{-}[Ru^{IV}(bpy)_3(py)(OH)]^{2+}$  and  $cis\text{-}[Ru^{IV}(bpy)_3(py)(H_2\text{O})]^{2+}$  couples.

• **Redox Potential Leveling:** Electrostatic effects also contribute to increases in redox potentials between adjacent couples. For the  $\text{Ru}(\text{VIII})-\text{Ru}(\text{III}/\text{II})$  couples,  $cis\text{-}[Ru^{IV}(bpy)_3Cl_2]^{2+}$  and  $cis\text{-}[Ru^{IV}(bpy)_3Cl]^{1+}$ ,  $\Delta E_{1/2} = E_{1/2}(2) - E_{1/2}(1) = 1.7$  V (1 M,  $\text{CH}_3\text{CN}$ ). This is typical for adjacent transition metal complex couples of charge types  $(n+2)^{+}/(n+1)^{+}$  and  $(n+1)^{+}/(n^0)$ .<sup>69</sup>

The influence of electrostatics on  $\Delta E^\circ$  can be seen in eq 21, which follows from eq 20. This is also an approximate result since it assumes spherical ions and the solvent as a dielectric continuum. In this equation,  $I'_n$  and  $I'_{n+1}$  are the promotion energies for two adjacent couples as defined above. Based on this result, a combination of electrostatics,  $2e^2/rD_s$ , and the difference in promotion energies,  $\Delta' = I'_{n+1} - I'_n$ , is the origin of the increase in  $\Delta E_{1/2}$  ( $\sim \Delta E^\circ$ ) with charge type. The latter can play an especially important role for non-transition-metal couples where bonding electrons are promoted, and odd electronic configurations are of relatively high energy.

$$\text{For couples } \text{Ox}_2^{(n+2)+}/\text{Red}_2^{(n+1)+} (E_2^{e^0}) \quad \text{and } \text{Ox}_1^{(n+1)+}/\text{Red}_1^{n+} (E_1^{e^0}): \\ \Delta E^\circ = E_2^{e^0} - E_1^{e^0} = \left(\frac{2e^2}{rD_s}\right) + I'_{n+1} - I'_n = \left(\frac{2e^2}{rD_s}\right) + \Delta' \quad (21)$$

$$\text{For couples } \text{Ox}_2^{e^+}/\text{Red}_2^{e^+} (E_2^{e^+}) \quad \text{and } \text{Ox}_1^{e^+}/\text{Red}_1^{n+} (E_1^{e^0}): \\ \Delta E^\circ = E_2^{e^+} - E_1^{e^+} = \Delta' \quad (22)$$

If there is no change in charge type, for example, between couples  $\text{Ox}^{e^+}/\text{Red}_2^{e^+}$  and  $\text{Ox}^{e^+}/\text{Red}_1^{n+}$ ,  $\Delta E^\circ$  is given by eq 22, and electrostatic effects play no, or a minimal, role. This is seen in the small difference in  $E_{1/2}$  values between the couples,  $cis\text{-}[Ru^{IV}(bpy)_3(py)(OH)]^{2+}/[Ru^{IV}(bpy)_3(py)(OH)]^{2+}$  ( $E_{1/2}(2)$ ) and  $cis\text{-}[Ru^{IV}(bpy)_3(py)(OH)]^{2+}/[Ru^{IV}(bpy)_3(py)(H_2\text{O})]^{2+}$  ( $E_{1/2}(1)$ ) with  $\Delta E_{1/2} = 0.08$  V from pH = 1 to 10.5 (Figure 2).

The latter is an example of **redox potential leveling** with PCET maintaining a constant charge type between adjacent couples. This is an important phenomenon for multi-electron catalysis. It allows the buildup of multiple redox equivalents over a narrow potential range and, with it, access to multielectron pathways such as hydride transfer in eq 4. It is especially important for membrane-bound biological redox couples (section 2.5.4). In these low dielectric environments, electrostatic charge is greatly destabilized compared to water; see, for example, refs 20 and 70–73.

• **Closely Spaced Redox Potentials:** The phenomenon of multiple, closely spaced redox couples with small  $\Delta'$  and  $\Delta E^\circ$  is a feature of the early to mid transition metal series. It is due to the relatively closely spaced, sequential ionization energies for the 3d, 4d, and 5d levels and efficient screening of the nuclear charge by the d electrons.<sup>74</sup>

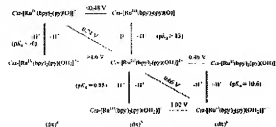


Figure 3. PCET thermodynamics. Acid-base, redox potential ( $E^{\circ'} - pK_a$ ) diagram for the Ru(IV/II) and Ru(IV/II) couples of *cis*-[Ru<sup>IV</sup>(bpy)<sub>2</sub>(py)(OH)]<sup>2+</sup> taken from Figure 2, showing the d<sub>xz</sub> electron configurations at the metal. Potentials are vs NHE at 25 °C,  $J = 0.1$  M. The vertical lines give  $pK_a$  values, and the slanted lines give  $E^{\circ'}$  values for pH-dependent couples at pH = 7, taken from ref 8.

$\Delta E'$  is also influenced by changes in bonding. For example, higher oxidation states of transition metal complexes are stabilized by ligand-to-metal electron donation, notably by  $\pi$ (ligand)  $\rightarrow$  d electron donation and multiple bond formation. The Ru<sup>IV</sup>—O<sup>2+</sup>/Ru<sup>III</sup>—OH<sup>2+</sup> and Ru<sup>III</sup>—OH<sup>2+</sup>/Ru<sup>II</sup>—OH<sup>2+</sup> couples in Figure 2 provide an example with Ru(IV) stabilized by the Ru<sup>IV</sup>—O multiple bond.<sup>74</sup>

• *Disproportionation:* Stabilization of a higher oxidation state by metal–ligand multiple bonding or a change in pH can become sufficient that  $E^{\circ'}_2 < E^{\circ'}_1$  for sequential couples, which leads to  $\Delta E^{\circ'} = E^{\circ'}_2 - E^{\circ'}_1 < 0$ . If  $\Delta E^{\circ'} < 0$ , the intermediate oxidation state in adjacent couples is “missing” thermodynamically because it is unstable with respect to disproportionation, e.g., 2Ru(II)  $\rightarrow$  Ru(II) + Ru(IV). This is the case for Ru<sup>III</sup>—OH<sup>2+</sup> above pH = 12.8 in Figure 2. It is a common phenomenon for organic and main group inorganic couples where  $\text{I}_1$ , radical intermediates or intermediate oxidation states such as Sn(II) or semiquinone,  $\text{OC}_6\text{H}_4\text{OH}$ , are unstable toward disproportionation.

• *Acid–Base Properties and Redox Potentials:* The difference in  $pK_a$  values between the higher and lower oxidation states of a couple can be used to calculate the difference in redox potentials between the protonated and deprotonated forms and vice versa. This is demonstrated for the Fe(II/II) aqua couple in eq 23 and more generally for the protonated (Ox-H/Red-H) and deprotonated (Ox/Red) couples in eq 24.

$$\begin{aligned} E^{\circ'}[(\text{Fe}(\text{H}_2\text{O})_6)^{3+/-2+}] - E^{\circ'}[(\text{Fe}(\text{H}_2\text{O})_6(\text{OH})^{2+/-1+})] = \\ 0.059[\text{p}K_a(\text{Fe}^{2+}) - \text{p}K_a(\text{Fe}^{3+})] = 0.43 \text{ V (25 }^{\circ}\text{C}) \quad (23) \end{aligned}$$

$$\begin{aligned} E^{\circ'}(\text{Ox-H/Red-H}) - E^{\circ'}(\text{Ox/Red}) = 0.059[\text{p}K_a \\ (\text{Red-H}) - \text{p}K_a(\text{Ox-H})] \quad (24) \end{aligned}$$

### 2.1.2. Redox Potential Diagrams: Implications for Reactivity

Acid–base constants and redox potentials at fixed pH are conveniently summarized in redox potential diagrams or “square schemes” such as the one shown for the *cis*-[Ru<sup>IV</sup>(bpy)<sub>2</sub>(py)(OH)]<sup>2+</sup>/[Ru<sup>IV</sup>(bpy)<sub>2</sub>(py)(OH)]<sup>2+</sup> and *cis*-[Ru<sup>IV</sup>(bpy)<sub>2</sub>(py)(OH)]<sup>2+</sup>/[Ru<sup>IV</sup>(bpy)<sub>2</sub>(py)(OH)]<sup>2+</sup> couples in Figure 3. The pH-dependences of organic redox couples can be equally complex.<sup>22–28</sup> This is illustrated for the quinone/hydroquinone (Q/H<sub>2</sub>Q) couple in Figure 4, which includes the one-electron semiquinone intermediate (HQ<sup>•</sup>/Q<sup>•-</sup>), as studied by Laviron and co-workers.<sup>81–83</sup>

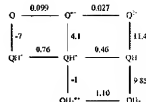


Figure 4. As in Figure 3 with potentials in V vs NHE, pH 7, 25 °C,  $J = 0.1$  M for the quinone/semiquinone/hydroquinone (Q/HQ/H<sub>2</sub>Q) couples; note refs 81–83.

In these diagrams, the values on the horizontal lines are potentials for pH-independent couples, Q/H<sup>+</sup>, HQ<sup>•</sup>/HQ<sup>•-</sup>, etc. The values on the vertical lines are  $pK_a$  values. The values on the slanted lines are potentials for pH-dependent couples at a specified pH, pH = 7 in Figure 3.<sup>24,83</sup>

The redox potential and  $pK_a$  data have important implications for oxidative activation and reactivity. From the summary in Figure 3, loss of a proton when *cis*-[Ru<sup>IV</sup>(bpy)<sub>2</sub>(py)(OH)]<sup>2+</sup> is oxidized to *cis*-[Ru<sup>IV</sup>(bpy)<sub>2</sub>(py)(OH)]<sup>2+</sup> could occur in three ways: (i) electron transfer to give Ru<sup>III</sup>—OH<sub>2</sub><sup>+</sup> followed by proton transfer to give Ru<sup>III</sup>—OH<sup>2+</sup> (ET-PT), (ii) proton transfer to give Ru<sup>III</sup>—OH<sup>2+</sup> followed by electron transfer to give Ru<sup>IV</sup>—OH<sup>2+</sup> (PT-ET), and (iii) electron–proton transfer (EPT) with simultaneous loss of both an electron and a proton, (section 1.1). Compared to the thermodynamic potential for the Ru<sup>III</sup>—OH<sup>2+</sup>/Ru<sup>III</sup>—OH<sub>2</sub><sup>+</sup> couple of 0.66 V at pH = 7, either mechanism (i) or (ii) incurs an energy penalty in the first step because Ru<sup>III</sup>—OH<sub>2</sub><sup>+</sup> and Ru<sup>III</sup>—OH<sup>2+</sup> are high-energy intermediates at the prevailing pH. For ET-PT, initial ET, Ru<sup>III</sup>—OH<sub>2</sub><sup>+</sup>  $\rightarrow$  e<sup>-</sup>  $\rightarrow$  Ru<sup>III</sup>—OH<sub>2</sub><sup>+</sup>, occurs at 1.02 V. The  $\Delta G^{\circ}$  difference of 0.36 eV is recovered in the subsequent PT step, Ru<sup>III</sup>—OH<sub>2</sub><sup>+</sup>  $\rightarrow$  Ru<sup>III</sup>—OH<sup>2+</sup> + H<sup>+</sup>, with  $\Delta G^{\circ} = 0.059(pK_a(\text{Ru}^{\text{III}}\text{—OH}^{\text{2+}}) - \text{pH})$  (at 25 °C). Similarly, the initial PT step in (ii) is unfavorable with  $\Delta G^{\circ} = +0.19$  eV.

Mechanisms involving Ru<sup>III</sup>—OH<sub>2</sub><sup>+</sup> or Ru<sup>III</sup>—OH<sup>2+</sup> add energy increments to the barrier for oxidative activation which can decrease rates. This is especially onerous for the second oxidation in Figure 3,



For this couple,  $\Delta G^{\circ'} > 0.9$  eV for initial ET and  $\Delta G^{\circ'} > 0.4$  eV for initial PT relative to the Ru<sup>IV</sup>—O<sup>2+</sup>/Ru<sup>III</sup>—OH<sup>2+</sup> couple at 0.74 V. This inhibits oxidative activation and imposes kinetic limitations that appear routinely, for example, at electrodes where pathways other than ET or PT are not accessible (sections 4.3 and 6.5.2).

PCET-induced barriers can be circumvented by utilizing EPT. In these pathways, both electrons and protons are transferred simultaneously and, therefore, at the thermodynamic potential for the PCET couple (section 4.3). Managing protons by EPT and proton transfer is critical in oxidative activation with the extraordinary example of the membrane-bound oxygen evolving complex of Photosystem II featured in section 7.2.

### 2.1.3. Coverage

In the remaining parts of Section 2, some thermodynamic aspects of selected PCET reactions will be described with the goal of highlighting the breadth of known pH-dependent phenomena by using known chemical examples.

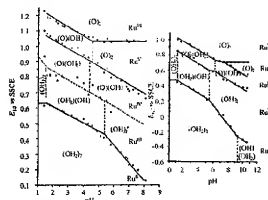


Figure 5.  $E_{1/2}$  vs pH diagrams for *cis*- (left) and *trans*-[Ru<sup>0</sup>(bpy)<sub>2</sub>(H<sub>2</sub>O)]<sup>2+</sup> (right) as in Figure 3 but showing the experimental points in  $E_{1/2}$ -pH diagrams (at 25 °C, vs SCE (+0.25 V vs NHE),  $I = 0.1$  M). The potential-pH lines for the various couples are indicated, as are regions where Ru(VI), Ru(V), Ru(IV), Ru(III), or Ru(II) are the dominant oxidation states and whether the fifth and sixth ligands are O<sup>2-</sup>, OH<sup>-</sup>, or H<sub>2</sub>O.<sup>58,89</sup>

## 2.2. Metal Complexes with Oxygen as the Donor Atom

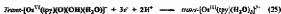
Changes in acidity with oxidation state and their impacts on the thermodynamics of PCET are ubiquitous for transition metal complexes containing ligands with acidic O–H bonds.<sup>56–58,86</sup>

### 2.2.1. *Aqua*/Hydroxy/Oxo Couples

2.2.1.1. *cis*- and *trans*-[Ru<sup>0</sup>(bpy)<sub>2</sub>(H<sub>2</sub>O)]<sup>2+</sup>. The  $E_{1/2}$ -pH diagrams for *cis*- and *trans*-[Ru<sup>0</sup>(bpy)<sub>2</sub>(H<sub>2</sub>O)]<sup>2+</sup> in Figure 5 illustrate two effects: the impact of a second water molecule in a Ru(II) poly(pyridyl) coordination environment and the role of coordination geometry. With two waters and PCET, the accessible oxidation states at the metal are extended to Ru(V) and Ru(VI), the latter as [Ru<sup>VI</sup>(bpy)<sub>2</sub>(O)]<sup>2+</sup>. In the higher oxidation states, Ru<sup>VI</sup>(<sup>3</sup>D), Ru<sup>VI</sup>(<sup>4</sup>S), and Ru<sup>VI</sup>(<sup>4</sup>D), there are vacancies in the d<sub>xz</sub>(Ru) levels and electronic stabilization by 2p<sub>z</sub>(O)  $\rightarrow$  d<sub>xz</sub> electron donation and Ru=O multiple bond formation.<sup>1,87–97</sup>

For the *cis* complex from pH ~2 to 6, successive 1e<sup>-</sup>/1H<sup>+</sup> oxidations occur from Ru<sup>0</sup> to Ru<sup>VI</sup> over a total potential range of 0.6 V, illustrating the role of PCET in redox potential leveling and M=O stabilization of higher oxidation states. For the *trans* complex, Ru(V) is missing in acidic solution because Ru(V) is stabilized by trans-O=Ru=O multiple bonding in *trans*-[Ru<sup>0</sup>(bpy)<sub>2</sub>(O)]<sup>2+</sup>. The missing oxidation state appears above pH = 7.3 because of differences in pH-dependences between the *trans*-[Ru(bpy)<sub>2</sub>(O)]<sup>2+/<sup>4</sup>V</sup> (Ru<sup>VI</sup>) and *trans*-[Ru<sup>0</sup>(bpy)<sub>2</sub>(O)]<sup>2+/<sup>4</sup>IV</sup> (Ru<sup>VI</sup>) couples.<sup>58,99</sup> Related behavior has been observed for other Ru and Os complexes.<sup>96–97</sup>

2.2.1.2. *trans*-[Os<sup>0</sup>(bpy)(H<sub>2</sub>O)]<sup>2+</sup>. A dramatic example of missing oxidation states due to differences in pH-dependent behavior and M=O stabilization occurs for *trans*-[Os<sup>0</sup>(bpy)(H<sub>2</sub>O)]<sup>2+</sup> (bpy is 2,2'-6',2''-terpyridine). Over a broad range of pH values, only a single 3e<sup>-</sup>/3H<sup>+</sup> Os(VI/III) wave is observed in cyclic voltammograms. Both Os(V) and Os(IV) are unstable toward disproportionation under these conditions, eq 25.<sup>99–101</sup>



2.2.1.3. *trans*-[Re<sup>V</sup>(py)<sub>4</sub>(O)]<sup>+</sup> and *trans*-[Re<sup>V</sup>(L)<sub>4</sub>(O)]<sup>+</sup>. The factors that cause “missing” oxidation states have been explored by Hupp *et al.* by comparing the pH-dependent electrochemical behaviors of *d*<sup>2</sup> *trans*-[Re<sup>V</sup>(py)<sub>4</sub>(O)]<sup>+</sup> and *trans*-[Re<sup>V</sup>(L)<sub>4</sub>(O)OMe]<sup>2+</sup> (L = pyridine or substituted pyridine).<sup>57,62</sup> In the reduction of *trans*-[Re<sup>V</sup>(py)<sub>4</sub>(O)]<sup>+</sup> to Re(II), *d*<sup>4</sup> Re(IV) is a missing oxidation state from pH = 1 to 14 due to *trans*-dioxo stabilization of O=Re<sup>V</sup>=O.

Redox potential and spectroscopic measurements reveal that Me<sup>4</sup> added to O in *trans*-[Re<sup>V</sup>(py)<sub>4</sub>(O)OMe]<sup>2+</sup> is a good surrogate for a proton. This makes the methoxy complex a reasonable model for *trans*-[Re<sup>V</sup>(py)(O)(OH)]<sup>2+</sup> but without a dissociable proton. For the member of this series with L = 4-MeOpy, the “missing” Re(VI/V) couple appears at  $\sim$ pH = 10 due to a difference in pH-dependences between the Re(V/IV) and Re(IV/III) couples.<sup>57,62</sup>

By using a mixture of aqueous and nonaqueous electrochemical measurements, estimates of  $pK_a = -10$  to  $-18$  were made for a series of *trans*-[Re<sup>V</sup>(L)<sub>4</sub>(O)(OH)]<sup>2+</sup> complexes, demonstrating that there is a low affinity for protons by the oxo group. In a related analysis, it was estimated that  $pK_a = 22$ –26 for *trans*-[Re<sup>V</sup>(L)<sub>4</sub>(OH)]<sup>2+</sup>.<sup>57,102</sup> This value illustrates the difficulty of deprotonating OH<sup>-</sup> when it is coordinated to a relatively low oxidation state at the metal.

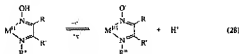
2.2.1.4. *[Re<sup>VI</sup>(Me<sub>3</sub>Scn)(O)]<sup>+</sup>*. Electrochemical reduction of *[Re<sup>VI</sup>(Me<sub>3</sub>Scn)(O)]<sup>+</sup>* (Me<sub>3</sub>Scn is 1,7-trimethyl-1,4-triazacyclonane) occurs by two quasi-reversible, pH-independent waves at  $-0.14$  and  $-0.36$  V vs SCE at pH = 1 corresponding to the Re(VII/VI) and Re(VI/IV) couples in eqs 26 and 27.<sup>103</sup>



2.2.1.5. *[([Bpy]2Mn<sup>IV</sup>(O)<sub>2</sub>Mn<sup>III</sup>(bpy)<sub>2</sub>)<sup>3+</sup>*. For the di-*μ*-oxo bridged complex *[([Bpy]2Mn<sup>IV</sup>(O)<sub>2</sub>Mn<sup>III</sup>(bpy)<sub>2</sub>)<sup>3+</sup>* and its 1,10-phenanthroline (phen) analogue, successive one-electron reductions over a wide pH range are accompanied by protonation at the bridge to give successively *[([Bpy]2Mn<sup>IV</sup>(O)<sub>2</sub>Mn<sup>III</sup>(bpy)<sub>2</sub>)<sup>3+</sup>]<sup>+</sup>* and *[([Bpy]2Mn<sup>IV</sup>(OH)<sub>2</sub>Mn<sup>III</sup>(bpy)<sub>2</sub>)<sup>3+</sup>]<sup>2+</sup>*.<sup>103–111</sup> Protonation at a  $\mu$ -oxo bridge accompanying reduction has also been observed for Os and Ru complexes. An example is *cis,cis*-*[([Bpy]2(H<sub>2</sub>O)Ru<sup>0</sup>(μ-OH)Ru<sup>0</sup>(H<sub>2</sub>O)](bpy)<sub>2</sub>)<sup>3+</sup>*.<sup>99,112,113</sup>

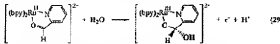
### 2.2.2. Other O-Based Couples

Related pH-dependent behavior has been observed for metal complex couples having oxime, hydroxamate, and dimethylglyoximate ligands. A generic example of the latter is shown for a M(II/II) couple in eq 28 with M = Ni, Fe.<sup>56,66,114</sup> For a linear hexadentate dioximate ligand with M = Ni, only a Ni(IV/II) couple is observed below pH 5 with Ni(IV/III) and Ni(II/II) couples appearing above pH 6.<sup>115–119</sup>



### 2.2.3. PCET Arising from pH-Dependent Chemical Changes

Electrochemical pH-dependent behavior can arise from reactions more complex than simple gain or loss of protons. In the example in eq 29, oxidation from Ru(II) to Ru(III) causes hydrolysis of the chelated aldehyde, creating a pH-dependence for the Ru(III/I) couple.<sup>129</sup>



### 2.3. pH-Dependent Metal Complex Couples Based on Donor Atoms Other than Oxygen

#### 2.3.1. Reversible Couples Based on N Donors

The appearance of pH-dependent redox potentials and associated redox phenomena also occurs for metal complex couples with acidic, dissociable protons bound to N, S, P, and even N as the donor atom.

**2.3.1.1.  $[M(bpy)_3(BiBzImH_2)]^{2+}$  (M = Ru and Os).** Oxidation of  $[M(bpy)_3(BiBzImH_2)]^{2+}$  (M = Ru and Os; BiBzImH<sub>2</sub> = 2,2'-bibenzimidazole; Figure 6) to M(III) and M(IV) occurs by pH-dependent couples with pH-dependences reminiscent of the oxo/aqua couples in Figures 2, 121,122. In this coordination environment, M(IV) is stabilized by double deprotonation and electron donation from  $\pi(BiBzIm^+)$  to M(IV). pH-dependent redox couples have also been observed for Fe and Ru complexes containing ligands related to bibenzimidazole.<sup>121-124</sup>

**2.3.1.2.  $[M(NH_3^+CMe_2CMe_2NH_2)_2Cl_2]$  (M = Ru and Os).** Oxidation of the 2,3-diamino-2,3-dimethylbutane complex  $[Os^{IV}(NH_3^+CMe_2CMe_2NH_2)_2Cl_2]^{2+}$  to Os(IV) over the pH range 1–5 occurs with loss of a single proton.<sup>125</sup> From pH = 0.5 to 2, oxidation of  $[Ru^{IV}(NH_3^+CMe_2CMe_2NH_2)_2Cl_2]$  occurs by reversible 1e- oxidation to Ru(III) followed by 1e-/2H+ oxidation to  $[Ru^{IV}(bpy)_3Cl_2(NH_3^+CMe_2CMe_2NH_2)]^{2+}$ . Above pH = 4, there is a single 2e-/2H+ oxidation to Ru(IV). Similar behavior is observed for the *tris*-2,3-diamino-2,3-dimethylbutane complex. In the oxidized complexes, Ru(IV) is stabilized by electron donation from 2p<sub>π</sub>(N) to d<sub>π</sub>(RuIV). This creates a Ru<sup>IV</sup>= $(NH_3^+CMe_2CMe_2)$  multiple bond interaction analogous to the M=O interaction in oxo complexes.<sup>126</sup>

**2.3.1.3. *trans*- $[Os^V(bpy)(Cl)_2(NNR_2)]^+$  and S- and P-Based Analogues.** As shown in eq 30, the Os(VI/V) hydrazido couple based on *trans*- $[Os^V(bpy)(Cl)_2(NNR_2)]^+$  with NR<sub>2</sub> = morpholine ( $\sim N(CH_2)_2O$ ) is pH-dependent in acidic solution. It becomes pH-independent above the pK<sub>a</sub> for *trans*- $[Os^V(bpy)(Cl)_2(NH_2)NR_2]^+$  ( $pK_a = 3.2$ ), where the couple is *trans*- $[Os^V(bpy)(Cl)_2(NNR_2)]^+$ /*trans*- $[Os^V(bpy)(Cl)_2(NNR_2)]$ . The deprotonated Os(V) complex undergoes further oxidation to Os(VI). The protonated Os(V) complex undergoes further reduction first by 2e-/3H+ to give the Os(II) hydrazido complex *trans*- $[Os^V(bpy)(Cl)_2(NH_2NR_2)]$  and then by further 2e-/3H+ reduction to the amine, eq 30.<sup>127-129</sup>

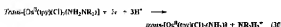


Figure 6.  $[M(bpy)_3(BiBzImH_2)]^{2+}$  with M = Ru and Os.



Figure 7.  $Tp^-$  = tris(pyrazol-1-yl)borate anion.

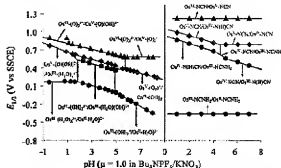


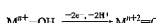
Figure 8.  $E_{1/2}$ -pH diagram for *mer*- $[Os^V(bpy)_2Cl_2(NCNC)]^-$  in 1:1 (v/v)  $H_2O/CH_3CN$  in  $1 = 1.0$  M  $Bu_4NPF_6/KNO_3$  with  $E_{1/2}$  values vs  $Ca^{2+}$  (saturated NaCl) rather than KCl). For comparison, the equivalent couples for *cis*- $[Os^V(bpy)_2(H_2O)_2]^{2+}$  at  $1 = 1.0$  M in  $H_2O$  are also shown. Vertical lines indicate  $pK_a$  values, and proton compositions of dominant forms are indicated for both sets of couples.<sup>132</sup>

Related acid–base behavior has been observed for the S–H based sulfonimido couple *trans*- $[Os^V(bpy)(Cl)_2(NS_2CH_2Me)_2]^{+}/trans- $[Os^V(bpy)(Cl)_2(NS(H_2)-p-C_6H_4Me)_2]^{+}$ <sup>130</sup> and the P–H based phosphonamido couple, *fac*- $[Os^V(bpy)(Cl)_2(N^+P^-(CH_2)_2Et_2)]^{+}/[Os^V(bpy)(Cl)_2(N^+P^-(CH_2)_2Et_2)]^-$  ( $Tp^-$  is the tris(pyrazol-1-yl)borate anion, Figure 7).<sup>131</sup> The kinetics of oxidation of the Os(V) complexes by quinone will be featured in the discussion on EPT pathways in chemistry in section 6.1.4 because they occur with colossal  $k(H_2O)/k(D_2O)$  kinetic isotope effects.$

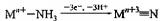
**2.3.1.4. Oxo-like Behavior in *mer*- $[Os^V(bpy)(Cl)_2(NCNC)]^-$ .** A dramatic example of pH-dependent redox behavior, reminiscent of the oxo complexes in Figures 2 and 5, occurs for the cyanonimido complex *mer*- $[Os^V(bpy)(Cl)_2(NCNC)]^-$ , which is prepared from the  $Os^{VI}$ -nitrido precursor by the reaction *mer*- $[Os^{VI}(bpy)(Cl)_2(N)]^- + CN^- \rightarrow$  *mer*- $[Os^V(bpy)(Cl)_2(NCNC)]^-$ .<sup>132,133</sup> It is based on reversible Os(V/V), Os(V/IV), Os(IV/III), and Os(III/II) couples and is compared to *cis*- $[Os^V(bpy)_2(H_2O)_2]^{2+}$  in Figure 8. From IR measurements, the first proton is added to *mer*- $[Os^V(bpy)(Cl)_2(N_2C_2N_2)]^-$  at  $N_2$  and the second is added at  $N_2$  accompanied by a proton shift from  $N_2$  to  $N_2^+$  to give *mer*- $[Os^V(bpy)(Cl)_2(NCNH_2)]^-$ .

#### 2.3.2. Oxidation of Coordinated Amines

There is a direct analogy between  $2e^-/2H^+$  oxidation of coordinated water to a higher oxidation state oxo complex,

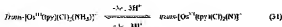


and  $3e^-/3H^+$  oxidation of coordinated ammonia to a nitroso complex. The analogy may be apt, but the oxidation

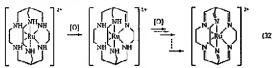


chemistry of coordinated ammonia is far more complex, with nitrosyl or  $\mu$ -N<sub>2</sub> products typically appearing instead of reversible PCET. <sup>8,134-140</sup>

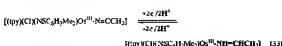
In sufficiently electron-rich coordination environments, NH<sub>3</sub>–N<sup>3+</sup> interconversion does become chemically reversible, as shown by the example in eq 31. <sup>141-143</sup> As discussed in section 4, these reactions are kinetically inhibited by slow proton transfer.



There is a related oxidative dehydrogenation chemistry of coordinated amines to imines and nitriles that is extensive. <sup>144-146</sup> This includes many examples from the Fe, Ru, and Os triad with one example illustrated in eq 32. <sup>147-151</sup> These are dehydrogenation reactions with electrons and protons lost from CII–NII bonds and the imine and nitrile ligands stabilizing M(II) by metal-to-ligand dπ–π\* backbonding. <sup>152-154</sup>



Oxidative dehydrogenation is typically irreversible because there are no facile pathways for re-reduction to the amine. Uncharacteristically, the nitrile complex [Os<sup>III</sup>(tpy)(Cl)(N≡CC<sub>2</sub>H<sub>5</sub>)(NS-3,5-Me<sub>2</sub>C<sub>6</sub>H<sub>3</sub>)]<sup>+</sup> undergoes reversible,  $2e^-/2H^+$  reduction to the imine, [Os<sup>IV</sup>(tpy)(Cl)(NH=CH<sub>2</sub>)(NS-3,5-Me<sub>2</sub>C<sub>6</sub>H<sub>3</sub>)]<sup>+</sup>, in 1:1 (v/v) CH<sub>3</sub>CN/H<sub>2</sub>O, at  $E_{1/2} = 0.29$  V (J = 0.2 M), eq 33. <sup>155</sup>



The unusual kinetic reversibility in this case may be due to the intervention of oxidation state isomers, e.g., [Os<sup>IV</sup>–N≡CC<sub>2</sub>H<sub>5</sub>]<sup>+</sup> + H<sup>+</sup>  $\rightarrow$  [Os<sup>IV</sup>–(NC(H)CH<sub>3</sub>)<sup>2</sup>]<sup>+</sup>. The reactivity of this complex extends to organic reactions where the coordinated nitrile/imine couple undergoes reversible reactions with alcohols to give ketones or aldehydes. <sup>155</sup>

## 2.4. Organic PCET

There is an extensive PCET electrochemistry for organic redox couples, <sup>26,77</sup> with notable examples appearing for quinones, aromatic hydrocarbons, and carbonyl compounds. <sup>15,19,80,156,157</sup> The compact potential– $pK_a$  scheme in Figure 4 for the reduction of quinone to hydroquinone provides a useful basis for summarizing redox properties in a variety of organic PCET reactions. <sup>85,158</sup> An example is shown in Figure 9, which summarizes the mechanism for reduction of a benzoin to the *cis* and *trans* endiols in aqueous solution. <sup>77,155,157</sup>

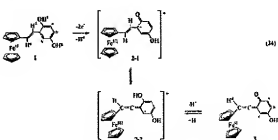
Another example is the reduction of aromatic hydrocarbons (A) such as anthraquinone. In dry DMF, two reversible waves appear due to successive reduction of A to A<sup>–</sup> and then to

A<sup>2–</sup>. Upon addition of a weak acid, typically a phenol, the A<sup>–</sup> reduction wave becomes irreversible because protonation of A<sup>2–</sup> gives AH<sub>2</sub><sup>–</sup>, which is unstable toward disproportionation into A and AH<sub>2</sub>. As the concentration of acid is increased, reduction to A<sup>–</sup> is followed by protonation to give HA and further 2e<sup>–</sup> reduction to give AH<sub>2</sub>. <sup>75,80</sup>

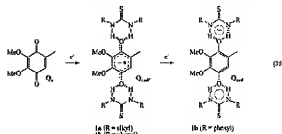
### 2.4.1. Reduction of Quinones

The influence of H-bonding and protonation on quinone reduction has been investigated for a series of quinones ranging from chloranil (tetrachloro-1,4-benzoquinone) to duroquinone (tetramethyl-1,4-benzoquinone). <sup>159</sup> In dry, pure benzonitrile, chemically reversible Q/Q<sup>–</sup> and Q<sup>–</sup>/Q<sup>2–</sup> couples appear separated by 0.8–0.9 V in cyclic voltammograms. With added weak acids, three different types of behavior were observed depending on the basicity of the quinone and the strength of the acid: (1) shift in  $E_{1/2}$  due to H-bonding, (2) reduction followed by disproportionation of the intermediate semiquinone, and (3) protonation of the quinone prior to reduction to Q<sup>2–</sup>.

Oxidation of the vinylene-bridged ferrocene-hydroquinone in eq 34 occurs by an initial 1e<sup>–</sup> oxidation to give a ferricinium form that subsequently loses a proton and a second electron to give the ferricinium-semiquinone. It is in equilibrium with the 2e<sup>–</sup>/2H<sup>+</sup> product, 6-(ferrocenylvinylene)-4-hydroxyhexa-2,4-dien-1-one, shown in eq 34. <sup>160</sup>



Reduction of ubiquinone to the corresponding semiquinone in CH<sub>2</sub>Cl<sub>2</sub> in the presence of [N-(n-Bu)<sub>4</sub>]ClO<sub>4</sub> occurs at  $E_{1/2} = -1.13$  V (vs Fe<sup>2+</sup>/Fe). Addition of the thiourea-based receptor shown in eq 35 gives a new oxidative wave at  $-0.3$  V following quinone reduction. This suggests that the intermediate semiquinone is stabilized by H-bonding to the thiourea, eq 35. Further reduction gives the hydroquinone



stabilized by H-bonding to the receptor anion. <sup>161</sup> This observation may be relevant to the possible role of H-bond stabilization of the semiquinone intermediate that appears following quinone reduction in bacterial reaction centers and in Photosystem II (section 7.3). <sup>162,163</sup>

The effects of H-bonding to amines on the oxidation of phenol to phenoxyl radical in the gas phase were investigated

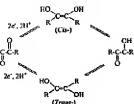
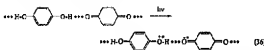


Figure 9. PCET reduction scheme for a benzoin.

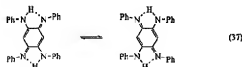
with GAUSSIAN 98.<sup>164</sup> The potential for phenol oxidation shifts negatively by as much as 1 V with added base.<sup>165</sup> This may be of relevance to a key step in Photosystem II, the oxidation of tyrosine Y<sub>2</sub>, which is 11-bonded to a neighboring histidine base (section 7.2).

#### 2.4.2. Quinhydrones and Intramolecular PCET

Quinhydrones have been described as H-bonded charge transfer (CT) complexes. They form in solutions that are concentrated in both quinone and hydroquinone by H-bonding interactions. Their formation is accompanied by the appearance of low-energy absorption bands arising from  $H_2Q \rightarrow Q$  charge transfer, eq 36.<sup>165–168</sup> For 1,4-benzoquinhydrone in the solid state<sup>169–171</sup> and for a series of extensively conjugated quinhydrones,<sup>172</sup> pressure induces a phase transition to a cooperative proton–electron transfer (PET) state. This state has been characterized as a molecular assembly of *11-bonded neutral radicals*.



Related processes occur in a class of organic molecules in which PCET interconverts degenerate tautomers.<sup>173–177</sup> For example, dynamic intramolecular, double electron–proton transfer has been shown to occur in azophenine (*N,N*-diphenyl-3,6-bis(phenylimino)-1,4-diamine) as illustrated in eq 37. The mechanism involves rate limiting  $1e^-/1H^+$  transfer both in solution and in the solid state.<sup>178</sup> A related mechanism has been invoked for interconversion of tautomers in free base porphyrins and the porphine radical anion.<sup>177,178</sup>



#### 2.5. Biological PCET

Except for single electron transfer carriers such as the cytochromes and ferredoxins, PCET is ubiquitous in biological redox reactions where molecular changes are tied to energy conversion. This includes photosynthesis and respiration, where coupled electron–proton transport chains create a transmembrane proton gradient and use it to produce ATP.<sup>179–188</sup>

##### 2.5.1. Iron–Sulfur Proteins

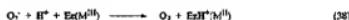
PCET has been clearly established for couples involved in dinitrogen reduction. A [4Fe–4S] cluster acts as a one-electron reductant for the [7Fe–Mo–9S–homocitrate] cofactor

(FeMoCo). It is present in the molybdenum–iron (MoFe) protein component where reduction of  $N_2$  occurs.<sup>189–194</sup> A [8Fe–7S] cluster ( $P^+$ ) has been proposed as an intermediate electron transfer site. It has sequential  $P^{2+}/P^+$ ,  $P^{1+}/P^0$  couples.<sup>192</sup> The  $P^{2+}/P^+$  couple is pH-dependent near pH = 7 with  $pK_a(P^+) = 6.0$  and  $pK_a(P^0) > 8.5$ . The P-cluster has O-serinate (beta-Ser 188), peptide amide (alpha-Cys88), and cysteinate S ligands.<sup>193</sup>

A voltammetric study on the [3Fe–4S] cluster in azobacter vinelandii Ferredoxin reveals that PCET occurs with reduction accompanied by protonation. Mechanistically, rate determining electron transfer is followed by proton transfer. The cluster is buried in a membrane and inaccessible to  $H_2O$ . Proton transfer is facile only if an aspartate (D15) resides on the membrane surface.<sup>194</sup> The kinetics and energetics of the coupled electron–proton transfer have been analyzed by protein–film voltammetry.<sup>195</sup> Proton transfer is mediated by a mobile carboxylate arm from an adjacent aspartate-15 residue. The possible roles of internal water molecules on the coupling of electrons and protons have been investigated by *ab initio* and molecular dynamics simulations.<sup>196</sup>

##### 2.5.2. Superoxide Dismutases

The Fe- and Mn-containing superoxide dismutase enzymes, Fe(SOD) and Mn(SOD), catalyze the disproportionation of superoxide, thus preventing  $O_2^-$ -initiated oxidative damage.<sup>197–202</sup> PCET is important in the reduction of  $O_2^-$  to  $H_2O_2$ , which is part of the disproportionation cycle in eqs 38–39. Ez is an abbreviation for the enzyme, and M = Fe or Mn.<sup>55,198–199</sup>



Reduction of  $Fe^{III}(SOD)$  to  $Fe^{II}(II)$  occurs with addition of a proton,<sup>203</sup> most likely at coordinated  $OH^-$ , eq 38. The coordination geometry at the active sites of the M(II) enzymes is trigonal bipyramidal with a ligand set consisting of three histidines, an aspartate anion, and  $OH^-$ . The proton equilibria for Mn(SOD) are consistent with  $pK_a = 11.8$  for the Mn(II) form of the enzyme and  $pK_a = 8.7$  for Mn(III).<sup>55,204,205</sup> In an alternate interpretation, it has been proposed that Tyr-34, which is universally conserved, is responsible for the  $pK_a$  claimed for Mn(III).<sup>206</sup>

##### 2.5.3. PCET in Flavodoxin

The electrochemistry of flavodoxin D, *Vulgaris* Hildenborough (Fld), has been investigated on nanocrystalline, mesoporous  $SnO_2$  electrodes. Binding to the electrode is promoted by poly-L-lysine. The electrochemical measurements reveal two reversible redox couples that have been attributed to the quinone/semiquinone and semiquinone/hydroquinone couples of the flavin mononucleotide (FMN) redox cofactor. For the  $Q/HQ^0$  couple,  $E_{1/2}$  decreases 51 mV/pH unit, consistent with a  $1e^-/1H^+$  couple (section 2.1). The rate of semiquinone oxidation is pH-dependent and consistent with rate limiting deprotonation of the semiquinone.<sup>71</sup>

##### 2.5.4. Membrane Effects on Redox Potentials

Electrostatic effects can have a significant impact on biological membrane redox potentials, including those involving PCET.<sup>207–213</sup> They arise from reorientation of surrounding dipoles in a rigid medium, local neutralization by a counterion, and rearrangement of solvent dipoles at

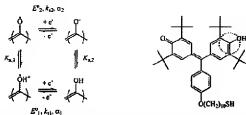


**Figure 10.** Kinetic scheme for pH-dependent reduction of the galvinoxyl/galvinoxyl couple of a  $C_{10}$ -alkanethiol-terminated galvinoxyl tethered to Au. The redox-active site is circled.

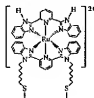


**Figure 11.** Structure of  $[Ru(dtbbipy)(bimpyH_2)]^{3+}$ .

surface-exposed sites. It has been proposed that long-range proton transfer in membranes may involve local, nonequilibrium conformations, equivalent to partial local denaturation.<sup>20</sup>

## 2.6. PCET on Surfaces

The proton-coupled electron transfer properties of solution-based couples have also been explored on surfaces and in thin films.

### 2.6.1. "Tethered" Surface Couples

On a Au microelectrode containing both adsorbed ferrocenyl-thiol,  $Fe-C(O-CH_2)_n-SH$ , and the hydroquinone derivative,  $H_2Q(CH_2)_n-SH$ , the quinone/hydroquinone couple retains its solution pH-dependence, with the  $Fe^{3+}/^{2+}$  couple providing an internal reference.<sup>20</sup>

The  $1e^-$  galvinoxyl/galvinoxyl couple of the  $C_{10}$ -alkanethiol-terminated derivative of galvinoxyl, illustrated in Figure 10, exhibits a pH-dependence when adsorbed to Au. The pH-dependence was explained by a kinetic scheme involving sequential ET-PT as shown in Figure 10. The surface reduction potential for the galvinoxyl/galvinoxyl couple decreased by 60 mV/pH unit up to  $pK_{1/2} = 12.7$ , past which it became independent of pH.<sup>20b,21b</sup>

Similarly, the merocouperide-dermatized Ru complex shown in Figure 11 retains its PCET properties when adsorbed to Au. The pH-dependence of the  $Ru(IV/III)$  couple was retained on the surface, although  $pK_{1/2}$  and  $pK_{2/1}$  for both  $Ru(IV)$  and  $Ru(II)$  increased by 2  $pK_e$  units compared to solution values.<sup>21</sup>

Cytochrome *c* ( $Cy-c$ ) was electrostatically bound to self-assembled monolayers (SAMs) of  $\omega$ -carboxyl alkanethiols,  $-S-(CH_2)_n-CO_2H$ , on Ag with  $n = 2, 3, 6, 11$ , and 16. The dynamics of electron transfer and from the electrode were measured by time-resolved, surface-enhanced resonance Raman spectroscopy following a potential jump. The measured  $k_{tr}$  decreased exponentially with increasing distance until  $n = 6$ , which coincided with an increase in  $k(H_2O)/k(D_2O)$  from 1.2 to 4.0. This effect was attributed to a

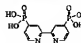


**Figure 12.**  $4,4'-(PO_3H_2)_2bipy$ .

rearrangement in H-bonding network surrounding Cyt-*c* between the oxidized and reduced states.<sup>21d</sup>

### 2.6.2. Directly Adsorbed Couples

Monolayers of the anthraquinone carboxylic acid shown in eq 40 on mercury microelectrodes undergo chemically and electrochemically reversible  $2e^-/2H^+$  reduction to the hydroquinone with  $E_{1/2}$  decreasing by 60 mV/pH unit at pH  $< 4$ .<sup>21c</sup>



The complex  $[Ru^{II}(tpy)(bipy)(H_2O)]^{2+}$  has successive  $Ru(IV/III)$  and  $Ru(III/II)$  couples at potentials only slightly shifted from those observed for *cis*- $[Ru^{II}(bipy)(tpy)(H_2O)]^{2+}$  in Figure 2. The phosphonate-derivative version,  $[Ru^{II}(tpy)(4,4'-(PO_3H_2)_2bipy)(H_2O)]^{2+}$ , adsorbs strongly to metal oxide surfaces, including  $TiO_2$  and  $Sn(IV)$ -doped  $In_2O_3$  (ITO) electrodes. The structure of the phosphonated ligand is shown in Figure 12. The pH-dependence of the  $Ru(IV/III)$  couple is retained on the surface at potentials comparable to those in solution. However, the appearance of the  $Ru(IV/II)$  couple and oxidation to adsorbed  $[Ru^{IV}(tpy)(4,4'-(PO_3H_2)_2bipy)]^{2+}$  are dependent on the extent of surface coverage.<sup>16</sup> Oxidation to  $Ru(IV)$  occurs by cross-surface disproportionation and not by direct oxidation (section 6.5.1).<sup>21d</sup> When adsorbed to surfaces of nanoparticle thin films of  $TiO_2$  on glass, adsorbed  $[Ru^{IV}(tpy)(4,4'-(PO_3H_2)_2bipy)(O)]^{2+}$  retains the extensive redox reactivity found for analogous polypyridyl  $Ru^{IV}=O$  complexes in solution.<sup>18,21e</sup>

### 2.6.3. Surface Couples

pH-dependent redox phenomena are also observed at the surfaces of metal oxides and on metal surfaces that have been oxidatively treated to produce surface oxide coatings. Such procedures produce clusters or layers of metal atoms with exposed oxo/hydroxo functional groups analogous to the single unit  $M=O$ ,  $M-OH$ , and  $M-OH_2$  groups in metal complexes.

An example of such behavior occurs on Pd, which, when coated with NaOH and heated at 800 °C, produces an oxide surface and a  $PdO/Pd$  electrode which acts as a linear pH sensor from pH = 3 to 11. The observed pH-dependence is consistent with the half reaction  $PdO + 2e^- + 2H^+ \rightarrow Pd(s) + H_2O$ .<sup>21f</sup>

Cyclic voltammetric sweeps of  $RuO_2$  electrodes on  $TiO_2$  display a broad but well-defined series of pH-dependent surface waves at  $\sim -0.1$ , 0.5, and 0.9 V in 1 M  $HClO_4$  vs SCE.<sup>21g</sup> Cyclic voltammograms of nanoparticles of hydrous  $Ru(II)$  oxide adsorbed on polished boron-doped diamond electrodes, a  $Ru(IV/III)$  couple appears that has a Nernstian response (0.059 mV/pH unit) from pH 1 to 13.<sup>21f</sup>

### 2.6.4. Solid State PCET

For a variety of oxide materials, the absolute valence and conduction band edge energies vary with the pH of the

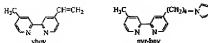


Figure 13. Vbpy and pyr-bpy ligands.



Figure 14. Phen (1,10-phenanthroline).

external solution with band edges shifting  $\sim 60$  mV per pH unit.<sup>211–223</sup> The origin of this effect has been explored in nanocrystalline  $\text{TiO}_2$  (anatase) electrodes by diffuse reflectance measurements of the conduction band gap,  $E_{\text{cb}}$ , and by electrochemical quartz crystal microbalance (EQCM) measurements.<sup>224</sup> Over a range in acidity from  $\text{H}^+ = -8$  to  $+23$ ,  $E_{\text{cb}}$  decreased by  $\sim 64$  mV/pH unit. The EQCM measurements revealed that the shifts in  $E_{\text{cb}}$  were accompanied by proton uptake over the whole pH range. The data were interpreted by assuming that, at increasingly applied negative potentials, reduction to  $\text{Ti}(\text{III})$  trap sites occurs accompanied by proton uptake,  $\text{Ti}^{\text{IV}}\text{O}_2 + \text{e}^- + \text{H}^+ \rightarrow \text{Ti}^{\text{III}}\text{O}(\text{OH})$ , which is reversible,  $\text{Ti}^{\text{III}}\text{O}(\text{OH}) \rightarrow \text{Ti}^{\text{IV}}\text{O}_2 + \text{e}^- + \text{H}^+$ . The conduction band edge energy is controlled by the potential of the pH-dependent,  $\text{Ti}(\text{IV}/\text{III})$  trap site couple in the nanocrystalline material.

The loss of pH-dependence at high acidity was attributed to equilibrium protonation of  $\text{Ti}(\text{IV})$  in the trap sites and the couple,  $[\text{Ti}^{\text{IV}}\text{O}(\text{OH})]^+ + \text{e}^- \rightarrow \text{Ti}^{\text{IV}}\text{O}(\text{OH})$ . Similarly, the loss of pH-dependence at low acidity was attributed to the couple  $\text{Ti}^{\text{IV}}\text{O}_2 + \text{e}^- \rightarrow [\text{Ti}^{\text{IV}}\text{O}_2]^-$ .<sup>224</sup>

## 2.7. PCET in Films

### 2.7.1. Electropolymerized Films

Thin polymeric films of metal complexes containing the vinylbipyridine or pyrrol-bipyridine ligands shown in Figure 13 can be prepared by electropolymerization on a variety of conducting substrates.<sup>225,226</sup> For vinylbipyridine complexes, reductive scans through bipy-based reductions in the potential region  $-0.7$  to  $-1.7$  V vs  $\text{SSCE}$  in  $\text{CH}_3\text{CN}$  result in well-defined films whose thicknesses can be controlled by varying the scan rate and the concentration of complex in solution. A similar procedure for pyrrole-containing ligands, but with oxidative scans past  $+0.8$  V, also results in well-defined thin films.

Electropolymerization followed by chemical or photochemical post-treatment was used to prepare thin films containing poly-*cis*-[Ru(vbpy)( $\text{H}_2\text{O}$ )<sub>4</sub>]<sup>2+</sup> or poly-*cis*-[Ru(pyr-bpy)( $\text{H}_2\text{O}$ )<sub>4</sub>]<sup>2+</sup>.<sup>227,228</sup> Electrochemical measurements revealed pH-dependent  $\text{Ru}(\text{IV}/\text{II})$  and  $\text{Ru}(\text{II}/\text{II})$  waves that were sensitive to cycling and aging effects. The films were electrocatalytically active toward oxidation of benzyl alcohol to benzaldehyde and of  $\text{Cl}^-$  to  $\text{Cl}_2$  based on the higher oxidation state  $\text{Ru}(\text{V}/\text{IV})$  and  $\text{Ru}(\text{IV}/\text{IV})$  couples.<sup>227</sup>

### 2.7.2. Ion-Exchanged Films

The complex  $[\text{Ru}(\text{tpy})(\text{phen})(\text{OH})]^+$  (phen is 1,10-phenanthroline, Figure 14) was incorporated into a carbon paste electrode containing added Dowex 50W  $\times 8$ , a strong cation exchanger. In the film, a reversible  $2\text{e}^-/\text{H}^+$  oxidation to  $[\text{Ru}(\text{tpy})(\text{phen})(\text{O})]^2+$  occurs, and the trapped  $[\text{Ru}^{\text{IV}}(\text{tpy})(\text{phen})(\text{O})]^2+/[\text{Ru}^{\text{IV}}(\text{tpy})(\text{phen})(\text{OH})]^+$  couple acts as an electrocatalyst toward oxidation of benzyl alcohol.<sup>229</sup>

Electrochemical and EQCM measurements have been applied to a series of polyoxometalates ( $[\text{PW}_{12}\text{O}_{40}]^{3-}$ ,  $[\text{SiW}_{12}\text{O}_{40}]^{4-}$ ,  $[\text{P}_2\text{W}_{18}\text{O}_{62}]^{3-}$ , and  $[\text{P}_2\text{W}_{18}\text{O}_{62}]^{4-}$ ) in slightly quantized poly-4-vinylpyridine (QPVP) and polyamine films. A  $1\text{e}^-$  reduction, e.g., QPVP/ $[\text{PW}_{12}]^{3-}$  +  $\text{e}^- \rightarrow$  QPVP/ $[\text{PW}_{12}]^{2-}$ , followed by a  $1\text{e}^-/2\text{H}^+$  reduction, QPVP/ $[\text{PW}_{12}]^{2-} + \text{e}^- + 2\text{H}^+ \rightarrow$  QPVP/ $[\text{H}_2\text{PW}_{12}]$ , was observed in all cases, with the difference in pH-dependence leading to a merging of the waves in acidic solution. A microenvironmental effect influences the  $\text{pK}_a$  properties of the doubly reduced clusters. It shifts the potential at which the pH-dependent and independent couples overlap at higher acidities.<sup>230</sup>

### 2.7.3. Liquid Crystal Films

The redox properties of the heme protein myoglobin (Mb) have been studied in thin liquid crystal films of didodecyltrimethylammonium bromide (DDAB) and phosphardicholines (PCs) by electrochemical and spectroscopic measurements. Two pH-dependent phenomena were observed. One, which occurs with  $\text{pK}_{\text{a},1} = 4.6$ , was attributed to protonation of a histidine residue in a near lying hydrophobic region,  $\text{MbFe}(\text{III}) + \text{H}^+ \rightarrow \text{MbFe}(\text{III})-\text{H}^+$ .<sup>231</sup> The second occurred at pH  $> 9$  and was attributed to the pH-dependent  $\text{Fe}(\text{III}/\text{II})$  couple of the myoglobin core,  $\text{MbFe}^{\text{II}}\text{OH} + \text{e}^- + \text{H}^+ \rightarrow \text{MbFe}^{\text{II}}\text{OH}$ .

## 2.8. Excited States

Electronic excited states have their own electronic structures and associated properties. This includes acid–base reactivity and PCET, which can be significantly different from those of the ground state.<sup>232,233</sup>

### 2.8.1. Excited State Superacids

The effects of changes in oxidation state or electron content on  $\text{pK}_a^*$  have been documented in previous sections. This extends to excited states where changes in electronic configuration can significantly change acid–base properties.<sup>234–238</sup> Excited states that are sufficiently long-lived to be thermally equilibrated with their surroundings have their own pseudo-thermodynamic properties including redox potentials,  $\text{pK}_a^*$ , etc.

The acid–base properties of excited and ground states are related through the Förster equation in eq 41, which is derived from a thermodynamic cycle.<sup>239</sup> It relates excited state ( $\text{pK}_a^*$ ) and ground-state  $\text{pK}_a$  values ( $\text{pK}_a$ ) through the  $0\text{--}0$  ground-state-to-excited-state energy differences between protonated ( $\text{Hv}(\text{HA})$ ) and unprotonated ( $\text{Hv}(\text{A}^-)$ ) forms. The latter are often approximated as absorption or emission maxima from the corresponding spectra.

$$\text{pK}_a^* = \text{pK}_a - \frac{[\hbar\nu(\text{HA}) - \hbar\nu(\text{A}^-)]}{2.3RT} \quad (41)$$

$$\Delta G = -2.3RT \log(K_a^*/K_a) = -0.059(\text{pK}_a - \text{pK}_a^*) \quad (\text{in eV at } 25^\circ\text{C}) \quad (42)$$

The Förster equation shows that the acidity of an excited state,  $\text{HA}^*$ , is enhanced, compared to the ground state, when its energy content is greater than that of the excited state of the basic form,  $\text{A}^-$ . Equation 41 is analogous to eqs 23 and 24, which relate  $\text{pK}_a$  values to redox potentials. The difference in  $\text{pK}_a$ 's between excited and ground states gives

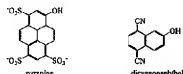
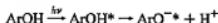


Figure 15. Pyranine and dicyanophenol.

the free energy change for proton transfer between the two excited states,  $HA^* + A^- \rightarrow A^* + HA$ , eq 42.

The Förster equation is useful conceptually but often not practical because of the difficulty in obtaining and analyzing relevant spectral data. It is also limited to those cases where acid–base equilibria are reached during the lifetime of the excited state, which is frequently not the case.

According to eq 41, if the 0–0 energy of  $HA^*$  is greater than the 0–0 energy of  $A^*$ ,  $pK_a^* < pK_a$  and the acidity of the excited state is greater than that of the ground state. The phenomenon of enhanced excited-state acidity has been studied extensively in aromatic hydroxyarenes. In the excited



states of these molecules, there is a redistribution of electron density away from the O-atom of the O–H bond which causes acidity to increase.

Substituent and solvent effects have been used to design excited states which function as “super” photacids. In these excited states, proton transfer is in competition with excited-state decay, proton loss induced quenching, and homolytic O–H bond cleavage.<sup>232</sup> The increase in excited-state acidity can be considerable. For example,  $pK_a^* = -4.5$  for the dicyano-2-naphthol derivative shown in Figure 15.

A related phenomenon has been reported for the Ir(III) complex  $[Ir^{III}(\text{phen})(\text{Cp}^*)\text{H}]^+$  (phen is 1,10-phenanthroline,  $\text{Cp}^*$  is pentamethylcyclopentadienyl anion,  $\text{C}_5\text{M}_5^-$ ). In this complex, visible, metal-to-ligand charge transfer,  $\text{H}^0 \rightarrow \text{phen}$  (MLCT) excitation in  $\text{CH}_3\text{OH}$ , followed by intersystem crossing ( $k = 3-4 \times 10^8 \text{ s}^{-1}$ ), gives a lowest lying MLCT excited state,  $[\text{Ir}^0(\text{phen}^*)(\text{Cp}^*)\text{H}]^{*+}$ . It subsequently undergoes  $\text{H}^+$  loss and internal electron transfer,  $[\text{Ir}^0(\text{phen}^*)(\text{Cp}^*)\text{H}]^{*+} \rightarrow [\text{Ir}^1(\text{phen})(\text{Cp}^*)] + \text{H}^+$  ( $k_1 = 8.1 \times 10^5 \text{ s}^{-1}$ ), which provides a basis for enhanced acidity.<sup>233</sup>

The kinetics of proton loss following excitation can be very rapid, limited by solvent relaxation in some cases.<sup>241–244</sup> Proton dissociation in the excited state of the sulfonated pyrrole derivative pyranine (8-hydroxy-1,3,6-trisulfonaphthalene) Figure 15 has been investigated by theory and femtosecond transient spectroscopy.<sup>235</sup> Based on this analysis, key microscopic elements in photoinduced proton transfer are the quantum nature of the proton nuclear motion and electrostatic coupling with surrounding polar solvent molecules. The barrier to proton transfer is dictated by solvent rearrangement and the proton tunneling distance rather than the barrier height.

Events occurring on three different time scales were observed for proton loss from excited pyranine. The first ( $< \sim 300 \text{ fs}$ ) was attributed to surrounding aqueous solvent dynamics, the second ( $\sim 2.2 \text{ ps}$ ) to a change in electronic state, and the third ( $\sim 87 \text{ ps}$ ) to the actual proton transfer event.

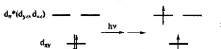


Figure 16. Schematic energy level diagram for  $d^4 \text{ trans-}[\text{Re}^{\text{V}}(\text{py})(\text{O})_2]^4+$  with the O–Re–O bonding axis defined as the  $z$ -axis. The diagram illustrates the effect of  $2p_{\pi}(\text{O})$  mixing with  $d_{xy}$  and  $d_{yz}$ , which imparts antibonding character, giving  $d\pi^*(\text{v}, \text{ax})$ . It also illustrates  $d_{xy} \rightarrow d\pi^*$  excitation to give the  $^1\text{E}_g$  excited state.

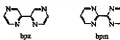


Figure 17. Bpz and bpm.

### 2.8.2. Proton Transfer Quenching of $\text{trans-}[\text{Re}^{\text{V}}(\text{py})(\text{O})_2]^4+$

Excited-state acid–base effects have been documented for other metal complex excited states.<sup>235,238</sup> For  $d^4 \text{ trans-}[\text{Re}^{\text{V}}(\text{py})(\text{O})_2]^4+$ , defining the O–Re–O bond axis as the  $z$ -axis, antibonding character is imparted to  $d_{xy}$  and  $d_{yz}$  by  $2p_{\pi}(\text{O})$  mixing. The in-plane  $d$  orbital  $d_{xy}$  remains relatively unaffected. This results in the schematic energy level diagram shown in Figure 16. As indicated in this diagram,  $d_{xy} \rightarrow d\pi^*$  interconfigurational excitation, followed by spin interconversion, gives the  $^1\text{E}_g$  excited state. It emits at 650 nm in  $\text{CH}_3\text{CN}$  with a lifetime of  $10 \mu\text{s}$ .<sup>246–250</sup>

In contrast to the case of the hydroxyarenes, the basicity of the  $^1\text{E}_g$  excited state is enhanced because excitation results in electron occupation of a  $d\pi^*$  orbital in the excited state. The electron density at the oxo groups is increased, as shown by an increase in Re–O bond length of  $0.07 \text{ \AA}$ .<sup>245</sup> The  $^1\text{E}_g$  excited state undergoes proton transfer quenching in  $\text{CH}_3\text{CN}$  with a variety of organic and inorganic acids<sup>247–249</sup> and even with metal hydrides.<sup>250</sup> The  $\Delta G$ -dependence of  $k_q$  for these reactions has been treated by application of Marcus–Hush electron transfer theory in a form originally applied to excited-state electron transfer quenching (section 5.1)<sup>251</sup> and later to proton transfer.<sup>252–257</sup> Analysis of these data gave  $pK_a^* \sim 11$  for  $\text{trans-}[\text{Re}^{\text{V}}(\text{py})(\text{O})(\text{OH})]^4+$  compared to  $pK_a < 0$  for the protonated ground state.<sup>247</sup>

### 2.8.3. MLCT Excited States

In polypryridyl  $d\pi^*$  complexes, such as  $[\text{Ru}(\text{ppy})_3]^{2+}$ , the lowest thermally equilibrated excited state is a largely triplet  $[\text{d}^2\pi^*]^1$  metal-to-ligand charge transfer (MLCT) excited state. In this state, the excited electron occupies a single ligand,  $[\text{Ru}^{III}(\text{bpy})_2(\text{bpy})]^{4+}$ , although the excited-state dipole rotates through the three ligands on the picosecond time scale.<sup>258–260</sup> Spin–orbit coupling and low symmetry split the triplet state into a manifold of three closely spaced states which behave kinetically as a single state at room temperature.<sup>264–269</sup>

In heteroleptic complexes containing bpy and the N heterocycles bpm (2,2'-bipyrimidine) and bpz (2,2'-bipyrazine), the bpm and bpz ligands offer external N–atom proton acceptor sites and lower  $\pi^*$  acceptor orbitals than bpy. The  $\pi^*$  energy ordering is bpz < bpm < bpy (Figure 17). In the one-electron reduced forms of the mixed ligand complexes, the electron is added to the ligand having the lowest  $\pi^*$  acceptor level.

In the series of nine possible homo- and heteroleptic complexes containing varying combinations of bpy, bpm, and bpz, those that contain at least one bpm or bpz ligand

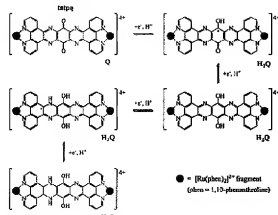


Figure 18. Stepwise photochemical  $e^-/H^+$  reduction of  $[(\text{phen})_2\text{Ru}(\text{tpy})\text{Ru}(\text{phen})]^{3+}$  in the presence of added  $\text{NEt}_3$ .<sup>205</sup>

act as proton acceptors in both the  $\text{I}^-$  reduced form and in the corresponding MLCT excited states. The electron is added to the ligand having the lowest  $\pi^*$  acceptor level.<sup>20,27</sup> Where it is observable, emission from the protonated excited states is significantly red-shifted compared to the deprotonated form with  $\Delta\lambda \sim 3000 \text{ cm}^{-1}$  for  $[\text{Ru}(\text{bpy})_3(\text{bpzH})]^{3+*}$ .<sup>21</sup> This is consistent with enhanced excited-state basicity with  $pK_a^* > pK_a$  since an electron is excited to a  $\pi^*(\text{bpy})$  or  $\pi^*(\text{bpz})$  level.<sup>270</sup> For example,  $pK_a^* = 4.4$  for  $[\text{Ru}^{3+}(\text{bpy})(\text{bpzH})]^{3+*}$  compared to  $pK_a < 0$  for the ground state of  $[\text{Ru}^{3+}(\text{bpy})(\text{bpzH})]^{3+}$ .<sup>272</sup> The once-reduced complexes are even stronger bases with  $pK_a = 9.2$  for  $[\text{Ru}^{3+}(\text{bpy})(\text{bpzH})]^+$ .

Protonation significantly increases the oxidizing power of the excited state with  $E^\circ = 1.44 \text{ V}$  (vs SCE) for the couple  $[\text{Ru}^{3+}(\text{bpy})(\text{bpzH})]^{3+*}/[\text{Ru}^{3+}(\text{bpy})(\text{bpzH})]^{2+}$  compared to  $E^\circ = 1.16 \text{ V}$  for  $[\text{Ru}^{3+}(\text{bpy})(\text{bpzH})]^{3+*}/[\text{Ru}^{3+}(\text{bpy})(\text{bpzH})]^+$ . The potential difference between the two can be calculated from the difference in excited- and ground-state  $pK_a$ 's by using eq 24.

MLCT excitation of the bridged complex  $[(\text{phen})_2\text{Ru}(\text{tpy})(\text{phen})]^{3+}$  in deaerated  $\text{CH}_3\text{CN}$  with added triethylamine ( $\text{NEt}_3$ ) results in reduction and protonation at the tpy bridging ligand (Figure 18). Continued photolysis results in stepwise  $4e^-$  reduction of the bridge.<sup>273</sup> The mechanism involves irreversible reductive MLCT quenching to give  $^{+*}\text{NEt}_3$  and the reduced complex, which undergoes proton loss and further oxidation.<sup>274</sup>

### 3. pH-Induced Redox Phenomena

#### 3.1. Introduction

PCET is induced by oxidation or reduction at single chemical sites or clusters. As shown by the example in eq 5 and application of the Nernst equation, changes in pH can cause electron transfer to occur by changing the equilibrium distribution of a pH-dependent reaction. A change in pH creates a driving force for molecular energy conversion or "transduction". Transduction, in this case, is induced by a change in pH and its effect on the equilibrium distribution between the components of a redox couple. In the example in eq 5, a change in pH above  $\text{pH} = 6.2$  results in a new equilibrium distribution which is reached by electron transfer,  $cis\text{-}[\text{Ru}^{3+}(\text{bpy})(\text{py})(\text{O})]^{2+} + [\text{Os}^{3+}(\text{bpy})]^{2+} + \text{H}^+ \rightarrow cis\text{-}[\text{Ru}^{3+}(\text{bpy})(\text{py})(\text{OH})]^{2+} + [\text{Os}^{3+}(\text{bpy})]^{3+}$ .



Figure 19. 4,4'-Bipy.

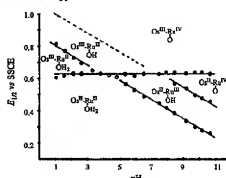


Figure 20.  $E_{1/2}$ -pH diagram for  $[(\text{tpy})(\text{bpy})\text{Os}^{3+}(4,4'\text{-bipy})\text{Ru}^{3+}]$  ( $\text{H}_2\text{O}$ ,  $I = 0.1 \text{ M}$ , vs SSCE). Oxidation state and proton compositions are indicated in those potential-pH domains where they are the dominant forms. The dashed line for the  $(\text{Os}^{3+})-\text{Ru}^{4+}/(\text{Os}^{3+})-\text{Ru}^{2+}$  couple was calculated by extrapolation.<sup>275</sup>

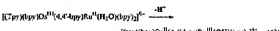
Reverse transduction occurs in biological membranes where local pH changes, induced by electron transfer, create a local pH gradient. The pH gradient drives long-range proton transfer and, in respiration, conversion of ADP to ATP.

#### 3.2. pH-Induced Electron Transfer, Energy Transfer, and Chemical Change

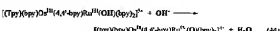
##### 3.2.1. pH-Induced Electron Transfer in Ligand-Bridged Complexes

The ligand-bridged complex  $[(\text{tpy})(\text{bpy})\text{Os}^{3+}(4,4'\text{-bipy})\text{Ru}^{3+}]$  contains both pH-dependent ( $\text{Ru}^{3+}-\text{OH}^{2+}/\text{Ru}^{3+}-\text{OH}^{2-}$ ) and pH-independent ( $\text{Os}^{3+}/\text{Os}^{2+}$ ) couples (Figure 19). In strongly acidic solution,  $1e^-$  oxidation gives the mixed-valence form  $[(\text{tpy})(\text{bpy})\text{Os}^{3+}(4,4'\text{-bipy})\text{Ru}^{3+}(\text{H}_2\text{O})-(4,4'\text{-bipy})\text{Ru}^{3+}(\text{H}_2\text{O})(\text{bpy})]^{3+}$ , loss of a second electron gives  $[(\text{tpy})(\text{bpy})\text{Os}^{3+}(4,4'\text{-bipy})\text{Ru}^{3+}(\text{H}_2\text{O})(\text{bpy})]^{2+}$ , and loss of a third gives  $[(\text{tpy})(\text{bpy})\text{Os}^{3+}(4,4'\text{-bipy})\text{Ru}^{3+}(\text{O})(\text{bpy})]^{3+}$ .

A potential-pH diagram for this complex is shown in Figure 20. In this complex, the pH-induced intramolecular electron transfer reaction in eq 43 was demonstrated by pH jump experiments.<sup>275</sup>



Similarly, the second pH-induced intramolecular electron transfer in eq 44 was demonstrated in the twice-oxidized complex,  $[(\text{tpy})(\text{bpy})\text{Os}^{3+}(4,4'\text{-bipy})\text{Ru}^{3+}(\text{OH})(\text{bpy})]^{3+}$ . Intramolecular electron transfer in this case forms  $\text{Ru}^{3+}=\text{O}$ , which has a significant impact on reactivity. A slight pH change results in a rate enhancement of  $\sim 1000$  in the oxidation of *isopropylbenzoate* anion to the corresponding ketone by the  $\text{Ru}^{3+}=\text{O}$  form.<sup>275</sup>



##### 3.2.2. pH-Induced Energy Transfer

Similarly, pH-induced, intramolecular energy transfer has been demonstrated in both  $[(\text{tpy})(\text{bpy})\text{Os}^{3+}(4,4'\text{-bipy})\text{Ru}^{3+}]$

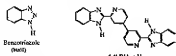
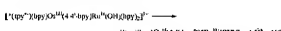


Figure 21. Benzotriazole and 2,2'-bis(benzimidazol-2-yl)-4,4'-bipyridine.

$(H_2O)(bpy)(Os^{II})^{4+}$  and its mixed-valence form, MLCT excitation of the  $Os^{(II)}-Ru^{(II)}$  complex at  $pH = 10$  is followed by rapid, efficient  $Ru^{III} \rightarrow Os^{II}$  energy transfer, eq 45. The sense of the energy transfer is reversed above  $pH = 10.3$ , eq 46.<sup>276</sup>



The mixed-valence form acts as a pH-dependent light switch. There is no emission from  $[(py)(bpy)Os^{III}(4,4'-bpy)^{3+}Ru^{(II)}(H_2O)(bpy)]^{4+}$  because of rapid nonradiative decay from the MLCT excited state  $[(py)(bpy)Os^{III}(4,4'-bpy)^{3+}Ru^{(II)}(H_2O)(bpy)]^{4+}$ . Excitation of  $[(py)(bpy)Os^{II}(4,4'-bpy)^{3+}Ru^{(II)}(H_2O)(bpy)]^{4+}$  leads to emission from the  $Os^{II}(py)^{4+}$  MLCT state.

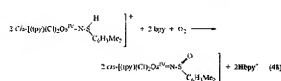
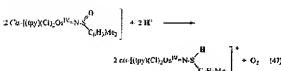
### 3.2.3. pH-Induced Changes in Electronic Coupling

Deprotonation of the mixed-valence complexes  $[(edta)Ru^{II}(OH)Ru^{II}(edta)]^{3-}$  (edta is ethylenediaminetetraacetate,  $\text{H}_2\text{edta}$  is benzotriazole) and  $[(\text{bipy})(\text{bbipy})_2]^{3+}$  because of rapid nonradiative decay from the MLCT excited state  $[(\text{bipy})(\text{bbipy})_2(4,4'-bpy)^{3+}Ru^{III}(H_2O)(bpy)]^{4+}$ . Excitation of  $[(\text{bipy})(\text{bbipy})_2(4,4'-bpy)^{3+}Ru^{III}(H_2O)(bpy)]^{4+}$  leads to emission from the  $Os^{II}(py)^{4+}$  MLCT state.

**3.2.3.1. pH-Induced Electronic Delocalization in Azurin.** In an engineered  $\text{Cu}_4$  center in azurin at  $pH = 7$  (Figure 22), EPR and UV-visible measurements point to a delocalized  $\text{Cu}^{1+}-\text{Cu}^{2+}$  core. Protonation causes changes in the absorption spectrum and a four-line EPR hyperfine spectrum, which are consistent with a trapped valence,  $\text{Cu}(\text{II})-\text{Cu}(\text{I})$ , core. Protonation occurs at the C-terminal histidine ligand (His-120), as shown by site-directed mutagenesis.<sup>278</sup>

### 3.2.4. Reversible $O_2$ Evolution from *cis*- $[\text{Os}^{IV}(\text{py})(\text{Cl})(\text{NS}(\text{O})(3,5-\text{Me}_2\text{C}_6\text{H}_3))]$

Oxidation of the sulfilimido complex *cis*- $[\text{Os}^{IV}(\text{py})(\text{Cl})_2(\text{NS}(\text{H})-3,5-\text{Me}_2\text{C}_6\text{H}_3)]^+$  by  $\text{Me}_2\text{N}^-\text{O}^-$  gives the corresponding sulfoximido complex *cis*- $[\text{Os}^{IV}(\text{py})(\text{Cl})(\text{NS}(\text{O})(3,5-\text{Me}_2\text{C}_6\text{H}_3))]$ . It is a pH-dependent  $O_2$  carrier undergoing rapid (less than millisecond) release of  $O_2$  upon addition of a strong acid by a reaction that is reversible upon addition of a base, eqs 47 and 48.<sup>279</sup>

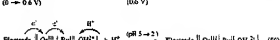


### 3.3. pH-Induced Redox Effects in Films

#### 3.3.1. Intra- and Interfilm Electron Transfer

The bilayer polymeric film structure, electrode II poly( $[\text{Os}^{(IV)}(\text{bpy})_2(\text{py})_2\text{PF}_6]_2$ )-nafion-*cis*- $[\text{Ru}^{(II)}(\text{bpy})(\text{py})(H_2\text{O})]^{2+}$  (bpy = 4-vinylpyridine, Figure 23), was prepared by reductive electropolymerization of the Os complex (section 2.7.1), followed by evaporative deposition of an outer film of Nafion and incorporation of *cis*- $[\text{Ru}^{(II)}(\text{bpy})(\text{py})(H_2\text{O})]^{2+}$  ( $\text{Ru}^{(II)}-\text{OH}^{2+}$ ) by ion exchange.

pH-induced electron transfer through the inner film was demonstrated by varying the pH in the external solution as illustrated in eqs 49–51.<sup>280</sup>



**Hydrolysis of the trimethoxysilane derivative  $[\text{BV-Q-BV}^{\bullet+}]$ .** (Figure 24) produces redox-active films on Pt by  $-\text{Si}-\text{O}-\text{Si}-$  cross-linking. The internal quinone/hydroquinone couple,  $\text{Q} + 2e^- + 2\text{H}^+ \rightarrow \text{H}_2\text{Q}$ , is mediated by the pH-independent  $\text{BV}^{\bullet+}/\text{BV}^{\bullet}$  couple; (1)  $\text{BV}^{\bullet+}-\text{Q}-\text{BV}^{\bullet+} + 2\text{e}^- \rightarrow \text{BV}^{\bullet+}-\text{Q}-\text{BV}^{\bullet+}$  followed by (2)  $\text{BV}^{\bullet+}-\text{H}_2\text{Q}-\text{BV}^{\bullet+}$ .<sup>281</sup>

#### 3.3.2. pH-Encapsulation\*

In films of the derivatized poly-4-vinylpyridine polymer in Figure 25 on glassy carbon electrodes, cyclic voltammetric

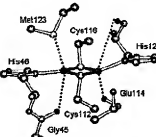


Figure 22. Structure of the  $\text{Cu}_4$  site in engineered  $\text{Cu}_4$  azurin showing the surrounding ligands: methionine (Met), histidine (His), glycine (Gly), and cysteine (Cys). Reprinted with permission from ref 278. Copyright 2004 National Academy of Sciences.

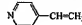


Figure 23. 4-vpy.

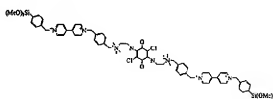


Figure 24.  $\text{BV}-\text{Q}-\text{BV}^{\bullet+}$ .

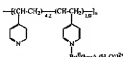


Figure 25. Derivatized poly-4-vinylpyridine polymer.



Figure 26. Nafion.

measurements as a function of pH revealed the presence of the expected pH-dependent  $\text{Ru}^{3+}-\text{OH}^{2+}/\text{Ru}^{2+}-\text{OH}_2^{2+}$  couple until the onset of the  $\rho K_a$  for the unbound pyridyl groups in the films ( $\text{pH} \sim 5$ ). Further increases in pH had no effect on  $E_{1/2}$ , which remained fixed at 0.63 V (vs SSCE). The effect is reversible, with the  $\text{Ru}(\text{II}/\text{III})$  wave reappearing when the pH of the external solution was decreased to 4.<sup>282</sup>

The loss of pH-dependence was described as a "pH encapsulation effect". When protonated, the interior of the film is impregnated with water and opened to the buffer components in the external solution. When deprotonated, the interior is nonpolar and water, and the buffer components are extruded.<sup>282</sup>

Related effects have been observed in thin films containing  $\text{cis}-[\text{Ru}^{3+}(\text{bpy})(\text{py})(\text{H}_2\text{O})]^2+$  or  $[\text{Ru}(\text{tpy})(\text{bpy})(\text{H}_2\text{O})]^2+$  ion-exchanged into Nafion (Figure 26) on glassy carbon electrodes.

The complexes partitioned into three different phases, only two of which were electroactive.  $E_{1/2}$  for a film-based  $\text{Ru}^{3+}-\text{OH}^{2+}/\text{Ru}^{2+}-\text{OH}_2^{2+}$  couple or couples decreased 59 mV/pH unit from  $\text{pH} = 1$  to 6. Past  $\text{pH} = 6$ , both pH-dependent and pH-independent waves appeared, the latter, at  $E_{1/2} = 0.56$  V (vs SSCE, 0.1 M  $\text{ClO}_4^-$ ), providing a second example of "pH encapsulation". Exchange among the three phases occurs on a time scale of seconds.<sup>283</sup>

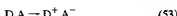
#### 4. Mechanistic Aspects of Proton-Coupled Electron Transfer

##### 4.1. Introduction

The examples in section 2 demonstrate a thermodynamic relationship between electron and proton transfer, and those in section 3 demonstrate that the relationship provides a basis for energy transduction. A second theme is mechanistic. How do PCET reactions occur? Are electrons and protons transferred singly or in concert? For concerted electron-proton transfer (EPT), what are the microscopic details defining reaction barriers and rates? A theoretical basis for understanding EPT is available from electron transfer theory, and it provides a useful starting point.

##### 4.2. Electron Transfer

For the generic intramolecular electron transfer reaction in eq 52 or electron transfer within an association complex of reactants in eq 53, the rate constant,  $k_{\text{ET}}$ , is given in the classical limit by eq 54. A barrier to electron transfer exists arising from changes in intramolecular structure at the electron transfer donor (D) and acceptor (A) and from reorientation of solvent molecules in the surrounding medium.



$$k_{\text{ET}} = \nu_{\text{ET}} (4\pi\lambda RT)^{-1/2} \exp - \left[ \frac{(\Delta G_{\text{ET}}^{\circ} + \lambda)^2}{4\lambda RT} \right] \quad (54)$$

In eq 54,  $\nu_{\text{ET}}$  is the frequency factor for electron transfer, and  $\lambda$  is the total reorganization energy. It is the sum of intramolecular,  $\lambda_{\text{in}}$ , and solvent,  $\lambda_{\text{so}}$ , reorganization energies; see eq 55. They include contributions from both reactants and are related to the reorganization energies for the  $\text{D}^{+0}$ ,  $\lambda_{\text{D}}$ , and  $\text{A}^{0-}$ ,  $\lambda_{\text{A}}$ , self-exchange reactions by eq 56.<sup>14,284-285</sup>

$$\lambda = \lambda_{\text{in}} + \lambda_{\text{so}} \quad (55)$$

$$\lambda_{\text{in}} = (\lambda_{\text{in},\text{A}} + \lambda_{\text{in},\text{D}})/2 \quad \text{and} \quad \lambda_{\text{so}} = (\lambda_{\text{so},\text{A}} + \lambda_{\text{so},\text{D}})/2 \quad (56)$$

$\Delta G_{\text{ET}}$  is the free energy change for the electron transfer step. Bimolecular electron transfer is a three-step process with preliminary association of the reactants, eqs 57–59. In this case,  $\Delta G_{\text{ET}}$  is the free energy change for electron transfer within the association complex. It is related to the overall  $\Delta G$  change in the prevailing medium,  $\Delta G^{\circ}$ , as shown in eq 60.



$$\Delta G_{\text{ET}} \approx \Delta G_c = \Delta G^{\circ} - (\Delta G_{\text{app}}^{\circ} - \Delta G_{\text{app}}^{\circ}) = \Delta G^{\circ} + \Delta \Delta G_{\text{app}}^{\circ} \quad (60)$$

As defined by Krishnalik, the quantity  $\Delta G_c$  in eq 60 is the free energy change between reactants and products in appropriate configurations (internuclear separation, relative orientations, ...) for electron transfer to occur (section 5.5.4).<sup>296–298</sup> For bimolecular electron transfer,  $\Delta G_{\text{ET}} \approx \Delta G_c$ . In eq 60,  $\Delta G_{\text{app}}^{\circ}$  and  $\Delta G_{\text{app}}^{\circ}$  are the free energy changes for forming the reactants and products in appropriate configurations for electron transfer with  $\Delta \Delta G_{\text{app}}^{\circ} = \Delta G_{\text{app}}^{\circ} - \Delta G_{\text{app}}^{\circ}$ . For charged reactants, the  $\Delta G_{\text{app}}^{\circ}$  terms include an electrostatic part, the "work" terms, for formation of the electron transfer precursor and successor complexes; note eq 77, below.<sup>287–289,294–295</sup>

##### 4.2.1. Reorganization Energies

In the limit that D and A in eqs 57–59 can be treated as non-interpenetrating spheres and the solvent as a dielectric electric continuum,  $\lambda_{\text{so}}$  is given by eq 61. In this equation,

$$\lambda = \epsilon \left( \frac{1}{2a_1} + \frac{1}{2a_2} - \frac{1}{d} \right) \left( \frac{1}{D_{\text{so}}} - \frac{1}{D_s} \right) \quad (61)$$

$D_{\text{so}}$  and  $D_s$  are the optical and static dielectric constants of the medium,  $a_1$  and  $a_2$  are the radii of D and A,  $d$  is the internuclear separation distance between D and A, and  $\epsilon$  is the unit electron charge. More accurate representations of the actual molecular geometry have been derived based on ellipsoidal cavities<sup>284,299</sup> and, more generally, by using a frequency-resolved cavity model (note refs 327, 328). Molecular-level solvent effects have been introduced by

separating  $\lambda_0$  into components arising from orientational fluctuations of solvent dipoles and density fluctuations.<sup>309–311</sup>

The effect of solvent on electron transfer has been investigated in detail both experimentally and theoretically.<sup>285,286,288–292,294,295,300–311</sup> Electronic delocalization along the electron transfer axis can greatly decrease the effective electron transfer distance compared to the molecular internuclear separation distance.<sup>312–314</sup>

There is experimental evidence for noncontinuum effects with  $\text{H}_2\text{O}/\text{D}_2\text{O}$  kinetic isotope effects as high as 1.5–2 observed for outer-sphere electron transfer and for electron transfer at electrodes.<sup>315,316</sup> Nonradiative decay of the MLCT excited state(s) of  $[\text{Ru}(\text{bpy})_3]^{2+}$  and related polyphenyl complexes of  $\text{Os}(\text{II})$  occurs with  $k(\text{H}_2\text{O})/k(\text{D}_2\text{O}) \sim 2.7$ .<sup>318</sup>

In these cases, there is no basis for specific interactions with the solvent and the isotope effects necessarily arise from quantum effects since there is no significant difference in dielectric properties between  $\text{H}_2\text{O}$  and  $\text{D}_2\text{O}$  until the onset of a series of water cluster librations at  $\sim 450 \text{ cm}^{-1}$ . Isotope effects may arise by coupling of electron transfer to water librations or  $\nu(\text{O}-\text{H})$  modes. The magnitudes of these effects are important since kinetic isotope effects of the same magnitude have been cited as evidence for multiple-site EPT mechanisms with the solvent acting as proton acceptor or proton donor (section 5.5).

$\lambda_i$  is given by a sum over coupled normal modes,  $j$ , in eq 62. Vibrational coupling to electron transfer occurs if there is a change in equilibrium structure and associated equilibrium displacement ( $\Delta Q_{ej} \neq 0$ ) between reactants,  $\text{D}^+ \text{A}$  or  $\text{D}, \text{A}$ , and products,  $\text{D}^+ \text{A}^-$  or  $\text{D}^+, \text{A}^-$ . In eq 62,  $f_j$  is the force constant for mode  $j$ .  $S_j$  is the electron-vibration coupling constant or Huang–Rhys factor, and  $\hbar\omega_j$  ( $=\hbar\nu_j$ ) is the vibrational quantum spacing.  $S_j$  is related to  $\Delta Q_{ej}$  as shown in eq 63 with  $M_j$  the reduced mass. Equation 62 assumes equal vibrational spacings (and force constants) for mode  $j$  in the reactants and products.

$$\lambda_i = \sum_j \frac{1}{2} f_j (\Delta Q_{ej})^2 = \sum_j S_j \hbar \omega_j \quad (62)$$

$$S_j = \frac{1}{2} (M_j \omega_j / \hbar) (\Delta Q_{ej})^2 \quad (63)$$

#### 4.2.2. Barrier Crossing

In the limit of weak electronic coupling, the dynamics of barrier crossing are controlled by slow electron tunneling, the nonadiabatic limit. In this limit,  $\nu_{\text{ET}} = \nu_c$  with  $\nu_c$  the electron tunneling frequency, defined in eq 64, which comes from time-dependent perturbation theory.  $H_{\text{b}}$  (or  $H_{\text{b}}^*$  or  $V_{\text{ET}}$ ) is the electron transfer matrix element, eq 65. It is the interaction energy arising from donor ( $\psi_D$ ) acceptor ( $\psi_A$ ) electronic wave function mixing. Mixing of the wave functions is induced by the electrostatic perturbation between  $\text{D}$  and  $\text{A}$  as represented by operator  $H$  in eq 65.

$$\nu_{\text{ET}} = \nu_c = \frac{2\pi}{\hbar} H_{\text{DA}}^2 \quad (64)$$

$$H_{\text{DA}} = \langle \psi_A | H | \psi_D \rangle \quad (65)$$

In the “adiabatic” limit, electronic coupling is sufficient (approximately tens of  $\text{cm}^{-1}$  or greater) that the transferring electron is always in equilibrium with the nuclear motions that create the electron transfer barrier. In this limit,  $\nu_{\text{ET}}$  is dictated by the dynamics of the slowest nuclear motion or

motions coupled to the interconversion between initial and final states and barrier crossing. These are typically collective solvent dipole reorientations, eq 66.<sup>119–221</sup> In the intermediate regime,  $\nu_{\text{ET}}$  is given by the kinetic average, eq 67.

$$\nu_{\text{ET}} = \nu_n \quad (66)$$

$$\nu_{\text{ET}}^{-1} = (\nu_c^{-1} + \nu_n^{-1}) \quad (67)$$

#### 4.2.3. Including Quantum Modes

The classical approximation is inappropriate for high- and medium-frequency vibrations with  $\hbar\nu = \hbar\omega \gg k_B T$ , and they must be treated quantum mechanically. For a single coupled mode or averaged mode with  $\hbar\omega \gg k_B T$ , only the  $v = 0$  level is significantly populated, and  $k_{\text{ET}}$  is given by eqs 68 and 69. These equations also assume that there is no change in frequency between reactants and products with  $\omega = \omega'$ .<sup>285,287–292,294,295,322–326</sup>

$$k_{\text{ET}} = \nu_{\text{ET}} \sum_{\nu'} \langle \chi(\nu') | \chi(\nu=0) \rangle^2 (4\pi R T \lambda_{\text{a,L}})^{1/2} \exp - \left[ \frac{(\Delta G_{\text{ET}} + \nu' \hbar \omega + \lambda_{\text{a,L}} \nu')^2}{4 \lambda_{\text{a,L}} R T} \right] \quad (68)$$

$$k_{\text{ET}} = \sum_{\nu'} k_{\text{ET},\nu'} \quad (69)$$

$$\langle \chi(\nu') | \chi(\nu=0) \rangle^2 = \exp - (S) \left( \frac{\sum_i}{\nu'!} \right) \quad (70)$$

$k_{\text{ET}}$  is a sum of  $k$ 's for separate vibrational channels starting with the  $v = 0$  level in  $\text{D}-\text{A}$  or  $\text{D}, \text{A}$  and ending up in the  $\nu'$  in  $\text{D}^+ \text{A}^-$  or  $\text{D}^+, \text{A}^-$ . For each channel,  $k_{\text{ET},\nu'}$  is a product of three terms: (1)  $\nu_{\text{ET}}$ , (2) the square of the vibrational overlap integral,  $\langle \chi(\nu') | \chi(\nu=0) \rangle^2$ , and (3) a classical exponential barrier crossing term. The latter gives the Boltzmann population of  $\text{D}-\text{A}$  or  $\text{D}, \text{A}$  pairs in the ensemble that have the free energy content and distribution among coupled vibrational and solvent modes required for electron transfer to occur with energy conservation. In the classical limit, this occurs at the top of the barrier where the energy-coordinate curves for reactants and products intersect.

The vibrational overlap integral gives the extent to which the initial and final states coincide along normal coordinate  $Q$ . It is the quantum equivalent of the intersection between energy curves in a classical barrier crossing. Its origin is the probabilistic uncertainty in spatial coordinates for particles at the quantum level. For a harmonic oscillator with no change in frequency between the initial and final states,  $\omega = \omega'$ , and the vibrational overlap integral is given by eq 70.

Coupled low-frequency modes are included in eq 68 through  $\lambda_{\text{a,L}}$  which is defined in eq 71.<sup>294</sup>

$$\lambda_{\text{a,L}} = \lambda_0 + \lambda_{\text{a,L}} \quad (71)$$

$\lambda_{\text{a,L}}$  is defined in eq 72. It is the reorganization energy contributed by low-frequency modes treated classically. The summation is over the coupled vibrations; note eq 62.

$$\lambda_{\text{a,L}} = \sum_i S_i \hbar \omega_i \quad (72)$$

For the more general case of a single coupled high-frequency mode or average mode with contributions from

levels above  $\nu = 0$  in the reactants, the expression for  $k_{\text{ET}}$  is given by eq 73.

$$k_{\text{ET}} = \nu_{\text{ET}} \sum_{\nu} \rho(\nu) \sum_{\nu'} \langle \chi(\nu') | \chi(\nu=0) \rangle^2 (4\pi RT \lambda_{\text{a},\nu})^{1/2} \times \exp \left[ -\frac{(\Delta G_{\text{ET}} + (\nu' - \nu)\hbar\omega + \lambda_{\text{a},\nu})^2}{4\lambda_{\text{a},\nu} RT} \right] \quad (73)$$

$$\Delta G_{\text{ET}}(\nu, \nu') = \Delta G_{\text{ET}} + (\nu' - \nu)\hbar\omega \quad (74)$$

In eq 73, the  $\rho(\nu)$  values are Boltzmann populations in level  $\nu$ ,  $\Delta G_{\text{ET}}(\nu, \nu')$  in eq 74 is the free energy change for the  $\nu \rightarrow \nu'$  vibrational channel. The expression for  $k_{\text{ET}}$  in eq 73 can be generalized to include multiple coupled modes and changes in frequency.<sup>32,33</sup>

As discussed in section 3, the result in eq 73 is of direct relevance to coupled electron–proton transfer (EPT). The same microscopic factors influencing reaction dynamics—intramolecular structural change, solvent coupling, electronic interactions, and coupling of quantum modes—are at play in each

#### 4.2.4. Bimolecular Reactions

For bimolecular reactions that occur well below the diffusion-controlled limit, the scheme in eqs 57–59 applies. As shown in eq 75, the experimental rate constant,  $k_{\text{obs}}$ , is given by the product of  $k_{\text{ET}}$  and a preassociation constant,  $K_{\text{A}}$ . As defined in eq 76,  $K_{\text{A}}$  is determined by the internuclear separation distance,  $d$ , Avogadro's number,  $N_{\text{A}}$ , and an electrostatic energy of association if the reactants are charged,  $w$ . From the Eigen–Fouss equation for spherical ions in a dielectric continuum,  $w$  is given by eq 77 with  $Z_1$  and  $Z_2$  the ion charges,  $e$  the unit electron charge,  $D_0$  the static dielectric constant of the medium,  $I$  the ionic strength, and  $\beta$  the Debye length ( $8\pi N_A e^2 / 1000 D_0 RT$ ).<sup>34–36,299,313–312</sup>

$$k_{\text{obs}} = K_{\text{A}} k_{\text{ET}} \quad (75)$$

$$K_{\text{A}} = \frac{4\pi N_A d^3}{3000} \exp \left( -\frac{w}{RT} \right) \quad (76)$$

$$w = \frac{Z_1 Z_2 e^2}{4D} \left( \frac{1}{1 + \beta d^{1/2}} \right) \quad (77)$$

More generally, electron transfer can occur over a range of separation distances and favored orientations that maximize electronic orbital overlap. In more complete analyses,  $K_{\text{A}}$  is replaced by an integral over a range of separations and relative orientations.<sup>367,284,296,297</sup> This is important in EPT, where a preformed H-bond or related interaction is required given the short-range nature of proton transfer (section 5.3).

In the generalized electron transfer mechanism in eqs 57–59,  $\Delta G_{\text{ET}}$  is determined by  $\Delta G^{\text{o}}$  and the association constants for the reactants,  $D + A \rightleftharpoons K_{\text{A}}$  ( $K_{\text{A}}$ ), and products,  $D^+ + A^- \rightleftharpoons D^+ A^-$  ( $K'_{\text{A}}$ ), with the three related as in eq 78. As mentioned above,  $\Delta G_{\text{ET}} \approx \Delta G_{\text{sp}}$  and  $\Delta G_{\text{sp}}$  the configurational free energy change. Also,  $K_{\text{A}} \approx \exp[-\Delta G_{\text{sp}}/RT]$  and  $K'_{\text{A}} \approx \exp[-\Delta G'_{\text{sp}}/RT]$  in eq 60.<sup>296–298</sup>

$$\Delta G_{\text{ET}} = \Delta G^{\text{o}} + RT \ln(K_{\text{A}}/K'_{\text{A}}) \quad (78)$$

Near the diffusion-controlled limit,  $10^9–10^{11} \text{ M}^{-1} \text{ s}^{-1}$  in water and polar organic solvents, rate constants for diffusion ( $k_{\text{D}}$ ) and electron transfer ( $k_{\text{ET}} K_{\text{A}}$ ) are comparable and kinetically coupled. They are related to the observed rate constant,  $k_{\text{obs}}$ , by eq 79.

$$\frac{1}{k_{\text{obs}}} = \frac{1}{k_{\text{D}}} + \frac{1}{k_{\text{ET}} K_{\text{A}}} \quad (79)$$

The classical electron transfer barrier expression in eq 54 can be expanded as shown in eqs 80 and 81, which neglects differences between  $K_{\text{A}}$  and  $K'_{\text{A}}$  and assumes corrections that can be made for diffusion, if needed, by using eq 79.

The expressions in eqs 80 and 81 account for the free-energy-dependence of  $k_{\text{ET}}$  in a closely related series of reactions where  $\Delta G^{\text{o}}$  is varied by varying the reactants.  $k_{\text{ET}}(0)$  is the rate constant for a hypothetical reaction in the series with  $\Delta G^{\text{o}} = 0$ . The behavior predicted by eqs 80 and 81 has been experimentally observed.<sup>330</sup> Based on these equations, when  $\lambda \gg \Delta G^{\text{o}}$ , the  $\Delta G^{\text{o}}/\lambda$  term is negligible and  $RT/k_{\text{ET}}$  is predicted to increase as  $-\Delta G^{\text{o}}/2$ .

$$k_{\text{ET}} = \nu_{\text{ET}} K_{\text{A}} (4\pi RT \lambda)^{-1/2} \exp \left[ -\frac{1}{4RT} \left( \lambda + 2\Delta G^{\text{o}} + \frac{\Delta G^{\text{o}}^2}{\lambda} \right) \right] \quad (80)$$

$$\ln k_{\text{ET}} = \ln k_{\text{ET}}(0) - \frac{\Delta G^{\text{o}}}{2RT} \left( 1 + \frac{\Delta G^{\text{o}}}{2\lambda} \right) \quad (81)$$

#### 4.2.5. Cross Reactions

From Marcus theory, it is possible to relate the rate constant for an outer-sphere electron transfer reaction,  $D + A^- \rightarrow D^+ + A$ ,  $k_{12}$ , to the free energy change,  $\Delta G_{12} = \Delta G^{\text{o}} - RT \ln K_{12}$ , and rate constants for the associated self-exchange reactions ( $k_{11}$  for  $D^+D$  and  $k_{22}$  for  $A^-A$ ). In the relationship in eq 82, the quantity  $f$  is defined in eq 83. Depending on time scale, self-exchange rate constants are typically measured by isotopic labeling or by NMR or EPR line broadening. Equation 82 follows from eq 54, assuming that  $\lambda_{12} = \lambda_{11} + \lambda_{22}$  and  $(\nu_{\text{ET},11} K_{\text{A},12}) - (\nu_{\text{ET},11} K_{\text{A},11}) (\nu_{\text{ET},22} K_{\text{A},22})^{1/2}$ , with the term  $(4\pi RT)^{1/2}$  included in  $\nu_{\text{ET},11}$  and  $\nu_{\text{ET},22}$ . For reactants and products of different charge types or with a significant mismatch in size, an electrostatics correction factor must be applied to eq 82.<sup>237,291–295</sup>

$$k_{12} = (k_{11} k_{22} K_{12})^{1/2} \quad (82)$$

$$\ln f = \frac{(\ln K_{12})^2}{\left( \frac{4 \ln(k_{11} k_{22})}{(\nu_{\text{ET},11} K_{\text{A},11}) (\nu_{\text{ET},22} K_{\text{A},22})} \right)} \quad (83)$$

Equation 82 was derived for outer-sphere electron transfer in the nonadiabatic limit. It has been successfully used to correlate electron transfer rate constants and to calculate quantities ( $k, \lambda$ ) for reactions for which experimental data are lacking. Although there is no direct theoretical justification for its application in such cases, it has also been found to correlate data involving bond rupture and formation,<sup>314–317</sup> hydride transfer,<sup>318</sup> proton transfer,<sup>292,339</sup> and H-atom transfer.<sup>340</sup>

### 4.3. PCET: Energetics and Mechanisms

#### 4.3.1. Stepwise Mechanisms

In the absence of coupled electron–proton transfer (EPT), PCET reactions occur by stepwise mechanisms: electron

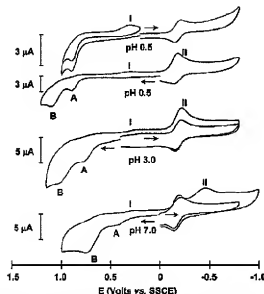


Figure 27. pH-dependent cyclic voltammograms for  $\text{trans-}[\text{Os}^{\text{IV}}(\text{py})\text{Cl}_2(\text{NH}_3)]^+$  in water,  $\text{I} = 0.1 \text{ M}$ , vs SSCE at  $100 \text{ mV/s}$ . Scan directions are indicated and waves labeled for the oxidation of  $\text{Os}^{\text{III}}$  to  $\text{Os}^{\text{V}}$  (A), for the oxidation of  $\text{Os}^{\text{V}}$  to  $\text{Os}^{\text{VI}}$  (B), and for reductions of an intermediate (I) and of  $\text{Os}^{\text{VI}}$  (II). The  $\text{Os}^{\text{IV}/\text{VI}}$  couple appears at  $E_{1/2} = -0.18 \text{ V}$ , taken from ref 134.

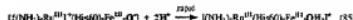
transfer followed by proton transfer, ET-PT, or proton transfer followed by electron transfer, PT-ET. For PCET, these mechanisms can impose high reaction barriers and low rates.<sup>32,34,342</sup> This includes electrochemical reactions at inert electrodes where the only available mechanisms are ET-PT or vice versa. Slow electron or proton transfer can cause irreversible electrochemistry, and complicated, pH-dependent current-potential waveforms.<sup>5,42,43,63,64</sup>

An example is the chemically reversible,  $3\text{e}^-/3\text{H}^+$  oxidation of  $[\text{Os}^{\text{IV}}(\text{tpy})(\text{Cl})(\text{NH}_3)]^+$  to  $[\text{Os}^{\text{V}}(\text{tpy})(\text{Cl})_2(\text{NH}_3)]^+$  in eq 31 (section 2.3.2). That the reaction is mechanistically complex is shown by the pH-dependent cyclic voltammograms of  $\text{trans-}[\text{Os}^{\text{IV}}(\text{tpy})(\text{Cl})_2(\text{NH}_3)]^+$  in Figure 27.<sup>134,139</sup>

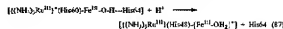
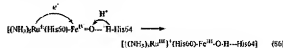
A qualitative mechanistic analysis of the data pointed to the importance of slow N-H transfer. It was suggested that rate-limiting proton transfer occurs from  $\text{trans-}[\text{Os}^{\text{IV}}(\text{tpy})(\text{Cl})_2(\text{NH}_3)]^+$  to  $\text{OH}^-$  (not  $\text{H}_2\text{O}$ ) followed by rapid oxidation to  $[\text{Os}^{\text{V}}(\text{tpy})(\text{Cl})_2(\text{NH}_3)]^+$ . Similarly, rate-limiting loss of  $2\text{H}^+$  to  $2\text{OH}^-$  is followed by rapid oxidation of  $[\text{Os}^{\text{V}}(\text{tpy})(\text{Cl})_2(\text{NH}_3)]^+$  to  $\text{Os}^{\text{VI}}$ . The possible intervention of MS-EPT pathways, as elucidated by Saveant and co-workers for other electrochemical reactions (section 6.5.3), was not considered in the analysis.

Another example, relevant to electron-proton coupling in biological reactions, occurs in the slow reduction of the oxyferryl heme site in cytochrome *c* peroxidase (CCP) by  $[\text{Ru}^{\text{II}}(\text{NH}_3)_6]^{2+}$  bound to His-60 (histidine-60). Slow electron transfer was attributed to a large reorganization energy at the oxyferryl heme.<sup>343</sup> A more likely explanation is that 1*c*-reduction of the ferryl,  $\text{Fe}^{\text{IV}}=\text{O} + \text{e}^- \rightarrow \text{Fe}^{\text{III}}-\text{O}^-$  (eq 84), is energetically unfavorable, much as reduction of  $\text{cis-}[\text{Ru}^{\text{IV}}(\text{tpy})(\text{py})\text{O}]^{2+}$  in eq 6.

Reduction of the oxyferryl heme site of horse heart myoglobin (HfMb) by  $[\text{Ru}^{\text{II}}(\text{NH}_3)_6]^{2+}$  attached to surface His48, 12.7 Å from the heme, was found to be pH-dependent



from pH = 5.8 to 7.<sup>344,345</sup> The pH-dependence is consistent with activation by protonation at distal His64 ( $\text{pK}_a \sim 6$ ). This group lies near the heme pocket and  $\text{Fe}^{\text{IV}}=\text{O}$ . This reaction may occur by MS-EPT (eq 86) followed by proton transfer, thus avoiding  $\text{Fe}^{\text{III}}-\text{O}^-$ .



The importance of H-bonding to an oxo ligand prior to electron transfer has been noted for horseradish peroxidase compound II (HRP-II),<sup>346–349</sup> the distal arginine of HRP,<sup>349–351</sup> cytochrome *c* peroxidase,<sup>352</sup> and other heme peroxidases.<sup>353–355</sup>

#### 4.4. Coupled Electron–Proton Transfer (EPT). Competition between Stepwise and EPT Mechanisms

As noted in sections 1.1 and 2.1.2, EPT is microscopically more complex than either ET or PT but can have a significant advantage in avoiding high-energy intermediates. This is illustrated in Figure 28 for the coproportionation reaction between *cis*- $[\text{Ru}^{\text{II}}(\text{bpy})_2(\text{py})(\text{O})]^{2+}$  and *cis*- $[\text{Ru}^{\text{II}}(\text{bpy})_2(\text{py})(\text{H}_2\text{O})]^{2+}$  in eq 10.<sup>7,9</sup> It compares energetics (at pH = 7) for (a) ET-PT, (b) PT-ET, and (c) EPT.<sup>356</sup>

Neither pathway (a) or (b) contributes significantly to the overall reaction in this case. This is shown by  $\Delta G^\circ$  values for initial PT or ET,  $>0.55$  and  $>0.59 \text{ eV}$ , that are in excess of the experimental free energy of activation,  $\Delta G^\ddagger = 0.44 \text{ eV}$  (Figure 28). Both involve initial formation of high-energy intermediates at the prevailing pH:  $\text{Ru}^{\text{III}}-\text{O}^- + \text{Ru}^{\text{II}}-\text{OH}_2^+$  or  $\text{Ru}^{\text{II}}-\text{OH}_2^+ + \text{Ru}^{\text{II}}-\text{O}^-$ . Although more complex, EPT in pathway (c) occurs at  $\Delta G^\ddagger$  for the net PCET reaction.

In other reactions, there can be a complex interplay among the three available mechanisms. The example of oxidation of tyrosine by  $[\text{Os}^{\text{IV}}(\text{bpy})]^{4+}$  is discussed in section 5.5.4.3.

An example of EPT of a different kind appears in the self-exchange reaction between  $\text{Fe}(\text{I})$  and  $\text{Fe}(\text{II})$  bi-imidazole complexes in eq 88 studied by Mayer and co-workers by <sup>1</sup>H NMR line broadening.<sup>357</sup> As illustrated in eq 89, proton transfer occurs between imidazole N-atoms which are ligand-based, and electron transfer occurs between dx orbitals that are mixed with ligand orbitals but largely dx( $\text{Fe}(\text{III})$ ) and dx( $\text{Fe}(\text{II})$ ) in character.

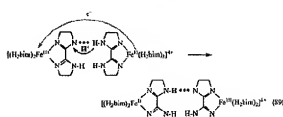
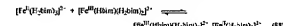




**Figure 28.** Thermodynamics of three PCET pathways for the disproportionation reaction in eq 10 at 25 °C and pH = 7, I = 0.1 M: (a) electron transfer followed by proton transfer (ET-PT); (b) proton transfer followed by electron transfer (PT-ET); and (c) coupled electron-proton transfer (EPT);  $\Delta G^\circ$  is the free energy of activation.<sup>39</sup>

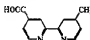


**Figure 29.** 4-CO<sub>2</sub>H-4'-MeBpy.

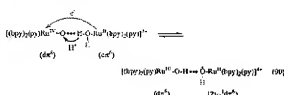
In a third example, quenching of  ${}^3\text{C}_{60}$  by phenols is enhanced by added pyridines with MS-EPT implicated as the pathway, eqs 13–15.<sup>34,38b</sup> With tyrosine ( $\text{TyrOH}$ ) as the phenol, EPT would be favored over ET,  ${}^3\text{C}_{60} + \text{TyrOH} \rightarrow {}^3\text{C}_{60} + \text{TyrOH}^{+*}$ , by  $\sim -0.4$  eV ( $\sim -9$  kcal/mol). This is due to the decrease in  $E^\circ$  from 1.34 V (vs NHE) for the  $\text{TyrOH}^{+*}$  couple to  $\sim 0.9$  V for the  $\text{TyrO}^{+*}\text{H}\text{-py}^*/\text{TyrO}\text{-py}$  couple (section 5.4.1).

## 5. Defining Electron–Proton Transfer

### 5.1. Electron–Proton Transfer (EPT)

Although pathways involving EPT may be preferred on energetic grounds, there are specific orbital requirements.

(1) *Electrons and protons transfer from different orbitals on the donor to different orbitals on the acceptor:* In H-atom transfer (HAT), both the transferring electron and proton come from the same bond. The distinction is not semantic. If disproportionation between *cis*-[Ru<sup>II</sup>(bpy)<sub>2</sub>(py)(H<sub>2</sub>O)]<sup>2+</sup> and *cis*-[Ru<sup>II</sup>(bpy)<sub>2</sub>(py)(H<sub>2</sub>O)]<sup>2+</sup> in eq 10 occurred by HAT rather than EPT, the immediate product would be a hydroxyl radical bound to Ru(II) rather than OH<sup>−</sup> bound to Ru(III), eq 90. It is at higher energy by  $> 2.1$  eV and not a viable intermediate for the thermal process.



(2) *The  $e^-/\text{H}^+$  donor orbitals and  $e^-/\text{H}^+$  acceptor orbitals interact electronically, enabling simultaneous  $e^-/\text{H}^+$  transfer:* In the reaction between  $[\text{Os}^{II}(\text{bpy})_4(4\text{-CO}_2\text{H-4'}\text{-MeBpy})]^{2+}$  and *cis*-[Ru<sup>II</sup>(bpy)<sub>2</sub>(py)]<sup>2+</sup>, there is no evidence for the EPT pathway,  $[\text{cis-}(\text{bpy})_2\text{Ru}^{2+}\text{O}^{2-}\text{H}^{+} \rightarrow [\text{cis-}(\text{bpy})_2\text{Ru}^{2+}\text{O}^{2-}\text{H}^{+}\text{O-C}(=\text{O})\text{MeBpy}]^{2+}]^{+}$   $\rightarrow [\text{cis-}(\text{bpy})_2\text{Ru}^{2+}\text{O}^{2-}\text{H}^{+}\text{O-C}(=\text{O})\text{MeBpy}]^{2+}$ .  $4\text{-CO}_2\text{H-4'}\text{-MeBpy}$  is shown in Figure 29. This is apparently a consequence of weak

electronic coupling between the spatially separated electron,  $\text{d}_{\text{Os}(II)}$ , and proton donor orbitals,  $\sigma_{\text{O}-\text{H}}(\text{COOH})^3$ .

(3) *As used here, simultaneous means rapid relative to the periods for coupled vibrations ( $\sim 100$  fs) and solvent modes ( $\sim 1$  ps):*<sup>19–33,35</sup> The intimate details of the coupled electron–proton transfer remain to be explored experimentally but are discussed theoretically in section 3.3.1.2. With the definition in (3), there is no discrete ET or PT intermediate equilibrated with its surroundings. If there were, the underlying thermodynamics would be those of the intermediate and not those of EPT. In the coupled electron–proton transfer step, the latter is typically the slow part with the electron coordinate always at equilibrium with the transferring proton.

### 5.1.1. Multiple Site Electron–Proton Transfer (MS-EPT)

In MS-EPT: (1) An electron–proton donor transfers electrons and protons to different acceptors or (2) an electron–proton acceptor accepts electrons and protons from different donors. Evidence for MS-EPT has been cited in the reduction of  ${}^3\text{C}_{60}$  by phenols in eqs 13–15 and possibly in the reduction of a ferryl ( $\text{Fe}^{IV}=\text{O}$ ) by appended  $-\text{Ru}^{\text{II}}(\text{NH}_3)^2$  in eq 86. The utilization of MS-EPT pathways appears to be common in biological PCET (section 7), where structural motifs have evolved and exploit long-range electron transfer with careful attention paid to the short-range nature of proton transfer (sections 5.3 and 7).

A variety of MS-EPT pathways is possible depending on the combination of protons and electrons that are transferred in concert. Possible examples are cited in the following sections of (1)  $\text{t}^{\bullet-}\text{H}^+$  MS-EPT, as in the oxidation of tyrosine  $\text{Y}_2$  by  $\text{P}_{\text{Sb}}^{\text{III}}$  in section 7.2.2, (2)  $2\text{e}^-/\text{H}^+$  MS-EPT, as in the activation of cytochrome *c* peroxidase in section 7.2.3, (3)  $1\text{e}^-/\text{H}^+$  MS-EPT in long-range PCET in oligonucleotides (section 6.4.4) and in the activation of the oxygen evolving complex in Photosystem II, (4) internal  $1\text{e}^-/\text{H}^+$  MS-EPT with intramolecular proton transfer accompanying ET (section 6.4.2), and (5) solvent-assisted  $\text{t}^{\bullet-}\text{H}^+$  MS-EPT with the solvent acting as the proton donor or acceptor (section 5.3.3).

### 5.2. Related Pathways

There are other concerted pathways for simultaneous electron–proton transfer which differs from EPT either in what is transferred or in the orbitals involved in the transfer.

#### 5.2.1. H-Atom Transfer (HAT)

In HAT, both electrons and protons are transferred from the same chemical bond. This is a characteristic reaction for hydrocarbons in which a C–H bond is the HOMO.<sup>36,37</sup> Illustrative examples that distinguish between EPT and HAT have come from the results of a DFT theoretical study on degenerate hydrogen self-exchange between benzyl radical/toluene and phenoxyl radical/phenol self-exchange. In the former,  $\text{PhCH}_2 + \text{PhCH}_3 \rightarrow \text{PhCH}_3 + \text{PhCH}_2$ , the  $2\text{p}_z$  acceptor orbital on the benzyl radical approaches along a C–H bond. In  $\text{PhO}^+ + \text{PhOH} \rightarrow \text{PhOH} + \text{PhO}^+$ , electron transfer occurs from a  $\pi$  orbital on phenol to a  $\pi$  orbital on phenoxyl radical. Proton transfer occurs within a H-bond between a  $\sigma$  lone pair on phenoxyl radical and  $\sigma_{\text{O}-\text{H}}$  of phenol. The key difference is the use of low lying  $\pi$  redox orbitals on the phenoxyl/phenol pair.<sup>32</sup>

A distinction can be made between EPT and HAT in many cases, with significant energy differences between the

different orbital pathways. The two have been compared theoretically by both Cukier<sup>163</sup> and Hammes-Schiffer.<sup>46</sup>

Nonetheless, there is a fundamental difference between reactions such as PhO<sup>+</sup>/PhOH exchange by EPT and the coproportionation pathway in eq 12 or MS-EPT in eq 14. In the latter reactions, electronic coupling is relatively weak, with the resulting resonance energy far less than the reorganization energy,  $H_{\text{OA}} < \lambda$ . This is because EPT occurs between spatially well separated sites. As discussed in section 5.2 and for related electron transfer reactions, reaction barriers are dictated largely by the reorganization energy and the changes that occur in intramolecular structure and surrounding solvent dipoles.

In HAT, or PhO<sup>+</sup>/PhOH exchange, electronic coupling is significant, comparable to the reorganization energy with  $H_{\text{OA}} \sim \lambda$ . The interaction or resonance energy plays a major role in defining the reaction barrier. In these strongly coupled cases, EPT and HAT are closely related even though their orbital interactions may differ in detail.

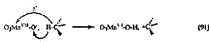
There are ambiguities of description, related to those that arise in defining oxidation states, as the extent of electronic coupling and delocalization increases. EPT and HAT become blurred as the energy differences between different HOMOs in the donor or LUMOs in the acceptor decrease, and/or as delocalization becomes extensive. A change in redox orbitals between reactants and products can also complicate mechanistic description.

In the oxidation of (Z,Z)-2,5-heptadiene by the Fe<sup>II</sup>—OH site in soybean lipoxygenase, DFT calculations point to proton transfer from the oxidized C=H bond to a σ lone pair on Fe<sup>II</sup>—OH while electron transfer occurs from a diene π orbital to a dπ(Fe(III)) orbital. This pathway has been described as PCET (EPT) because the electron and proton come from different orbitals, but there is no prior H-bonding and the H<sup>1</sup> source is a C=H bond with strong electronic coupling (section 7.4.4).<sup>164,353</sup>

### 5.2.2. Hybrid Mechanisms

The definition of EPT and the distinction between EPT and HAT focus on the separate orbital characteristics of the donor and acceptor couples. Many reactions occur by hybrid mechanisms involving couples of both kinds. Large  $k_{\text{H}}/k_{\text{D}}$  KIEs have been observed in the oxidation of  $d_{10}$ -ethylbenzene by a Fe<sup>IV=O</sup> pyridyl complex<sup>354</sup> and in methane oxidation by the diiron enzyme methane monooxygenase.<sup>355</sup> In these examples, and in the oxidation of aromatic hydrocarbons such as toluene, ethylbenzene, and diphenylmethane by MnO<sub>4</sub><sup>-</sup>, oxidation of the organic compounds is by HAT with EPT occurring at the oxidant since different proton and electron acceptor orbitals are used.<sup>360–361</sup>

In MnO<sub>4</sub><sup>-</sup> oxidations, coupled electron–proton transfer occurs from O<sub>C=H</sub> to dπ(Mn) and proton transfer to an O<sup>2-</sup> lone pair, eq 91. As for soybean lipoxygenase in the previous



section, there is no prior orientation by H-bonding. Orientation effects still exist in the association complex between reactants in order to maximize overlap.<sup>294,287,298,360,361,363</sup> Another example is oxidation of [Fe<sup>II</sup>(H<sub>2</sub>bim)]<sup>2+</sup> by PhCH<sub>3</sub><sup>+</sup>, eq 92, in which “H-atom abstraction” from the Fe(II) complex occurs by transfer of an electron from dπ(Fe(II)) and a proton from σ<sub>N-H</sub> (imidazole) to a sp<sup>3</sup>(C) orbital to form the C–H bond.<sup>340</sup>

Mayer and co-workers have demonstrated the existence of an empirical Marcus-like cross-reaction correlation for a series of reactions such as those in eq 92 which occur by a combination of HAT and hybrid HAT-EPT pathways. The Marcus cross-reaction equation relates the rate constant for electron transfer to the self-exchange rate constants for the component couples and the equilibrium constant. Note eq 82 in section 4.2.5. There is no obvious discrimination between the two pathways in the data.

These reactions are different in kind from the coproportion or MS-EPT examples in eqs 12 and 14 in that, as noted above, there is strong electronic coupling in the transfer of electrons and protons. There is no theoretical basis for application of Marcus theory to these reactions since it was derived for reactions in which electronic coupling is weak with  $H_{\text{OA}} (H_{\text{DA}}, V_{\text{ET}}) < \lambda$  (section 4.2).<sup>284–293</sup>

The HAT and EPT pathways in these correlations involve strong electronic coupling with  $H_{\text{DA}}$  probably comparable to or greater than  $\lambda$ . They may reflect more of an averaging of bond energies between self-exchange and cross-reactions than surface crossing between harmonic energy curves.

### 5.2.3. Energetics of HAT and “H-Atom Abstraction”

In the oxidation of a series of hydrocarbons (toluene, ethylbenzene, ...) by both radicals (OH<sup>·</sup>, RO<sup>·</sup>, ROO<sup>·</sup>) and the transition metal oxidants (MnO<sub>4</sub><sup>-</sup> and CrO<sub>2</sub>Cl<sub>2</sub>), a correlation was found between log  $k$  and the bond dissociation energy (BDE) of the hydroxyl products, ROH, HOMnO<sub>3</sub>, etc. This correlation demonstrated the importance of reaction energetics rather than radical character in the oxidant as a determinant of reactivity.<sup>368,369,370</sup> Related correlations have been found for a multitude of HAT reactions<sup>371–373</sup> and for the *trans*-[Ru<sup>2+</sup>(L)(O)]<sup>2+</sup> (L = 1,12-dimethyl-3,4,9,10-dibenzo-1,2-diaz-5,8-dioxacyclpentadecane) oxidations of a series of phenols which occur by EPT (section 6.1.2).<sup>374,375</sup>

In Photosystem II (section 7.2), an important step is oxidation of the CaMn<sub>2</sub> cluster in the oxygen evolving complex (OEC) by a tyrosyl radical, Y<sup>·</sup>. Babcock and co-workers proposed that oxidation by Y<sup>·</sup> occurs by “H-atom abstraction” (HAT) as a way to avoid high-energy intermediates (section 7.2).<sup>24,25,27,28,296,397</sup> This pathway is illustrated in eq 93 for the oxidation of a Mn<sup>II</sup>—OH<sub>2</sub> cluster site. “H-atom abstraction” would circumvent the high-energy ET products Mn<sup>II</sup>—OH<sub>2</sub> + TyrO<sup>·</sup>, with Mn<sup>II</sup>—OH and TyrOH the stable forms at pH = 7 (section 7.2.3). Consistent with terminology used here, the H-atom abstraction or HAT pathway would better be described as EPT since HAT would give the excited state, Mn<sup>II</sup>—O<sup>2-</sup>—H, and a high-energy tautomer of tyrosine with the proton on σ<sub>O-H</sub>, rather than σ<sub>O-H</sub>.

The H-atom abstraction (EPT) pathway in eq 93 is enthalpically viable if BDE(TyrOH) > BDE(Mn<sup>II</sup>—OH). For tyrosine, BDE(TyrO—H) = 87 kcal/mol.<sup>24,25,27,376–381</sup> Based



atom abstraction” would circumvent the high-energy ET products Mn<sup>II</sup>—OH<sub>2</sub> + TyrO<sup>·</sup>, with Mn<sup>II</sup>—OH and TyrOH the stable forms at pH = 7 (section 7.2.3). Consistent with terminology used here, the H-atom abstraction or HAT pathway would better be described as EPT since HAT would give the excited state, Mn<sup>II</sup>—O<sup>2-</sup>—H, and a high-energy tautomer of tyrosine with the proton on σ<sub>O-H</sub>, rather than σ<sub>O-H</sub>.

The H-atom abstraction (EPT) pathway in eq 93 is enthalpically viable if BDE(TyrOH) > BDE(Mn<sup>II</sup>—OH). For tyrosine, BDE(TyrO—H) = 87 kcal/mol.<sup>24,25,27,376–381</sup> Based

on redox potentials,  $\Delta G^\circ = 3.45$  eV (80 kcal/mol) for the bond dissociation reaction in eq 94.



The analysis developed by Babcock and co-workers provides a powerful basis for understanding the thermodynamic importance of coupled electron–proton transfer. It can be extended by including the differential energetics of formation of the initial,  $\text{Mn}^{II}-\text{OH}_2\cdots\text{O}^\bullet\text{Tyr}$ , and final,  $\text{Mn}^{II}-\text{O}^\bullet\cdots\text{H-O}^\bullet\text{Tyr}$ , H-bonded adducts and by using free energy rather than enthalpic changes. For example,  $\Delta G$  for eq 93 is favorable if  $E^\circ(\text{TyrO}^\bullet\text{TyrOH}) > E^\circ(\text{Mn}^{II}-\text{OH}^\bullet/\text{Mn}^{II}-\text{OH}_2)$  with  $E^\circ(\text{TyrO}^\bullet\text{TyrOH}) = 0.93$  V (vs NHE) at  $\text{pH} = 7$ .<sup>382</sup>

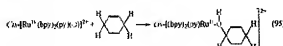
The results of recent structural analyses of PSII at 3 and 3.5 Å resolution appear to rule out an EPT pathway for TyrO<sup>•</sup> oxidation of Mn–OH<sub>2</sub>. In these structures, Y<sub>2</sub> is too far removed from the OEC cluster for EPT to be viable<sup>383</sup> (section 7.2.4). However, an alternate pathway is proposed in section 7.2.3.1 in which both Mn–OH<sub>2</sub> and TyrO<sup>•</sup> undergo EPT but with different EPT acid–base pairs rather than with each other (section 7.2.4).

#### 5.2.4. Related Pathways

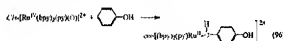
**5.2.4.1. Hydride Transfer.** In hydride transfer, two electrons and a proton are transferred from the same chemical bond. This was the suggested pathway for the oxidation of formate anion by *cis*-[Ru<sup>IV</sup>(bpy)<sub>2</sub>(py)]<sup>2+</sup> in eqs 2–4.<sup>4</sup> Examples where hydride transfer has been invoked include reversible oxidation of alcohols to aldehydes or ketones by the enzyme liver alcohol dehydrogenase (LADH)<sup>384–386</sup> and aqueous oxidation of toluene by MnO<sub>4</sub><sup>–</sup>.<sup>348</sup>

**5.2.4.2. Two-Electron–Proton Transfer (2e<sup>–</sup>/1H<sup>+</sup> EPT).** As discussed in more detail in section 6.1.1, 2e<sup>–</sup>/1H<sup>+</sup> EPT has been invoked in the oxidation of anilines by *cis*-[Ru<sup>IV</sup>(bpy)<sub>2</sub>(py)]<sup>2+</sup>. Microscopically, this involves simultaneous transfer to *cis* [Ru<sup>IV</sup>(bpy)<sub>2</sub>(py)]<sup>2+</sup> of two electrons from a π aniline orbital and a proton from  $\sigma_{\text{Bp-N}}$ .<sup>387</sup>

**5.2.4.3. C–H Insertion.** In the oxidation of activated C–H bonds, a mechanism has been proposed in which an oxo group inserts into a C–H bond in a concerted manner, as suggested, for example, in the oxidation of cyclohexene by *cis*-[Ru<sup>IV</sup>(bpy)<sub>2</sub>(py)]<sup>2+</sup> in eq 95.<sup>388</sup>



**5.2.4.4. Electrophilic Ring Attack.** Similarly, in the oxidation of phenol by *cis*-[Ru<sup>IV</sup>(bpy)<sub>2</sub>(py)]<sup>2+</sup>, eq 96, a mechanism has been proposed involving initial electrophilic addition of the oxo group to the aromatic ring, analogous to Br<sup>+</sup> addition to activated aromatics.<sup>389</sup>



### 5.3. Theory of Coupled Electron–Proton Transfer

#### 5.3.1. Introduction

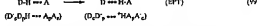
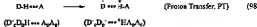
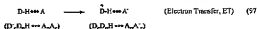
Theories of electron transfer (section 4.2) and proton transfer<sup>390–396</sup> provide a basis for understanding EPT including quantum effects. In one approach, HAT and EPT have

been analyzed theoretically by treating the transferring proton as a particle with quantum-tunneling corrections to transition state theory.<sup>392,393–396</sup> EPT theory has been developed systematically in a series of papers by Cukier et al.,<sup>11,39,39–39,36,395</sup> by Hammes-Schiffer et al.,<sup>12,40,41,44–47,40,405–411</sup> and by others.<sup>412–414</sup> Both Cukier and Hammes-Schiffer have dealt with PCET mechanisms, generally including competition between EPT and stepwise ET-PT or PT-ET.

Cukier makes a distinction between EPT (ETPT in his terminology) and H-atom transfer (HAT), which is different from the usage adopted here. In his terminology, the term EPT (ETPT) is used when electron and proton coupling between donor and acceptor are weak, with both in the nonadiabatic regime. HAT is used when electron transfer occurs over a distance comparable to the scale of proton transfer with strong coupling and both electron and proton transfer occurring in the adiabatic regime.

As noted by Hammes-Schiffer et al., three physically distinct types of HAT-EPT appear to be relevant: (1) electronically adiabatic proton transfer and electron transfer, (2) electronically nonadiabatic proton transfer and electron transfer, and (3) electronically adiabatic proton transfer and electronically nonadiabatic electron transfer.<sup>45</sup> Adiabatic in this context has the conventional meaning that there is sufficiently strong electronic coupling between the diabatic (non-interacting) reactant and product states that electron or proton transfer involves a change of coordinates within a single electronic state and not a transition between states.<sup>45–47</sup>

**5.3.1.1. Mixing of Diabatic States.** In the treatment of Hammes-Schiffer, the wave functions for the initial diabatic (non-interacting) states are represented as shown in eqs 97 and 98. They are labeled as to the transferring electron,  $D_e$ ,<sup>48</sup> and proton,  $D_p$ ,<sup>49–57</sup>



Adiabatic free energy surfaces for the transferring proton are constructed for the initial proton reactant state,  $\text{D}-\text{H}^\bullet-\text{A}$ , by mixing the diabatic states,  $\text{D}_e\text{D}_p\text{H}^\bullet-\text{A}_e\text{A}_p$  and  $\text{D}_e\text{D}_p\cdots\text{H}\text{A}_p\text{A}_e^\bullet$ . Similarly, free energy surfaces are constructed for the final product proton state by mixing  $\text{D}_e\text{D}_p\cdots\text{H}\text{A}_p\text{A}_e^\bullet$  and  $\text{D}_e\text{D}_p\text{H}^\bullet-\text{A}_e\text{A}_p$ . The coupling energy  $V_{\text{PT}}$  is assumed to be the same for both initial and product states. Proton vibrational levels and wave functions are then calculated for the resulting reactant (I) and product (II) diabatic states, giving rise to separate energy-coordinate curves and vibrational wave functions for the reactants and products. States I and II are diabatic with regard to electronic coupling but adiabatic in the transferring proton.

Examples of energy surfaces that illustrate this analysis are shown in Figure 30.<sup>47,49</sup> This figure was used originally to illustrate energy-coordinate curves, vibrational wave functions, and vibrational overlaps for three different solvent configurations for a single reaction. In Figure 30, they are used to illustrate the effect of changing  $\Delta G$  in a related series of reactions. It shows the lowest vibrational levels ( $\mu = 0$  and  $\nu = 0$ ) as a function of the proton coordinate,  $r_p$  in Å,

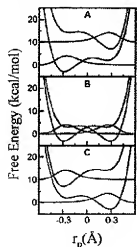
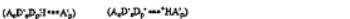
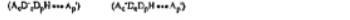
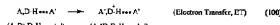


**Figure 36.** Energy-coordinate diagrams for EPT showing the variation in energy with proton coordinate,  $r_p$ , the position of the hydrogen nucleus relative to the midpoint of the donor and acceptor, for reactant (I, blue) and product (II, red) states and the associated vibrational wave functions for three cases: (A)  $\Delta G > 0$ ; (B)  $\Delta G = 0$ ; and (C)  $\Delta G < 0$ . Modified with permission from ref 409. Copyright 2001 American Chemical Society.

for three cases: (A)  $\Delta G > 0$ ; (B)  $\Delta G = 0$ ; and (C)  $\Delta G < 0$ . The initial reactant diabatic state,  $I$ , is shown in blue, and the final state,  $II$ , is shown in red. In this example,  $r_p$  varies from the minimum for the reactant state,  $-0.3$  Å, to the maximum for the product state,  $+0.3$  Å, with the difference between them the proton transfer distance. This would be the tunneling distance in a particle tunneling calculation.<sup>47,49</sup>

The same approach can be used to analyze MS-EPT. For example, for MS-EPT from a common electron–proton donor to separate electron,  $A_e$ , and proton,  $A_p$ , acceptors, the initial and final ET, PT, and EPT wave functions are as given in eqs 100–102.



**5.3.1.2 Transition between Reactants and Products.** Electronic coupling between  $D$ – $H$  and  $A$  in  $D$ – $H$ – $A$  and between  $D$  and  $H$ – $A$  in  $D$ – $H$ – $A$  mixes the initially diabatic reactant (I) and product (II) states. Application of time-dependent perturbation theory and the Golden Rule to the transition between states I and II leads to eq 103. It gives an

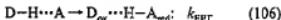
$$k_{\text{EPT}} = \frac{2\pi}{\hbar} \sum_{\mu} P_{\mu} \sum_{\nu} |V_{\mu\nu}|^2 (4\lambda_{\mu\nu} k_B T)^{-1/2} \exp - \frac{[(\Delta G_{\mu\nu} + \lambda_{\mu\nu})^2]}{4\lambda_{\mu\nu} k_B T} \quad (103)$$

$$\Delta G_{\mu\nu} = \Delta G_{\text{EPT}} + (\mu - \nu)\hbar\omega \quad (104)$$

expression for the rate constant for coupled electron–proton transfer,  $k_{\text{EPT}}$ .<sup>36,39,45,47,49</sup> In this equation, the summations are over the initial, coupled  $D$ – $H$ – $A$  vibrational levels  $\mu$  in  $(D^*, D, H \cdots A_p A_p)$  and the final coupled  $D$ – $H$ – $A$  levels  $\nu$  in  $(D, D^*, H \cdots A_p A_p)$ .  $P_{\mu\nu}$  is the Boltzmann population in vibrational level  $\mu$  in initial state  $D$ – $H$ – $A$ .  $\lambda_{\mu\nu}$  is the reorganization energy arising from the solvent and low-frequency modes for the  $\mu \rightarrow \nu$  vibrational channel.

$\Delta G_{\mu\nu}$  is the associated  $\mu \rightarrow \nu$  free energy change. It is related to the overall free energy change for EPT within the H-bonded association complex,  $\Delta G_{\text{EPT}}$ , by eq 104, in which  $\hbar\omega$  is the vibrational quantum spacing.<sup>45–47</sup>

The overall EPT mechanism, including preassociation, is shown in eqs 105–107.  $\Delta G_{\text{EPT}}$  is related to the overall free energy change,  $\Delta G$ , and the association constants for the EPT reactants ( $K_A$ ) and products ( $K_A'$ ) by eq 108, which is analogous to eq 78 for electron transfer.



$$\Delta G_{\text{EPT}} = \Delta G - RT \ln (K_A / K_A') \quad (108)$$

The expression for  $k_{\text{EPT}}$  in eq 103 has been extended to include coupled high-frequency vibrations treated quantum mechanically and anharmonic modes such as the  $w_{0-H}$  mode coupled to the proton transfer coordinate.<sup>41,41,45,46</sup> In form, it is similar to eq 73 for electron transfer, but there are important differences. The reorganization energies, free energy change, and couplings are different for each vibrational channel because of slight differences in the proton transfer distance.<sup>45–47,49</sup> The summation over  $\nu$  typically involves a limited number of levels ( $\leq 4$ ), those for which  $\Delta G_{\mu\nu}$  is not greatly different from  $\lambda_{\mu\nu}$ . It is for these levels that the classical exponential barrier term is maximized.

As for electron transfer in eq 73,  $k_{\text{EPT}}$  for each channel is produced of three terms: the Boltzmann population in initial level  $\nu$ , the classical barrier for the  $\mu \rightarrow \nu$  transition including solvent and low-frequency vibrations, and the barrier crossing term,  $(2\pi\hbar T)|V_{\mu\nu}|^2 (4\pi\lambda_{\mu\nu} k_B T)^{1/2}$ .  $V_{\mu\nu}$  is the EPT matrix element. If the Condon approximation separating nuclear and electronic motions is valid, it is given by eq 109, in which  $\phi_{\mu}^1$  and  $\phi_{\nu}^1$  are proton vibrational wave functions for the initial and final proton states.  $V_{\text{ET}}$  is the electron transfer matrix element,  $H_{\text{DA}}$  in eq 65. The square of the vibrational overlap integral,  $\langle \phi_{\mu}^1 | \phi_{\nu}^1 \rangle^2$ , gives a quantitative measure of the extent to which the reactants and products coexist spatially along the proton transfer coordinate.

$$V_{\mu\nu} \approx V_{\text{ET}} \langle \phi_{\mu}^1 | \phi_{\nu}^1 \rangle \quad (109)$$

Because site-to-site transfer distances for EPT are large, vibrational overlap integrals are typically small. Barrier crossing dynamics depend on the product  $V_{\text{ET}} \langle \phi_{\mu}^1 | \phi_{\nu}^1 \rangle$ . In contrast to ET, the frequency factor for EPT can vary with  $V_{\text{ET}}^2$  even if electronic coupling is large.<sup>45–47</sup> With significant electronic coupling in electron transfer, barrier crossing dynamics are dictated by the slowest mode or modes coupled to the reaction; note eqs 64–67. These are typically reorientation modes in the solvent. In this interpretation, the limiting factor in the dynamics of coupled electron–proton

transfer is the proton. The coordinate of the transferring electron is always at equilibrium with the proton coordinate.

The EPT frequency factor,  $\nu_{\text{EPT}}$ , is given by eq 110, which includes the prediction that  $\nu_{\text{EPT}}$  is temperature-dependent.

$$\nu_{\text{EPT}} = \frac{2\pi}{\hbar} V_{\text{ET}}^{-2} \sum_{\mu} P_{\mu} \sum_{\nu} \langle \phi_{\mu}^{\text{ET}} | \phi_{\nu}^{\text{ET}} \rangle^2 (4\pi\lambda_{\mu\nu} k_{\text{B}} T)^{-1/2} \quad (110)$$

As the extent of electronic coupling increases further and becomes comparable to the reorganization energy, the Condon approximation breaks down. In that case,  $\nu_{\text{ET}}$  becomes a function of the coordinates of both the transferring electron and proton. Procedures are available for solving the Schrödinger equation in this limit, giving wave functions and energies that depend on both electronic and nuclear coordinates.<sup>40,417-419</sup>

In applications using eq 103, the key input parameters are (1) the gas-phase coupling matrix elements  $V_{\text{ET}}$  and  $V_{\text{TR}}$ , which are calculated by molecular mechanics fits to electronic structure calculations or experimental data,<sup>420-421</sup> (2) the solvent reorganization energy, which is treated by standard dielectric continuum theory (section 4.2.1),<sup>311</sup> or more elaborate two-cavity models such as the frequency-resolved cavity model (FRCM) developed by Newton *et al.*,<sup>422,423</sup> (3) quantum modes that are based on frequency of bond distance changes and vibrational frequencies,<sup>420</sup> and (4) the proton transfer distance, which, in the absence of structural information, is obtained by fits to experimentally measured rate constants and kinetic isotope effects.

Theoretical analysis of EPT has been extended to quantum and dynamical effects in the proton donor–acceptor mode which has been treated both classically and quantum mechanically. Nonadiabatic expressions for  $k_{\text{EPT}}$  have been derived in the limits of slow classical and fast quantum modes. Expressions have also been derived which incorporate dynamical fluctuations in both electronic coupling and the energy gap between reactant and product states.<sup>41,414</sup> Quantitative applications of eq 103 to EPT in both chemistry and biology have been made, the results of which will be discussed in sections 6 and 7.<sup>415-417</sup>

### 5.3.2. Kinetic Isotope Effects

Large kinetic isotope effects (KIEs) are sometimes observed for EPT, an example being  $k(\text{H}_2\text{O})/k(\text{D}_2\text{O}) = 16.1$  for the comproportionation reaction between *cis*–[Ru<sup>IV</sup>(bpy)<sub>2</sub>(py)(O)]<sup>2+</sup> and *cis*–[Ru<sup>IV</sup>(bpy)<sub>2</sub>(py)(D<sub>2</sub>O)]<sup>2+</sup> in eq 10. KIEs of this magnitude are larger than the O–H/O–D classical limit of 7.9, pointing to the importance of quantum effects.<sup>424</sup> Large KIEs are known for other reactions involving H or D transfer, including (1) enzymatic C–H oxidations,<sup>40,425-429</sup> which have been treated by a theoretical description of isotope effects originally developed by Bigeleisen and Mayer,<sup>430,431</sup> (2) values of up to 50 for proton transfer and up to 250 for H-atom abstraction by free radicals in the pre-1980s literature,<sup>424</sup> (3) a value  $\geq 6 \times 10^3$  for alpha H-atom transfer from ethanol by methyl radicals in ethanol glasses at 77 K,<sup>432</sup> and (4) a value of  $> 10^4$  for intramolecular HAT in the triplet excited states of an aromatic ketone at 20 K.<sup>433-435</sup>

In addition to  $k_{\text{EPT}}$ , interpretation of KIEs for EPT must account separately for the equilibrium isotope effect in forming a H-bonded precursor complex, eq 105. Analogous

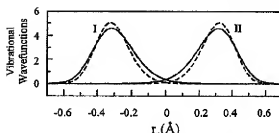


Figure 31. Reactant (I) and product (II) vibrational wave functions, H (solid curve) and D (dashed curve), for the  $\mu = 0 \rightarrow \nu = 0$  vibrational channel for the *cis*–[Ru<sup>IV</sup>(bpy)<sub>2</sub>(py)(O)]<sup>2+</sup>/*cis*–[Ru<sup>IV</sup>(bpy)(H<sub>2</sub>O)<sub>2</sub>]<sup>2+</sup> comproportionation reaction in eq 10, illustrating enhanced vibrational overlap for X = H compared to X = D. Reprinted with permission from ref 410. Copyright 2002 American Chemical Society.

to electron transfer in eq 57, the experimental rate constant,  $k_{\text{obs}}$ , is related to  $K_{\text{A}}$  and  $k_{\text{EPT}}$  by  $k_{\text{obs}} = K_{\text{A}} k_{\text{EPT}}$ .

For a substrate having solvent exchangeable protons, the isotopic preference in the H-bonded precursor complex is given by the isotopic fractionation factor,  $\varphi = [\text{D}(\text{H} \cdots \text{A})/\text{D}(\text{D}(\text{deuterium}) \cdots \text{A})]/[\chi_{\text{D}}/\chi_{\text{H}}]$ , with  $\chi_{\text{D}}/\chi_{\text{H}}$  the mole fraction ratio of D to H in a H<sub>2</sub>O/D<sub>2</sub>O solvent mixture.<sup>436-438</sup> Isotopic fractionation factors from 0.3 to 2, and even greater, have been observed in stable H-bonded bridges over an extensive range of H-bond distances.<sup>439-442</sup>

Fractionation factors of less than 1 arise when the zero point vibrational energies ( $\omega/2$ ) of the products are increased relative to the reactants. This can happen if there are frequency changes or if there is a change in the number of normal modes in the isotopic equilibrium.<sup>433-439</sup> An example of the latter is the equilibrium  $2\text{OH}^- + \text{D}_2\text{O} \rightleftharpoons 2\text{DO}^- + \text{H}_2\text{O}$ , for which  $K = 0.21$  because the heavier isotope concentrates in water, which has three normal modes compared to two for  $2\text{OH}^-$ .<sup>431-433</sup> The appearance of inverse kinetic isotope effects with  $k(\text{H}_2\text{O})/k(\text{D}_2\text{O}) < 1$  has been used as a criterion to distinguish rate limiting proton transfer from proton transfer occurring in a pre-equilibrium prior to the rate limiting step.

The magnitudes of KIEs for EPT follow directly from eq 103. Zero point energies and vibrational energy levels for X–D compared to X–H are lower in the vibrational energy wells by a factor of 0.7, the square root of the ratio of the O–H/O–D reduced masses,  $\{m_{\text{H}}(m_{\text{X}} + m_{\text{D}})/m_{\text{D}}(m_{\text{X}} + m_{\text{H}})\}^{1/2}$ . Alternatively, the larger mass of D can be viewed as leading to a more localized wave function, which leads to decreased vibrational wave function overlaps.

The example in Figure 31 shows the calculated  $\mu = 0 \rightarrow \nu = 0$  vibrational overlap for the *cis*–[Ru<sup>IV</sup>(bpy)<sub>2</sub>(py)(O)]<sup>2+</sup>/*cis*–[Ru<sup>IV</sup>(bpy)<sub>2</sub>(py)(H<sub>2</sub>O)]<sup>2+</sup> and *cis*–[Ru<sup>IV</sup>(bpy)<sub>2</sub>(py)(O)]<sup>2+</sup>/*cis*–[Ru<sup>IV</sup>(bpy)<sub>2</sub>(py)(D<sub>2</sub>O)]<sup>2+</sup> comproportionation reactions in eq 10.<sup>410</sup> Note also the form of the harmonic oscillator vibrational overlap integral in eq 70 and the dependence of  $S$  on reduced mass in eq 63.

The total KIE is the sum of KIEs for the individual, Boltzmann-weighted vibrational channels,  $P_{\mu\nu} k_{\text{obs}}$  in eq 103.

### 5.3.3. Temperature-Dependence

Equation 103 predicts that  $k_{\text{EPT}}$  should also be temperature-dependent due to the Boltzmann population and classical barrier terms. A smaller temperature-dependence arises from the pre-exponential term, eq 110. Since each  $\mu \rightarrow \nu$

vibrational channel has its own temperature-dependence, this leads to a precise but complex interpretation of the apparent energy of activation.

At low temperatures, populations above  $\mu = 0$  become negligible. EPT is then dominated by a vibrational channel or channels from  $\mu = 0$  to a  $\nu$  level or levels for which  $\Delta G_{\mu\nu} + \lambda$  is minimized. This causes the apparent energy of activation ( $E_a$ ) to decrease with temperature with a residual temperature-dependence arising from the classical modes and solvent at low temperatures.

The magnitude of the  $k_{\text{EPT}}/k_{\text{D}}$  KIE is predicted to be temperature-dependent in a complex way. On a level-by-level basis,  $\langle \phi_{\mu} | \phi^{\dagger} \rangle^2$  is decreased for X-D compared to X-H. However, the quantum spacing to the next higher  $\mu$  level is smaller for D than for H by  $\sim 0.7$ . This increases relative populations in levels above  $\mu = 0$  where  $\langle \phi_{\mu} | \phi^{\dagger} \rangle^2$  is greater. For the heavier isotope, levels above  $\mu = 0$  play a more important role, and this increases the magnitude of the apparent  $E_a$ .

### 5.3.4. $\Delta G$ -Dependence

The Boltzmann-weighted sum in eq 103 predicts that  $k_{\text{EPT}}$  is dependent on  $\Delta G$  but in a complex way. It arises from the  $\Delta G$ -dependences of the individual vibrational channels,  $\exp[-(AG_{\mu\nu} + \lambda)^2/4k_{\text{B}}T]$ , weighted by  $P_{\mu\nu}$  and  $\langle \phi_{\mu} | \phi^{\dagger} \rangle^2$ .<sup>2</sup> If the  $\mu = 0 \rightarrow \nu = 0$  vibrational channel dominates with  $\lambda \gg |\Delta G_{\mu\nu}|$ ,  $RT \ln k_{\text{EPT}}$  is predicted to vary as  $-\Delta G_{\text{EPT}}/2$ . The same result was obtained for classical electron transfer in eq 81.

As  $\Delta G_{\text{EPT}}$  increases or decreases, other channels with higher vibrational overlaps play an increasingly important role. This contributes a  $G$ -dependence in addition to the quadratic  $\Delta G$ -dependence of the exponential term. It also explains why experimental slopes for plots of  $RT \ln k_{\text{EPT}}$  vs  $-\Delta G$  for EPT have been found that are considerably different from 0.5 even when  $\lambda \gg |\Delta G_{\text{EPT}}|$ , as described in later sections.

*Inverted Region.* Both classical and quantum results for electron transfer in eqs 54 and 73 predict that the electron transfer barrier decreases as  $-\Delta G$  increases. This continues until  $-\Delta G = \lambda$ , at which point classical electron transfer becomes barrierless with  $k_{\text{EPT}} = \nu_{\text{E}}$ ; note eq 54. As  $-\Delta G$  is increased further, the energy-coordinate curve for the reactant state is imbedded in the curve for the product state along at least one of the coupled vibrations. Further increases in  $-\Delta G$  cause the classical barrier to increase as  $-\Delta G$  is increased further, as predicted by Marcus<sup>45</sup> and as observed experimentally.<sup>29,35,46</sup> A decrease in  $k_{\text{EPT}}$  is predicted by both the classical and quantum results in eqs 53 and 73 although with different dependences on  $\Delta G$ .

Although EPT in its equivalent "inverted region" has been discussed, at least in a preliminary way,<sup>46</sup> it does not appear to have been systematically explored experimentally.

## 5.4. H-Bonding and Distance-Dependence

The distance-dependence of electron transfer has been investigated in depth both experimentally and theoretically.<sup>1,2,35,39,45,46,47</sup> For EPT, both  $\nu_{\text{E}}$  and  $\langle \phi_{\mu} | \phi^{\dagger} \rangle$  are distance-dependent, but in different ways, since they involve electronic ( $\nu_{\text{E}}$ ) and vibrational overlaps.  $\lambda_{\text{c}}$  is also distance-dependent, as discussed in section 5.5.1.

From the expression for the de Broglie wavelength,  $\lambda = h/(2\pi E)^{1/2}$ , and the masses of the electron and proton, the proton wavelength is shorter than the electron wavelength

at a fixed energy by 40 for the proton and by  $\sim 60$  for the deuteron. The radial-dependence of vibrational wave functions falls off far more rapidly than that of electronic wave functions. This greatly decreases the distance between interacting centers for significant vibrational overlap. Relatively small changes in the proton transfer distance,  $r_p$ , can lead to large changes in  $\langle \phi_{\mu} | \phi^{\dagger} \rangle$  which can significantly impact  $k_{\text{EPT}}$  and  $\lambda_{\text{EPT}}$ .

The distance-dependence of EPT is dominated by proton transfer because of its short-range nature. Meeting the demands imposed by proton transfer raises a key structural issue for EPT, one that is dealt with routinely in biological PCET (section 7).

### 5.4.1. Precursor H-Bonding

Given the short-range nature of  $\text{H}^+$  transfer, a preformed interaction by H-bonding is an important element in EPT. H-bonding establishes an orbital pathway for proton transfer. It also minimizes the proton transfer distance and supports donor-acceptor electronic coupling.

H-bonding is common for H-X bonds with X an electronegative atom, especially F, O, N, and Cl. Strong H-bonds have bond energies in the range 15–60 kcal/mol.<sup>37,48–49</sup> There is even experimental evidence for H-bonding involving C–H bonds.<sup>48–49</sup> This suggests that prior H-bonding could play a role in some HAT or EPT reactions.

A correlation has been found between the strength of a H-bond,  $X-\text{H}\cdots Y$ , and the difference in  $\text{X}-\text{H}$  and  $\text{H}\cdots Y$  bond lengths,  $\Delta r$ , with  $\Delta r = r(\text{X}-\text{H}) - r(\text{H}\cdots Y)$ .<sup>43,48–49</sup> This observation is relevant to EPT because  $\Delta r$  is a measure of the proton transfer distance  $r_p$ .  $\Delta r = 0$  in  $\text{F}-\text{H}\cdots \text{F}^-$ , where there is strong electronic coupling across the H-bond, and the proton is "delocalized". The relationship between H-bond energy,  $\Delta r$ , and through-bond electronic coupling in  $\text{X}-\text{H}\cdots Y$  is conceptually related to the interplay between electronic delocalization and reorganization energy in the localized-to-delocalized transition in mixed-valence compounds.<sup>26,28,39,40,44,48–49</sup>

### 5.4.2. Distance-Dependence

The distance-dependence of EPT has been invoked to explain the decrease in  $k(\text{H}_2\text{O})/k(\text{D}_2\text{O})$  KIE from 16.1 for comproportionation between *cis*-[Ru<sup>IV</sup>(bpy)<sub>3</sub>(H<sub>2</sub>O)]<sup>2+</sup> and *cis*-Ru<sup>IV</sup>(bpy)<sub>3</sub>(py)(H<sub>2</sub>O)<sup>2+</sup> to 11.3 for [Ru<sup>IV</sup>(py)(bpy)(H<sub>2</sub>O)]<sup>2+</sup>/[Ru<sup>IV</sup>(py)(bpy)(H<sub>2</sub>O)]<sup>2+</sup>.<sup>7,8,49</sup> Theoretical calculations by Jordanova and Hammes-Schiffer point to a decrease in  $\Delta r$  for the latter from 2.70 Å to 2.64 Å due to decreased steric and electrostatic repulsion.<sup>49</sup>

Bonding effects and the nature of the donor-acceptor orbitals play a major role in dictating the magnitudes of  $\Delta r$  and  $r_p$ . Enhanced  $\text{X}-\text{H}\cdots Y$  electronic coupling across the H-bond decreases asymmetry and  $r_p$ . An example occurs in the  $[\text{Fe}^{\text{II}}(\text{H}_2\text{bim})(\text{Hbim})]^{2+}/[\text{Fe}^{\text{II}}(\text{H}_2\text{bim})]^{2+}$  self-exchange reaction in eq 89, for which  $k_{\text{H}}/k_{\text{D}} = 2.3 \pm 0.3$ .<sup>37</sup> In this case, the H-bond is relatively symmetrical, which decreases  $r_p$  and the classical isotope effect. Calculations show that the reactant proton state is a mixture of 66% of the initial, diabatic proton transfer state and 34% of the final, diabatic proton transfer state (section 6.1.5.1).<sup>49</sup>

Hybridization plays a role. In *cis*-[Ru<sup>IV</sup>(bpy)<sub>3</sub>(py)(O)]<sup>2+</sup>/*cis*-[Ru<sup>IV</sup>(bpy)<sub>3</sub>(py)(H<sub>2</sub>O)]<sup>2+</sup> comproportionation, hybridization at Ru<sup>IV</sup>=O<sup>2+</sup> is sp<sup>3</sup>. It is sp<sup>3</sup> at Ru=OH<sub>2</sub><sup>+</sup>. This creates a less symmetrical H-bond, increasing  $\Delta r$  and  $r_p$ . Proton transfer in the pseudo-self-exchange reaction, [Ru<sup>IV</sup>(bpy)(bpy-

$(\text{OH})^{2+} + \text{cis}-[\text{Ru}^{\text{II}}(\text{bpy})(\text{py})(\text{H}_2\text{O})]^{\text{2+}} \rightarrow [\text{Ru}^{\text{II}}(\text{py})(\text{bpy})(\text{H}_2\text{O})]^{\text{2+}} + \text{cis}-[\text{Ru}^{\text{II}}(\text{bpy})(\text{py})(\text{OH})]^{\text{2+}}$ , occurs between  $\text{sp}^2$ -hybridized O atoms, and the KIE falls to 5.8.<sup>8</sup>

## 5.5. Solvent

The charge transfer characteristics of EPT between single donors and acceptors are different from ET or PT since both electrons and protons are transferred simultaneously. Although there is a dearth of experimental evidence, it is possible to predict that there should be a solvent-dependence. Both electrons and protons are transferred in EPT. As a consequence, as can be seen for the EPT reactions in eqs 10 and 89, a charge dipole is transferred rather than a unit charge, as in an electron or proton transfer. Charge dipole transfer couples EPT to the polarization field of the surrounding medium, creating a solvent reorganization energy. This is in contrast to HAT, where both the transferring electron and proton come from the same orbital.<sup>4,40,43,46,49</sup> In addition to generalized solvent effects, it is possible for the solvent, especially  $\text{H}_2\text{O}$ , to be directly involved in EPT, with individual solvent molecules acting as proton donors or acceptors.

### 5.5.1. Solvent Effects on $\lambda_a$ and $\Delta G$

Solvent reorganization in EPT has been treated by assuming the solvent to be a dielectric continuum with application of an ellipsoidal cavity model developed by Kirkwood and Westheimer.<sup>12,16,493</sup> More recently, a frequency-resolved cavity model has been applied as in section 4.2.1 for electron transfer.<sup>327,328</sup>

There are limited experimental results on solvent effects,<sup>494</sup> but useful conclusions about solvent participation have been drawn based on theoretical analyses of experimental data: (1)  $\lambda_a$  for EPT can be comparable to  $\lambda_a$  for ET. For the  $[\text{Fe}^{\text{II}}(\text{HbIn})]^{\text{2+}}/[\text{Fe}^{\text{II}}(\text{HbIn})]^{\text{2+}}$  self-exchange reaction in eq 89, the calculated  $\lambda_a$  for EPT is 10 kcal/mol, and for ET, it is 13 kcal/mol.<sup>494</sup> (2) For a multiple-site EPT pathway with the electron and proton transferring to different external acceptors,  $\text{A}-\text{D}^{\text{H+}}-\text{A}' - \text{A}'-\text{D}^{\text{H+}}-\text{H}-\text{A}'$ ,  $\lambda_a(\text{EPT}) > \lambda_a(\text{ET})$  because of the separate reorganization energies for the transferring electron and proton.<sup>495</sup>

### 5.5.2. Proton Inventory

For EPT with protons exchangeable with the solvent, the determination of a KIE by single point rate constant measurements in pure  $\text{H}_2\text{O}$  and pure  $\text{D}_2\text{O}$  can mask participation by multiple protons in the solvent or by multiple exchangeable sites in the polypeptide structure of an enzyme, for example. Single point measurements also fail to uncover possible parallel pathways having the same rate law but different KIEs.

These effects have been explored experimentally by obtaining kinetic data in  $\text{H}_2\text{O}/\text{D}_2\text{O}$  mixtures, which is referred to in the biochemical literature as the proton inventory method.<sup>496</sup> Based on analyses by Kresse, Gold, and Albery and Davies,<sup>497</sup> it is possible to establish the number of exchangeable sites contributing to the KIE by studies of this kind.<sup>416,427,497-499</sup>

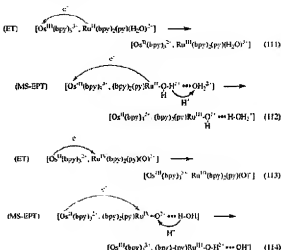
In one limiting form, plots of  $k_{\text{H}}/k_{\text{D}}$  vs  $\chi$  are made with  $\chi$  the mole fraction of  $\text{D}_2\text{O}$  in  $\text{H}_2\text{O}/\text{D}_2\text{O}$  mixtures.  $k_{\text{H}}$  is the rate constant in  $\text{H}_2\text{O}$ ,  $k_{\text{D}}$  is the rate constant in the mixture, and  $k_{\text{D}}$  is the rate constant in  $\text{D}_2\text{O}$ . If a single proton is involved and a single pathway,  $k_{\text{H}}/k_{\text{D}} = 1 + \chi(k_{\text{D}}/k_{\text{H}} - 1)$ ,

In this limit,  $k_{\text{H}}/k_{\text{D}}$  is predicted to vary linearly with  $\chi$ , with  $k_{\text{D}}/k_{\text{H}}$  obtained from the slope. Linear relationships of this kind have been found for EPT, for example, for the  $\text{cis}-[\text{Ru}^{\text{IV}}(\text{bpy})(\text{py})(\text{O})]^{\text{2+}}/\text{cis}-[\text{Ru}^{\text{II}}(\text{bpy})(\text{py})(\text{H}_2\text{O})]^{\text{2+}}$  reaction in eq 10, consistent with transfer of a single proton and a single pathway.

### 5.5.3. The Solvent as Proton Donor or Acceptor. Solvent-Assisted MS-EPT

For PCET reactions in  $\text{H}_2\text{O}$  with EPT unavailable to the reactants, coupled proton transfer to or from individual  $\text{H}_2\text{O}$  molecules or water clusters can provide a basis for MS-EPT, at least in principle. A solvent-assisted MS-EPT pathway of this kind is usually kinetically indistinguishable from stepwise ET-PT with ET followed by rapid proton equilibration. In some cases, it may be possible to infer which is operative based on extrakinetic measurements such as isotope effects or by rate constant and activation parameter comparisons.

The two mechanisms are compared for oxidation of  $\text{cis}-[\text{Ru}^{\text{II}}(\text{bpy})(\text{py})(\text{H}_2\text{O})]^{\text{2+}}$  by  $[\text{Os}^{\text{III}}(\text{bpy})]^{\text{2+}}$  within the association complex of the reactants in eqs 111 and 112, and for the reduction of  $\text{cis}-[\text{Ru}^{\text{IV}}(\text{bpy})(\text{py})(\text{O})]^{\text{2+}}$  by  $[\text{Os}^{\text{II}}(\text{bpy})]^{\text{2+}}$  in eqs 113 and 114; note eqs 5-7.<sup>5</sup>



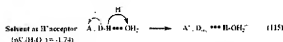
In considering a possible role for water and protons, it is useful to first consider the state of the local water structure around a proton. Two different cluster structures have been suggested. One is the Zundel cation  $\text{H}_2\text{O}_2^+$  ( $\text{H}_2\text{O}\cdots\text{H}^+\cdots\text{H}\cdots\text{O}_2^+$ ),<sup>500</sup> and the other is the Eigen cation  $\text{H}_3\text{O}_2^+$  ( $\text{H}_3\text{O}^+\cdots\text{H}_2\text{O}$ ).<sup>501-504</sup> These structures undergo dynamical interchange.<sup>502-504</sup> There is also experimental evidence for proton transfer through individual solvent molecules acting as bridges.<sup>505</sup>

The suggested solvent-assisted MS-EPT pathways in eqs 112 and 114 are reasonable, but individual water molecules or water clusters are neither good proton donors nor good acceptors given  $pK_{\text{a}}(\text{H}_2\text{O}) = 15.7$  and  $pK_{\text{a}}(\text{H}_2\text{O}^+) = -1.74$ ,<sup>439,506,507</sup> Thermodynamically, this favors ET followed by PT over solvent-assisted MS-EPT, except for the strongest acids and bases.

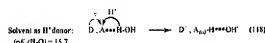
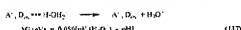
For example, for ET within the association complex in eq 111,  $\Delta G_{\text{ET}} \sim \Delta G^{\text{o}} = +0.21 \text{ eV} (+4.8 \text{ kcal/mol})$ , neglecting  $\Delta G$  differences in forming the initial and final association complexes,  $\Delta G_{\text{app}}$  in eq 60. For EPT in eq 112,  $\Delta G_{\text{EPT}} \sim$

$$+0.21-0.059(pK_a(H_2O^+) - pK_a(D_2O^{\text{H}^+}-OH_2^{2+})) = +0.36 \text{ eV} (+8.3 \text{ kcal/mol}).$$

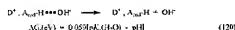
General expressions for the configurational free energy change,  $\Delta G_c \sim \Delta G_{\text{ET}} \text{ or } \Delta G_{\text{PT}}$ , are given in eqs 115 and 120. In these equations,  $F$  is the Faraday constant (1 eV/V in SI units),  $D_m$  is the oxidized form of  $D$ , and  $A_m$  is the reduced form of  $A$ . Also shown are expressions for the subsequent free energies of dilution, or transposition, of released  $H_2O^+$  or  $OH^-$ ,  $\Delta G_f$ .<sup>20,29,510</sup>



$$\Delta G_f(\text{eV}) = -F(pK_a(A^+ \cdot D_m) - pK_a(H_2O^+) - pK_a(D_m)) + \Delta G_{\text{PT}} \quad (116)$$



$$\Delta G_f(\text{eV}) = -F(pK_a(A^+ \cdot D_m) - pK_a(H_2O^+) + 0.059(pK_a(H_2O) - pK_a(A^+ \cdot D_m)) + \Delta G_{\text{PT}}) \quad (119)$$



Because of the kinetic indistinguishability of MS-EPT and ET-PT in water, and in the absence of energetic, isotope effect, or other arguments sufficiently ruling out one or the other, it is not clear when or if solvent-assisted MS-EPT plays a role in a particular reaction. *ET-PT is expected to dominate except for reactions involving the formation of very strong acids and bases.* This conclusion is based on the  $pK_a$  values for  $H_2O$ , a decreased  $\Delta_f$  for  $A$ , and the impact of vibrational overlap and tunneling on decreasing the magnitude of the EPT pre-exponential term in eq 103.

The appearance of relatively large  $\Delta_f(H_2O)/\Delta_f(D_2O)$  KIEs has been cited as evidence for solvent-assisted MS-EPT.<sup>49,51-1518</sup> Although it may be a useful criterion in some cases, as noted in section 4.2.1,  $H_2O/D_2O$  KIEs of up to 2 have been observed for outer-sphere and electrochemical ET because of coupling with quantum modes in the solvent. Conclusions based on isotope effects must be drawn with care. Complications may also exist from buffer components acting as proton donors or acceptors rather than solvent molecules (section 6.4.4).

There is a possible kinetic distinction between ET-PT and solvent-assisted MS-EPT based on the initial products of the electron transfer step. In ET-PT, electron transfer occurs prior to proton loss, and there is a discrete intermediate on the time scales for vibrational and solvent equilibration. In solvent-assisted MS-EPT, the loss of the proton is synchronous with electron transfer, and there is no intermediate, only equilibration and dilution following the elementary reaction.

Three different elementary steps have been identified for spontaneous loss of protons. For highly favored reactions, proton transfer can be ultrafast in tight acid-base complexes with the proton donor and acceptor directly linked by H-bonding. If the proton donor and acceptor are linked by an intermediate water bridge, proton transfer is largely controlled by reorganization in the solvent. In solutions dilute

in both proton donor and acceptor, proton transfer is diffusion limited.<sup>319,320</sup>

Ultrafast transient infrared measurements on pyranine-8-hydroxy-1,3,6-pyrenetriisulfonate (HPTS) in  $D_2O$  (section 2.8.1) reveal that proton loss occurs to  $D_2O$  on a time scale less than 150 fs, limited by the time resolution of the experiment. Subsequent transfer of  $D^+$  from  $D_2O^+$  to the added base  $CICH_2COO^-$  ( $pK_a(CICH_2COOH) = 2.7$ ) occurs more slowly, with  $\tau = 25 \text{ ps}$  ( $k = 4 \times 10^9 \text{ s}^{-1}$ ), even though  $\Delta G'' = -0.26 \text{ eV}$  (6.0 kcal/mol).<sup>502</sup> For HPTS, initial proton loss from the excited state is very rapid, approaching the vibrational time scale. In other cases, proton loss appears to be dynamically tied to solvent relaxation.<sup>241-244</sup>

Cukier has treated the problem of MS-EPT in the limit that the interaction between the final PCET products is repulsive and proton loss dissociative. The existence of a repulsive surface is attributed to the weakness of the H-bond, with proton dissociation aided by solvent electronic polarization.<sup>39,496</sup>

#### 5.5.4. pH Variations and the Distinction between $\Delta G_c$ and $\Delta G$

As noted by Krishnalik, the standard free energy change,  $\Delta G$ , does not completely characterize the energetics of an elementary step since it depends on the choice of standard states.<sup>296,307,510</sup> For ET or EPT, Krishnalik factors the driving forces into two terms. The first is the free energy change for the chemical transformation that occurs in an elementary step,  $\Delta G_c$ , the configurational free energy change (section 4.4.2). Neglecting  $\Delta G_{\text{app}}$ , it is related to  $\Delta G$ , the overall free energy change, as shown in eq 121. The summations are over the mole fractions of final (f) and initial (i) components in their standard states.

$$\Delta G_c = \Delta G^o + RT \sum_i^n \ln X_i^o - RT \sum_f^n \ln X_f^o \quad (121)$$

The second term, the transpositional free energy change  $\Delta G_t$ , arises from the change in entropy associated with the mutual transposition of particles in solution in forming association complexes between reactants and products. In an ideal solution, it is given by eq 122, again neglecting  $\Delta G_{\text{app}}$ .

$$\Delta G_t = RT \sum_i^n \ln X_f - RT \sum_f^n \ln X_i \quad (122)$$

For the overall reaction,  $\Delta G = \Delta G_c + \Delta G_t$ . For reactions where there is no change in the number of particles in the elementary step,  $\Delta G_c = \Delta G$ , neglecting  $\Delta G_{\text{app}}$ . However, for PCET reactions that occur by EPT in the elementary step, the difference between the two can be significant because of the transpositional term  $\Delta G_t$ ; note eqs 115–120.

*One consequence of this analysis is that  $\Delta G_{\text{app}}$  is independent of pH changes in the external solution.* At the microscopic level, this arises because there is no basis for coupling a local gain or loss of proton to the surrounding ensemble of solvent, protons, buffer, etc. that defines the final equilibrium state, including the pH. Because of an absence of a pH-dependence for  $\Delta G_{\text{app}}$ ,  $k_{\text{app}}$  is also independent of pH.

That this should be so can also be seen by considering simple acid dissociation of a generic acid,  $HA$ , to give  $H_2O^+ + A^-$ . This reaction can be written as the sum of the

elementary step for acid dissociation,  $\text{H}_2\text{O}\cdots\text{H}\cdots\text{A} \rightarrow \text{H}_2\text{O}^{\cdots\cdots\text{A}^+}$ , followed by dilution,  $\text{H}_2\text{O}^{\cdots\cdots\text{A}^+} \rightarrow \text{H}_2\text{O}^+ + \text{A}^-$ . Except for generalized medium effects, the elementary step is unaffected by pH changes in the external solution.

When pH-dependent PCET rate laws do appear, they may have a variety of origins. This has been discussed in a general way by Krishnaih.<sup>50f</sup> Specific examples are discussed below. Another example is discussed in section 6.4.5, involving intramolecular oxidation of a phenol linked to a  $[\text{Ru}^{\text{II}}(\text{bpy})_3]^{2+}$  derivative in which a linear dependence of  $\Delta G^\circ$  on pH has been observed.

**5.5.4.1. pH-Dependence. Proton Transfer followed by Electron Transfer (PT-ET).** (a) *Rate limiting proton transfer (PT-ET).* In the oxidation of  $cis\text{-}[\text{Ru}^{\text{II}}(\text{bpy})_2(\text{py})(\text{OH})]^{2+}$  by  $[\text{Os}^{\text{III}}(\text{bpy})_3]^{4+}$  above pH = 6.2, eq 5, a pH-dependent term appears in the rate law that has been attributed to rate limiting proton loss to  $\text{OH}^-$ ,  $cis\text{-}[\text{Ru}^{\text{II}}(\text{bpy})_2(\text{py})(\text{OH})]^{2+} + \text{OH}^- \rightarrow cis\text{-}[\text{Ru}^{\text{III}}(\text{bpy})_2(\text{py})(\text{O}^-)]^{3+} + \text{H}_2\text{O}$ . This reaction is slow, with  $k \leq 0.1 \text{ M}^{-1} \text{ s}^{-1}$ .<sup>51</sup>

Thermodynamically favored proton transfer reactions involving  $\text{OH}^-$  or  $\text{H}_2\text{O}^+$  can be rapid, with rate constants as high as  $\sim 2 \times 10^4 \text{ M}^{-1} \text{ s}^{-1}$  for the former and  $2 \times 10^{12} \text{ M}^{-1} \text{ s}^{-1}$  for the latter.<sup>51b,52b</sup> Since it is so slow, proton transfer from  $cis\text{-}[\text{Ru}^{\text{II}}(\text{bpy})_2(\text{py})(\text{O}^-)]^{2+}$  to  $\text{OH}^-$  is presumably highly unfavorable with  $pK_a(\text{Ru}^{\text{II}}-\text{OH}^2+) > 14$ .

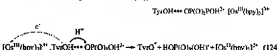
(b) *Acid-base pre-equilibria with rate limiting electron transfer (PT-ET).* Oxidation of ferrocene  $\text{Fe}(\text{C}_5\text{H}_5)_2$ ,  $\text{Fc}$ , by quinone (Q) is pH-dependent,  $2\text{Fc} + \text{Q} + 2\text{H}^+ \rightarrow 2\text{Fc}^+ + \text{H}_2\text{O}_2$ . The kinetics are also pH-dependent, but it has been suggested that the pH-dependence arises from prior protonation of Q ( $pK_a = -7$ ) followed by Fe reduction of  $\text{HQ}^+$ ,  $\text{Fc} + \text{HQ}^+ \rightarrow \text{Fc}^+ + \text{HQ}^-$ . Even though  $\text{HQ}^-$  is a high-energy intermediate with  $pK_a(\text{HQ}^-) = -7$ , it dominates electron transfer reactivity because it is a stronger oxidant than Q by 0.6 V.<sup>52b,53,521,522</sup>

**5.5.4.2. pH-Dependence. Parallel ET-PT and PT-ET Mechanisms.** A pH-dependence is introduced into a PCET mechanism if more than one form of a pH-dependent couple is involved. In this case, the pH-dependence originates in the effect of pH on the distribution between reactive forms, not from its influence on  $\Delta G$ . Note the redox potential square schemes in Figures 3 and 4.

The kinetics of oxidation of  $[\text{Os}^{\text{III}}(\text{bpy})_3]^{4+}$  by  $cis\text{-}[\text{Ru}^{\text{II}}(\text{bpy})_2(\text{py})(\text{OH})]^{2+}$  in acidic solution in eq 5 are pH-dependent because of the pH-dependent distribution between  $cis\text{-}[\text{Ru}^{\text{II}}(\text{bpy})_2(\text{py})(\text{H}_2\text{O})]^{2+}$  and  $cis\text{-}[\text{Ru}^{\text{II}}(\text{bpy})_2(\text{py})(\text{OH})]^{2+}$ .  $cis\text{-}[\text{Ru}^{\text{II}}(\text{bpy})_2(\text{py})(\text{H}_2\text{O})]^{2+}$  is more reactive than its hydroxo analogue by  $7 \times 10^4$ , but its  $pK_{\text{a},1}$  is 0.85. There is a pH dependence because  $cis\text{-}[\text{Ru}^{\text{II}}(\text{bpy})_2(\text{py})(\text{OH})]^{2+}$  plays an increasingly important role as the pH is raised, and its concentration relative to the aqua complex increases.<sup>5</sup> Another example is the pH-dependent oxidation of ascorbic acid ( $\text{H}_2\text{A}$ ) by  $[\text{Fe}(\text{CN})_6(\text{thiourea})]^{4-}$ , with oxidative reactivity in the order  $\text{A}^{2-} > \text{HA}^- > \text{H}_2\text{A}$ .<sup>523</sup>

**5.5.4.3. Buffer Effects.** In pH-dependent kinetic studies near pH = 7,  $\text{OH}^-$  and  $\text{H}^+$  are in low concentration, and buffers are used to control and vary pH. However, electron transfer data obtained under such conditions must be interpreted with care since the buffer itself can be an active component. The kinetics of oxidation of tyrosine ( $\text{TyrOH}$ ) by  $[\text{Os}^{\text{III}}(\text{bpy})_3]^{4+}$ , and a related series of polyridyl complexes, were investigated in a  $1\text{M} \text{PO}_4^{3-}/1\text{M} \text{PO}_4^{2-}$  buffer over a range of buffer concentrations.<sup>524</sup>

There is a background reaction between tyrosine and  $[\text{Os}^{\text{III}}(\text{bpy})_3]^{4+}$ . It occurs by ET,  $[\text{Os}^{\text{III}}(\text{bpy})_3]^{4+} + \text{TyrOH} \rightarrow [\text{Os}^{\text{II}}(\text{bpy})_3]^{2+} + \text{TyrO}^{1+}$ , followed by PT and is relatively slow,  $k(23^\circ\text{C}, I = 0.8) = 1.7 \times 10^2 \text{ M}^{-1} \text{ s}^{-1}$ , because  $\Delta G^\circ = +0.5 \text{ eV}$  for the initial ET step. Added buffer catalyzes the reaction, with the experimental rate law consistent with initial association between  $\text{TyrOH}$  and  $\text{HPO}_4^{2-}$ , eq 123, followed by two parallel pathways. In one pathway, deprotonation of  $\text{TyrOH}$  by proton loss to  $\text{HPO}_4^{2-}$  occurs followed by rapid oxidation of  $\text{Tyr}^-$  by  $[\text{Os}^{\text{III}}(\text{bpy})_3]^{4+}$ . In the other, eq 124, the buffer component acts as the proton acceptor in a MS-ET pathway.



Based on the results of a detailed kinetic study over a wide range of buffer concentrations,  $K_A = 30$  in eq 123 and  $K_A = 2.1$  for the EPT step in eq 124, in 0.8 M NaCl at room temperature.<sup>524</sup>

As discussed in later sections, the participation by buffer components may be a general phenomenon. It may play a role in other reactions and require reinterpretation of earlier data on the oxidation of DNA bases and other biological reductants in buffered solutions. The MS-EPT pathway in eqs 123 and 124 is also important as a mimic for the suggested MS-EPT oxidation of tyrosine  $\text{Y}_2$  in Photosystem II (section 7.2.2).

## 6. Coupled Electron-Proton Transfer in Chemistry

EPT pathways, both EPT and MS-EPT, have been invoked mechanistically in a number of PCET reactions. Examples have also been documented for discrete molecules adsorbed on, or bound to, surfaces and at the surfaces themselves, following "activation" procedures which produce O-containing functional groups.

### 6.1. EPT in Metal Complexes

#### 6.1.1. *cis*- $[\text{Ru}^{\text{IV}}(\text{bpy})_2(\text{py})(\text{O})]^{2+}$ and Related Complexes

**6.1.1.1. Comproportionation.** The  $k(\text{H}_2\text{O}/\text{D}_2\text{O})$  KIE of 16.1  $\pm 0.2$  for comproportionation between  $cis\text{-}[\text{Ru}^{\text{IV}}(\text{bpy})_2(\text{py})(\text{O})]^{2+}$  and  $cis\text{-}[\text{Ru}^{\text{II}}(\text{bpy})_2(\text{py})(\text{H}_2\text{O})]^{2+}$  in eqs 10–12 includes both isotopic fractionation in the H-bonded association complex and EPT (section 5.3.2).<sup>7–9</sup> From a theoretical analysis by Fordanova and Hammes-Schiffer (section 5.3),<sup>41b</sup> the O–O distance in the H-bond was calculated to be 2.70 Å by fitting the rate constant and KIE with  $\lambda = 0.53 \text{ eV}$  (12 kcal/mol). This analysis neglected the  $\nu(\text{Ru}=\text{O})$  mode and assumed a fixed O–O separation.

The distributions through vibrational channels, shown as fractions in parentheses, starting from initial level  $\mu = 0$  to levels  $\nu$  in the products were as follows: (1) *coordinated*  $\text{H}_2\text{O}$ ,  $\nu = 1$  (0.73),  $\nu = 2$  (0.18),  $\nu = 3$  (0.09), and  $\nu = 4$  (0); (2) *coordinated*  $\text{D}_2\text{O}$ ,  $\nu = 1$  (0.06),  $\nu = 2$  (0.10),  $\nu = 3$  (0.18), and  $\nu = 4$  (0.62). These data illustrate the effect of the smaller quantum spacing for O–D ( $\hbar\nu_{\text{D}} \sim 0.7\hbar\nu_{\text{H}}$ ) on the distribution through vibrational channels at room tem-

perature, with higher vibrational overlap occurring between  $\mu = 0$  and levels above  $\nu = 0$  for  $D_2O$ .<sup>410</sup>

Farrar and Thorp studied compartmentalization between  $[Ru^{IV}(\text{tpy})(\text{bpy})(\text{O})]^{2+}$  and  $[Ru^{IV}(\text{tpy})(\text{bpy})(\text{H}_2\text{O})]^{2+}$  and for a series of tpy- and bpy-substituted derivatives. This allowed  $\Delta G$  for compartmentalization to be varied over a range of 0.06 eV (1.4 kcal/mol).<sup>492</sup> For the tpy complex, the enhanced rate constant ( $\sim 7$ ) and decrease in  $k(\text{H}_2\text{O})/k(\text{D}_2\text{O})$  (11.4 compared to 16.1) at the same  $\Delta G$  were explained by invoking enhanced steric crowding for the tpy complex, which increases the O–O separation distance. This increases the proton transfer distance and decreases vibrational overlap (section 5.4.2).<sup>410</sup> Experimental slopes of plots of  $\ln k_{\text{H}_2\text{O}}/k_{\text{D}_2\text{O}}$  vs  $\Delta G$  were  $0.66 \pm 0.06$  in  $\text{H}_2\text{O}$  and  $0.64 \pm 0.05$  in  $\text{D}_2\text{O}$  rather than 0.5. This is consistent with intervention of  $\mu = 0 \rightarrow \nu$  vibrational channels above  $\nu = 0$  (section 5.3.4).

The pseudo-self-exchange reaction between  $[Ru^{IV}(\text{tpy})(\text{bpy})(\text{OH})]^{2+}$  and  $cis-[Ru^{IV}(\text{tpy})(\text{H}_2\text{O})]^{2+}$  mentioned in section 5.4.2 occurs by pH-dependent and independent pathways. The pH-dependent pathway occurs by outer-sphere electron transfer between  $[Ru^{IV}(\text{tpy})(\text{bpy})(\text{OH})]^{2+}$  and  $cis-[Ru^{IV}(\text{bpy})(\text{tpy})(\text{OH})]^{+}$ , is more rapid by  $\sim 110$ , and occurs with  $k(\text{H}_2\text{O})/k(\text{D}_2\text{O}) = 1.5$ . The pH-independent pathway occurs by EPT with  $k(\text{H}_2\text{O})/k(\text{D}_2\text{O}) = 5.8$  at  $25^\circ\text{C}$  ( $J = 0.005$  M).<sup>78</sup> Based on the discussion in section 5.3.2, the large  $k(\text{H}_2\text{O})/k(\text{D}_2\text{O})$  KIEs for compartmentalization arise from unsymmetrical H-bonds in the association complex, which increases the proton transfer distance and decreases vibrational overlap.

**6.1.1.2. Oxidation of  $\text{H}_2\text{O}_2$ .** Oxidation of  $\text{H}_2\text{O}_2$  to  $\text{O}_2$  by  $cis-[Ru^{IV}(\text{bpy})(\text{tpy})(\text{O})]^{2+}$  ( $k(\text{H}_2\text{O}_2, 25^\circ\text{C}) = 1.74 \pm 0.18$ ) and  $cis-[Ru^{IV}(\text{bpy})(\text{tpy})(\text{OH})]^{2+}$  ( $k = 8.09 \pm 0.27 \times 10^{-2}$   $\text{M}^{-1} \text{s}^{-1}$ ) occurs by EPT,  $[\text{Ru}^{IV}(\text{O}^\bullet\text{H})\text{H}_2\text{O}_2\text{OH}]^{2+} \rightarrow [\text{Ru}^{IV}(\text{O}^\bullet\text{H})\text{O}^\bullet\text{H}]^{2+}$ , to give  $\text{H}_2\text{O}_2$ . Experimental KIEs for the KIEs are  $22.0 \pm 1.2$  and  $16.2 \pm 0.7$  ( $25^\circ\text{C}$ ,  $J = 0.1$  M).<sup>323</sup> The HOMO on  $\text{H}_2\text{O}_2$  is a combination of  $\sigma_{\text{O}-\text{O}}$  and an orbital of  $\pi^*$  symmetry.<sup>324</sup>

**6.1.1.3. Oxidation of  $\text{H}_2\text{Q}$ .** Oxidation of hydroquinone ( $\text{H}_2\text{Q}$ ) by  $cis-[Ru^{IV}(\text{bpy})(\text{tpy})(\text{O})]^{2+}$  occurs with  $k(\text{H}_2\text{Q}, 25^\circ\text{C}, J = 0.1 \text{ M}) = 9.6 \pm 0.3 \times 10^3 \text{ M}^{-1} \text{s}^{-1}$  and  $k(\text{H}_2\text{O})/k(\text{D}_2\text{O}) = 28.7 \pm 1.0$  at  $15^\circ\text{C}$ . From the results of a mole fraction study (section 5.5.2), a single proton is involved, consistent with EPT,  $[\text{Ru}^{IV}(\text{O}^\bullet\text{H})\text{H}_2\text{Q}\text{OH}]^{2+} \rightarrow [\text{Ru}^{IV}(\text{O}^\bullet\text{H})\text{O}^\bullet\text{H}\text{H}_2\text{Q}]^{2+}$ . Oxidation of  $\text{H}_2\text{Q}$  by  $cis-[Ru^{IV}(\text{bpy})(\text{tpy})(\text{OH})]^{2+}$  also occurs by EPT with  $k(\text{H}_2\text{Q}/\text{D}_2\text{O}) = 9.3 \pm 0.1$  and  $k(\text{H}_2\text{O}, 25^\circ\text{C}, \mu = 0.1 \text{ M}) = (1.16 \pm 0.1) \times 10^6 \text{ M}^{-1} \text{s}^{-1}$ .<sup>32</sup> Consistent with the discussion in section 5.4.2, the difference in magnitudes between KIEs for the oxidants may be a consequence of a more unsymmetrical H-bond in the former due to the change in hybridization at the oxo group.

**6.1.1.4. Comparisons.** KIE data are collected in Table 1 for reactions involving  $cis-[Ru^{IV}(\text{bpy})(\text{tpy})(\text{O})]^{2+}$  ( $\text{Ru}^{IV}=\text{O}^\bullet$ ) and  $cis-[Ru^{IV}(\text{bpy})(\text{tpy})(\text{OH})]^{2+}$  ( $\text{Ru}^{IV}=\text{OH}^{2+}$ ) as the oxidants with a series of reductants.<sup>32</sup> The data include differences in enthalpies,  $\Delta H^\ddagger$ , and entropies,  $\Delta S^\ddagger$ , of activation between reactions studied in  $\text{H}_2\text{O}$  and  $\text{D}_2\text{O}$ . The data were treated by using the reaction rate theory expression in eq 125. In this interpretation,  $k = k_{\text{H}_2\text{O}}/k_{\text{D}_2\text{O}}$ , and the differences between  $\Delta H^\ddagger$  and  $\Delta S^\ddagger$  include  $\Delta H^\ddagger$  and  $\Delta S^\ddagger$  for H-bonded pre-equilibria with their associated isotopic fractionation factors (section 5.3.2).<sup>336</sup>

The higher  $\Delta H^\ddagger$  values in  $\text{D}_2\text{O}$  are consistent with greater use of vibrational channels above vibrational level  $\mu = 0$ ,

Table 1.  $\text{H}_2\text{O}/\text{D}_2\text{O}$  Kinetic Isotope Effects and Activation Parameters for Oxidations by  $cis-[Ru^{IV}(\text{bpy})(\text{tpy})(\text{O})]^{2+}$  and  $cis-[Ru^{IV}(\text{bpy})(\text{tpy})(\text{OH})]^{2+}$  in Water ( $J = 0.1$  M) at  $25^\circ\text{C}$

Reaction <sup>a</sup>	$\text{D}_2\text{O} - \text{H}_2\text{O}$		
	$k_{\text{H}_2\text{O}}/k_{\text{D}_2\text{O}}$	$\Delta H^\ddagger$ kcal/mol	$\Delta S^\ddagger$ cal/ $^\circ\text{C}$ mol
$\text{Ru}^{IV}=\text{O}^\bullet + \text{Ru}^{IV}\text{OH}_2^{2+} \rightleftharpoons$ ( $\text{ca}^1$ ) ( $\text{de}^1$ )	16.1 $\pm$ 0.7	+1.6	-0.3
$\text{Ru}^{IV}=\text{O}^\bullet + \text{HO}-\text{C}_6\text{H}_4-\text{OH}$ ( $\text{ca}^1$ ) ( $\text{nr}^1$ )	28.7 $\pm$ 1.0	+1.5	-1.7
$\text{Ru}^{IV}=\text{O}^\bullet + \text{H}-\text{O}-\text{H}$ ( $\text{ca}^1$ ) ( $\text{nr}^1$ )	71.6 $\pm$ 1.7	+3.2	-2.0
$\text{Ru}^{IV}=\text{OH}^{2+} + \text{HO}-\text{C}_6\text{H}_4-\text{OH}$ ( $\text{de}^1$ ) ( $\text{nr}^1$ )	0.3 $\pm$ 0.1	NA	NA
$\text{Ru}^{IV}=\text{OH}^{2+} + \text{H}-\text{O}-\text{H}$ ( $\text{ca}^1$ ) ( $\text{nr}^1$ )	16.7 $\pm$ 1.7	NA	NA

<sup>a</sup>The electronic configurations of the electron transfer donors and acceptors are indicated for the individual entries.

$$k = \frac{k_B T}{h} \exp\left(\frac{-\Delta G^\ddagger}{RT}\right) = \frac{k_B T}{h} \exp\left(\frac{-\Delta H^\ddagger}{RT}\right) \exp\left(\frac{\Delta S^\ddagger}{RT}\right) \quad (125)$$

eq 103, and the smaller O–D quantum spacing (section 5.3.3). KIEs for  $\text{Ru}^{IV}=\text{OH}^{2+}$  may be lower due to the difference in hybridization at  $\text{Ru}=\text{OH}$  compared to  $\text{Ru}=\text{O}$  which decreases proton transfer distances (section 5.4.2).

### 6.1.2. Oxidation of Phenols by $trans-[Ru^{IV}(\text{L})(\text{O})]^{2+}$ ( $\text{L} = 1,12\text{-Dimethyl-3,4,9,10-dibenzo-1,2-diaza-5,8-dioxacyclopentadecane}$ )

The oxidation of a series of phenols by  $trans-[Ru^{IV}(\text{L})(\text{O})]^{2+}$  was investigated in water and  $\text{CH}_3\text{CN}$ .<sup>317</sup> For phenol in water, pH-dependent and -independent pathways were observed consistent with  $k(\text{25 }^\circ\text{C}, J = 0.1 \text{ M}) = 12.5 \text{ M}^{-1} \text{s}^{-1}$  for  $\text{PhOH}$  and  $k(\text{25 }^\circ\text{C}, J = 0.1 \text{ M}) = 8.0 \times 10^6 \text{ M}^{-1} \text{s}^{-1}$  for  $\text{PhO}^\bullet$ . The pH-independent pathway occurred with  $k(\text{H}_2\text{O})/k(\text{D}_2\text{O}) = 4.8$ . Based on the KIE and the influence of bulky substituents in the oxidation of sterically hindered phenols, it was concluded that pH-independent phenol oxidation occurs by a HAT (EPT) pathway, eq 126. Following the  $1e^-/1\text{H}^\bullet$  oxidation in eq 126, the phenoxyl radical undergoes further  $3e^-$  oxidation by  $trans-[Ru^{IV}(\text{L})(\text{O})]^{2+}$  and  $trans-[Ru^{IV}(\text{L})(\text{O})\text{O}]^{2+}$  to give  $\rho$ -benzoquinone, in competition with coupling of the radical to give 4,4'-biphenolquinone.<sup>315</sup>



$\text{L} = 1,12\text{-Dimethyl-3,4,9,10-dibenzo-1,2-diaza-5,8-dioxacyclopentadecane}$

In the oxidation of a series of substituted phenols by  $trans-[Ru^{IV}(\text{L})(\text{O})]^{2+}$  in  $\text{CH}_3\text{CN}$ , a straight line correlation was observed between  $\log k$  and the bond dissociation energy of the phenol. A separate correlation was observed for phenols with bulky 2,6-di-*tert*-butyl substituents close to the  $-\text{O}^\bullet\text{H}$  group, resulting in significantly decreased rate constants.<sup>315</sup> The comparison between the two provides graphic, if

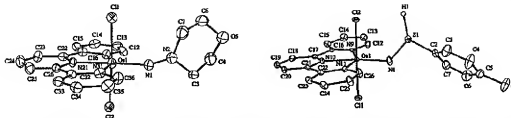
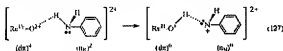


Figure 32. Representative structures of Os complexes as  $\text{PF}_6^-$  salts: (A)  $\text{trans-}[\text{Os}^{4+}(\text{tpy})(\text{Cl})_2(\text{N}(\text{H})\text{N}(\text{CH}_2)_4\text{O})]^{6-}$  with  $\text{OsN1} = 1.865(8)$  Å and  $\text{OsN1N2} = 158.9(12)^\circ$ ; (B)  $\text{trans-}[\text{Os}^{4+}(\text{tpy})(\text{Cl})(\text{p-NS(H)C}_6\text{H}_4\text{Me})]^{6-}$  with  $\text{OsN1} = 1.912(9)$  Å and  $\text{OsN1S1} = 128.6(6)^\circ$ .<sup>31</sup>

qualitative, evidence for the importance of the proton transfer distance on EPT vibrational overlaps (section 5.4.2).

#### 6.1.3. Two-Electron-Proton Transfer ( $2e^-/1\text{H}^+$ EPT) in the Oxidation of Aniline

Aniline undergoes  $6e^-$  oxidation by  $\text{cis-}[\text{Ru}^{4+}(\text{bpy})_2(\text{PhNHNHPh})](\text{O}_2)^{2+}$  in  $\text{CH}_3\text{CN}$ . The products of the first stage are diphenylhydrazine ( $\text{PhNHNHPh}$ ) and phenylhydroxylamine ( $\text{PhNHOH}$ ). The reaction is first order in each reactant with  $k(25.1^\circ\text{C}) = (2.05 \pm 0.18) \times 10^2 \text{ M}^{-1} \text{ s}^{-1}$ . In water, the reaction occurs with  $k(\text{H}_2\text{O})/k(\text{D}_2\text{O}) = 1.55 \pm 2.2$ . Given the absence of one-electron oxidation polyaniline products, the initial redox step appears to involve a  $2e^-$  change.<sup>38</sup> It has been proposed that  $2e^-/1\text{H}^+$  EPT occurs to give the intermediate nitrene or protonated nitrene shown in eq 127.



The relationship between  $2e^-/1\text{H}^+$  EPT and hydride transfer is analogous to that between EPT and HAT. In  $2e^-/1\text{H}^+$  EPT, the electrons and proton are transferred from different orbitals in the electron–proton donor. Proton transfer occurs from  $\sigma_{\text{N-H}}$  and electron transfer occurs from a  $\pi$  orbital. This is in contrast to the oxidation of formate anion ( $\text{HCO}_2^-$ ) in eq 4, in which both electrons and the proton come from the same C–H bond.

Following the redox step, the nitrene intermediate is captured competitively by  $\text{PhNH}_2$  to give  $\text{PhNHNHPh}$  or by  $\text{H}_2\text{O}$  to give  $\text{PhNHOH}$ . The hydroxylamine does not build up in solution since it undergoes rapid oxidation to give nitrosobenzene ( $\text{PhNO}$ ).<sup>38</sup>

#### 6.1.4. "Colossal" Kinetic Isotope Effects in the Oxidation of $\text{Os}^{(V)}\text{Hydrazido}$ and Related Complexes by Quinone

In section 2.3.1.3, pH-dependent  $\text{Os}^{(V)/V}$  couples such as  $\text{trans-}[\text{Os}^{4+}(\text{tpy})(\text{Cl})_2(\text{NNR}_2)]^{4-}/\text{trans-}[\text{Os}^{4+}(\text{tpy})(\text{Cl})_2(\text{N(H)-NR}_2)]^{4-}$  ( $pK_a = 3.21$ ) were mentioned in the context of PCET thermodynamics. The change in proton content with oxidation state is reminiscent of those in the oxo/hydroxo/acqua couples  $\text{cis-}[\text{Ru}^{4+}(\text{bpy})(\text{py})(\text{O})]^{2+}/\text{cis-}[\text{Ru}^{4+}(\text{bpy})(\text{py})(\text{H}_2\text{O})]^{2+}$  and  $\text{cis-}[\text{Ru}^{4+}(\text{bpy})(\text{py})(\text{H}_2\text{O})]^{2+}/\text{cis-}[\text{Ru}^{4+}(\text{bpy})(\text{py})(\text{OH})]^{2+}$ . Kinetic studies on the oxidations of  $\text{trans-}[\text{Os}^{4+}(\text{tpy})(\text{Cl})_2(\text{N(H)N}(\text{CH}_2)_4\text{O})]^{6-}$  (note eq 128),  $\text{trans-}[\text{Os}^{4+}(\text{tpy})(\text{Cl})_2(\text{N(H)N}(\text{CH}_2)_4\text{O})]^{6-} + \text{O}_2 \rightarrow$

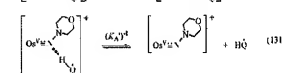
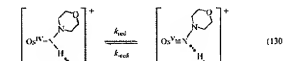
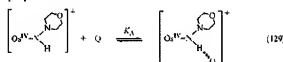


$\text{trans-}[\text{Os}^{4+}(\text{tpy})(\text{Cl})_2(\text{NS(H)-p-C}_6\text{H}_4\text{Me})]^{6-}$ , and  $\text{trans-}[\text{Os}^{4+}(\text{Tp}^-)(\text{Cl})_2(\text{NP(H)Et}_2)]^{6-}$  ( $\text{Tp}^-$  is tris(pyrazol-1-yl)borate anion) by quinone (Q) in 1:1 (v/v)  $\text{CH}_3\text{CN}/\text{H}_2\text{O}$  have revealed the

existence of EPT accompanied by colossal H/D KIEs.<sup>13,111,57,58</sup> Representative structures of the complexes are shown in Figure 33.

For  $\text{trans-}[\text{Os}^{4+}(\text{tpy})(\text{Cl})_2(\text{N(H)N}(\text{CH}_2)_4\text{O})]^{6-}$ , EPT occurs at the N directly bound to Os. In  $\text{trans-}[\text{Os}^{4+}(\text{tpy})(\text{Cl})(\text{NS(H)-p-C}_6\text{H}_4\text{Me})]^{6-}$  and  $\text{trans-}[\text{Os}^{4+}(\text{Tp}^-)(\text{Cl})(\text{NP(H)Et}_2)]^{6-}$ , EPT occurs at S or P proton donor atoms once removed.<sup>51</sup> Driving forces are small for all three with  $\Delta G = -0.05, +0.08$ , and  $+0.06 \text{ eV}$ , which allowed the kinetics to be studied in both forward and reverse directions.<sup>51</sup>

pH-dependent kinetic studies revealed both pH-dependent and pH-independent pathways. The pH-independent pathways occur by EPT. Saturation kinetics and direct spectral measurements provide evidence for intermediates in all three reactions. In the representative mechanism shown for the hydrazido complex in eqs 129–132, H-bonding with Q is proposed in the intermediate.



The appearance of saturation kinetics allows separation of  $k_{\text{red}}$  and  $K_A$ . A proton inventory experiment was conducted as described in section 5.5.2. The variation of  $k_{\text{red}}/k_{\text{H}}$  with mole fraction of D and  $\chi_D$  followed the relationship  $k_{\text{red}}/k_{\text{H}} = 1 + \chi_D(k_0/k_1 - 1)$ , with  $k_0$ ,  $k_1$ , and  $k_2$  as the rate constant in pure  $\text{H}_2\text{O}$  in  $\text{D}_2\text{O}$ , and in a mixed solvent of mole fraction  $X$ . Values of  $k_0/k_1$  and  $k_2$  were obtained by extrapolation. The results, shown replotted as  $k_{\text{red}}/k_{\text{H}}$  versus  $\chi_D$  in Figure 33, show that  $k(\text{H}_2\text{O})/k(\text{D}_2\text{O}) = 439 \pm 8^{111,58}$ . As shown by the data in Table 2, all three reactions proceed with giant kinetic isotope effects.

Based on an analysis of these data by Iordanova and Hammes-Schiffer,<sup>47</sup> (1)  $\Delta G_{\text{eff}}$  is large and positive for all three reactions (+18 kcal/mol (0.78 eV) to 21 kcal/mol (0.91

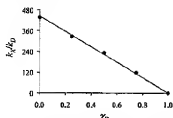


**Figure 33.** Plot of  $k_p/k_t$  versus  $x_D$  for the reaction between quinone and *trans*-[Cs<sup>2+</sup>(npy)(Cl)<sub>2</sub>(N(H)(N)(CH<sub>2</sub>)<sub>2</sub>)O]PF<sub>6</sub>, eq 128, in 1:1 (v/v) CH<sub>3</sub>CN/H<sub>2</sub>O-D<sub>2</sub>O mixtures,  $\mu = 0.1$  M, at 25.0  $\pm$  0.1 °C, at  $[Q] < 2.80 \times 10^{-3}$  M.  $k_p$  and  $k_t$  are rate constants in pure H<sub>2</sub>O and in H<sub>2</sub>O-D<sub>2</sub>O mixtures of mole fraction  $x_D$ .

**Table 2.** H<sub>2</sub>O/D<sub>2</sub>O Kinetic Isotope Effects for the Oxidation of Do(IV) Complexes by Quinone<sup>31</sup>

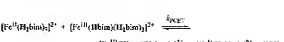
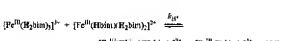
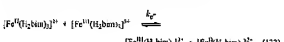
$\Delta \log k_{\text{ET}}$	Oxidant <sup>a</sup>			
	$\eta$	$\eta$	$\eta$	$\eta$
$\text{Fe}^{\text{IV}}(\text{Ph}_3\text{P})_3^{\text{II}}$	$-1.8 \pm 0.1 \times 10^0$	$12.5 \pm 0.02 \times 10^0$	$(1.32 \pm 0.09) \times 10^0$	
$\text{Fe}^{\text{IV}}(\text{Cl})_2^{\text{II}}$	$-1.23 \pm 0.04 \times 10^0$	$12.10 \pm 0.02 \times 10^0$	$(1.27 \pm 0.03) \times 10^0$	
$\text{Fe}^{\text{IV}}(\text{H}_2\text{O})^{\text{II}}$	$-1.23 \pm 0.02 \times 10^0$	$95.4 \pm 0.04 \times 10^0$	$(3.69 \pm 0.02) \times 10^0$	
$\text{Fe}^{\text{IV}}(\text{D}_2\text{O})^{\text{II}}$	$-1.42 \pm 0.04 \times 10^0$	$63.0 \pm 0.05 \times 10^0$	$(2.69 \pm 0.02) \times 10^0$	
$\text{Fe}^{\text{IV}}(\text{D}_2\text{O})_{\text{pD-DO}}$	$-2.01 \pm 0.05 \times 10^0$	$77 \pm 5$	$109 \pm 6$	

<sup>a</sup>25.0  $\pm$  0.1 °C in 1:1 v/v CH<sub>3</sub>CN/H<sub>2</sub>O-D<sub>2</sub>O,  $\mu = 0.1$  M.

eV)), and the reactions occur from initial levels  $\mu = 0, 1, 2, \dots, \nu = 0$  in the products and (2) the longest proton transfer distance is for P-H, but its KIE (at 25 °C) is the smallest. This is because the calculated P-H vibrational spacing is lowest, which leads to higher Boltzmann populations in levels above  $\mu = 0$ , in which vibrational overlaps are higher.

### 6.1.5. Metal Complex Self-Exchange

**6.1.5.1.  $[\text{Fe}^{\text{IV}}(\text{H}_2\text{bim})_2^{\text{II}}]^{\text{2+}} \times [\text{Fe}^{\text{II}}(\text{H}_2\text{bim})]^{\text{2+}}$  Self-Exchange.** The  $[\text{Fe}^{\text{IV}}(\text{H}_2\text{bim})_2^{\text{II}}]^{\text{2+}} \times [\text{Fe}^{\text{II}}(\text{H}_2\text{bim})]^{\text{2+}}$  self-exchange reaction, eq 89 in section 4.4, was studied by <sup>1</sup>H NMR line broadening in CD<sub>3</sub>CN ( $\mathcal{I} = 0.1$  M) as part of a comprehensive study of electron transfer in eq 133, proton transfer in eq 134, and PCET in eq 135.<sup>337</sup>



PCET occurs by EPT and a small KIE,  $k(\text{H}-\text{H})/k(\text{N}-\text{D}) = 2.3 \pm 0.3$  at 51 °C,<sup>337</sup> consistent with a largely symmetrical H-bond, eq 89, in agreement with calculations by Iordanova, Decornez, and Hammes-Schiffer (section 5.4.2).<sup>405</sup> Rate constants for electron transfer,  $\Delta \log \mathcal{I} = 1.7 \pm 10^{-1}$  M<sup>-1</sup> s<sup>-1</sup>, and EPT are comparable due to compensating effects. The solvent reorganization energy is smaller for EPT, and electronic coupling is larger for ET.<sup>337</sup>

**6.1.5.2. Related Metal Complex Self-Exchange Reactions.** Self-exchange rate measurements have also been

conducted on the 2,2'-bis(tetrahydro)pyrimidine (H<sub>2</sub>bip) couple,  $[\text{Fe}^{\text{IV}}(\text{H}_2\text{bip})_2^{\text{II}}]^{\text{2+}}/[\text{Fe}^{\text{IV}}(\text{H}_2\text{bip})_2]^{\text{2+}}$  in CD<sub>3</sub>CN (Figure 34). At temperatures near ambient, both electron transfer self-exchange between  $[\text{Fe}^{\text{IV}}(\text{H}_2\text{bip})_2^{\text{II}}]^{\text{2+}}$  and  $[\text{Fe}^{\text{IV}}(\text{H}_2\text{bip})_2]^{\text{2+}}$  and EPT self-exchange occur with negative enthalpies of activation with  $\Delta H^\ddagger = -1.5 \pm 0.5$  kcal/mol for EPT self-exchange. The negative  $\Delta H^\ddagger$  values have been attributed to self-exchange occurring preferentially from low-spin forms of the Fe(II) and Fe(III) complexes. The  $k_{\text{ET}}/k_{\text{EPT}}$  KIE was 1.6  $\pm$  0.5 at 25 °C.<sup>338</sup>

In a comprehensive study at 25 °C in CD<sub>3</sub>CN, Soper and Mayer investigated PCET self-exchange between  $[\text{Os}^{\text{IV}}(\text{Tp})(\text{Cl})_2(\text{NH}_2\text{Ph})]^{\text{2+}}$  (Tp<sup>-</sup> is tris(pymol-1-yl)borate anion) in CH<sub>3</sub>CN, electron transfer self-exchange between  $[\text{Os}^{\text{IV}}(\text{Tp})(\text{Cl})_2(\text{NH}_2\text{Ph})]^{\text{2+}}$  and  $[\text{Os}^{\text{IV}}(\text{Tp})(\text{Cl})_2(\text{NH}_2\text{Ph})]^{\text{3+}}$  and proton exchange between  $[\text{Os}^{\text{IV}}(\text{Tp})(\text{Cl})_2(\text{NH}_2\text{Ph})]^{\text{2+}}$  and  $[\text{Os}^{\text{IV}}(\text{Tp})(\text{Cl})_2(\text{NH}_2\text{Ph})]^{\text{3+}}$  and between  $[\text{Os}^{\text{IV}}(\text{Tp})(\text{Cl})_2(\text{NH}_2\text{Ph})]^{\text{2+}}$  and  $[\text{Os}^{\text{IV}}(\text{Tp})(\text{Cl})_2(\text{NH}_2\text{Ph})]^{\text{+}}$  and  $[\text{Os}^{\text{IV}}(\text{Tp})(\text{Cl})_2(\text{NH}_2\text{Ph})]^{\text{2+}}$ .<sup>339</sup> This study revealed that the ET and PT self-exchange reactions were  $\geq 10^6$  times more rapid than EPT with  $k_{\text{ET}} \sim 3 \times 10^{-3}$  M<sup>-1</sup> s<sup>-1</sup>. This rate constant may be an upper limit because of acid and base catalysis of competitive ET-PT or PT-ET PCET mechanisms.

The slowness of the EPT pathway was attributed to a possibly weaker and longer H-bond in the EPT precursor complex which "raises the barrier to HAT-PCET self-exchange and increases its nonadiabaticity".<sup>339</sup> Consistent with this notion and the discussions in sections 5.4 and 6.1.4, there is presumably a highly unsymmetrical H-bond in the  $[\text{Os}^{\text{IV}}(\text{Tp})(\text{H})\text{N}^+\text{-HN}(\text{Ph})(\text{H})\text{O}^{\text{II}}]^{\text{+}}$  association complex and a long proton transfer distance. There is a large  $\pi K_{\text{a1}}$  difference of  $\geq 25$  pK<sub>a</sub> units between  $[\text{Os}^{\text{IV}}(\text{Tp})(\text{Cl})_2(\text{NH}_2\text{Ph})]^{\text{2+}}$  and  $[\text{Os}^{\text{IV}}(\text{Tp})(\text{Cl})_2(\text{NH}_2\text{Ph})]^{\text{+}}$ .<sup>339</sup>

### 6.1.6. EPT in Metal Complex PCET

**6.1.6.1.  $\text{Mn}_4\text{O}_4(\text{O}_2\text{PPh}_2)_6$ .** The cluster  $[\text{Mn}_4(\mu\text{-O})(\text{O}_2\text{PPh}_2)_6]^{\text{2+}}$  is reversibly oxidized to  $[\text{Mn}_4(\mu\text{-O})(\text{O}_2\text{PPh}_2)_6]^{\text{3+}}$ . Reduction by phenothiazine (PTZH) in CH<sub>2</sub>Cl<sub>2</sub> gave  $[\text{Mn}_4(\mu\text{-O})(\mu\text{-OH})(\text{O}_2\text{PPh}_2)]^{\text{2+}}$  and PTZ<sup>+</sup>. Reduction of the neutral cluster with PTZ-H gave the same product and PTZ<sup>+</sup>. The two reactions were described as occurring by hydride transfer and H-atom transfer, respectively, but the  $k_{\text{ET}}/k_{\text{EPT}}$  kinetic isotope effect is negligible, and the mechanisms could involve ET-PT.<sup>311,312</sup>

**6.1.6.2. Mn Macrocycles as Superoxide Dismutase Mimics.** In a study of superoxide dismutase (SOD) mimics based on a series of pentazia macrocyclic complexes of Mn, the kinetics of  $\text{O}_2^-$  reduction were studied for the complex shown in eq 136 in its aqua form.<sup>333</sup> This reaction occurs with both acid-dependent and -independent pathways, with the latter attributed to reduction of  $\text{HO}_2^-$  by the aqua form of the complex as shown in eq 136. For this pathway,  $k(\text{H}_2\text{O}/\text{D}_2\text{O}) = 2$ . However, assuming that  $K_{\text{a}}(\text{HO}_2^-)$  is in equilibrium isotope effect comparable to that of acetic acid,

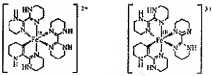
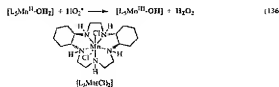
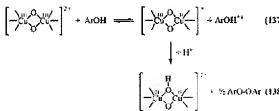


**Figure 34.**  $[\text{Fe}^{\text{IV}}(\text{H}_2\text{bip})_2]^{\text{2+}}$  and  $[\text{Fe}^{\text{IV}}(\text{H}_2\text{bip})_2]^{\text{2-}}$ .



$K_{\text{d}}(\text{HOAc})/K_{\text{d}}(\text{DOAc}) = 3.3$ ,<sup>534</sup> the KIE for the redox step,  $k_{\text{red}}$ , could be  $\sim 6$ . The mechanism was described as HAT, but electron transfer comes from a d-orbital on the metal and the proton from  $\sigma_{\text{O}-\text{H}}$  on the bound water to give d<sup>4</sup> Mn(III) and H<sub>2</sub>O<sub>2</sub>. The elementary step is probably better described as EPT.<sup>533</sup>

**6.1.6.3. Oxidation of Phenols by DiIyoxigen Complexes.** The kinetics of reduction of d<sup>7</sup>[Cu<sup>II</sup>(μ-peroxo)Cu<sup>II</sup>] and Cu<sup>II</sup>(μ-O<sub>2</sub>)<sup>2+</sup> dimers by a series of phenols in acetone at  $-180^{\circ}\text{C}$  have been investigated (Figures 35). The reaction for the Cu(II)-Cu(II) dimer is illustrated in eq 137. In these reactions, ArOH/ArOD  $k_{\text{h}}/k_{\text{D}}$  KIEs were obtained ranging from 1.21 to 1.56.<sup>535</sup>



Linear relationships were found to exist between  $RT \ln k$  and  $-\Delta G$  over a range of  $\Delta G$  values of 0.2 eV (4.6 kcal/mol) with slopes of 0.7 in both cases. Based on these slopes, a mechanism was proposed involving pre-equilibrium electron transfer followed by EPT. In the oxidation of this series of phenols by cumyloperoxy radical under the same conditions, ArOH + PhCMc<sub>2</sub>O<sub>2</sub>· → ArO<sup>+</sup> + PhCMc<sub>2</sub>O<sub>2</sub>H, rate constants were essentially independent of D<sub>A</sub>, consistent with PT-ET.

In the series of copper-dioxxygen adducts shown in Figure 36, electronic structural properties were varied systematically by varying the ligand pyridyl donor substituents with R = H, MeO, and MeN. Detailed mechanistic studies were used to distinguish whether the initial step involved EPT or ET-PT. At low driving forces for ET, ET-PT dominates. At high driving forces, EPT dominates.<sup>536</sup>

In the catalytic oxidative dehydrogenation of 3,5-di-*tert*-butylcatechol and 2-aminophenol by O<sub>2</sub> in the presence of dioximato-cobalt(II), iron(II), and Mn(II) complexes, the rate determining step is H-atom abstraction (EPT) from the phenol by the MO<sub>2</sub> complexes.<sup>537</sup>

## 6.2. EPT in Organic PCET

### 6.2.1. Excited States

**6.2.1.1. Intramolecular Proton Transfer.** Changes in electronic structure induced by proton transfer have been observed in organic excited states that are related to EPT. In a series of α-hydroxy ketones in Figure 37, S<sub>0</sub> → S<sub>1</sub> excitation is followed by internal proton transfer and formation of a high-energy tautomer. Relaxation to the lowest triplet of the tautomer and optical pumping provide a basis for amplified spontaneous emission, lasing action, and an intramolecular proton transfer laser.<sup>538–541</sup>

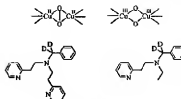


Figure 35. Bridging Cu and ancillary ligand structures L(py); and L(py)·.

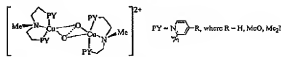


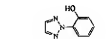
Figure 36. Copper-dioxxygen adducts.



Figure 37. 2-Methyl-3-hydroxychromone.



2-(2-Hydroxyphenyl)benzonitrile (BZT1)



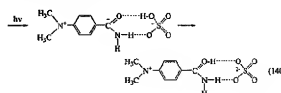
5-(2-Hydroxyphenyl)isoxazole (BZT2)

Similarly, intermolecular proton transfer and tautomerism is observed on concerted double proton transfer have been observed following excitation of pyrrolpyridines. Concerted double proton transfer is illustrated for the 7-azaindole (7-AI) dimer in eq 139.<sup>542–546</sup>



(139)

Intramolecular charge transfer (ICT) dual fluorescence from *p*-dimethylaminobenzamide (DMABA) in acetonitrile is selectively quenched by HSO<sub>4</sub><sup>-</sup>. This may be due to proton transfer in the ICT excited state, eq 140, leading to enhanced nonradiative decay.<sup>547</sup>



Orthohydroxyphenyl benzotriazoles are used as ultraviolet absorbers because their excited states undergo ultrafast nonradiative decay. The decay mechanism involves excited-state intramolecular proton transfer (ESIPT) through a conical intersection.<sup>548–554</sup> Complete active space self-consistent-field (CASSCF) calculations on 2-(7'-hydroxyphenyl)benzotriazole without the fused benzo group, BZT2, reinforce a mechanism involving (1) excitation to give an internal charge transfer state (ICT), (2) intramolecular proton transfer involving twisted geometries, and (3) rapid decay from the keto state following proton transfer (Figure 38).<sup>555</sup>



Figure 39. Benzocouline N-oxide.

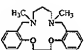
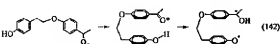


Figure 40. 1,12-Dimethyl-3,4,9,10-dibenzo-1,2-diaza-5,8-dioxacyclopentadecane.

**6.2.1.2. EPT in Gas-Phase Clusters.** Excitation of phenol in small ammonia clusters in the gas phase gives the  $S_1(\pi\pi^*)$  excited state. It undergoes surface crossing to a singlet  $\pi^*$  Rydberg state which is dissociative along the OH coordinate. This state subsequently undergoes EPT to the surrounding ammonia cluster.<sup>346,357</sup>

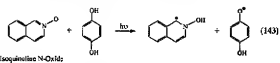
**6.2.1.3 Aromatic Excited State Quenching by Phenols and Hydroquinine.** **6.2.1.3.1. Aromatic Ketones.** Aromatic  $n \rightarrow \pi^*$  carbonyl triplets such as the benzophenone triplet are quenched by phenols. One pathway for quenching is by reduction, eq 141.<sup>358–359</sup> Kinetic isotope effects in 9:1 CH<sub>3</sub>Cl:



CH<sub>3</sub>CN/H<sub>2</sub>O or 9:1 CH<sub>3</sub>CN/D<sub>2</sub>O vary from 1.2 to 4.5 depending on the ketone and the phenol, pointing to HAT at the ketone and EPT at the phenol in the quenching step. Geometrical effects on intramolecular HAT-EPT have also been studied in oxyethyl-linked phenolic ketones; note eq 142.<sup>359,360</sup>

In a closely related study, the quenching of excited-state fluorenone by a series of phenols was investigated in H-bonded pairs in organic solvents.<sup>360</sup> Quenching of both singlet and triplet excited states occurs with rate constants that increase with the reducing ability of the phenol. Energetic arguments based on acidities before and after electron transfer greatly favor EPT as the mechanism and emphasize the importance of H-bonding prior to EPT.<sup>361</sup> HAT (EPT) mechanisms have also been invoked in the quenching of a series of benzophenone triplet excited states by *p*-cresol.<sup>361</sup>

**6.2.1.3.2. *N*-Oxides.** Application of transient absorption and IR monitoring following UV excitation of isoquinoline *N*-oxide and benzocouline *N*-oxide (Figure 39) were used to demonstrate that quenching of their excited triplet states by hydroquinone occurs by EPT, eq 143.<sup>362</sup>

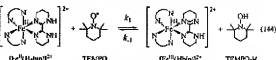


## 6.2.2. Organic Radicals

**6.2.2.1. Correlations with Bond Dissociation Energies and  $\Delta G$ .** In sections 5.2.2 and 5.2.3, mention was made of the extensive correlations that exist for HAT between  $\log k$  and bond dissociation energies. These correlations extend to EPT involving organic radicals, including the oxidation of phenols by *trans*-[Ru<sup>IV</sup>(L)(O)]<sup>2+</sup> (L = 1,12-dimethyl-3,4,9,10-dibenzo-1,2-diaza-5,8-dioxacyclopentadecane, Figure 40),<sup>373</sup> and peroxy radicals<sup>362</sup> and to a Marcus cross-

reaction correlation for a series of EPT, and hybrid HAT-EPT pathways involving metal complexes and organic radicals (section 5.2.2).<sup>363</sup>

**6.2.2.2. Oxidation of TEMPO by [Fe<sup>II</sup>(H<sub>2</sub>bp)<sub>2</sub>(Hbp)]<sup>2+</sup>.** Oxidation of the stable nitroxyl radical TEMPO by [Fe<sup>II</sup>(H<sub>2</sub>bp)<sub>2</sub>(Hbp)]<sup>2+</sup>, eq 144, is an example of a metal complex–radical reaction used in the Marcus correlation described above. Temperature-dependent kinetic measurements in CH<sub>3</sub>CN revealed a negative enthalpy of activation,  $\Delta H^\ddagger = -2.7 \pm 0.4$  kcal/mol,<sup>363</sup> which was rationalized by using a form of the Marcus cross-reaction equation interrelating  $\Delta H^\ddagger$  and  $\Delta H$  for the overall reaction. The large negative  $\Delta S^\ddagger$  value of  $-30 \pm 2$  cal mol<sup>-1</sup> K<sup>-1</sup> was attributed to a spin state change between the Fe(II) and Fe(III) forms of the complex.

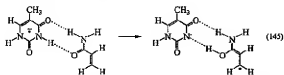


**6.2.2.3. Oxidation of Phenols by Galvinoxyl Radical.** Oxidation of a series of substituted phenols (ArOH) by the stable radical galvinoxyl (GO<sup>•</sup>; note the structure in Figure 10), ArOH + G  $\rightarrow$  ArO<sup>•</sup> + GOH, has been studied in toluene. The rate constant for the reaction with 2,4,4-*terti*-butylphenol (TBP) is solvent-dependent, with  $k$  varying by a factor of 30, decreasing markedly in polar solvents, qualitatively consistent with theoretical predictions (section 5.1). Kinetic isotope effects,  $k_H/k_D$ , of up to  $6.3 \pm 0.3$  were observed for the reactions.<sup>364</sup>

**6.2.2.4. Other Reactions.** The effects of guanyl radical production in plasmid DNA following  $\gamma$ -irradiation have been detected by using an *Escherichia coli* base excision repair endonuclease to convert stable end products to strand breaks. Addition of micromolar amounts of substituted phenols strongly attenuates excision by capturing guanyl radicals. Based on an energetic analysis, it was concluded that capture of the radicals by phenols occurs by EPT.<sup>364</sup> The oxidation of *p*-cresol (*p*-MeC<sub>6</sub>H<sub>4</sub>OH) by the cation radical of 2,4,4-*terti*-butylphenol (Me-Iu<sup>+</sup>) occurs with  $k(H_2O)/k(D_2O) = 2.4 \pm 0.1$ , consistent with EPT.<sup>365</sup>

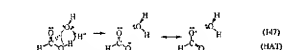
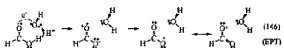
**6.2.2.5. Theory.** **6.2.2.5.1. EPT in Amino Acid Model Compounds.** Quantum chemical calculations based on the density functional theory method B3LYP have been conducted on net HAT reactions involving amino acid model compounds<sup>366</sup> H-bonded to vinyl alcohol and methoxy radicals.<sup>367</sup> Depending on the radical-bridge-acceptor combination, three different mechanisms were identified: (1) proton governed hydrogen transfer, in which a proton is first transferred to a neighboring amino acid residue followed by electron transfer (PT-EET), (2) overlap governed hydrogen transfer (EPT), in which the transferring proton and electron take different paths, and (3) HAT. Intramolecular hydrogen atom migration in amide and peptide radicals also occurs by EPT, based on combined B3LYP-MP2 calculations. These calculations show that the migrating H-atom has negligible spin density and substantial positive charge with electron transfer occurring in parallel through a  $\pi$ -orbital system in the same or opposite direction from proton transfer.<sup>367</sup>

**6.2.2.5.2. Thymine Radical and DNA.** A theoretical study of oxidation within the thymine radical–acrylamide complex, eq 145, and the thymine–DNA radical complex was conducted based on the CASSCF method by using a frequency-resolved cavity model for the solvent. The calculations revealed that the preferred pathway depends on the



surrounding environment. ET dominates for the solvated thymine radical-acyl amide complex, and EPT dominates for the solvated DNA radical complex.<sup>564</sup> The difference in behavior is due to decreased solvent accessibility in the presence of DNA, which alters the relative free energies of the initial ET and EPT products.

**6.2.2.5.3. Other Reactions.** High-level *ab initio* electronic structure calculations have been applied to the gas-phase bimolecular reaction,  $\text{HCOOH} + \text{OH} \rightarrow \text{HCOO}^+ + \text{H}_2\text{O}$ , and to the intramolecular reaction,  $\text{OOCCH}_2\text{OH} \rightarrow \text{HOOCCH}_2\text{O}^+$ . Both are of environmental interest. For both, EPT is a lower energy pathway than HAT. The two mechanisms are illustrated for the bimolecular reaction in eqs 146 and 147. An important factor favoring EPT over HAT is the higher triplet repulsion energy for HAT arising from the unpaired electrons localized on the participating O-atoms.<sup>565</sup>



Oxidation of a series of *o*-, *m*-, *p*-methyl and dimethyl-phenyl derivatives by  $\text{HO}_2^+$  was studied by using the B3LYP functional. The calculations suggest that the phenol-hydroperoxy reactions proceeded by PCET (EPT) rather than H-atom transfer (HAT).<sup>570</sup> Oxidation of phenol by  $\text{HO}_2^+$  occurs by EPT and of tolucene by HAT.<sup>571</sup>

For the self-exchange reaction between  $\text{R}_2\text{C}=\text{NO}^+$  and  $\text{R}_2\text{C}=\text{NOH}$ , DFT calculations reveal a pathway for exchange involving a five-center, cyclic PCET (EPT) pathway. In this pathway, the proton is transferred between electron pairs on the O-atoms and the electron transfers between in-plane orbitals on the N-atoms over a distance of 2.65 Å.<sup>572</sup>

### 6.3. PCET through "Salt Bridges"

The dynamics of excited-state electron transfer within molecular assemblies held together by H-bonding through "salt bridges" have been investigated by laser flash photolysis by Nocera and co-workers.<sup>50,53,573–575</sup> In one series of experiments, laser flash excitation of the Ru(bpy) chromophore shown in Figure 41 was used to access metal-to-ligand charge transfer (MLCT) [Ru<sup>III</sup>(bpy)<sup>4</sup>]<sup>2+</sup> excited states. Excitation was followed by oxidative quenching by nitrobenzene derivatives linked to the chromophore by amidinium-carboxylate H-bonded bridges.

Two types of assemblies were studied, one with the amidinium bound to the Ru(bpy) chromophore shown in Figure 41 as assembly (1), and the other with the amidinium bound to the quencher shown in Figure 41 as assembly (2). Both quenching and back-electron transfer were investigated in  $\text{CH}_2\text{Cl}_2$  at 22 °C with the back-electron transfer step illustrated in Figure 41 for both assemblies.<sup>50,534</sup> The H-bonded assemblies in these cases are favored by two secondary H-bond interactions.<sup>576,577</sup> In these reactions,

excited-state electron transfer across the H-bonded interface creates an organic radical anion which increases the basicity of the acceptor. The resulting changes in local charge distribution couple electron and proton motion when back-electron transfer occurs.

Back-electron transfer is highly favored with  $\Delta G' \sim -2$  eV ( $\sim -46$  kcal/mol) and occurs in the inverted region with  $|\Delta G| > \lambda$ ; note the discussion on the inverted region in section 5.3.4.  $\lambda$  is the sum of the intramolecular and solvent reorganization energies, as discussed in section 4.2.1.

In the inverted region, the rate constant for electron transfer decreases as  $-\Delta G$  increases and the reaction becomes more favorable in contrast to the normal region,  $|\Delta G| < \lambda$ . This result is predicted by both the classical and quantum results in eqs 53 and 73 although they differ in detail. Based on the latter, in the average mode approximation with  $|\Delta G| \gg \Delta\omega$  and  $\hbar\omega \gg k_B T$ ,  $k_{\text{ET}}$  varies with the "energy gap",  $E_0$ , between the initial and final states as shown in eq 148.<sup>567,594,524,463</sup>

$$k_{\text{ET}} \propto \exp \left( \frac{\gamma E_0}{S\eta\omega} \right) \quad (148)$$

$$\gamma = \ln \left( \frac{E_0}{S\eta\omega} \right) - 1 \quad (149)$$

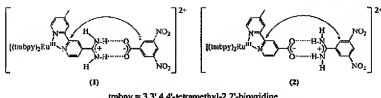
$$|\Delta G| = E_0 + \lambda_{\text{qJ}} \quad (150)$$

The rate constant for back-electron transfer is more rapid by  $\sim 40$  for assembly (1), in which the amidinium part of the interface is oriented toward the reduced dinitrobenzene quencher. The electrostatic effect of the positive charge on the amidinium and the dipole orientation within the H-bond interface stabilize the quencher radical anion by  $\sim 0.37$  eV compared to assembly (2). In assembly (2), the anionic carboxylate group is on the same side as the reduced quencher with the orientation of the interfacial dipole reversed.<sup>574</sup> The dipole stabilization effect in assembly (1) decreases the energy gap (and  $-\Delta G$ ), increasing  $k_{\text{ET}}$  as predicted by eq 148.

A theoretical analysis<sup>565</sup> predicts ET-PCT to be far more rapid than EPT for excited-state quenching in assembly (1) and more rapid by a factor of 30 or more for assembly (2). Similar conclusions were reached in an analysis which included just the bpy ligand and not the Ru(bpy) complex.<sup>496,565</sup> The latter predicts that ET dominates back-electron transfer in assembly (1) and that a mixture of ET and EPT dominates in assembly (2).<sup>568</sup>

Related observations have been made in an amidinium-carboxylate Ru(bpy) assembly with a H-bonded, *p*-dimethylaminole derivative where fast reductive electron transfer quenching occurs following laser flash excitation.<sup>573</sup> In a porphyrin-based study, fast oxidative quenching occurs following laser flash excitation of a Zn(porphyrin)-dinitrobenzene assembly through a carboxylic acid-carboxylic acid H-bonded interface.<sup>578</sup> Electron transfer quenching and subsequent back-electron transfer have also been investigated in a Zn(porphyrin) bound to a naphthalene-dimide acceptor through an amidinium-carboxylate interface. Transient absorption measurements were used to time resolve the quenching and back-electron transfer reactions.<sup>579</sup>

Temperature-dependent isotope effects have been measured for electron transfer from an excited-state  $\text{Zn}(\text{II})$  porphyrin to a naphthalene imide acceptor through an amidinium-carboxylate H-bonded interface. An inverse



tmppy = 3,3',4,4'-tetramethyl-2,2'-bipyridine

Figure 41. Back-electron transfer coupled to proton motion through amidinium-carboxylate salt bridges following oxidative quenching of the Ru(ppy) MLCT excited states in  $\text{CH}_2\text{Cl}_2$  at 22 °C.

kinetic isotope effect with  $k_{\text{H}}/k_{\text{D}} < 1$  was observed at low temperature with  $k_{\text{H}}/k_{\text{D}} = 0.9$  at 120 K increasing to 1.2 at 300 K. The temperature-dependence of the isotope effect was attributed to the influence of bath-induced dynamics on the coordinate of the transferring proton.<sup>586</sup>

#### 6.4. Multiple-Site Electron-Proton Transfer (MS-EPT)

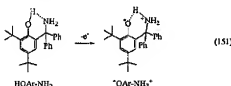
##### 6.4.1. Phenol Quenching of $^3[\text{C}_{60}]$

Flash photolysis studies on the quenching of  $^3[\text{C}_{60}]$  by phenols in the presence of added pyridines show that the quenching products are  $[\text{C}_{60}]^{\cdot-}$ ,  $\text{ArO}^{\cdot}$ , and  $^1\text{H-py}$ , consistent with MS-EPT,  $^3[\text{C}_{60}]\text{ArO}^{\cdot-} \rightarrow \text{C}_{60}^{\cdot-}\text{ArO}^{\cdot-}\text{H}^{\cdot} \text{py}^{\cdot+}$ , eqs 13–15.<sup>438</sup>  $k_{\text{H}}/k_{\text{D}}$  kinetic isotope effects of up to 1.65 ± 0.10 were observed for these reactions.<sup>438,587</sup>

In a closely related study, oxidation of photochemically generated diphenyliodonium radical,  $\text{Ph}_2\text{COH}^{\cdot+}$ , by 1,2,4,5-tetra-*tert*-butylbenzene (TCB) was studied in 1,2-dichloroethane. Direct ET between  $\text{Ph}_2\text{COH}^{\cdot+}$  and TCB,  $\text{Ph}_2\text{COH}^{\cdot+} + \text{TCB} \rightarrow \text{Ph}_2\text{COH}^{\cdot+} + \text{TCB}^{\cdot+}$ , is endergic by 0.4 eV and does not occur. Electron transfer does occur in the presence of the N-bases 2,6-lutidine, 3-chloropyridine, and 2-chloropyridine. These reactions occur by MS-EPT with electron transfer from the ketyl radical to TCB coupled to proton transfer to the H-bonded base,  $\text{TCB} \cdots \text{B} \rightarrow \text{TCB}^{\cdot+} \text{Ph}_2\text{COH}^{\cdot+} \cdots \text{H-B}$ . There is a  $k_{\text{H}}/k_{\text{D}}$  kinetic isotope effect of 3.2 and transient spectroscopic evidence for H-bonding in the lutidine adduct.<sup>588</sup>

##### 6.4.2. An Intramolecular Analogue, Internal MS-EPT

Rhile and Mayer have demonstrated an intramolecular analogue of phenol-pyridine MS-EPT in an amino-derivative, 2,4-di-*tert*-butylphenol, eq 151.<sup>589–594</sup> This phenol undergoes 1 $\text{e}^-$  oxidation to the H-bonded phenoxy radical at a potential of 0.73 V lower than the potential for oxidation of 2,4,6-tri-*tert*-butylphenol. The results of kinetic studies with a series of oxidants are consistent with an elementary step in which electron transfer is coupled to intramolecular proton transfer in a pathway that could be described as *internal MS-EPT*, eq 151.



The results of a related study on electrochemical oxidation of aminophenols, originally interpreted as occurring by ET followed by slow PT,<sup>595</sup> have been reinterpreted as most likely occurring by *internal MS-EPT*.<sup>596</sup>

Figure 42. 2-HO-C<sub>6</sub>H<sub>2</sub>-3,5-(i-Bu)<sub>2</sub>-CONH<sub>2</sub>

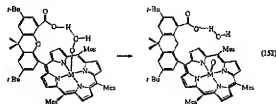
A similar effect may be operative in a series of H-bonded phenols such as 2-HOC<sub>6</sub>H<sub>2</sub>-3,5-(i-Bu)<sub>2</sub>-CONH<sub>2</sub> (Figure 42).<sup>597</sup> Decreased peak potentials for oxidation of the phenols to  $\text{ArO}^{\cdot+}$  were explained by the influence of intramolecular H-bonding in enhancing the acidity of the phenolic proton but is most likely due to the intervention of MS-EPT. Much larger shifts of 0.7–0.11 V were observed for  $\text{ArOH}$  couples H-bonded to amine bases.<sup>588–599</sup>

##### 6.4.3. Proton Activation of Bound $\text{HO}_2^-$

A series of heme-based proteins exists which reacts with oxygen or hydrogen peroxide to generate oxidatively active ferryl ( $\text{Fe}^{\text{IV}}=\text{O}$ ) in their active site cavities; see, e.g., section 7.3.2.<sup>391–395</sup> They play an important role as oxidants (e.g., the family of cytochrome P450 enzymes) and as catalases which catalyze the disproportionation of  $\text{H}_2\text{O}_2$ ,  $\text{H}_2\text{O}_2 \rightarrow \text{H}_2\text{O} + \text{O}_2$ .

Synthetic procedures have been developed for adding a H-bonding scaffold to trimethyl Mn and Fe porphyrins. In the presence of  $\text{H}_2\text{O}_2$ , they display enhanced reactivities toward epoxidation and catalase activity. The key activation step has been suggested to be heterolytic O–O bond cleavage, which occurs by proton-coupled two-electron transfer,  $2\text{e}^-/\text{H}^+\text{EPT}$ , eq 152. In this mechanism, 2 $\text{e}^-$  transfer occurs from Mn(III) or Fe(II) to bound hydroperoxide ( $\text{HO}_2^-$ ), and a proton is transferred from an external H-bond through an appended carboxylic acid. The activation process gives the reactive  $\text{Mn}^{\text{V}}=\text{O}$  or  $\text{Fe}^{\text{IV}}=\text{O}$  groups at the porphyrin core.<sup>595</sup>

An  $\text{O}=\text{Fe}^{\text{IV}}(\text{porph}^{\cdot+})$  intermediate has been observed directly by stopped flow spectroscopic measurements. It was generated by protonation and heterolytic cleavage of bound *m*-chloropropoxybenzoic to give the peroxy intermediate shown in eq 152.<sup>596</sup>



##### 6.4.4. Oxidation of DNA Bases

###### 6.4.4.1. Oxidation by Polypyridyl Complexes.

The kinetics of oxidation of guanine in 2'-deoxyguanosine 5'-

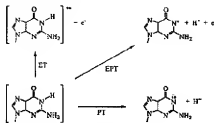


Figure 43. Pathways for guanine oxidation.

triphosphate, double-stranded herring testes DNA, and guanine-containing oligonucleotide hybridized to its Watson-Crick complement, al<sup>1</sup> by [Ru<sup>II</sup>(bpy)<sub>3</sub>]<sup>2+</sup>, were studied in a phosphate buffer at pH = 7 by stopped-flow and electrochemical methods. There were two separate kinetic components involving non-interconvertible forms of the reactants.<sup>311</sup> The pathways for initial proton loss, electron loss, and EPT from guanine are illustrated in Figure 43.<sup>311,312</sup>

Oxidation of the mononucleotide occurred with  $k(\text{H}_2\text{O})/k(\text{D}_2\text{O}) = 1.4$  with  $k(\text{H}_2\text{O})/k(\text{D}_2\text{O}) = 2.1$  for the DNA. Oxidation of guanine by a series of polyoxypyridyl complexes of Fe, Ru, and Os having varying M(III/II) redox potentials,  $E^\circ$ , showed that  $RT \ln k$  increased with  $E^\circ$  with a slope of  $0.8 \pm 0.2$ . A parallel variation with  $-\Delta G = f(E^\circ)(M^{\text{III}}) - E^\circ(\text{guanine}^{\text{radical}})$  presumably exists since the guanine<sup>•+</sup> couple remains constant through the series.

These studies were extended to oxidation of both 7-deazaguanine and 7-deazacaudine, for which plots of  $RT \ln k$  vs  $E^\circ$  were linear with slopes of 2.1 to 2.2. In the oxidations of deoxyguanosine-5-monophosphate (dGMP) and herring testes DNA, plots of  $k$  versus mole fraction D<sub>2</sub>O were linear, consistent with the involvement of a single proton.<sup>311,312</sup>

The large KIE values and mole-fraction-dependencies for these reactions are consistent with EPT in the elementary step. Slopes of plots of  $RT \ln k$  vs  $E^\circ$  that are >0.5 point to participation by vibrational channels,  $\mu = m - v = n$  above  $n = 0$  (section 5.5.4).

Based on these results, it was suggested that the solvent acts as the proton acceptor (solvent-assisted MS-EPT), eq 153. However, in work in progress by Fecenko, it has been

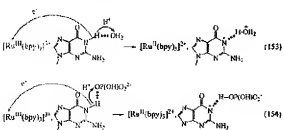
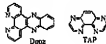


Figure 44. Possible H-bond interactions with the phosphate base buffer component at the primary and secondary amines of guanine.

H<sub>2</sub>O as the base, with PT favored by  $\sim -0.5$  eV ( $\sim 12$  kcal/mol) given the values  $pK_a(\text{H}_2\text{O}) = -1.74$  and  $pK_a(\text{H}_2\text{PO}_4^-) = 7.1$ .

A second, rapid kinetic component was also reported in the oxidation of guanine. Conceivably, it could arise from a parallel MS-EPT pathway with HPO<sub>4</sub><sup>2-</sup> hydrogen bonded to the primary amine rather than the secondary amine (Figure 44). Following MS-EPT at this site, internal PCET would give the more stable secondary amine radical.

**6.4.4.2. Oxidation by MLCT Excited States.** TAP is the acceptor ligand in the lowest MLCT excited state of [Ru<sup>II</sup>(TAP)(dppz)<sup>2+</sup>] (TAP is 1,4,5,8-tetraazaphenanthrene; dppz is dipyrro[3,2-*a*:2',3'-*c*]phenazine). The excited state is a strong oxidant with  $E^\circ = 1.44$  V (vs NHE). It is rapidly quenched by guanosine-5'-monophosphate with  $k(\text{H}_2\text{O})/k(\text{D}_2\text{O}) = 1.7$  in a phosphate buffer at pH = 7,  $k(\text{H}_2\text{O}) = 1.7 \times 10^9 \text{ M}^{-1} \text{ s}^{-1}$ .<sup>397</sup> Based on the isotope effect, it was suggested that oxidation occurs by solvent-assisted MS-EPT with water as the proton acceptor. Given the discussion in the previous section, HPO<sub>4</sub><sup>2-</sup> may be the actual proton acceptor. It is also possible that quenching occurs by EPT with the excited state acting as a  $\text{le}^-/\text{H}^+$  acceptor, eq 155.



Assuming that  $pK_a$  for the reduced complex,  $[\text{Ru}(\text{TAP}^{\text{•}})\text{H}](\text{TAP})(\text{dppz})^{2+}$ , is the same as that for  $[\text{Ru}(\text{bpy})_3](\text{bpz}^2-)\text{H}^+$  (bpz is 2,2'-bipyrimidine and bpz<sup>2-</sup> is 2,2'-bipyrimidine,  $pK_a = 9.2$ , section 2.8.3),  $\Delta G^\circ \sim -0.31$  eV ( $\sim -7.2$  kcal/mol) for EPT in eq 155. This calculation is based on  $E^\circ = 1.44$  V (vs NHE) for the G-H<sup>+</sup> couple and  $pK_a = 3.9$  for the guanine radical cation, G-H<sup>+</sup>.<sup>398</sup>

Similarly, the back-reaction between  $[\text{Ru}^{\text{II}}(\text{TAP}^{\text{•}})\text{H}](\text{TAP})(\text{dppz})^{2+}$  and G-H<sup>+</sup> following quenching occurs with  $k(\text{H}_2\text{O})/k(\text{D}_2\text{O}) = 2.1$  and may also involve EPT or MS-EPT. It has been suggested that oxidation of the ubiquinol analogue 2,3-climethoxy-5-methyl-1,4-benzozquinol (UQH<sub>2</sub>) by the MLCT excited state of  $[\text{Ru}(\text{bpy})_3](\text{pbim})^{\text{•}+}$  (pbim is 2-(2-pyridyl)benzimidazolate anion) occurs by EPT,  $[\text{Ru}^{\text{II}}(\text{bpy})_3](\text{pbim})^{\text{•}+} + \text{UQH}_2 \rightarrow [\text{Ru}^{\text{II}}(\text{bpy})_3](\text{pbim}-\text{H})^{\text{•}+} + \text{UQH}^{\text{•}}$ .<sup>616</sup>

**6.4.4.3. Radical Oxidations.** Related observations have been made by Shafirovich and co-workers in a series of papers concerning electron transfer between DNA base analogues in an aqueous phosphate buffer.<sup>313-318</sup> For example, two-photon ionization of 2-amino-9- $\beta$ -D-ribofuranosylpurine (2Aप) and 2-aminopurine (2Aप') is followed by rapid deprotonation to give the corresponding radicals [2Aप<sup>•-</sup>(H)<sup>•</sup>] or [2Aप'<sup>•-</sup>(H)<sup>•</sup>] (Figure 45). The kinetics of their subsequent reactions with D-deoxyguanosine-5'-monophosphate (dGMP), e.g., [2Aप<sup>•-</sup>(H)<sup>•</sup>] + dGMP  $\sim$  [2Aप<sup>•</sup>] + dGMP<sup>•-</sup>, were followed by transient UV measurements. In these studies,  $k(\text{H}_2\text{O})/k(\text{D}_2\text{O})$  values in the range 1.5–2.0 were observed which led to the suggestion that these reactions occurred by solvent-assisted MS-EPT.<sup>311,313</sup>

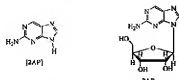
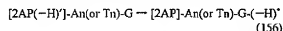
Figure 45. 2-Aminopurine and 2-amino-9- $\beta$ -D-ribofuranosylpurine.

Figure 46. Line structures for the oligonucleotides.

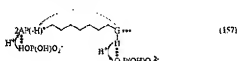
Long-range PCET in the 2-aminopurine–guanine ([2AP]-G) base pair system was subsequently investigated in a series of oligonucleotides with thymidine (T) or adenine (A) spacers.<sup>51–56</sup> Two-photon ionization led to  $[2AP(-H)]^+$  followed by intrstrand PCET, eq 156. The subsequent reaction was monitored by transient UV measurements for both single-strand and duplex, double-strand forms.



In the duplex, oligonucleotides were complexed with their complementary strands. The duplex structures were used to avoid possible looping mechanisms with electron transfer occurring by outer-sphere, intrstrand electron transfer. Line structures indicating the sequence of bases investigated with the number of adenine (A) and thymine (T) spacers used in one study are shown in Figures 46.<sup>51</sup>

From kinetic measurements in  $H_2O$  and  $D_2O$ ,  $k(H_2O)/k(D_2O) = 1.3–1.7$ . At the multiangstrom distance over which intrstrand electron transfer occurs in these oligonucleotides, EPT is not a feasible pathway because of the short-range nature of proton transfer (sections 5.3 and 5.4).

Although not proposed in the original reference, this reaction may occur by the  $1e^-/2H^+$  multiple-site-EPT pathway illustrated in eq 157. In this pathway, long-range



electron transfer is coupled to two spatially separated proton transfers. The proton transfers occur with the separate phosphate buffer components H-bonded to the electron transfer donor and acceptor sites. Related pathways may also play a role in oxidative activation of the oxygen evolving complex of Photosystem II by tyrosine radical  $Y_2^{\cdot+}$  (section 7.2.4).

Related pathways and ambiguities exist in related chemical reactions. For example, quenching of the benzophenone triplet by diethylaniline or triethylamine occurs by ET-PT. Initial electron transfer is followed by proton transfer to reduced benzophenone from either the oxidized amine or an added proton source.<sup>59</sup>

#### 6.4.5. pH-Dependent MS-EPT with Solvent as the Proton Acceptor?

Oxidative quenching of the Ru-bpy-tyrosine assembly in Figure 47 by methyl viologen cation,  $MV^{2+}$ ,  $[Ru^{II}(bpy)_3]^+$

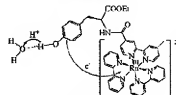
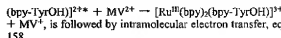


Figure 47. Proposed solvent-assisted MS-EPT in the oxidation of the linked tyrosine in  $[Ru^{II}(bpy)_3(bpy\text{-}TyOH)]^{2+}$ . See text. Reprinted with permission from ref 495. Copyright 2003 American Chemical Society.

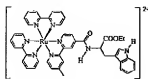


As shown by laser flash photolysis measurements in  $NaH_2PO_4$  or  $NaH_2BO_3$  buffers,  $k_{int}$  is pH-dependent over a wide pH range.<sup>58,601–603</sup>  $\log k_{int}$  was found to increase linearly with  $[OH^-]$  up to  $pH = 10$ , where the dominant form of the complex becomes  $[Ru^{II}\text{-TyrO}^-]^{2+}$  ( $pK_a(\text{TyrOH}) = 10$ ).  $[Ru^{II}\text{-TyrO}^-]$  undergoes rapid, pH-independent intramolecular electron transfer,  $[Ru^{II}\text{-TyrO}^-] \rightarrow [Ru^{II}\text{-TyO}^{\cdot-}]$ , with  $k \approx 5 \times 10^9 \text{ s}^{-1}$ . The rate acceleration is expected given the decrease in  $E^\circ$  for the  $\text{TyrO}^-/\text{TyO}^{\cdot-}$  couple (0.72 V vs NHE) compared to  $\text{TyO}^{\cdot-}/\text{TyOH}$  (1.34 V).<sup>58,603,605,597</sup> Oxidation of  $[Ru^{II}\text{-TyrOH}]^{2+}$  is kinetically independent of  $[Ru^{II}\text{-TyrO}^-/\text{TyO}^{\cdot-}]^{2+}$  because proton loss from  $[Ru^{II}\text{-TyrOH}]^{2+}$  is slow compared to the time scale for electron transfer.

The pH-dependence of electron transfer within  $[Ru^{II}\text{-TyrOH}]^{2+}$  was explained by invoking the reaction in eq 158 as an elementary step. In this analysis, the driving force was assumed to increase with pH as  $\Delta G^\circ = -F(E^\circ(Ru^{IIH}) - E^\circ(\text{TyOH}^-) - 0.059(\text{pH} - pK_a(\text{TyOH}^-)))$  with  $F$  the Faraday constant (1 eV in SI units) and  $pK_a(\text{TyOH}^-) = -2.8,603,604$ . This pathway was analyzed theoretically by Hannes-Schiffer and co-workers, who accounted for the pH-dependence through its influence on  $\Delta G^\circ$ .<sup>605</sup> They also found that the increased electron transfer reactivity for  $[Ru^{II}\text{-TyrO}^-/\text{TyO}^{\cdot-}]^{2+}$  compared to  $[Ru^{II}\text{-TyrOH}]^{2+}$  was due to a smaller  $\lambda_m$  and the rate diminution for  $[Ru^{II}\text{-TyrOH}]^{2+}$  was due to the small degree of vibrational overlap for proton transfer to solvent.

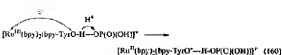
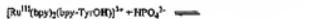
Given the discussion in section 5.5.4, this interpretation of the pH-dependence raises significant questions. The elementary step proposed is not the solvent-assisted MS-EPT step shown in Figure 47 with a  $H_2O$  molecule or localized water cluster acting as the proton acceptor. Following the analysis of Krishnamoorthy, sections 5.5.3 and 5.5.4, if it were, the driving force would be independent of pH with  $\Delta G$  fixed at  $G_c$  (eV)  $\sim 0.08–0.09(pK_a(H_2O) - pK_a(\text{TyOH}^-)) = 0.04 \text{ eV}$  (0.9 kcal/mol). In this analysis, the pH-dependence for the reaction in eq 158 arises from the dilution of  $H_2O^+$  after EPT occurs with  $\Delta G_c$  (eV)  $= 0.059(pK_a(H_2O^+) - \text{pH})$ ; note eqs 115–117. As noted in section 5.5.4, the EPT step is independent of pH because there is no microscopic basis for coupling an elementary step in which a proton is lost to the surrounding ensemble of solvent, protons, buffer, etc. that define the final equilibrium state.

Other possible interpretations have been considered by Hammarström and co-workers and ruled out. A PT-ET

Figure 48. Structure of  $[\text{Ru}^{II}(\text{bpy})_3(\text{bpy-Typr})]^{2+}$ .

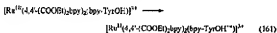
mechanism with initial proton transfer to  $\text{OH}^-$ ,  $[\text{Ru}^{III}-\text{TyrOH}]^{4+} + \text{OH}^- \rightarrow [\text{Ru}^{III}-\text{TyrO}^{2-}]^{3+} + \text{H}_2\text{O}$ , followed by rapid electron transfer,  $[\text{Ru}^{III}-\text{TyrO}^{2-}]^{3+} \rightarrow [\text{Ru}^{II}-\text{TyrO}^{2-}]$ , was ruled out because, at the low concentrations of hydroxide in these experiments, proton transfer is too slow to explain the data.<sup>519,520,604</sup>

The oxidation of  $\text{TyrOH}$  by  $[\text{Os}(\text{bpy})_3]^{4+}$  in phosphate buffer (section 5.5.4.3) provides an "untheorized" analogue of the reaction in eq 158. In this mechanism, eqs 123 and 124, a pH-dependence arises indirectly by participation of the basic form of the buffer ( $\text{HPO}_4^{2-}$  or  $\text{HBO}_3^{2-}$ ) as the proton acceptor, eqs 159 and 160. Although there is evidence for



such a pathway at high buffer concentrations,<sup>606</sup> it does not account completely for the results reported earlier, and a significant issue remains in interpreting the pH-dependence microscopically. pH-dependent oxidation of bpy ligands has been well documented for  $[\text{Ru}(\text{bpy})_3]^{2+}$  and related polypyridyl complexes but is too slow to explain the results.<sup>607,608</sup>

The studies of PCET in light-driven intramolecular electron transfer were extended to two additional assemblies. In one, the bpy ligands in the structure in Figure 47 were replaced by the diester-bpy ligand 4,4'-(COOEt)<sub>2</sub>bpy, which increases  $E^\circ$  for the  $\text{Ru}(\text{III}/\text{II})$  couple from 1.26 to 1.53 V. With the increased driving force for electron transfer, direct oxidation of  $\text{TyrOH}$  was observed, eq 161.<sup>604</sup> For this pathway,  $k(\text{H}_2\text{O})/k(\text{D}_2\text{O}) = 2$ .

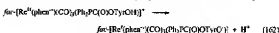


A pH-dependent pathway was also observed for this complex having the same pH-dependence as intramolecular oxidation of  $[\text{Ru}^{II}(\text{bpy})_3(\text{bpy-TyprOH})]^{2+}$ . For the pH-dependent pathway,  $k(\text{H}_2\text{O})/k(\text{D}_2\text{O}) > 10$ , pointing to the importance of EPT in the rate limiting step.

For appended tryptophan in  $[\text{Ru}^{II}(\text{bpy})_3(\text{bpy-Typr})]^{2+}$  (Figure 48), deprotonation of the tryptophan radical cation ( $pK_a = 4.7$ ) is observed following intramolecular electron transfer,  $[\text{Ru}^{II}(\text{bpy})_3(\text{bpy-Typr})]^{2+} + \text{H}_2\text{O} \rightarrow [\text{Ru}^{II}(\text{bpy})_3(\text{bpy-Typr})]^{2+} + \text{H}_3\text{O}^{+}$ .<sup>604</sup>

Nocera and co-workers have reported similar pH-dependent intramolecular electron transfer events following laser flash photolysis of  $\text{f}_{67}\text{C}(\text{Phen})(\text{CO})(\text{Ph}_3\text{PCo})(\text{O}^-\text{TyprOH})$ .<sup>4</sup> In this assembly, the  $\text{Re}^6(\text{phen}^-)$  MLCT excited state is a stronger oxidant, and intramolecular electron transfer occurs directly from  $\text{TyrOH}$  to the excited state, eq 162.<sup>609</sup> Intramolecular electron transfer is pH-dependent with the pH-dependence also attributed to the pH-dependence of  $\Delta G^\circ$ .

as for the reaction in eq 158. It is unclear whether or not buffer effects and MS-EPT played a role in this study.



## 6.5. EPT on Surfaces

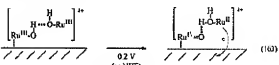
The role of PCET at surfaces, either at surface sites or at linked molecules, was discussed in section 2.6. Evidence has also been found for EPT pathways at both types of electrode surfaces. The appearance of PCET at surface sites typically occurs following activation pretreatments that create O-based surface functional groups.

### 6.5.1. Adsorbed Molecules

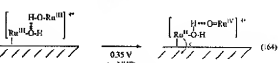
6.5.1.1.  $[\text{Ru}^{II}(\text{tpy})(4,4'-(\text{PO}_3\text{H}_2)_2\text{bpy})(\text{H}_2\text{O})]^{2+}$  on ITO. As discussed in section 2.6.2,  $[\text{Ru}^{II}(\text{tpy})(4,4'-(\text{PO}_3\text{H}_2)_2\text{bpy})(\text{H}_2\text{O})]^{2+}$  (the ligand structure is shown in Figure 12) adsorbs to optically transparent Sn(IV)-doped  $\text{In}_2\text{O}_3$  (ITO) electrodes. Surface coverage effects were observed with the  $[\text{Ru}^{IV}=\text{O}]^{2+}/[\text{Ru}^{II}\text{OH}]^{2+}$  couple only appearing at complete monolayer coverages,  $\Gamma = 0.8 \times 10^{-10} \text{ mol/cm}^{-2}$ .<sup>106</sup>

Direct oxidation of  $[\text{Ru}^{II}\text{OH}]^{2+}$  to  $[\text{Ru}^{IV}=\text{O}]^{2+}$  occurs at  $E_{1/2} \approx 1.6 \text{ V}$  (vs NHE), past the solvent limit. The appearance of the  $\text{Ru}(\text{IV}/\text{III})$  wave due to enhanced surface coverage was explained by invoking "cross-surface" EPT,  $2[\text{Ru}^{II}\text{OH}]^{2+} \rightarrow [\text{Ru}^{IV}=\text{O}]^{2+} + [\text{Ru}^{II}\text{OH}_2]^{2+}$ , analogous to the solution reaction in eq 12. It is followed by oxidation of  $[\text{Ru}^{II}\text{OH}_2]^{2+}$  and rapid proton loss from  $[\text{Ru}^{II}-\text{OH}_2]^{2+}$ . Proton inventory experiments (section 5.5.2) suggest a  $\text{H}_2\text{O}/\text{D}_2\text{O}$  KIE as large as  $\sim 60$  in pure  $\text{D}_2\text{O}$ , pointing to restricted motion and a longer proton transfer distance on the surface compared to in solution.<sup>106</sup>

The  $\text{Ru}(\text{IV}/\text{III})$  wave appears even on partially loaded surfaces if catalytic amounts of  $[\text{Ru}^{II}(\text{tpy})(\text{bpy})(\text{H}_2\text{O})]^{2+}$  ( $2 \mu\text{M}$ ) are added to the external solution. Similarly, catalysis of the solution  $[\text{Ru}^{IV}(\text{tpy})(\text{bpy})(\text{O})]^{2+}/[\text{Ru}^{II}(\text{tpy})(\text{bpy})(\text{H}_2\text{O})]^{2+}$  couple occurs by disproportionation to give adsorbed  $[\text{Ru}^{II}(\text{tpy})(4,4'-(\text{PO}_3\text{H}_2)_2\text{bpy})(\text{H}_2\text{O})]^{2+}$  followed by its oxidation to  $\text{Ru}(\text{III})$ . The proposed EPT surface pathways are illustrated in eqs 163 and 164.<sup>610</sup>



Solvation-Surface EPT



Surface-Solvation EPT

6.5.1.2. *Cis* and *Trans* Isomers of  $[\text{Ru}^{II}(\text{tpy})(4-(\text{PO}_3\text{H}_2)_2\text{4'-Mebpy})(\text{H}_2\text{O})]^{2+}$  and Cross-Surface EPT. As can be seen in Figure 49, when bound to ITO, there are isomers of  $[\text{Ru}^{II}(\text{tpy})(4-(\text{PO}_3\text{H}_2)_2\text{4'-Mebpy})(\text{H}_2\text{O})]^{2+}$ . They differ in the positions of the phosphonate group (*cis* vs *trans*) relative to the  $\text{Ru}-\text{OH}_2$  axis. The redox properties of the surface  $[\text{Ru}^{II}-\text{OH}]^{2+}/[\text{Ru}^{II}-\text{OH}_2]^{2+}$  couple on ITO are nearly superimposable with the corresponding solution couple independent of surface coverage. On fully loaded surfaces with monolayer coverages, there is evidence for catalysis of the  $[\text{Ru}^{IV}=\text{O}]^{2+}/$

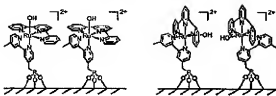


Figure 49. Proposed surface structures for the adsorbed *trans* and *cis* isomers of  $[\text{Ru}^{\text{II}}(\text{bpy})(4-(\text{P}(\text{O})_3\text{H}_2)-4'\text{-M(bpy)})(\text{H}_2\text{O})]^{\text{2+}}$ .

$[\text{Ru}^{\text{II}}-\text{OH}]^{\text{2+}}$  wave by cross-surface EPT but only for the *cis* isomer.<sup>411</sup>

6.5.1.3.  $[\text{Os}^{\text{III}}(\text{bpy})_2(4\text{-pyCH}_2\text{NH}_2)(\text{H}_2\text{O})]^{\text{2+}}$  Tethered to Au. The complex  $[\text{Os}^{\text{III}}(\text{bpy})_2(4\text{-pyCH}_2\text{NH}_2)(\text{H}_2\text{O})]^{\text{2+}}$  was attached by amide coupling to a mixed surface containing  $11\text{S}(\text{Cl})_{12}\text{OH}$  (12-mercaptoodecanoic acid) and  $\text{HS}(\text{CH}_2)_{10}\text{CO}_2\text{H}$  (16-mercaptohexadecanoic acid) on gold bead electrodes. Electrochemical measurements of  $[\text{Os}^{\text{III}}-\text{OH}]^{\text{2+}}$  oxidation and  $[\text{Os}^{\text{III}}-\text{OH}]^{\text{2+}}$  reduction gave asymmetrical Tafel plots, pH-independent rate constants, and transfer coefficients and were inconsistent with an ET-PT mechanism.<sup>412</sup>

### 6.5.2. Oxidative Activation of Carbon Electrodes

Typical electrode materials are conductive and chemically inert, providing stable interfaces for electron transfer. In the absence of special structural features, these surfaces are unable to participate in complex pathways such as EPT. This can result in slow reactions, large overvoltages, and electrochemical irreversibility (section 4.3.1).<sup>63,64</sup> Procedures have been developed for "activating" graphite,<sup>61,64</sup> or glassy carbon electrodes based on plasma treatments in an oxygen atmosphere, chemical or electrochemical oxidation,<sup>65–69</sup> or addition of adsorbed aromatics containing catechol functionalities.<sup>62,66–68</sup> These modifications can dramatically enhance the electrochemical response for PCET reactions.

Oxidative activation gives phenolic and quinoidal groups on the surface, as shown by XPS measurements.<sup>61,68</sup> They can enable EPT, as shown, for example, by the surface catalyzed oxidation of reduced nicotinamide adenine dinucleotide (NADP) at an activated glassy C electrode.<sup>65</sup> Surface activation has also been used to enhance electrochemical responses for metal complex aqua couples such as  $[\text{Ru}(\text{NH}_3)_6(\text{H}_2\text{O})]^{\text{2+}}$ <sup>62</sup> and *cis*- $[\text{Ru}^{\text{II}}(\text{bpy})_2(\text{H}_2\text{O})_2]^{\text{2+}}$ , note Figure 5.<sup>69,70</sup>

The impact of surface activation on the electrochemical oxidation of catechol in eq 165 is shown in Figure 50. As the extent of surface activation is increased, a transition occurs from two overlapping, 1e<sup>-</sup> irreversible waves to a single, reversible 2e<sup>-</sup>/2H<sup>+</sup> wave. All catalyzed surface waves display significant H<sub>2</sub>O/D<sub>2</sub>O KIEs.<sup>69</sup>

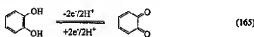


Figure 50. Cyclic voltammograms vs SSCE of solutions containing catechol, eq 165, in 0.1 M  $\text{H}_2\text{SO}_4$  following surface activation periods of 0 min (A), 2 min (B), 12 min (C), and 28 min (D). The scan rate is 100 mV/s.<sup>69</sup>

EPT, and H-bond adduct formation between Os(V) and a phenolic O–H.<sup>62</sup>

Related effects have been observed on other electrode surfaces. On TiO<sub>2</sub> (In<sub>2</sub>O<sub>3</sub>:Sn(IV)), Thorp *et al.* have reported significant pH effects on the potential–current waveforms for the Mn(IV)–Mn(III)/Mn(III)–Mn(II) couple of  $[(\text{bpy})_3\text{Mn}(\mu\text{-O})_2\text{Mn}(\text{bpy})_2]^{\text{1+}}$  and the Ru(IV/III) couple of  $[\text{Ru}(\text{py})^2(\text{bpy})(\text{H}_2\text{O})]^{\text{2+}}$ . Raising the pH to 7 greatly improves resolution of the waves and decreases peak-to-peak separations in cyclic voltammograms.<sup>111</sup>

Electrochemical oxidation of a series of alcohols and amines at oxide coated Ni, Ag, Cu, and Co anodes has been investigated with evidence found for H-atom abstraction by surface oxide sites. At a Ni anode, there is a KIE of 7.0 for oxidation of  $\text{CH}_3\text{OH}$  compared to  $\text{CD}_3\text{OH}$ .<sup>69</sup>

### 6.5.3. EPT at Electrodes

In  $\text{CH}_3\text{Cl}$  and DMF in the presence of water,  $\text{O}_2$  is initially reduced to  $\text{O}_2^-$ . A second wave appears in cyclic voltammograms for further reduction of  $\text{O}_2^-$ . The latter occurs with a transfer coefficient, the symmetry factor  $\alpha$ , much smaller than the value 0.5 typically found for outer-sphere electron transfer. Reduction at the electrode was proposed to occur by solvent-assisted MS-EPT,  $\text{O}-\text{O}^- \cdots \text{H}-\text{OH} + \text{e}^- \rightarrow \text{O}-\text{O}-\cdots\text{OH}^-$ .<sup>42</sup> A related pathway involving pre-protonation may be operative in the reduction of the anion radical of the orthoquinone 3,5-di-*tert*-butyl-1,2-benzoquinone in the presence of weak acids.<sup>43</sup>

A theory has been developed to account for EPT in electrochemical reactions with an expression derived for the electrochemical rate constant as a function of the applied electrode potential.<sup>42</sup> In this theory, key factors are the solvent and intramolecular reorganization energies for both electron and proton transfer and the pre-exponential factor, which includes proton tunneling. For the reduction of  $\text{O}_2$  mentioned above, the small value of the transfer coefficient observed was attributed to a pre-exponential factor decreased in magnitude due to the requirement for vibrational wave function overlap.

Surface catalysis of the Os(IV/V) hydrazido couple of *trans*- $[\text{Os}^{\text{IV}}(\text{tpy})(\text{Cl})_2(\text{N}(\text{H})\text{N}(\text{CH}_2)\text{O})]^{\text{2+}}$  (section 6.1.4) occurs at oxidatively activated glassy carbon electrodes. Activation induces both catalysis and strong surface binding, with the latter reminiscent of H-bond complex formation with quinone prior to EPT in eq 129 or surface activation by adsorbed catechols.<sup>62,66–68</sup> The proposed mechanism includes surface adduct formation by H-bonding, surface-solution

## 7. PCET in Biology

### 7.1. Introduction

PCET is common in biology. Vital reactions, such as nitrogen fixation, water oxidation in Photosystem II, and respiration, all involve multiple-electron, multiple-proton changes. A molecular level understanding of how these reactions occur is emerging from X-ray structures, spectroscopy, theory, mechanism, and site-directed mutagenesis. Recent results combining molecular structure with density functional theory (DFT) have been especially revealing.<sup>52,53,60–63</sup> With the insight gained in these studies, it is becoming apparent that EPT, especially multiple-site-EPT (MS-EPT), plays an essential role mechanistically.

The goal of this section is to focus on selected examples where EPT has been invoked, with a special emphasis on Photosystem II and the light driven oxidation of water.

### 7.2. PCET in Photosystem II

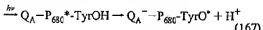
#### 7.2.1. Introduction

Photosystem II (PSII) is a multi-polypeptide complex found in thylakoid membranes of chloroplasts. Plants and algae use water as the electron donor in the photochemical oxidation of water to oxygen, eq 166. In green plants, electrons produced in this reaction reduce a quinone to hydroquinone, transferring reductive equivalents to Photosystem I, where they enter the Calvin cycle for reduction of  $\text{CO}_2$ . Photosystem II turns over rapidly, producing up to 50 molecules of  $\text{O}_2$  per second.<sup>54,55,27,28,63,64</sup>



A great deal has been learned about reactivity<sup>54,55,27,51,179,381,634,644–647</sup> and mechanism in Photosystem II.<sup>55,60–61</sup> The structure has been determined to 3.0 Å resolution.<sup>53,62</sup> Oxidation of  $\text{H}_2\text{O}$  is triggered by light absorption by antenna pigments and sensitized excitation of chlorophyll  $\text{P}_{680}$ .  $\text{P}_{680}$  consists of  $\text{Chl}_{\text{D}1}$  and  $\text{Chl}_{\text{D}2}$ , with  $\text{Chl}_{\text{D}2}$  acting as an antenna fragment.

Following excitation of  $\text{P}_{680}$ , the  $\text{P}_{680}^*$  excited state undergoes long-range electron transfer (10.6 Å) through a pheophytin bridge ( $\text{Pheo}_{\text{D}1}$  in Figure 51) to bound plastocyanin,  $\text{Q}_\text{A}$ , to create a  $\text{P}_{680}^*-\text{Q}_\text{A}^+$  redox-separated pair. Light-driven electron transfer is followed by rapid ( $\mu\text{s}$  to  $\text{ns}$ ) electron transfer from tyrosine Tyr161 on the D1 polypeptide ( $\text{Y}_2$ ) to  $\text{P}_{680}^*$ , giving the neutral tyrosine radical,  $\text{Y}_2^{\cdot-}$ , with release of a proton, eq 167. The structure of the excited state-electron transfer array, including the close proximity of  $\text{Y}_2$  to the oxygen evolving complex (OEC), is shown in Figure 51, which is taken from refs 383 and 662.



Oxidation of  $\text{Y}_2$  to  $\text{Y}_2^{\cdot-}$  is essential in extending the separation distance between the photochemically produced oxidative and reductive equivalents. This increases the time scale for back-electron transfer from the 200  $\mu\text{s}$  time scale for  $\text{Q}_\text{A}^{\cdot-} \rightarrow \text{P}_{680}^*$  back-electron transfer, avoiding loss of the transiently stored redox equivalents.

In a following step,  $\text{Y}_2^{\cdot-}$  oxidizes the OEC. The OEC contains a 4Mn cluster with  $\text{Ca}^{2+}$  and  $\text{Cl}^-$  as cofactors. In order to release  $\text{O}_2$ , the OEC undergoes four sequential light absorption-electron transfer cycles coupled with loss of four

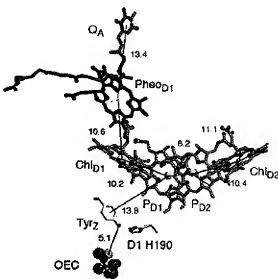


Figure 51. Molecular structure of the reaction center of Photosystem II illustrating the  $\text{Y}_2-\text{Chl}_{\text{D}1}-\text{Chl}_{\text{D}2}(\text{Pheo}_{\text{D}1})-\text{Pheo}_{\text{D}1'}-\text{Q}_\text{A}$  donor-chromophore-acceptor ( $\text{D}-\text{C}-\text{A}-\text{A}'$ ) array and the proximity of  $\text{Y}_2$  to the oxygen evolving complex (OEC). Reprinted with permission from ref 383 (<http://www.sciencemag.org>). Copyright 2004 AAAS.

protons. The sequence of photochemically induced transitions between states from  $\text{S}_0$  to  $\text{S}_4$  is known as the Kok cycle, with the subscripts identifying the number of electrons lost.<sup>63</sup>

$\text{S}_0$  is the stable resting state in the dark.  $\text{S}_0$ ,  $\text{S}_1$ ,  $\text{S}_2$ , and  $\text{S}_3$  all have been trapped in high yield by a variety of chemical and physical manipulations and stabilized by rapid freezing in the dark.<sup>604–608</sup> Recently, spectroscopic evidence has been obtained for an intermediate, postulated to be  $\text{S}_4$ , by measurements under high partial pressures of  $\text{O}_2$ .<sup>639</sup> Additional evidence for transient behavior has come from application of transient X-ray absorption spectroscopy (XAS) to the K edge for Mn on the 10  $\mu\text{s}$  time scale.<sup>670</sup>

Based on X-ray absorption near edge spectroscopy (XANES), the oxidation state distributions in the  $\text{S}$  states are thought to be  $\text{Mn}(\text{II})-\text{Mn}(\text{III})-\text{Mn}(\text{V})-\text{Mn}(\text{IV})$  for  $\text{S}_0$  and  $\text{Mn}(\text{II})-\text{Mn}(\text{III})-\text{Mn}(\text{IV})-\text{Mn}(\text{V})$  for  $\text{S}_1$ .<sup>53,61,62,63,641</sup> This conclusion is in agreement with  $\text{K}\beta$  XES data<sup>670,612,633</sup> and with  $^{55}\text{Mn}$  ENDOR spectra of  $\text{S}_2$ .<sup>633</sup> The presence of  $\text{Mn}^{\text{II}}$  in  $\text{S}_0$  has been questioned recently based on low-temperature electron-spin-lattice relaxation measurements.<sup>634</sup>

Activation energies for the four steps in the Kok cycle range from  $E_a = 0.05$  to 0.4 eV (1–9 kcal/mol), rate constants vary from  $10^3$  to  $10^5 \text{ s}^{-1}$ , and  $k(\text{H}_2\text{O})/k(\text{D}_2\text{O})$  kinetic isotope effects of 1.2–2.9 have been measured.<sup>379,645,648</sup> Oxidation of  $\text{S}_3$  occurs through  $\text{S}_4$  as a transient, which does not build up, giving  $\text{S}_2$  and  $\text{O}_2$  instead. In membrane-containing samples, 1.00–1.75 protons are released in the  $\text{S}_0 \rightarrow \text{S}_1$  transition, depending on pH, with the higher number observed at lower pH. Proton changes in  $\text{S}_0 \rightarrow \text{S}_1$  appear to correlate inversely with  $\text{S}_1 \rightarrow \{\text{S}_2\} \rightarrow \text{S}_3$ .<sup>636</sup> The overall proton release patterns depend somewhat on sample type and pH. In intact samples, the proton release pattern appears to be 1:0:1:2 although a pattern of 1:1:1:1 has been observed with spinach core particles.<sup>637</sup>

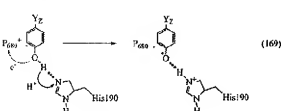
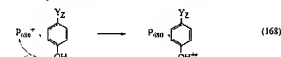
In PSII, there are two redox-active tyrosines,  $\text{Y}_2$  and  $\text{Y}_{\text{D}2}$ . Each is oxidized by  $\text{P}_{680}^*$  to form a phenoxy! radical with

$Y_2$  oxidized more rapidly.  $Y_2$  can be selectively oxidized photochemically at 1.8 K in PSII enriched membranes with  $Y_2'$  detected by EPR. Warming the samples to 77 K results in a relaxation process leading to a stable form of the radical.<sup>688</sup> Based on the results of 2H ESEEM (electron spin-echo envelope modulation spectroscopy), both  $Y_2'$  and  $Y_2''$  appear to be coordinated by two H-bonds.<sup>689</sup>

In PSII-containing particles isolated from several D<sub>1</sub>-His190 mutants in the cyanobacterium *Synechocystis* sp. PCC 6803, rate constants for oxidation of  $Y_2$  by  $P_{680}^{+}$  are decreased dramatically, and  $Q_A^{+} \rightarrow P_{680}^{+}$  back-electron transfer dominates; note Figure 51. Addition of imidazole and other small organic bases greatly accelerates  $P_{680}^{+}$  oxidation of  $Y_2$ . These results are consistent with D<sub>1</sub>-His190 acting as the immediate  $Y_2$  proton acceptor with the transferred proton bound to His190 during the lifetime of  $Y_2''$ .<sup>690</sup>

### 7.2.2. Possible Role for MS-EPT in the Oxidation of $Y_2$ by $P_{680}^{+}$

As suggested by Babcock and co-workers and by Krishnamoorthy, both the formation of  $Y_2''$  and subsequent oxidation of the OEC appear to utilize EPT pathways in order to avoid high-energy intermediates.<sup>24,25,27,306–309,379,646,652,691–693</sup> Oxidation of  $Y_2$  by  $P_{680}^{+}$  by electron transfer, eq 168, occurs with  $\Delta G^{\circ} \sim +0.08 \text{ eV}$  based on the recently revised estimate of  $E^{\circ}(P_{680}^{+})^{694} = 1.26 \text{ V}$  (vs NHE).<sup>691,692</sup> By contrast, MS-EPT with electron transfer from  $Y_2$  to  $P_{680}^{+}$  and proton transfer to histidine 190, eq 169, is exergoergic with  $\Delta G^{\circ} \sim -0.36 \text{ eV}$  ( $\sim -8.4 \text{ kcal/mol}$ ) although this estimate is based on solution values for  $pK_a(H^+ \text{-His})$  ( $\approx 5.5$ ) and  $E^{\circ}$  for the tyrosine couple.<sup>693</sup> The lower barrier for MS-EPT with  $P_{680}^{+}$  as the electron acceptor may be critical since, as noted above, this step is in competition with  $Q_A^{+} \rightarrow P_{680}^{+}$  back-electron transfer, which occurs on a time scale of 200  $\mu\text{s}$ . The microscopic involvement of MS-EPT is also consistent with a  $\text{H}_2\text{O}/\text{D}_2\text{O}$  kinetic isotope effect of 3.64 at  $p\text{H} = 7$  and the implied requirement for a nitrogen base as shown by the mutant results described in the previous section. There is evidence for single proton involvement in a Mn-depleted PSII core complex isolated from a site-directed mutant.<sup>690,695</sup>



### 7.2.3. Oxidation of the OEC by $Y_2'$

**7.2.3.1. Structure.** The structure of Photosystem II from *Thermosynechococcus elongatus*, presumably in S<sub>1</sub>, which is the stable resting state in the dark, has been determined recently to 3  $\text{\AA}$ <sup>692</sup> and 3.5  $\text{\AA}$  resolution.<sup>382</sup> In Figure 52 is shown a modified version of one stereoview of the 3.5  $\text{\AA}$  structure taken from ref 650. In this version, the original 3.5  $\text{\AA}$  structure<sup>383</sup> was modified to include possible coordination details around Ca and the Mn(3) and Mn(4) cluster sites.

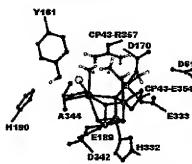


**Figure 52.** Structure of the PSII OEC from reference 383 with reprinted permission as modified in reference 650. Copyright 2004 Science and 2004 American Chemical Society. Elements are colored as follows: C, dark gray; O, red; N, dark blue; Mn, purple; Ca, green. Hydrogen atoms are not included in the published structure. Numbering of amino-acid residues is in accord with the sequences of *Thermosynechococcus elongatus*, the organism from whose protein the crystal structure was derived, with the abbreviations D for aspartate, E for glutamate, H for histidine, and A for alanine. The residues shown belong to the D1 subunit of PSII. Those bound to the Mn ions are shown as truncated side-chains except for C-terminal D<sub>1</sub>-Ala144, which is shown in its entirety. The two water ligands proposed to act as substrates in water oxidation are labeled with asterisks.

Suggested positions of H-atoms on the side chains of D<sub>1</sub>-Tyr161 ( $Y_2'$ ) and CP43-Arg357 were also added. Although suggestive and useful for discussing the mechanism, *at the resolution of the current structures, there is no definitive information about the water molecules designated as coordinating to Mn(4) and Ca or the putative oxo bridges shown in the cluster structure, and questions remain about local coordination environments at the CaMn<sub>3</sub> cluster*. In recent work, Batista and Siegbahn have generated computational structures, including coordinated water molecules, starting from the low-resolution X-ray crystal structures, which are consistent with both X-ray and EXAFS data.<sup>695</sup>

Based on earlier EXAFS studies on S<sub>1</sub>, it was proposed that the OEC was composed of 2–3 di- $\mu$ -oxo bridged Mn units with Mn–Mn separation distances of  $\sim 2.7 \text{ \AA}$ <sup>636,641,642,697–702</sup>. A more recent extended range EXAFS study on S<sub>1</sub> reveals three Mn–Mn vectors in the CaMn<sub>3</sub> cluster, two at  $\sim 2.7 \text{ \AA}$  and one at  $\sim 2.8 \text{ \AA}$  with one or two Mn–Mn interactions at  $3.3 \text{ \AA}$ .<sup>674</sup>

The more recent structure of the OEC at 3  $\text{\AA}$  resolution is shown in Figure 53. In this structure, Mn–Mn distances were restrained by the results of EXAFS studies with Mn(1)–Mn(2) and Mn(2)–Mn(3) distances of 2.7  $\text{\AA}$  and a Mn(3)–Mn(4) distance of 3.3  $\text{\AA}$ . Ca is equidistant from Mn(1), Mn(2), and Mn(3) in this structure at  $\sim 3.4 \text{ \AA}$ .<sup>676</sup>

A complication in interpreting these structures at the molecular level is that the X-ray results include the effects of radiation damage and its impact on local structure through disorder and reduction of Mn(II) and Mn(IV) to Mn(II) by X-ray generated radicals.<sup>701</sup> Important features in both structures are (1) the six or seven ligating amino acid residues, including aspartate, glutamate, histidine, and alanine, with Glu333 and Asp342 required ligands as shown by mutagenesis,<sup>703,704</sup> (2) a CaMn<sub>3</sub> cluster at the core of the structure, (3) outlining Mn(4) which is linked to the CaMn<sub>3</sub> cluster and lies near Asp170 with Asp61, both of which appear to be in the second coordination sphere, and (4)  $Y_2'$  and its associated histidine base in the near vicinity of the OEC.

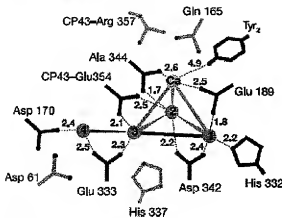


**Figure 53.** Schematic view of the  $\text{CaMn}_4$  cluster of the OEC with distances given in angstroms. The abbreviations are alanine (Ala), arginine (Arg), aspartate (Asp), glutamate (Glu), and histidine (His). The distances between Mn (red) and Ca (orange), as illustrated by the connecting lines, are as follows: gray, 2.7 Å; blue, 3.3 Å; green, 3.4 Å. In the labeling scheme, amino acids in black are in the first coordination sphere, and those beyond that sphere are in gray. Reprinted with permission from ref 662 (<http://www.nature.com>). Copyright 2005 Nature Publishing Group.

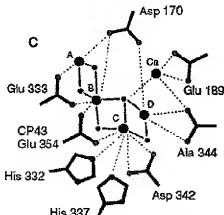


**Figure 54.** The favored EXAFS structure for the OEC in  $S_1$ . Mn- $\mu$ -oxo bonds are shown as solid green lines. Bonds to other possible ligand atoms are shown as dotted lines, with black indicating a distance less than 3.0 Å and blue indicating distances greater than 3.0 Å. Reprinted with permission from ref 683 (<http://www-sciencemag.org>). Copyright 2006 AAAS.

The 3 and 3.5 Å structures are related but differ in (1) the apparent bridging rather than terminal roles for Asp342, Glu189, and Glu333 as ligands and (2) coordination of Ala344 to Mn(2) rather than Ca, consistent with FTIR results.<sup>701</sup>

More recent EXAFS results have been reported on  $S_1$  from measurements on single crystals free of radiation damage.<sup>683</sup> The EXAFS results were consistent with three different but topologically related structures, with the most favored shown in Figure 54. In this structure  $\text{Mn}_4$  is  $\text{Mn}(4)$  in Figures 52 and 53,  $\text{Mn}_5$  is  $\text{Mn}(3)$ ,  $\text{Mn}_6$  is  $\text{Mn}(2)$ , and  $\text{Mn}_7$  is  $\text{Mn}(1)$ .

In the EXAFS structure, the base cluster and ligand frameworks are retained. Notable features include di- $\mu$ -oxo bridging between each pair of Mn partners, a single tri- $\mu$ -oxo bridge between Ca and Mn(2) and Mn(3), and a long Mn(4)–O distance between Mn(4) and Asp170.

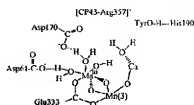
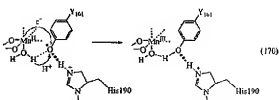


**Figure 55.** Schematic diagram illustrating possible structural features at the OEC. It is based on the EXAFS and XRD structures in Figures 5 and 6. The water molecules shown are not observed in either the EXAFS or XRD structures.

A schematic drawing of the OEC based on the EXAFS structure is shown in Figure 55. As suggested by the EXAFS structure, it includes coordinative stabilization of Mn(4) by triple bridging. It also includes features not seen in the 3.0 or 3.5 Å structures but proposed in the mechanistic discussion that follows. They include (1) three coordinated water molecules at Mn(4) in  $S_1$ , (2) two waters and a hydroxide in  $S_1$ , (3) a H-bond interaction between Mn(4)–OH<sub>2</sub> and Asp170, and (4) Asp170 in the second coordination sphere rather than bound to Mn(4). The latter is consistent with FTIR results; see below.

**7.3.2.2. Thermodynamics.** Once formed,  $\text{Y}_2$  oxidatively activates the OEC sequentially through the four steps of the Kok cycle. Babcock and co-workers suggested intervention of the “H-atom abstraction” pathway illustrated for the  $\text{S}_1 \rightarrow \text{S}_2$  transition in eq 170.<sup>23–28</sup> It involves simultaneous  $\text{e}^-/\text{H}^+$  transfer from  $\text{d}_{\alpha}^4\text{Mn}(\text{II})$  and  $\sigma_{\alpha-4}$  to  $\text{Tyro}^{\cdot+}$ . In the parlance of this review, this pathway would be described as  $\text{e}^-/\text{H}^+$  MS-EPT.

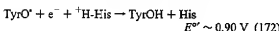
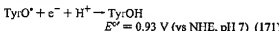


The structures in Figures 52 and 53 appear to rule out this pathway. They show that, although  $\text{Y}_2$  is H-bonded to His190, it is  $\sim 5$  Å from the  $\text{Ca}^{2+}$  ion in the cluster and even further from the Mn ions, with the nearest being Mn(4) at  $\sim 7$  Å. Although these are reasonable distances for electron transfer, they are unreasonable for proton transfer given its short-range character.

The suggestion of an “H-abstraction” mechanism by Babcock followed from an analysis of the thermodynamic requirements for water oxidation. The standard reduction potential for the couple  $\text{O}_2 + 4\text{e}^- + 4\text{H}^+ \rightarrow 2\text{H}_2\text{O}$  at pH = 7 is 0.815 V (vs NHE) or, excluding the free energy of dilution of the released  $\text{O}_2$ , 0.884 V (section 5.5.4).<sup>294–298</sup> This makes water oxidation thermodynamically accessible to  $\text{P}_{\text{H}_2\text{O}}$  with  $E'' \sim 1.26$  V. However, the potential relevant to the activation of the OEC is  $E''$  for the  $\text{Tyro}^{\cdot+}/\text{TyroOH}$  couple at pH = 7, eq 171, or, more appropriately, for the  $\text{Tyro}^{\cdot+}/\text{H-His}/\text{Tyro-O-H-His}$  couple given the evidence for participation by His as a proton acceptor, eq 172.

These potentials are approximations to the true membrane values and neglect differences in  $\Delta G$  for formation of the H-bonded pairs  $\text{Tyro}^{\cdot+}/\text{H-His}$  and  $\text{Tyro-O-H-His}$ . Experimental estimates place  $E''(\text{Y}_2/\text{Y}_2^{\cdot+})$  at potentials 40–110 mV more negative than  $E''(\text{P}_{\text{H}_2\text{O}}/\text{H}_2\text{O})$ , from which  $E''(\text{Y}_2/\text{Y}_2^{\cdot+})$ , eq

173, lies between 1.1 and 1.2 V.<sup>60</sup> It is notable that these estimates are still well below the solution value for the  $\text{TyrOH}^+/\text{TyrO}^-$  couple at  $E^\circ = 1.34$  V vs NHE.<sup>58,69,60</sup> This supports the formulation  $\text{TyrO}^{\cdots\cdots\cdots\text{H}}\text{His}/\text{TyrO-H}\cdots\text{His}$ , for the  $\text{Y}_2^{\cdots\cdots\cdots\text{H}}$  couple.



An increase in potential for the  $\text{Y}_2^{\cdots\cdots\cdots\text{H}}$  couple in the membrane compared to solution is expected<sup>70b</sup> and seen in the 0.2–0.3 V increase for the  $\text{Y}_2^{\cdots\cdots\cdots\text{H}}$  couple compared to the solution couple in eqs 172 and 173. In the nonpolar membrane, oxidation of  $\text{TyrO}^{\cdots\cdots\cdots\text{H}}\text{His}$  to  $\text{TyrO}^{\cdots\cdots\cdots\text{H}}\text{His}$  occurs without benefit of a charge compensating counterion, and stabilization of the positive charge by polarization interactions with the membrane is greatly decreased compared to water.

Given the estimated potentials for the  $\text{Y}_2^{\cdots\cdots\cdots\text{H}}$  and  $\text{O}_2/\text{H}_2\text{O}$  couples, the driving force for water oxidation by  $\text{Y}_2$  is  $\sim 0.3$  eV ( $\sim 7$  kcal/mol). This entails a mechanism which avoids high-energy intermediates and meets the  $4\text{e}^-/4\text{H}^+$  demands of the net reaction. The latter explains the use of four photons in the Kok cycle by the OEC to make  $\text{O}_2$ , which avoids the one-, two-, and three-electron intermediates  $\text{OH}^-$ ,  $\text{H}_2\text{O}_2$ , and  $\text{HO}_2^-$ . A  $1\text{e}^-$  pathway to give hydroxyl radical,  $\text{OH}^-$ ,  $\text{Y}_2^{\cdots\cdots\cdots\text{H}}$ , and  $\text{H}_2\text{O}$ — $\text{Y}_2 + \text{OH}^- + \text{H}_2\text{O}$ , can be ruled out in any case because  $\Delta G^\circ \sim +1.1-1.2$  eV for this reaction, and the highest activation energy for the individual steps in the Kok cycle is  $E_a \sim 0.4$  eV.<sup>70</sup>

PCET and the loss of four protons are part of the stoichiometric requirement for water oxidation. PCET must also play an important role in the oxidative activation of the OEC by avoiding positive charge buildup. This causes redox potential leveling, enabling the accumulation of multiple oxidative equivalents over a narrow potential range (section 2.1.1).<sup>70b-71</sup>

The importance of PCET is illustrated by the stepwise oxidation of a series of exo and sulfido metal clusters in which the uncompensated buildup of positive charge contributes to an increase in  $E^\circ$  of 0.3–0.4 V for each electron loss.<sup>67</sup> Injection of a positive charge into a membrane with dielectric constant  $\epsilon_S = 3.5$  by electron transfer would require 31 kcal/mol (1.35 eV).<sup>72</sup> Redox potential leveling by PCET has been demonstrated by the influence on  $E^\circ$  of proton loss from the  $\mu$ -hydroxo group in  $\text{Mn}^{38}\text{Mn}^{\text{IV}}(\mu\text{-O})(\mu\text{-OH})(\text{salpn})_2$  ( $\text{salpn} = 1,3\text{-bis}(\text{salicylideneamino})\text{propane}$ )<sup>60</sup> and by proton loss from  $\text{H}_2\text{O}$  in  $[\text{Mn}_2\text{L}_2(\text{H}_2\text{O})_2]^{4+}$  ( $\text{L} = 2\text{-hydroxy-1,3-bis}(3,5\text{-X}_2\text{-salicylideneamino})\text{propane}$ ,  $\text{X} = \text{Cl, H, di-}tert\text{-butyl}$ ).<sup>70b,71</sup>

Estimates of  $E^\circ$  have been made for the successive transitions in the Kok cycle.<sup>67</sup> From the Krishnaiak value for the configurational potential of  $E_c^\circ = 0.88$  V for water oxidation,  $\Delta G_c = 3.52$  eV with  $n = 4$ . In order for water oxidation to proceed to completion or near completion,  $E_1^\circ + E_2^\circ + E_3^\circ + E_4^\circ \geq 3.6$  eV with  $E_1^\circ$ , etc. the formal potentials for the separate S state transitions. This sets the average potential for the S state transitions at  $E_{\text{ave}}^\circ \geq 0.9$  V.

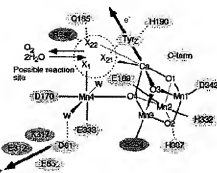


Figure 56. Schematic view of the OEC illustrating: (A) possible H-bond interactions between  $\text{Y}_2$  and histidine 190 and between  $\text{Mn}_4^{\text{III}}-\text{OH}_2$  and aspartate D61 shown as light blue dotted lines; (B) the hydrophilic exit channel for proton transfer from the entryway at aspartate D61 to the lumen; and (C) possible substrate water binding positions to  $\text{Mn}(4)$  ( $\text{X}_1$ ) and to  $\text{Ca}$  ( $\text{X}_2$  and  $\text{X}_3$ ) and another possible coordinated water molecule, not identified at 3.5 Å resolution, shown as  $\text{W}$ . Residues in the D1, D2, and CP43 subunits are shown in yellow, orange, and green, respectively. Reprinted with permission from ref 383 (<http://www.sciencemag.org>). Copyright 2004 AAAS.

Given this value and the potential of 1.1–1.2 V for the  $\text{Y}_2^{\cdots\cdots\cdots\text{H}}$  couple, only a narrow potential window exists for the individual couples. Estimated values for  $\text{S}_1/\text{S}_0$  and  $\text{S}_2/\text{S}_1$  are 0.80 and  $\sim 1.0$  V.<sup>60</sup> The average value of potentials for the  $\text{S}_0/\text{S}_1$  and  $\text{S}_1/\text{S}_2$  couples,  $(E_3^\circ + E_4^\circ)/2$ , must be  $\geq 0.9$  V in order for water oxidation to be spontaneous.

There are model systems that illustrate the possible role of PCET on redox potential leveling in the OEC. One is  $cis\text{-}[\text{Ru}^{\text{II}}(\text{bpy})_2(\text{H}_2\text{O})_2]^{2+}$  (Figure 6), which undergoes four sequential  $\text{e}^-/\text{H}^+$  steps over a potential range of 0.6 V to give  $cis\text{-}[\text{Ru}^{\text{V}}(\text{bpy})_2(\text{O})]^{2+}$ . Similarly,  $cis,cis\text{-}[(\text{bpy})(\text{H}_2\text{O})\text{-O}_2^{\text{III}}\text{-O}-\text{O}_2^{\text{III}}(\text{H}_2\text{O})(\text{bpy})_2]^{4+}$  undergoes a series of electron–proton transfers to give  $cis,cis\text{-}[(\text{bpy})(\text{O})\text{Os}^{\text{V}}\text{-O}-\text{Os}^{\text{V}}(\text{O})(\text{bpy})_2]^{4+}$  over a comparable potential range.<sup>72</sup> The Ru analogue,  $cis,cis\text{-}[(\text{bpy})(\text{O})\text{Ru}^{\text{V}}\text{-O}-\text{Ru}^{\text{V}}(\text{O})(\text{bpy})_2]^{4+}$ , oxidizes water on the sub-100 ms time scale.<sup>73</sup> Other examples of metal complex catalyzed water oxidation have been reported, including  $\mu\text{-oxo}$  complexes of  $\text{Mn}$ .<sup>50,53,71,76</sup>

#### 7.2.4. Oxidation of $\text{Y}_2$ Mechanism

A number of accounts have appeared which address mechanistic details of how water is oxidized at the OEC. Proton involvement<sup>4,23,31,17,18</sup> and electron–proton coupling<sup>7,53,64,65,68</sup> have been discussed, and detailed models have been proposed.<sup>63,64,64,64,64,65,65,70-72</sup> In the account that follows, a mechanism for oxidative activation and water oxidation is presented that emphasizes the possible roles of EPT and proton transfer. It is a summary of a more detailed version that has appeared elsewhere.<sup>73</sup>

As noted above, the stable dark resting state for the OEC is  $\text{S}_1$ , and the dark-adapted, light-driven Kok cycle begins with the  $\text{S}_1 \rightarrow \text{S}_2$  transition. For convenience in presenting the mechanism, it is useful to begin with the  $\text{S}_0 \rightarrow \text{S}_1$  transition and follow the sequential buildup of four redox equivalents as the cycle progresses.

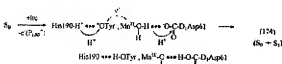
**7.2.4.1. The  $\text{S}_0 \rightarrow \text{S}_1$  Transition.** With the “H-abstraction” mechanism of Babcock and co-workers unlikely, McEvoy

and Brudvig have proposed that CP43-Arg357 in Figure 52 helps to organize a H-bonding network and functions as the "proton-abstractor" for the higher  $S_2 \rightarrow S_3 \rightarrow (S_4) \rightarrow S_0$  transitions.<sup>630</sup> This residue is required for  $O_2$  evolution, and its terminal N-atoms are  $\sim 4$  Å from the active face of the CaMn<sub>3</sub> cluster. However, with its  $pK_a$  value of  $\sim 12$ , it is protonated and presumably unavailable as a base.<sup>731-733</sup>

*1e<sup>-</sup>/2H<sup>+</sup> MS-EPT.* Examination of Figure 55 reveals another possible EPT pathway not considered by Babcock and co-workers. As shown in eq 174, it utilizes the apparent H-bond between a water molecule bound to Mn(4) and an aspartate residue, "OOC-D<sub>1</sub>Asp61". As discussed below and illustrated in Figure S6, Asp61 appears to be the entryway to a hydrophilic proton exit channel.<sup>734-737</sup> In order to clarify the mechanism as it evolves in the discussion, the S state transition in which the reaction is proposed to occur will be indicated in parentheses.

The suggested electron transfer in eq 174 occurs over 7 Å from Mn<sup>II</sup>—OH<sub>2</sub> to Y<sub>2</sub>'. It acts in concert with a double proton transfer, one from Mn—OH<sub>2</sub> to "OOC-D<sub>1</sub>Asp61" and the other from "H—His190 to TyrO".

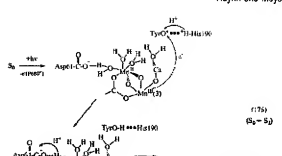
The pathway in eq 174 can be described as *1e<sup>-</sup>/2H<sup>+</sup> MS-EPT*. It exploits the relatively long-range nature of electron transfer<sup>16,671</sup> while meeting the short-range requirements for proton transfer.<sup>390-396</sup> It avoids the high-energy intermediates Mn<sup>III</sup>—OH<sup>+</sup> and TyrO<sup>+</sup> and delivers the released proton at an entryway for proton transfer to the lumen.



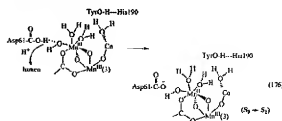
The proton transferred from TyrOH to His190 in the oxidation of Y<sub>2</sub> by P<sub>450</sub><sup>1</sup> in eq 169 is transferred back in eq 174. This "proton-rocking" mechanism was first proposed by Renger and co-workers<sup>738</sup> and has been elaborated by several groups.<sup>66,690,739,740</sup> *Proton-rocking increases the potential of TyrO<sup>+</sup> as an oxidant in the [TyrO<sup>•+</sup>—H—His190]/[TyrO<sup>•+</sup>—H—His190] couple compared to the [TyrO<sup>•+</sup>—H—His190]<sup>+</sup> couple by  $\sim 0.2$ – $0.3$  V. The increase in potential is required thermodynamically for the tyrosyl radical to oxidize water to oxygen.* The [TyrO<sup>•+</sup>—H—His190]/[TyrO—H—His190] and [Mn<sup>II</sup>—O—H—Asp61]/[Mn<sup>II</sup>—OH<sub>2</sub>—OOC-Asp61] couples act as "EPT modules" in meeting the combined orbital requirements for *1e<sup>-</sup>/2H<sup>+</sup> MS-EPT*.

*Stepwise 1e<sup>-</sup>/1H<sup>+</sup> MS-EPT.* S<sub>0</sub>  $\rightarrow$  S<sub>1</sub> oxidation at Mn(4) may also occur in a stepwise manner. This is illustrated in eq 175, which is based on Figure 55. In eq 175, initial 1e<sup>-</sup> oxidation of the CaMn<sub>3</sub> cluster is shown as occurring at Mn(3) and is followed by 1e<sup>-</sup>/1H<sup>+</sup> MS-EPT oxidation of Mn(4).

*Proton Transfer to the Lumen.* After the proton is released at Asp61, it appears on the lumen surface of the protein, eq 176, in as little as 12  $\mu$ s.<sup>687,738,741–<sup>742</sup> Since proton transfer</sup>

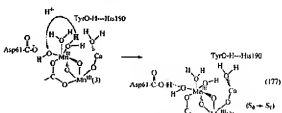


is spontaneous, and the pH of the lumen is as low as 5,  $pK_a(\text{D}_1\text{Asp61}) \leq 5$ .



The proton exit channel appears to consist of a cluster of titratable residues beginning with D<sub>1</sub>Asp61 and terminating in a series of Pb<sub>60</sub>O residues. The four residues in subunits D<sub>1</sub> and D<sub>2</sub>, D<sub>1</sub>Asp61, D<sub>2</sub>Glu65, D<sub>2</sub>Glu312, and D<sub>2</sub>Lys315, are fully conserved.<sup>734-737</sup> From the results of a theoretical analysis based on the linearized Poisson–Boltzmann equation,  $pK_a$  values increase monotonically along the exit channel. Alternate exit and water intake channels were also identified.<sup>737</sup> In these calculations, charge was allowed to build up on the CaMn<sub>3</sub> cluster rather than invoking PCET and redox potential leveling. This led to greatly enhanced acidities for residues near the cluster, which was the suggested origin of released protons in the Kolo cycle.<sup>737</sup>

*Intracoordination Sphere Proton Transfer.* As shown in eq 177, the next step in the proposed mechanism is intracoordination sphere proton transfer from in-plane Mn—OH<sub>2</sub>, labeled X<sub>1</sub> in Figure S6, to Mn<sup>III</sup>—OH<sup>+</sup>.<sup>743</sup> It appears to be favored by conversion of a repulsive Mn—OH<sub>2</sub>—OOC-D<sub>1</sub>Asp61 interaction into a Mn<sup>III</sup>—OH<sub>2</sub>—OOC-D<sub>1</sub>Asp61 hydrogen bond and a favorable electrostatic interaction between OH<sup>+</sup> at X<sub>1</sub> with the positively charged side chain  $-\text{N}(\text{H})\text{C}(\text{NH}_2)^+$  (R357 in Figure S6).



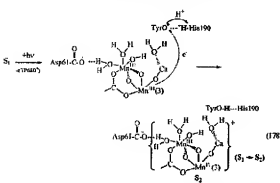
*Coordination of Asp170?* The results of site-directed mutagenesis studies point to involvement of Asp170 in the

formation of the  $\text{CaMn}_4$  cluster by providing a ligand at the high-affinity site that binds the first  $\text{Mn}^{3+}$ .<sup>735,736</sup> However, FTIR difference spectra on *Synechocystis* sp. PCC 6803 show that there are no shifts in cluster carboxylate modes between  $S_1$  states.<sup>655,700,747–749</sup> Given the sensitivity of these modes to oxidation state, these data are consistent with the structures in Figures 54 and 55, in which Asp170 is in the second coordination sphere of  $\text{Mn}^{4+}$  rather than coordinated. This enables it to act as an internal base at a later stage in the mechanism; see below.

**7.2.4.2. The  $S_1 \rightarrow S_2$  Transition.** Given the 1:0:1.2 proton release pattern for intact samples in the Kok cycle,<sup>186,678,685–687,730–733</sup> there are no protons released to the lumen during the  $S_1 \rightarrow S_2$  transition although, as noted above, a pattern of 1:1:1:1 has been observed in spinach core particles.<sup>744,745</sup> The results of EXAFS studies show that  $S_1$  and  $S_2$  have essentially the same structures.<sup>678,699</sup>

Results of resonant inelastic X-ray scattering (RIXS) measurements point to electron loss from a delocalized orbital,<sup>753,757</sup> ( $\text{OOC}^-$ ) carboxylate band shifts are consistent with oxidation at the  $\text{CaMn}_4$  cluster in the  $S_1 \rightarrow S_2$  transition.<sup>705,754–760</sup> Electrochromic band shifts have been observed in  $S_2$  which arise from a positive charge deeply buried from bulk solvent in a low dielectric environment.<sup>761,763</sup> The appearance of a positive charge occurs only during the  $S_1 \rightarrow S_2$  transition and is coupled with protein conformational changes.

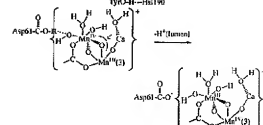
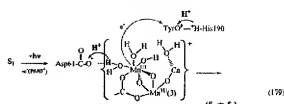
Cluster oxidation from  $\text{Mn}^{(4)\text{III}}\text{CaMn}_3^{(\text{II})\text{IV}}\text{JV}$  to  $\text{Mn}^{(4)\text{IV}}\text{CaMn}_3^{(\text{V})\text{IV}}\text{JV}$  in the  $S_1 \rightarrow S_2$  transition, eq 178, is consistent with these experimental observations.<sup>184,379,712,760</sup>



Oxidation of the cluster could also occur by initial  $1\text{e}^-/2\text{H}^+$  MS-EPT to oxidize  $\text{Mn}^{(\text{III})}$  to  $\text{Mn}^{(\text{IV})}$  followed by  $1\text{e}^-/1\text{H}^+$  MS-EPT with electron transfer from the  $\text{CaMn}_3$  cluster to  $\text{Mn}^{(\text{IV})}$ , eq 179.

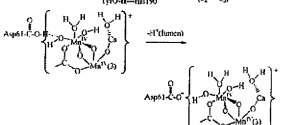
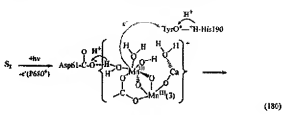
The sequence of steps leading from  $S_0$  to  $S_2$  in eqs 174–178 meets the requirements suggested in a theoretical analysis by Siegbahn and Cmířová. They predicted that the active Mn site in  $S_0$  is  $\text{Mn}^{(\text{II})}$  coordinated to two  $\text{H}_2\text{O}$  ligands and that it acts as the precursor to the active site for water oxidation. They also predicted that it cycles through  $\text{H}_2\text{O} - \text{Mn}^{(\text{IV})} = \text{O}$  as a reactive intermediate, a step that is discussed below.<sup>643</sup>

**7.2.4.3. The Transitions  $S_2 \rightarrow S_3 \rightarrow S_3'$ .  $\text{O}^- \text{O}^+$  coupling** has been proposed to occur following oxidation of  $S_2$  to  $S_3$ <sup>642,656,658,659,677,754–769 in a reaction that may involve high-oxidation state  $\text{Mn}^{(\text{IV})} = \text{O}$  or  $\text{Mn}^{(\text{IV})} = \text{O}^-$  intermediates.<sup>25,630,639</sup> It has been suggested that such intermediates would undergo nucleophilic attack at the electrophilic, terminal  $\text{OxO}$  group by  $\text{Ca} - \text{OH}^-$  ( $X_{22}$ ).<sup>647</sup> EXAFS data point to a significant</sup>



structural change between  $S_2$  and  $S_3$ , but different interpretations have been offered in different studies.<sup>636,640,701,724,738,758,770–773</sup> It has also been proposed that there is an equilibrium between at least two states in  $S_3$ .<sup>677,770</sup> From XANES measurements, K edge difference spectra for the  $S_1 \rightarrow S_2$  and  $S_2 \rightarrow S_3$  transitions are significantly different, with oxidation of  $\text{Mn}^{(\text{III})}$  to  $\text{Mn}^{(\text{V})}$  occurring in the former.<sup>776,777</sup> At 0.4 eV the energy of activation for the  $S_2 \rightarrow S_3$  transition is the highest of the four S state transitions.<sup>764,769,787,788,799</sup>

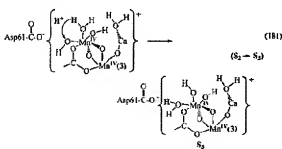
**The Transition  $S_3 \rightarrow S_3'$ .** Given the formulation of  $S_3$  in eq 178, a second light-driven  $1\text{e}^-/2\text{H}^+$  MS-EPT oxidation of  $S_2$  with D. Asp61 as the proton acceptor would give  $\text{Mn}^{(\text{IV})}$ , (4), but as the dihydroxo form shown in eq 180. This is consistent with comparative XANES results on PSII and Mn model compounds which suggest the absence of higher oxidation state  $\text{Mn}=\text{O}$  intermediates in all S states from  $S_0$  to  $S_3$ .<sup>780</sup>



There is a debate in the literature as to whether oxidation at this stage is  $\text{Mn}^{51,673,686,721,736,781–782}$  or  $\text{O}$ -ligand based.<sup>659,672,674,676,776,783–785</sup> In this terminology, there is more ligand than metal character in the redox orbital, leading to the description  $\text{Mn}^{(\text{IV})}\text{O}^-$ .

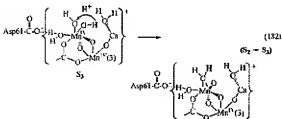
Following Mn-based oxidation and proton loss to the lumen, intracoordination sphere proton transfer, utilizing the

putative third water molecule in the structure in Figure 55, rests the  $\text{Mn}^{(4)}\text{OH}_2\cdots\text{O}$  Asp161 MS-EPT interface. This results in the intermediate labeled  $S_3$  in eq 181, perhaps the first of two forms of  $S_3$  proposed by Renger.<sup>78</sup>



**$\text{O} \cdots \text{O}$  Coupling: The  $S_1 \rightarrow S_1'$  Transition.** Ca depletion inhibits photosynthesis by blocking the  $S_2 \rightarrow S_3$  transition and, by inference, its involvement in  $\text{O} \cdots \text{O}$  coupling.<sup>72,265,377</sup> From the 3 Å and 3.5 Å structures, coordination details around Ca are unclear but are consistent with the coordinated water molecule labeled  $S_{22}$  in Figure 56. It is aligned toward putative  $\text{Mn}^{(4)}\text{OH}$  at position  $X_1$  in Figure 56. This has been proposed as the site for  $\text{O} \cdots \text{O}$  coupling.<sup>383,559</sup>

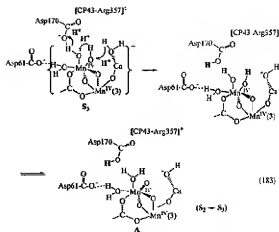
$\text{O} \cdots \text{O}$  coupling is expected to occur at an oxo site at  $\text{Mn}^{(4)}$ .<sup>52,191,647</sup>  $\text{Mn}=\text{O}$  is available at  $\text{Mn}(4)$  through the dihydro-oxo-oxo equilibrium,  $\text{Mn}^{IV}(\text{OH}_2) \rightleftharpoons \text{Mn}^{IV}(\text{O})\text{H}_2\text{O}$ , shown in eq 182. There is precedence for related equilibria in metal complexes.<sup>136–138</sup>



$\text{O} \cdots \text{O}$  coupling is expected to be preceded by deprotonation of  $\text{Ca}=\text{OH}_2$  ( $X_{22}$ ).<sup>647</sup> This avoids a high-energy, protonated peroxy intermediate,  $(\text{H}_2\text{O}_2)\text{Mn}(\text{H}_2\text{O})$ , but requires an internal base. As shown in eq 183, this is a role that may be played by Asp170 through intervention of a local proton transfer channel involving the coordinated hydroxyl ligands in the  $\text{Mn}^{IV}(\text{OH}_2)$  form of  $\text{Mn}(4)$ . Although this provides a role for Asp170 as an internal base, a number of other amino acid residues can functionally substitute for Asp170. Both the Arg and Met mutants can evolve oxygen at 10–20% of the wild-type rate.<sup>78</sup>

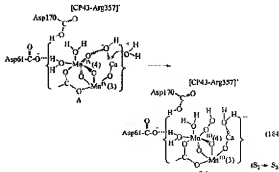
As shown in eq 183, proton loss from  $\text{Ca}=\text{OH}_2$  and  $\text{Mn}^{(4)}\text{O}$  formation would give the species labeled intermediate A in eq 183, the immediate precursor to  $\text{O} \cdots \text{O}$  coupling. It is proposed as a high-energy intermediate, not observed spectroscopically, due to the unfavorable  $\text{Mn}^{IV}(\text{OH}_2)/\text{Mn}^{IV}(\text{O})\text{H}_2\text{O}$  equilibrium and proton loss from  $\text{Ca}=\text{OH}_2$ . Its thermodynamic instability may contribute to the high energy of activation (0.4 eV) for the  $S_2 \rightarrow S_3$  transition.

Mutagenesis studies show that CP43-Arg357<sup>+</sup>, which spans the active face of the  $\text{CaMn}_4$  cluster, is required for  $\text{O}_2$  evolution.<sup>789</sup> Its electrostatic influence may decrease  $pK_a$



for  $\text{Ca}=\text{OH}_2$ , decreasing the  $\Delta G$  difference between intermediate A and  $S_2$ .

$\text{O} \cdots \text{O}$  coupling in intermediate A is shown in eq 184. In this reaction,  $\text{Ca}=\text{OH}_2$  redox nucleophilic attack occurs on  $\text{Mn}=\text{O}$ . Two electrons are transferred, either sequentially or in concert, one to  $\text{Mn}^{IV}(4)$  and the other to the  $\text{Mn}^{IV,IV,V}$  cluster.



The product of  $\text{O} \cdots \text{O}$  coupling in eq 184 is a  $\text{Mn}^{IV}$  hydroperoxide,  $\text{Mn}^{IV}\text{OOH}$ . It is proposed as the second of two possible intermediates suggested by Renger,  $S_1'$ .<sup>677,770</sup> There is evidence for  $\text{Mn}(\text{III})$  in  $S_1$  at liquid helium temperature in EPR and near IR measurements.<sup>644,655,783,790</sup>

Based on density functional theory (DFT) and the B3LYP functional for geometry optimization, Slegbaek and Crabtree have concluded that  $\text{Mn}^{IV}\text{OOH}$  is in thermodynamic equilibrium with an activated  $\text{Mn}^{IV}=\text{O}$  precursor in  $S_2$ . Renger has proposed that a rapid redox equilibrium exists between a Mn peroxide and a form having two terminal hydroxyl ligands.<sup>78</sup> Water-exchange studies show that  $\text{O} \cdots \text{O}$  coupling occurs at a site that undergoes rapid exchange with external solvent, presumably  $\text{Ca}=\text{OH}_2$  ( $X_{22}$ ), and one that undergoes slow exchange. The slow exchange site is presumably  $\text{O}=\text{Mn}^{IV}(\text{H}_2\text{O})$  or  $\text{Mn}^{IV}(\text{OH}_2\text{H}_2\text{O})$ , with exchange occurring before  $\text{O} \cdots \text{O}$  coupling.<sup>168,715,718,791–794</sup>

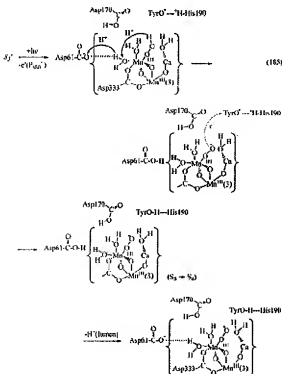
Although not located in the X-ray structures of PSII,  $\text{Cl}^-$  is a cofactor for water oxidation. Chloride-depleted samples are reconstituted to catalytically active forms by addition of a variety of anions.<sup>795–798</sup> In a recent combined EPR/FT-IR study,  $\text{N}_3^-$  was shown to bind in the immediate vicinity of the Mn cluster in competition with  $\text{Cl}^-$  binding.<sup>799</sup> As discussed by Brudvig *et al.*,<sup>544</sup>  $\text{Cl}^-$  may be transferred from

Ca to Mn=O, which would increase  $pK_a$  for Ca—OH<sub>2</sub> (X<sub>2</sub>) and help initiate O···O coupling.

**7.2.4.4. The Transition  $S_3 \rightarrow \{S_4\} \rightarrow S_0 + O_2$  States  $S_0$ ,  $S_1$ ,  $S_2$ , and  $S_3$  all have been trapped and investigated spectroscopically with evidence obtained recently for two intermediates past  $S_3$ . Inhibition of O<sub>2</sub> evolution from cyanobacteria was observed at high O<sub>2</sub> pressure with spectroscopic evidence for an intermediate.<sup>669</sup> Time-resolved X-ray absorption spectroscopy (XAS) on the 10  $\mu$ s time scale revealed a lag phase of 250  $\mu$ s followed by oxidation of Mn and reduction of Y<sub>2</sub> in 1.1 ms.<sup>670</sup> The lag phase has been attributed to a proton transfer step.<sup>670</sup> Proton transfer preceding electron transfer has been proposed by Rappaport and Lavergne.<sup>263</sup> Following excitation of  $S_3$ , Y<sub>2</sub> release and O<sub>2</sub> release both occur on the approximately millisecond time scale.<sup>669</sup>**

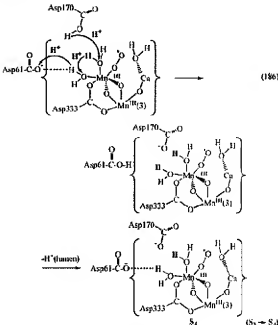
These observations are consistent with a multistep mechanism.<sup>739</sup> In the first step, eq 185, light-driven 1e<sup>-</sup>/1H<sup>+</sup> MS-EPT oxidation of Y<sub>2</sub> is followed by a lag phase in which proton transfer occurs from Mn—OOH to Asp61, eq 185. One possible proton transfer channel is illustrated, and others might operate utilizing coordinated H<sub>2</sub>O or HOOC-Asp170 as proton transfer bridges.

In eq 185, proton loss activates coordinated peroxide toward electron transfer to Y<sub>2</sub><sup>+</sup> with all subsequent steps rapid, on the ~1 ms time scale. Electron transfer may occur stepwise with initial oxidation at Mn(4), Mn<sup>III</sup>(OO<sup>2-</sup>), Y<sub>2</sub><sup>+</sup> → Mn<sup>IV</sup>(OO<sup>2-</sup>), followed by intramolecular electron transfer, Mn<sup>IV</sup>(OO<sup>2-</sup>) → Mn<sup>III</sup>(OO<sup>2-</sup>). Electron transfer is followed by proton transfer to the lumens.



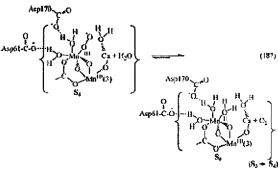
Proton transfer to Asp61 would open a long-range proton transfer channel from HOOC-Asp170 to Asp61. As shown in eq 186, utilization of this channel for loss of the proton on HOOC-Asp170 followed by proton transfer to the lumen would explain the 1:0:1:2 proton release pattern and loss of

the second of two protons in the  $S_1 \rightarrow \{S_4\} \rightarrow S_0 + O_2$  transition. It would also reset the EPT interface at Asp61.



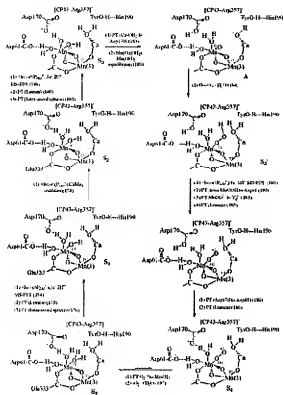
The final product is a superoxide complex of Mn(II), Mn<sup>II</sup>(OO<sup>2-</sup>), which is tentatively identified as  $S_0$ . This is presumably the intermediate observed under high pressures of O<sub>2</sub>.<sup>669</sup> In the net reaction in eqs 185 and 186, electron transfer occurs from coordinated “OOH to Y<sub>2</sub><sup>+</sup> with coupled-proton transfer to the lumen, Y<sub>2</sub><sup>+</sup>Mn<sup>III</sup>(OOH) → Y<sub>2</sub><sup>+</sup>Mn<sup>II</sup>(OO<sup>2-</sup>) + H<sup>+</sup>(lumen). There is no change in oxidation state at Mn, and the lag time is due to intracoordination sphere proton transfer.

The final step, shown in eq 187, is intramolecular O<sub>2</sub><sup>2-</sup> → Mn<sup>II</sup><sup>+</sup> electron transfer. It is followed by loss of O<sub>2</sub> and coordination of H<sub>2</sub>O which returns the catalytic system to the  $S_0$  state.



### 7.2.5. S State Mechanistic Summary

The reactions proposed for the complete Kok cycle are shown in the Mechanistic Summary below. They correspond to equations in the text by the numbers in parentheses. In constructing the summary: (1) the abbreviations used are  $+h\nu$  for a light driven reaction, 1e<sup>-</sup>/mH<sup>+</sup> MS-EPT for multisite EPT, and PT and ET for proton transfer and electron transfer; (2) Asp170 is assumed to be uncoordinated and



available as an internal base; (3) in the  $S_0 \rightarrow S_1$  transition, oxidation of  $Mn^{IV}(H_2O)$  by  $O_2$  occurs by  $1\sigma^2/2H^+$  M-S-EPT; (4) oxidation in the  $S_1 \rightarrow S_2$  transition is assumed to occur at the  $CaMn_4$  cluster; (5) it is assumed that there are two forms of  $S_2$ , with a  $Mn^{IV}(OH_2)$  intermediate; (6) deprotonation of  $Ca-OH_2$  by Asp170 and equilibrium formation of  $(H_2O)Mn^{IV}O$  from  $Mn^{IV}(OH)$  give intermediate  $A$ ; (7)  $O_2 \cdots O$  coupling occurs in intermediate  $A$  to give  $Mn^{IV}OH$ , which is identified as  $S_3'$ ; (8) following photochemical formation of a fourth  $Y_2'$ , a lag phase arising from proton loss from  $Mn^{IV}OH$  is followed by rate limiting intramolecular electron transfer to give  $Mn^{IV}(O_2^+)$ ; and (9) deprotonation of  $HOOC\text{-Asp170}$  and proton transfer to the heme produce  $S_4$ , an intermediate identified under high partial pressures of  $O_2$ .

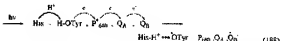
### 7.2.6. Conclusions

This analysis of PCET in Photosystem II reveals the extraordinary attention paid in the structure to "proton-wiring" and the movement of protons. The movement of protons is short range in both coupled electron-proton transfer and the sequential proton transfer steps that make up long-range proton transfer chains. The distance-dependence of electron transfer is less demanding and a relative afterthought in the spatial design of the biological assembly.

PCET plays a critical role in the operation of the OEC. One is thermodynamic by avoiding charge buildup, enabling redox potential leveling. Similarly, repetitive use of MS-EPT avoids high-energy intermediates and directs protons to Asp61, which is the entryway to the proton exit channel to the lumen.

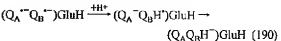
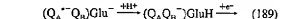
### 7.3. Reduction of $Q_3$

Absorption of a photon in PSII is followed by oxidative quenching through a phenophenyl bridge to plastiquinone  $Q_A$  (Figure 51). Subsequent  $Q_A \rightarrow Q_B$  electron transfer is gated by a protein conformational change and mediated by a non-heme iron.<sup>26,83,861-863</sup> The net reaction is shown in eq 188



As discussed in the previous section, subsequent PCET by a  $1e^-/2H^+$  MS-EPT mechanism results in oxidation of the OEC and advancement of the S state cycle by one from  $S_{0,1}$  to  $S_{1,1}$ . In the photosynthetic reaction center from *Rhodobacter sphaeroides*, absorption of two photons is followed by  $2e^-/2H^+$  reduction of  $Q_a$  to give hydroquinone,  $H_2Q_a$ . The protons in this reaction come from the cytoplasm.  $H_2Q_a$  subsequently diffuses from the reaction center and is oxidized by the cytochrome *bc* complex.

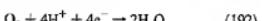
The initial  $Q_A \rightarrow Q_A$  electron transfer is coupled to protonation of a nearby carboxylic acid, Glu-L212, but the proton and electron transfers are sequential and the mechanism is ET-PT, cq 189. Similarly, a second light-induced electron transfer creates the semiquinone pair,  $(Q_A^{\cdot-}, Q_B^{\cdot-})$ . After it forms, protonation at  $Q_A^{\cdot-}$  and  $Q_A^{\cdot-} \rightarrow Q_B^{\cdot-}$  electron transfer occur to give  $HQ_A^{\cdot-}$ , cq 190. In the final step, the proton at Glu-L212 is transferred to give the quinol,  $HQ_B^{\cdot-}$ , cq 191. All of these steps appear to involve sequential electron-proton transfer and not EPT.<sup>163,183,184,188-190</sup> The binding of  $Cd^{2+}$  to His126 and His128, which are located near the proton entry point to the reaction center, inhibits PCET.<sup>189</sup>



$$(Q_A Q_B H^-) \text{GluH} \rightarrow (Q_A H_2 Q_B) \text{Glu}$$

## 7.4. PCET-EPT in Other Biological Systems

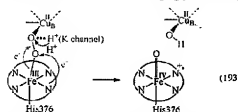
**Cytochrome c oxidase (CcO)** is an enzyme that catalyzes respiratory oxygen reduction. It is located in mitochondrial or bacterial membranes of all aerobic organisms. The active site includes a low-spin heme (heme a) and a copper complex (Cu<sub>b</sub>). The enzyme catalyzes the reduction of O<sub>2</sub> on 192, which is coupled to proton translocation across the membrane surface. A  $\Delta \text{P}_i$  is generated. 28.8.10-8.11



During its activation,  $O_2$  initially binds to the heme. Of the four electrons required in the net reduction, two come from: Fe(II) to give Fe(IV), one comes from  $Cu_B$ , and one comes from a nearby tyrosine.<sup>32,81-84</sup> Protons are available to the heme- $Cu_B$  site from two different channels, K and D.

Theoretical studies based on density functional theory (DFT) and the B3LYP functional,<sup>815-817</sup> with structural details from X-ray studies on mammalian<sup>818</sup> and bacterial<sup>819</sup> CCo's, have been applied to the O-O bond cleavage step.<sup>82</sup> In a first step or stage,  $\text{La}^{3+}$  transfer occurs from Cu<sup>II</sup>, which

is coordinated by three histidines, His291, His240, and His 290. Subsequent reduction of the bridging peroxide, eq 193,



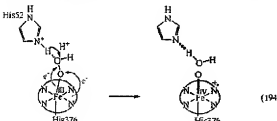
is triggered by protonation with the proton coming from one of the proton channels, most likely the K channel. Simultaneous electron transfer occurs from both Fe(II) and the porphyrin ring to the antibonding  $\pi^*$  orbital of the peroxide, eq 194. The porphyrin macrocycle structure and an axially bound histidine (His376) are both indicated schematically in eq 193.

The pathway proposed in eq 193 could be described as solvent-assisted 2e<sup>-</sup>/1H<sup>+</sup> MS-EPT. However, the calculations suggest that, in the initial step, solvent-assisted 1e<sup>-</sup>/1H<sup>+</sup> MS-EPT occurs with proton transfer to the peroxo-bridge, and a single electron transfer from Fe(III). MS-EPT is followed by ET, in this case from a porphyrin  $\pi$  orbital.<sup>52</sup> Following formation of the ferryl, Fe<sup>IV=O</sup>, a final electron transfer occurs to the porphyrin cation radical, from nearby tyrosine 244, which is bound to His240 and part of the H-bonding network of the proton channel.

#### 7.4.2. Cytochrome *c* Peroxidase (Cp)

The heme-containing peroxidases oxidize a variety of substrates by using hydrogen peroxide as the oxidant. Cp is part of the mitochondrial electron transport chain with cytochrome *c* as its redox partner.<sup>52,810–814,820–823</sup> The key step in the catalytic cycle is cleavage of the O—O bond of H<sub>2</sub>O<sub>2</sub> with an Fe(II)-heme oxidized to Fe<sup>IV=O</sup> and a nearby tryptophan (Trp191) to its radical. Trp191 is connected to the heme by H-bonding via a His-Asp-Trp grouping with the histidine bound to Fe in an axial position. From site-directed mutagenesis studies on both Cp<sup>297</sup> and horseadish peroxidase,<sup>822</sup> a distal histidine, His52, is important residue.

The initial step in the activation of H<sub>2</sub>O<sub>2</sub><sup>52,818</sup> involves binding to Fe(II) with loss of a proton to His52. In the transition state for O—O cleavage, a key element is transfer of the proton initially bound to His52 to the terminal O-atom of the bound peroxide. Proton transfer is coupled to a slight motion and 2e<sup>-</sup> transfer. One electron is transferred from Fe(II) and one from the porphyrin. This results in the ferrylporphyrin cation radical shown in eq 194. Electron transfer

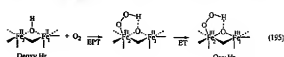


to the porphyrin cation radical from Tryptophan191 occurs in a subsequent step.<sup>52</sup> Assuming that the calculations are correct, this is another example of 2e<sup>-</sup>/1H<sup>+</sup> MS-EPT with the electrons coming from separate Fe(III) and porphyrin

electron donor orbitals. It is also an example of histidine acting sequentially as a proton donor and acceptor, much as His190 does in the TyrO<sup>•</sup>—H—His EPT module in PSII (section 7.2.4).

#### 7.4.3 Dioxygen Binding to Hemerythrin

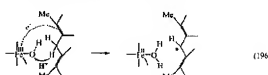
Hemerythrin (Hr) contain magnetically exchange-coupled non-heme iron centers and are capable of reversibly binding dioxygen.<sup>824–828</sup> In the net sense, addition of O<sub>2</sub> to the deoxygenated form of Hr, deoxyHr, is accompanied by 2e<sup>-</sup>/1H<sup>+</sup> PCET to give the oxy form, oxyHr, eq 195. Density



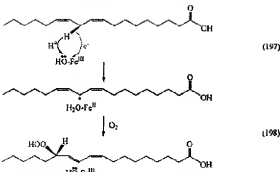
functional theory (DFT) has been applied to both the deoxy and oxy forms<sup>829</sup> and to the reversible addition of O<sub>2</sub>.<sup>830</sup> The latter calculations point to a stepwise process with a mixed HAT—EPT step followed by ET. On the binding side of the equilibrium, electron transfer occurs from (Fe(II))<sub>2</sub> in eq 195 to a  $\pi^*$  orbital on O<sub>2</sub> with coupled-proton transfer from the bridging hydroxide to give coordinated HOO<sup>•</sup>. ET occurs in a following step from Fe(II) to a  $\pi^*$  orbital on the terminal hydroperoxide (HOO<sup>•</sup>).

#### 7.4.4. H-Atom Abstraction by Lipoxygenases (LO)

The lipoxygenase (LO) enzymes catalyze the regio- and stereospecific hydroperoxidation of (Z,Z)-pentadiene-containing fatty acid substrates.<sup>831–835</sup> The results of detailed kinetic studies are available for the reaction with linoleic acid.<sup>827,828,835,843,847</sup> In the ferrous form, the iron site contains three coordinated histidines, one C-terminal isoleucine carboxylate, and a water with an asparagine in the sixth coordination position but 3 Å away from the iron.<sup>834,839,838</sup> Based on spectroscopic measurements, the Fe(II) form is five coordinate.<sup>835</sup> DFT calculations on the initial step of the hydroxylation of (Z,Z)-2,5-heptadiene by the Fe<sup>II</sup>—OH form of the enzyme show that the reaction occurs by a net H-atom transfer. However, the acceptor orbital is largely d<sub>xy</sub>(Fe(III)) mixed with 2p<sub>x</sub>(O), and the donor orbital is a pure  $\pi$  orbital on the diene with oxidation leading to a delocalized carbon-based radical, eq 196.<sup>865</sup>



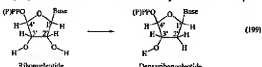
The theoretical studies have been extended to linoleic acid.<sup>839</sup> The reaction in eqs 197 and 198 shows that, following transfer of the pro-S hydrogen atom to Fe<sup>II</sup>—OH, a reaction with O<sub>2</sub> gives hydroperoxyoctadecadienoic acid. Based on calculations on the initial EPT step, a number of conclusions were reached: (1)  $\lambda_0 \sim 19$  kcal/mol, which comes largely from the reorganization energy at the Fe cofactor and is significantly greater than  $\lambda_0 \sim 2.4$  kcal/mol. (2)  $\Delta G^\circ = -5.4$  kcal/mol, which partly compensates for  $\lambda$  leading to a weak temperature-dependence. (3) The high  $k_3/k_0$  of 81 is a consequence of a large proton transfer distance and the dominance of the  $\mu = 0 \rightarrow \nu = 0$  vibrational channel. (4) There is no H-bond, and the maximal proton transfer distance



is considerably less (2.69 Å vs 2.88 Å) than the equilibrium distance calculated by using a docking model.<sup>360</sup>

#### 7.4.5. Long-Range PCET in Class I Ribonucleotide Reductase

The ribonucleotide reductase enzymes (RNRs) catalyze the conversion of nucleotides to deoxynucleotides, eq 199, and play an essential role in DNA replication and repair.



There are three classes of RNRs, and reviews have covered the mechanisms of nucleotide reduction for all three.<sup>349–845</sup> In class I RNRs, there are two types of homodimeric subunits, R1 and R2. R1 subunits contain five cysteines essential for catalysis with three at the active site. They control turnover and specificity. R2 subunits contain two dithiobisulfite clusters and 1.2 stable tyrosine radicals (Y<sup>•</sup>) per dimer, both of which are essential for the radical-initiated reduction of ribonucleotides.

A significant question is how Y<sup>•</sup> on the R2 (Y122) subunit generates a tyral radical (S<sup>•</sup>) at cysteine Cys439 on the R1 subunit. A docking model suggests that they are separated by 35 Å, and the reaction is reversible. Intervening between the two final redox sites are several tyrosines and a tryptophan residue. The cysteine residue is the final redox site.

Mechanisms have been proposed involving a series of sequential H-atom transfer steps, probably better described as EPT, and involving TyrO<sup>•</sup>/TyrOH, cysteine, tryptophane, and a dithiobisulfite cluster. This sequence of reactions is triggered by initial EPT between TyrO<sup>•</sup>(Y122) and Fe<sup>2+</sup>–OH<sub>2</sub>.<sup>349–847</sup>

The 1e<sup>−</sup>/2H<sup>+</sup> MS-EPT pathway suggested for the OEC in water oxidation may play a role in long-range EPT in the RNRs as well. In the OEC, 7 Å electron transfer occurs from Mn<sup>4+</sup>–OH<sub>2</sub> to Y<sub>2</sub><sup>•</sup> in concert with a double proton transfer: one from Mn<sup>4+</sup>–OH<sub>2</sub> to OOC–D<sub>1</sub>Asp6 and the other from <sup>1</sup>H–His190 to TyrO<sup>•</sup>, eq 174. In the RNRs, long-range electron transfer could be achieved by a sequence of 1e<sup>−</sup>/2H<sup>+</sup> MS-EPT steps based on membrane-embedded EPT couples. EPT directionality would be incorporated into the membrane structure by having EPT couples such as TyrO<sup>•</sup>–<sup>1</sup>H–His/Ty<sup>•</sup>OH–His aligned in the membrane so as to create a redox potential gradient.

In a recent model, it has been proposed that long-range electron transfer occurs from Y356, through W48, to Y122<sup>•</sup> in the R2 subunit.<sup>17</sup> In this model, electron transfer is accompanied by short-range proton transfer to/from local

hydrogen-bonded residues. It is known that proton transfer is not obligatory at position 356 since unnatural fluorotyrosine amino acids with lower pK<sub>a</sub>'s have been incorporated at this position and yet remain active.<sup>848</sup>

It has also been shown that the activity of RNR can be changed from a conformationally gated regime to one in which EPT and radical transport are rate limiting by increasing the reduction potential at position 356. The results of studies utilizing photoinitiated radical generation support an EPT model for radical transport between Y731, Y730, and C439 in the R1 subunit. These three residues are all within hydrogen bond contact in the crystal structure of R1, ensuring short proton tunneling distances. Based on this interpretation, both EPT and MS-EPT pathways appear to be utilized in RNR.<sup>17</sup>

#### 8. Summary

Some of the important conclusions reached in this analysis of PCET are summarized below. The sections in which they are discussed are also cited.

(1) PCET describes reactions in which there is a change in both electron and proton content between reactants and products. It originates from the influence of changes in electron content on acid–base properties and provides a molecular-level basis for energy transduction between proton transfer and electron transfer (section 1).

(2) Coupled electron–proton transfer or EPT is defined as an elementary step in which electrons and protons transfer from different orbitals on the donor to different orbitals on the acceptor. There is (usually) a clear distinction between EPT and H-atom transfer (HAT) or hydride transfer, in which the transferring electrons and proton come from the same bond. Hybrid mechanisms exist in which the elementary steps are different for the reaction partners (sections 5.1 and 5.2).

(3) EPT pathways such as PhO/PhOH exchange have much in common with HAT pathways in that electronic coupling is significant, comparable to the reorganization energy with  $H_{0A} \sim \lambda$ .

(4) *Multiple-Site Electron–Proton Transfer (MS-EPT)* is an elementary step in which an electron–proton donor transfers electrons and protons to different acceptors, or an electron–proton acceptor accepts electrons and protons from different donors. It exploits the long-range nature of electron transfer while providing for the short-range nature of proton transfer (section 5.1).

(5) A variety of EPT pathways exist, creating a taxonomy based on what is transferred, e.g., 1e<sup>−</sup>/2H<sup>+</sup> MS-EPT (section 5.1).

(6) PCET achieves “*redox potential leveling*” between sequential couples and the buildup of multiple redox equivalents, which is of importance in multielectron catalysis (section 2.1).

(7) There are many examples of PCET and pH-dependent redox behavior in metal complexes, in organic and biological molecules, in excited states, and on surfaces (section 2).

(8) Changes in pH can be used to induce electron transfer through films and over long distances in molecules. Changes in pH, induced by local electron transfer, create pH gradients and a driving force for long-range proton transfer in Photosystem II and through other biological membranes (sections 3 and 7.2).

(9) In EPT, simultaneous transfer of electrons and protons occurs on time scales short compared to the periods of coupled vibrations and solvent modes. A theory for EPT has

been developed which rationalizes rate constants and activation barriers, includes temperature and driving force ( $\Delta G^\circ$ ) dependences implicitly, and explains kinetic isotope effects. The distance-dependence of PCT is dominated by the short-range nature of proton transfer, with electron transfer being far less demanding (sections 4.2 and 5).

(10) Changes in external pH do not affect an EPT elementary step. Solvent molecules or buffer components can act as proton donor acceptors, but individual H<sub>2</sub>O molecules are neither good bases ( $pK_a(\text{H}_2\text{O}) = -1.74$ ) nor good acids ( $pK_a(\text{H}_2\text{O}) = 15.7$ ) (section 5.5.3).

(11) There are many examples of mechanisms in chemistry, in biology, on surfaces, and in the gas phase which utilize EPT (sections 6 and 7).

(12) PCET and EPT play critical roles in the oxygen evolving complex (OEC) of Photosystem II and other biological reactions by decreasing driving force and avoiding high-energy intermediates (section 7.2).

## 8.1. Addenda

During the lengthy period for review of this manuscript, a number of significant publications have appeared which feature various aspects of PCET. Among them are reviews on water oxidation in Photosystem II<sup>189,190</sup> and on the role of PCET in oxygen activation.<sup>190,191</sup> The theory of EPT has been extended by Hammes-Schiffer<sup>82,193</sup> An analysis of the role of driving force and water as the proton donor or acceptor by Costentin and Saveant has appeared<sup>194</sup> as has a report of MLCT excited state quenching by EPT.<sup>195</sup>

**Acknowledgments** are made to the Los Alamos National Laboratory and the National Science Foundation for support that led to the writing of this review.

## 9. References

- Yang, E. S.; Chan, M. S.; Wahl, A. C. *J. Phys. Chem.* **1975**, *79*, 2949.
- Zwickl, A.; Taube, H. *J. Am. Chem. Soc.* **1961**, *83*, 793.
- Cardin, L. P.; Halperin, J. *Inorg. Chem.* **1965**, *4*, 766.
- Roecker, L.; Meyer, T. J. *J. Am. Chem. Soc.* **1966**, *108*, 4066.
- Lebeau, E. L.; Binsted, R. A.; Meyer, T. J. *J. Am. Chem. Soc.* **2001**, *123*, 10535.
- (For loss of a proton at the prevailing pH,  $\Delta G^\circ$  in eV is given by  $\Delta G^\circ = 0.059(pK_a - \text{pH})$ , and for gain of a proton,  $\Delta G^\circ = -0.059(-pK_a + \text{pH})$  at 25 °C.)
- Binsted, R. A.; Meyer, B. A.; Samuels, G. J.; Meyer, T. J. *J. Am. Chem. Soc.* **1981**, *103*, 2897.
- Binsted, R. A.; Meyer, T. J. *J. Am. Chem. Soc.* **1987**, *109*, 3287.
- Binsted, R. A.; Stultz, L. K.; Meyer, T. J. *Inorg. Chem.* **1995**, *34*, 546.
- Meyer, T. J.; Taube, H. *Inorg. Chem.* **1968**, *7*, 2369.
- Cukier, R. I.; Nocera, D. G. *Ann. Rev. Phys. Chem.* **1998**, *49*, 337.
- Costentin, H.; Hammes-Schiffer, S. *J. Phys. Chem. A* **2000**, *104*, 9370.
- Prausnitz, J. M.; Robert, M.; Saveant, J. M. *J. Am. Chem. Soc.* **2001**, *123*, 4886.
- Bicak, L.; Linschitz, H. *J. Phys. Chem.* **1995**, *99*, 1843.
- Bicak, L.; Gupta, N.; Linschitz, H. *J. Am. Chem. Soc.* **1997**, *119*, 12601.
- Gray, H. B.; Winkler, J. R. *Proc. Natl. Acad. Sci. U.S.A.* **2005**, *102*, 3533.
- Reese, S. Y.; Hodgeson, J. M.; Stubbe, J.; Nocera, D. G. *Philos. Trans. R. Soc. London, Ser. A* **2006**, *364*, 153.
- Meyer, T. J.; Hayns, M. V. H. *Inorg. Chem.* **2003**, *42*, 8149–8160 and references therein.
- Meyer, T. J.; Tausi, M.; Ugo, R. *Fundamental Research in Heterogeneous Catalysis*; Plenum Press: New York, 1977, p 169.
- Williams, R. J. P. *J. Theor. Biol.* **2002**, *219*, 389.
- Cukierman, S. *Frontiers Biosci.* **2003**, *8*, S118.
- DeCoursey, T. E. *Physiol. Rev.* **2003**, *83*, 475.
- Borucki, P.; Larson, G. *Biochim. Biophys. Acta Bioenerg.* **2003**, *1605*, 1.
- Tommos, C.; Babcock, G. T. *Acc. Chem. Res.* **1998**, *31*, 18.
- Heganson, C. W.; Babcock, G. T. *Science* **1997**, *277*, 1953.
- Renay, A.; Gerwitz, K. *Nature Struct. Biol.* **2003**, *10*, 637.
- Babcock, G. T.; Eager, M. P.; Horsman, C.; Lydiard-Simantov, N.; McCracken, J.; Shi, W. J.; Styring, S.; Tommos, C.; Warecke, K. *Acta Chim. Scand.* **1997**, *51*, 533.
- Prochalyukov, D. A.; Prusker, M. A.; Babcock, G. T. *Proc. Natl. Acad. Sci. U.S.A.* **1998**, *95*, 8020 and references therein.
- Hsieh, J.; Dodson, R. W. *J. Am. Chem. Soc.* **1956**, *78*, 911.
- Friedman, H. L.; Newton, M. D. *J. Electroanal. Chem.* **1986**, *204*, 21.
- Reynolds, W. L.; Lamery, R. W. *J. Chem. Phys.* **1955**, *23*, 2460.
- Reynolds, T. T.; Taube, H. Unpublished result, 1966.
- Binsted, R. A.; McGuire, M. E.; Doylelogian, A.; Seok, W. K.; Roecker, L. E.; Meyer, T. J. *J. Am. Chem. Soc.* **1992**, *114*, 173.
- Thor, H. *H. Chem. Abst. Inorg. Chem.* **1991**, *13*, 171.
- Li, W.; Thor, H. *Excited-State Proton Transfer Reactions of Multiply-Bonded Ligands. Advances in Transition Metal Coordination Chemistry*, Vol. 1, p 187.
- Cukier, R. I. *J. Phys. Chem.* **1994**, *98*, 2377.
- Seok, W. K. *J. Phys. Chem.* **1995**, *99*, 16101.
- Zhang, X. G.; Cukier, R. I. *J. Phys. Chem.* **1995**, *99*, 945.
- Cukier, R. I. *J. Phys. Chem.* **1996**, *100*, 15428.
- (40) and references therein.
- Fang, J.-Y.; Hammes-Schiffer, S. *J. Chem. Phys.* **1997**, *105*, 8442 and references therein.
- Fang, J.-Y.; Hammes-Schiffer, S. *J. Chem. Phys.* **1997**, *107*, 8933 and references therein.
- Costentin, C.; Evans, D. H.; Robert, M.; Saveant, J. M.; Singh, P. S. *J. Am. Chem. Soc.* **2005**, *127*, 12490.
- Lehman, M. W.; Evans, D. H. *J. Phys. Chem. B* **2001**, *105*, 8877.
- Hammes-Schiffer, S. *Proton-coupled electron transfer. In Electron Transfer in Chemistry, Vol. 1: Principles, Theories, Methods and Techniques*; Balazs, A. V., Ed.; Wiley-VCH: Weinheim, 2001; Vol. 1, p 189.
- Hammes-Schiffer, S. *Acc. Chem. Res.* **2001**, *34*, 273.
- Hammes-Schiffer, S. *Chem. Phys. Chem.* **2002**, *3*, 33.
- Hammes-Schiffer, S.; Iordanova, N. *Biochim. Biophys. Acta* **2004**, *1635*, 29.
- Mayer, J. M. *Am. Rev. Phys. Chem.* **2004**, *55*, 363.
- Mayer, J. M.; Rihle, I. *J. Biochim. Biophys. Acta Bioenerg.* **2004**, *1655*, 51.
- Chen, C. I.; Chang, M. C. Y.; Damrauer, N. H.; Nucera, D. G. *Biochim. Biophys. Acta Bioenerg.* **2004**, *1655*, 13.
- Hayns, M. H. V.; Meyer, T. J. *Proc. Natl. Acad. Sci. U.S.A.* **2004**, *101*, 13138.
- Himo, F.; Siegbahn, P. E. M. *Chem. Rev.* **2003**, *103*, 2421.
- Lovell, T.; Himo, F.; Han, W. G.; Noddlein, L. *Coord. Chem. Rev.* **2003**, *238*, 211.
- Ram, M. S.; Steenjones, L. M.; Johnson, C. S.; Zhang, X. L.; Stern, C.; Yoon, D. L.; Selensky, D.; Hupp, T. J. *J. Am. Chem. Soc.* **1995**, *117*, 1411 and references therein.
- Whitman, M. W.; Whitman, J. W. *Biochemistry* **1997**, *36*, 8923.
- Whitman, J. M.; Whitman, A. R.; Goldsby, K. A. *Electrochemistry: Proton-Coupled Systems. In Comprehensive Organometallic Chemistry*; McCleverty, J. A.; Meyer, T. J., Eds.; 2003; Vol. 2, p 223 and references therein.
- Bates, C. F., Jr.; Messner, R. E. *The Hydrolysis of Metal Cations*; Kreiger, R. E. Publishing Co.: Malabar, FL, 1986.
- Sjödin, M.; Styring, S.; Akermark, B.; Sun, L.; Hammarström, L. *J. Am. Chem. Soc.* **2000**, *122*, 3952.
- And, J. C.; Porta, G.; Fang, J. Y.; Srechan, E. *Trans. Faraday Soc.* **1961**, *57*, 882.
- Meyer, B. A.; Meyer, T. J. *J. Am. Chem. Soc.* **1978**, *100*, 3601.
- Meyer, B. A.; Meyer, T. J. *Inorg. Chem.* **1981**, *20*, 436.
- For E<sub>1/2</sub> red/reactions written as reduction potentials,  $\text{Ox}^\bullet + \text{e}^- \rightarrow \text{Red}$ ,  $E_{1/2}$  values obtained by voltammetry are related to the formal potential,  $E^\circ$ , at 25 °C by  $E_{1/2} = E^\circ - (0.059 \text{ ln}(m_{\text{red}}/m_{\text{ox}}))^{1/2}$ . In this equation,  $m_{\text{red}}/m_{\text{ox}}$  is the ratio of mass transfer coefficients (in cm/s) for the oxidized (ox) and reduced (red) forms of the couple. The formal potential is the electrode potential in the prevailing redox couple,  $[\text{Ox}^\bullet]/[\text{Red}]$ .  $\alpha_{\text{red}}$  and  $\alpha_{\text{ox}}$  are the potential when the ratio of activities,  $a_{\text{red}}/a_{\text{ox}}$ .
- Zandio, P. *Inorganic Electrochemistry: Theory, Practice and Application*; Royal Society of Chemistry: Cambridge, 2003.
- Bard, A. J.; Faulkner, L. R. *Electrochemical Methods: Fundamentals and Applications*, 2nd ed.; J. Wiley: New York, 2001.
- Bard, A. J.; Parsons, R.; Jordon, J. *Standard Potentials in Aqueous Solution*; Marcel Dekker: New York, 1985.
- More generally, for the Ru(II/III) couple over the entire pH range in Figure 2,  $E_{1/2}$  varies with pH as  $E_{1/2} = E^\circ(\text{Ru}(\text{II})/\text{Ru}(\text{III})) - 0.059( - \log(K_{\text{diss}}^{\text{ox}} + [\text{H}^+]) - \log(K_{\text{diss}}^{\text{red}} + [\text{H}^+])$ , with  $K_{\text{diss}}^{\text{ox}}$  and  $K_{\text{diss}}^{\text{red}}$  the dissociation constants for the Ru(II) and Ru(III) aqua complexes.<sup>6</sup>
- Johnson, D. A. *Some Thermodynamic Aspects of Inorganic Chemistry*; Cambridge University Press: London, 1958.

(65) Buckingham, D. A.; Sorenson, A. M. In *Cleaving Agents and Metal Chelators*; Doherty, P. J., Mellor, D. P., Eds.; Academic Press: New York, 1964; Chapter 6.

(66) Heath, G. A.; Moose, K. A.; Sharp, D. W. A.; Yellowlees, L. J. *J. Chem. Soc., Chem. Commun.* 1985, 1303.

(67) Gunn, M. R.; Honig, B. *Proc. Natl. Acad. Sci. U.S.A.* 1991, 88, 9151.

(68) Astuti, Y.; Tuppiglidi, E.; Briscoe, P. B.; Fanuzzi, A.; Gilardi, G.; Durrant, J. R. *J. Am. Chem. Soc.* 2004, 126, 8901.

(69) Huang, B.; Niu, Y. *Adv. Science* 1995, 268, 114.

(70) Lamantia, C. R. D. *Proc. Roy. Soc. London Ser. A* 2003, 545, 52.

(71) Cotton, F. A.; Wilkinson, G.; Murrillo, C. A.; Bochmann, M. *Advanced Inorganic Chemistry*; Wiley & Sons, Inc.: New York, 1999.

(72) Nadjo, L.; Savant, J. M. *J. Electroanal. Chem.* 1971, 33, 419.

(73) Lund, H.; Hammerich, O. *Carbonyl Compounds: Organic Electrochemistry*; Marcel Dekker: New York, 2001, Chapter 12.

(74) Lund, H.; Baltz, M. *Organic Electrochemistry: An Introduction and Guide*; Marcel Dekker: New York, 1991.

(75) Chambers, J. Q. In *The Chemistry of Quinonoid Compounds*; Patai, S., Rappoport, Z., Eds.; Wiley: New York, 1988; Vol. II, p 199.

(76) Meunier-Prest, R.; Laviron, E.; Gepard, C.; Raveau, S. *Electrochim. Acta* 2001, 46, 1847 and references therein.

(77) Ammar, F.; Nadjo, L.; Savant, J. M. *J. Electroanal. Chem.* 1973, 48, 146.

(78) Laviron, E. *J. Electroanal. Chem.* 1984, 164, 213.

(79) Laviron, E. *J. Electroanal. Chem.* 1984, 169, 29.

(80) Laviron, E. *J. Electroanal. Chem.* 1984, 208, 357.

(81) Laviron, E.; Meunier-Prest, R. *J. Electroanal. Chem.* 1992, 324, 1.

(82) Meunier-Prest, R.; Laviron, E. *J. Electroanal. Chem.* 1992, 328, 33.

(83) Slattery, S. J.; Blaha, J. K.; Leinen, J.; Goldby, K. A. *Coord. Chem. Rev.* 1998, 174, 391.

(84) Liu, X. P.; Theil, E. C. *Acc. Chem. Res.* 2005, 38, 167.

(85) Machera, B. *Coord. Chem. Rev.* 2005, 249, 591.

(86) Espinosa, J. H. *Coord. Chem. Rev.* 2005, 249, 329.

(87) Hurst, T. J. *Coord. Chem. Rev.* 2005, 249, 313.

(88) Borovik, A. S. *Acc. Chem. Res.* 2006, 38, 54.

(89) Muthukumar, S.; Sankar, S. K.; Bhaider, S.; Armstrong, W. H. *Chem. Rev.* 2004, 104, 3531.

(90) Moussavi, J.; de Vries, P. S.; Shukla, S. *Chem. Rev.* 2004, 104, 3947.

(91) Lewis, B. A.; Tolman, W. B. *Chem. Rev.* 2004, 104, 1047.

(92) Emeneki, J. H.; Cooney, J. A. *Chem. Rev.* 2004, 104, 1175.

(93) Che, C. M.; Yam, W. W. *Adv. Inorg. Chem.* 1992, 35, 233.

(94) Che, C. M.; Yam, W. W. *Adv. Transition Met. Chem.* 1996, 1, 209.

(95) Gilbert, J. A.; Eggleston, D. S.; Murphy, R. Jr.; Geselovitz, D. A.; Gersten, S. W.; Hodgson, D. J.; Meyer, T. J. *J. Am. Chem. Soc.* 1984, 106, 3555.

(96) Dobson, J. C.; Takeuchi, K. J.; Pipes, D. W.; Geselovitz, D. A.; Meyer, T. J. *Inorg. Chem.* 1986, 25, 2557.

(97) Pipes, D. W.; Meyer, T. J. *J. Am. Chem. Soc.* 1984, 106, 7653.

(98) Pipes, D. W.; Meyer, T. J. *Inorg. Chem.* 1986, 25, 4042.

(99) Pipes, D. W.; Meyer, T. J. *Inorg. Chem.* 1986, 25, 3255.

(100) Doevangelou, A.; Adeyemi, S. A.; Lynn, M. H.; Hodgson, D. J.; Meyer, T. J. *Am. Chem. Soc.* 1990, 112, 8389.

(101) Lebeau, E. L.; Meyer, T. J. *Inorg. Chem.* 1999, 38, 2174.

(102) Adeyemi, S. A.; Doevangelou, A.; Gudipati, A.; Meyer, T. J. *Inorg. Chem.* 1992, 31, 1373.

(103) Adeyemi, S. A.; Gudipati, A.; Dobbel, F.; Gullberg, L. A.; Maris, P. J.; T. J. *Am. Chem. Soc.* 1998, 120, 12246.

(104) Neyhart, G. A.; Hupp, J. T.; Curtiss, C. J.; Timson, C. J.; Meyer, T. J. *Am. Chem. Soc.* 1996, 118, 2347.

(105) Che, C.-M.; Cheng, J. Y. K.; Chong, K.-K.; Wong, K.-Y. *J. Chem. Soc., Dalton Trans.* 1997, 13, 2347.

(106) Manchanda, R.; Thorp, H. H.; Brudvig, G. W.; Cahrlree, R. H. *Inorg. Chem.* 1992, 31, 4040.

(107) Manchanda, R.; Thorp, H. H.; Brudvig, G. W.; Cahrlree, R. H. *Inorg. Chem.* 1992, 31, 4040.

(108) Thorp, H. H.; Brudvig, G. W.; Cahrlree, R. H. *Inorg. Chem.* 1990, 29, 293.

(109) Thorp, H. H.; Brudvig, G. W.; Cahrlree, R. H. *J. Electroanal. Chem. Interfacial Electrochem.* 1990, 290, 293.

(110) Gilbert, J. A.; Geselovitz, D.; Meyer, T. J. *J. Am. Chem. Soc.* 1986, 108, 1493.

(111) Liope, A.; Doppelt, P.; Meyer, T. J. *Inorg. Chem.* 1988, 27, 514.

(112) Linguri, R.; Morris, J. J.; Staley, W. C.; Bell-Loucelle, E. T.; Turner, M.; Boyko, W. J.; Bessel, C. A. *Inorg. Acta* 2001, 315, 53.

(113) Mohanty, J. G.; Chakravorty, A. *Inorg. Chem.* 1976, 15, 2912.

(114) Mohanty, J. G.; Singh, R. P.; Singh, A. N.; Chakravorty, A. *J. Indian Chem. Soc.* 1977, 54, 210.

(115) Singh, A. N.; Singh, R. P.; Mohanty, J. G.; Chakravorty, A. *Inorg. Chem.* 1977, 16, 2597.

(116) Mohanty, J. G.; Chakravorty, A. *Inorg. Chem.* 1977, 16, 1561.

(117) Levy, N. M.; Larrazabal, M. C.; Neves, A.; Franco, C. V. *J. Coord. Chem.* 1998, 38, 259.

(118) Doh, A. M.; Haga, M. A. *J. Am. Chem. Soc.* 1990, 112, 6132.

(119) Doh, A. M.; Haga, M. A. *Inorg. Chem.* 1992, 31, 507.

(120) Xiao, X. M.; Haga, M. A.; Matsumura, T.; Re, Y.; Addison, W.; Kano, K. *J. Chem. Soc., Dalton Trans.* 1993, 15, 277.

(121) Ayers, T.; Caylor, N.; Ayers, G.; Godwin, C.; Hascrook, D. J.; Stomann, V.; Slattery, S. J. *Inorg. Chem. Acta* 2002, 328, 33.

(122) Haga, M.; Arai, T.; Kano, K.; Yamabe, S. *Inorg. Chem.* 1991, 30, 3843.

(123) Chin, K. F.; Wong, K. Y.; Che, C. M. *J. Chem. Soc., Dalton Trans.* 1993, 1, 197.

(124) Haga, M.; Hwang, K. K.; Che, C. M. *J. Chem. Soc., Dalton Trans.* 1994, 16, 3699.

(125) Hayn, M. H. V.; El-Samandy, E. S.; Dennis, K. D.; Meyer, T. J.; White, P. S. *J. Am. Chem. Soc.* 1999, 121, 1403.

(126) Hayn, M. H. V.; El-Samandy, E. S.; Dennis, K. D.; White, P. S.; Meyer, T. J. *Inorg. Chem.* 2000, 39, 3075.

(127) Hayn, M. H. V.; El-Samandy, E. S.; White, P. S.; Meyer, T. J. *Inorg. Chem.* 1999, 38, 3760.

(128) Hayn, M. H. V.; El-Samandy, E. S.; Dennis, K. D.; Meyer, T. J. *Inorg. Chem.* 2000, 39, 4101.

(129) Hayn, M. H. V.; Meyer, T. J. *Angew. Chem., Int. Ed.* 2001, 40, 1395.

(130) Hayn, M. H. V.; Meyer, T. J. *Angew. Chem., Int. Ed.* 2002, 41, 1395.

(131) Hayn, M. H. V.; Meyer, T. J. *Angew. Chem., Int. Ed.* 2002, 41, 1395.

(132) Hayn, M. H. V.; Meyer, T. J.; Baker, R. T. *J. Am. Chem. Soc.* 2003, 125, 2832.

(133) Hayn, M. H. V.; White, P. S.; Carter, C. A.; Meyer, T. J. *Angew. Chem., Int. Ed.* 2001, 40, 3037.

(134) Coia, G. M.; Dennis, K. D.; Meyer, T. J. *J. Am. Chem. Soc.* 2000, 122, 2212.

(135) Nagert, W. A.; Meyer, J. A. *Metal-Ligand Multiple Bonds*; Wiley: New York, 1958; Chapter 3.

(136) Che, C. M. *Appl. Chem.* 1995, 67, 225.

(137) Bahr, J. D.; Winkler, J. R.; Turner, H. *Inorg. Chem.* 1980, 19, 2416.

(138) Bahr, J. D.; Turner, H. *Inorg. Chem.* 1979, 18, 2208.

(139) El-Samandy, E. S.; Dennis, K. D.; Meyer, T. J. *Inorg. Chem.* 2001, 40, 3677.

(140) Ishizaki, O.; White, P. S.; Meyer, T. J. *Inorg. Chem.* 1996, 35, 2167.

(141) Pipes, D. W.; Bakir, M.; Vials, S. E.; Hodgson, D. J.; Meyer, T. J. *J. Am. Chem. Soc.* 1990, 112, 5507.

(142) Asefa, Z.; Stenbury, D. M. *J. Am. Chem. Soc.* 1997, 119, 521.

(143) Hayn, M. H. V.; White, P. S.; John, K. D.; Meyer, T. J. *Angew. Chem., Int. Ed.* 2001, 40, 4049.

(144) Keene, F. R. *Coord. Chem. Rev.* 1999, 187, 121 and references therein.

(145) Acock, P. A.; Keene, F. R. *J. Am. Chem. Soc.* 1981, 103, 6494.

(146) Acock, P. A.; Keene, F. R.; Smythe, R. S.; Snow, M. R. *Inorg. Chem.* 1984, 23, 2336.

(147) Bernhard, P.; Bell, D. J.; Burgi, H. B.; Osvath, P.; Ruselli, A.; Sorenson, A. M. *Inorg. Chem.* 1997, 36, 2834.

(148) Bernhard, P.; Sorenson, A. M. *J. Chem. Soc., Chem.* 1998, 27, 1516.

(149) Bernhard, P.; Sorenson, A. M.; Anson, F. C. *Inorg. Chem.* 1988, 27, 2754.

(150) Bernhard, P.; Sorenson, A. M. *J. Am. Chem. Soc.* 1989, 111, 597.

(151) Bernhard, P.; Anson, F. C. *Inorg. Chem.* 1989, 28, 3272.

(152) Lane, B. C.; Lester, J. E.; Basilio, F. J. *J. Am. Chem. Soc., Chem. Commun.* 1978, 24, 1618.

(153) Mahoney, D. F.; Bostick, J. K. *Inorg. Chem.* 1973, 12, 2561.

(154) Keene, F. R.; Salma, D. J.; Meyer, T. J. *J. Am. Chem. Soc.* 1976, 98, 1834.

(155) Huynh, M. H. V.; Baker, R. T.; Morris, D. E.; White, P. S.; Meyer, T. J. *Angew. Chem., Int. Ed.* 2002, 41, 3870.

(156) Chambers, J. Q. In *The Chemistry of Quinonoid Compounds*; Patai, S., Rappoport, Z., Eds.; Wiley: New York, 1974; Vol. I, Chapter 14, p 737; 1988; Vol. II, Chapter 12, p 719.

(157) Evans, D. H. In *Encyclopedia of Electrochemistry*; Bard, A. J., Eds.; Marcel Dekker: New York, 1978; Vol. 12.

(158) Laviron, E. *J. Electroanal. Chem.* 1983, 146, 15 and references therein.

(159) Gupta, N.; Linschitz, H. *J. Am. Chem. Soc.* 1997, 119, 6384.

(160) Kurihara, M.; Sano, H.; Murata, M.; Nishihara, H. *Inorg. Chem.* 2001, 40, 4.

(161) Graves, M. D.; Niemi, A.; Rettig, V. M. *J. Am. Chem. Soc.* 1999, 121, 266.

(162) Parson, W. W. In *Photosynthesis*; Arnon, I., Ed.; Elsevier: New York, 1987; p 43.

(163) Feher, G.; Allen, J. P.; Okamura, M. Y.; Rees, D. C. *Nature* 1989, 339, 11.

(164) Fang, Y.; Liu, L.; Feng, Y.; Li, X. S.; Guo, Q. *J. Phys. Chem. A* 2002, 106, 4669.

(165) Bernstein, J.; Cohen, M. D.; Letserowitz, L. In *The Chemistry of Quinonoid Compounds*; Patai, S., Ed.; John Wiley & Sons Ltd.: Chichester, 1974; p 37.

(166) Föster, R.; Formanek, M. L. In *The Chemistry of Quinonoid Compounds*; Patai, S., Ed.; John Wiley & Sons Ltd.: Chichester, 1974, p 257.

(167) Depew, M. C.; Wan, J. K. S. In *The Chemistry of Quinonoid Compounds*; Patai, S., Ed.; John Wiley & Sons Ltd.: Chichester, 1983; Vol. II, p 963.

(168) Ringer, H.; Linsbach, H. H. *J. Am. Chem. Soc.* 1989, 111, 5429 and references therein.

(169) Mitani, T.; Saito, G.; Urayama, H. *Phys. Rev. Lett.* 1988, 60, 2299.

(170) Mitani, T. *Mol. Cryst. Liq. Cryst.* 1989, 171, 343.

(171) Mitani, T. *Surf. Met.* 1988, 27, B49.

(172) Nakajishi, K.; Sugihara, K.; Kitagawa, T.; Toyoda, J.; Okamoto, H.; Okanishi, K.; Mitani, T.; Yamamoto, H.; Mitora, I.; Kawamoto, A.; Tanaka, J. *J. Am. Chem. Soc.* 1991, 113, 1862.

(173) Linsbach, H. H. In *The Use of NMR Spectroscopy in the Study of Hydrogen Bonding in Solution*. In *Advanced Processors*; Gormley, J. W.; Wijn-Jones, E., Eds.; Elsevier: Amsterdam, 1983; Chapter 16.

(174) Linsbach, H. H.; Henning, J.; Geriken, D.; Rumpf, H. *Faraday Discuss.* *Chem. Soc.* 1982, 74, 822.

(175) Hennig, J.; Linsbach, H. H. *J. Am. Chem. Soc.* 1984, 106, 392.

(176) Schulbach, M.; Wehrle, B.; Linsbach, H. H.; Bunnemann, E.; Katergrat, A.; Shin, A. Y.; Tof, R.; Djereci, C. *J. Am. Chem. Soc.* 1984, 106, 393.

(177) Wehrle, B.; Linsbach, H. H.; Zinnemann, H. *J. Am. Chem. Soc.* 1988, 110, 7014 and references therein.

(178) Braun, J.; Schwesinger, R.; Williams, P. G.; Morimoto, H.; Wemmer, D. E.; Linsbach, H.-H. *J. Am. Chem. Soc.* 1996, 118, 11101 and references therein.

(179) Mitchell, P. *Nature* 1961, 191, 144.

(180) Williams, R. J. *Biochim. Biophys. Acta* 1991, 1058, 71.

(181) Beacock, G. T.; Wikström, M. *Nature* 1992, 355, 301.

(182) Williams, R. J. *Adv. Chem.* 1993, 26, 332.

(183) Ranville, D. E.; Maitland, B. G.; Winkler, J. R.; Gray, H. B. *Proc. Natl. Acad. Sci. U.S.A.* 1995, 92, 11949.

(184) Rich, P. R.; Meunier, B.; Mitchell, R.; Moody, A. J. *Biochim. Biophys. Acta* 1996, 1275, 91.

(185) Neude, K.; Pebay-Peyroula, E.; Edman, K.; Royston, A.; Navarro, J.; Landau, E. M. *Biochim. Biophys. Acta* 2002, 1555, 144.

(186) Rappaport, F.; Lavigne, J. *Biochim. Biophys. Acta* 2001, 1503, 246.

(187) Hofacker, I.; Schulten, K. *Proteins: Struct., Funct., Genet.* 1998, 31, 100.

(188) Winkler, M. *Curr. Opin. Struct. Biol.* 1998, 8, 480.

(189) Burgess, B. K.; Lowe, D. J. *Chem. Rev.* 1996, 96, 2583.

(190) Sosofit, L. C.; Dean, D. R. *Chem. Rev.* 1997, 97, 20, 266.

(191) Howard, J. B.; Rees, D. C. *Ann. Rev. Biochem.* 1994, 63, 235.

(192) Peters, J. W.; Fisher, K.; Dean, D. R. *Ann. Rev. Microbiol.* 1995, 49, 335.

(193) Lanzilotta, W. N.; Christiansen, J.; Dean, D. R.; Sosofit, L. C. *Biochemistry* 1998, 37, 1376.

(194) Hirst, J.; Duff, J. L. C.; Jameson, G. N. L.; Kemper, M. A.; Burgess, B. K.; Armstrong, F. A. J. *Am. Chem. Soc.* 1998, 120, 7083.

(195) Hirst, J. R.; Jung, Y. S.; Huisken-Wang, L. M.; Burgess, B. K.; Stor, C. D.; Hirst, J.; Armstrong, F. A. *Biochemistry* 2003, 42, 10369.

(196) Meuwly, M.; Karplus, M. *Faraday Discuss.* 2003, 124, 297.

(197) Miller, A.-F.; Sorkin, D. L. *Comments Mol. Cell. Biophys.* 1997, 9, 1.

(198) Fridovich, I. *Free Radic. Res.* 1998, 7, 2688.

(199) Fridovich, I. *J. Biol. Chem.* 1997, 272, 18515.

(200) Musco, C.; Cuzzocrea, S.; Riley, D. P.; Zweier, J. L.; Thiemermann, C.; Wang, Z. Q.; Salvenen, D. B. *Br. J. Pharma.* 2003, 149, 445.

(201) Miller, A.-F.; Miller, D. F.; Domniczak, A. F. *Hypertension* 1999, 34, 539.

(202) Salvenen, D.; Cuzzocrea, S. *Crit. Care Med.* 2003, 31, S29.

(203) Bell, C.; Fee, J. A. *J. Am. Chem. Soc.* 1985, 107, 3295.

(204) Miller, A. F.; Padmavath, K.; Sorkin, D. L.; Karapetian, A.; Vance, C. K. *J. Inorg. Biochem.* 2003, 93, 71.

(205) Schwartz, A. L.; Yilmaz, E.; Vance, C. K.; Vathyam, S.; Koder, R. L.; Miller, A. F. *J. Inorg. Biochem.* 2006, 90, 247.

(206) Meakin, J.; Karapetian, A.; Vance, C.; Yilmaz, E.; Wu, Q.; Jackson, T. C.; Bond, T. C.; Spiro, T. G.; Miller, A. F. *J. Am. Chem. Soc.* 2002, 124, 15064.

(207) Hickman, J. J.; Oler, D.; Laibinis, P. E.; Whitesides, G. M.; Wrighton, M. S. *Science* 1991, 252, 688.

(208) Haddox, R. M.; Fleckle, H. O. *J. Electroanal. Chem.* 2003, 539-551, 351.

(209) Broussau, L. C.; Zhao, Q.; Shultz, D. A.; Feldheim, D. L. *J. Am. Chem. Soc.* 1998, 120, 7645.

(210) Murguia, D. H.; Hildebrandt, P. *J. Am. Chem. Soc.* 2001, 123, 4052.

(211) Haga, H.; Hong, H. G.; Shiozawa, Y.; Kawata, Y.; Morishiro, H.; Fukui, A. *J. Inorg. Chem.* 2000, 39, 4566.

(212) Foster, R. J. *J. Electrochem. Soc.* 1997, 144, 1165.

(213) Honstein, B.; Datalbaum, D. M.; Schonover, J.; Meyer, T. J. Unpublished results.

(214) Gallagher, L. A.; Meyer, T. J. *J. Am. Chem. Soc.* 2001, 123, 5308.

(215) Grubis, W. T.; King, L. H. *Anal. Chem.* 1980, 52, 273.

(216) Anikado, T.; Iwakura, C.; Tamura, H. *Electrochim. Acta* 1978, 23, 9.

(217) McKenzie, K. J.; Marken, F. *Electrochim. Solid-State Lett.* 2002, 5, E47.

(218) Bolts, J. M.; Wriggins, M. S. *J. Phys. Chem.* 1976, 80, 2641.

(219) Watanabe, T.; Fujishima, A.; Tatsuki, O.; Honda, K. *Bull. Chem. Soc. Jpn.* 1976, 51, 49.

(220) Gerischer, H. *Electrochim. Acta* 1989, 34, 1005.

(221) Natale, M. J.; Wrighton, M. S. *J. Phys. Chem.* 1987, 91, 248.

(222) Hwang, H. O. *Semiconductor Electrodes*; Elsevier: New York, 1988; Chapter 2.

(223) Lyon, L. A.; Hupp, J. T. *J. Phys. Chem.* 1993, 97, 4623.

(224) Murray, R. W. *Molecular Design of Electronic Surface*; John Wiley and Sons: New York, 1992; Vol. 22.

(225) Dennerz, A.; Moulet, J. C. *Coord. Chem. Rev.* 1996, 147, 339.

(226) Gaudapal, A. R.; Chen, X. H.; Sullivan, B. P.; Meyer, T. J. *Inorg. Chem.* 1993, 32, 5502.

(227) Danner, R. C.; Meyer, T. J. *Inorg. Chem.* 1988, 27, 3283.

(228) Kates, W.; Meyer, T. J.; Murray, R. W. *J. Electroanal. Chem.* 1985, 195, 373.

(229) Mahmood, A.; Keita, B.; Nadj, L.; Cung, O.; Creutz, R.; Brown, S.; de Kouchkovsky, V. *J. Electroanal. Chem.* 1999, 463, 129.

(230) Nassar, A. E. F.; Zhang, Z.; Hu, N. F.; Rusling, J. F.; Kumeinski, T. F. *J. Phys. Chem.* 1997, 101, 2224.

(231) Föster, R. *Elektrochim.* 1950, 34, 531.

(232) Föster, R. *Reaktionen* 1951, 1952, 139.

(233) Ireland, J. F.; Wynn, P. A. *Adv. Phys. Org. Chem.* 1976, 12, 131.

(234) Shizuka, H. *Adv. Chem. Res.* 1985, 18, 141.

(235) Arnaut, L. G.; Formosinho, S. J. *J. Photochem. Photobiol.* 1993, 73, 1.

(236) Tolbert, L. M.; Soltishev, K. M. *Acc. Chem. Res.* 2003, 35, 19.

(237) Voir, J. G. *Polyhedron* 1992, 18, 2235.

(238) Walker, A. *J. Electrochim.* 1952, 36, 662.

(239) Suenaga, K.; Goto, K. M.; Ono, S.; Fukuzumi, S. *Angew. Chem.* 2003, 21, 6027.

(240) Cohen, B.; Huppert, D. *J. Phys. Chem.* 2001, 105, 2980.

(241) Kim, T. G.; Topp, M. R. *J. Phys. Chem.* A 2004, 108, 1060.

(242) Stolow, A. *Annu. Rev. Phys. Chem.* 2003, 54, 89.

(243) Yu, W.-S.; Cheng, C.-C.; Cheng, Y.-M.; Wu, P.-C.; Song, Y.-H.; Chi, Y.; Chou, P.-T. *J. Am. Chem. Soc.* 2003, 125, 16800.

(244) Hynes, J. T.; Tran-Thi, T. H.; Grancucci, G. J. *Photochem. Photobiol.* 2002, 14/14, 3 and references therein.

(245) Winkler, M.; Gray, H. H. *J. Inorg. Chem.* 1988, 24, 346.

(246) Liu, W. T.; Thorp, H. H. *J. Inorg. Chem.* 1994, 33, 1026.

(247) Liu, W. T.; Welch, T. W.; Thorp, H. H. *Inorg. Chem.* 1992, 31, 4044.

(248) Liu, W. T.; Thorp, H. H. *J. Am. Chem. Soc.* 1995, 117, 982.

(249) Liu, W. T.; Thorp, H. H. *J. Am. Chem. Soc.* 1993, 115, 11048.

(250) Goll, J. G.; Liu, W. T.; Thorp, H. H. *J. Am. Chem. Soc.* 1993, 115, 11048.

(251) Goll, J. G. R.; Connor, J. A.; Gutierrez, A. R.; Meyer, T. J.; Whitten, D. G.; Sullivan, B. P.; Nagle, J. K. *J. Am. Chem. Soc.* 1979, 101, 4815.

(252) Krasznahodder, S. S.; Norton, J. R. *J. Am. Chem. Soc.* 1991, 113, 4366.

(253) Wubbels, G. G. *Acc. Chem. Res.* 1983, 16, 285.

(254) Krausz, A. *J. Am. Chem. Soc.* 1973, 2, 475.

(255) McEwen, J.; Yates, K. *J. Am. Chem. Soc.* 1987, 109, 5800.

(256) Albany, W. J. *Annu. Rev. Phys. Chem.* 1980, 31, 227.

(257) Yates, K. *J. Phys. Org. Chem.* 1989, 2, 300 and references therein.

(258) Wittenberg, D. J.; Danner, E. M.; Papanikolas, J. M.; Meyer, T. J. *Chem. Phys.* 2004, 236, 71.

(259) Ormsby, K. M.; Schoeniger, J. R.; Treadaway, J. A.; Lenseur, R. M.; Dyer, R. B.; Meyer, T. J. *J. Am. Chem. Soc.* 1997, 119, 7013.

(260) Dalling, G. B.; Woodruff, W. H. *J. Am. Chem. Soc.* 1979, 101, 4391.

(261) Shaw, G. B.; Brown, C. L.; Papanikolas, J. M. *J. Phys. Chem. A* 2002, 106, 1483.

(262) Ormsby, J. P.; Batoi, C.; Kelley, D. F. *J. Phys. Chem. A* 1997, 101, 7222.

(263) Wallin, S.; Davidson, J.; Modia, J.; Hammarstrom, L. *J. Phys. Chem. A* 2005, 109, 6697.

(264) Hicks, C.; Ye, G. Z.; Levi, C.; Gonzales, M.; Rutenburg, L.; Fan, J. W.; Helmy, R.; Kassis, A.; Gafney, H. D. *Coord. Chem. Rev.* 2001, 211, 207.

(265) Meyer, T. J. *Pure Appl. Chem.* 1986, 58, 1193.

(266) Shan, R. Z.; Zhao, Q.; Gersmow, N.; Eichhorn, D. M.; Rillema, D. P. *Coord. Chem. Rev.* 2001, **211**, 117.

(267) Balzani, V.; Juris, A. *Coord. Chem. Rev.* 2004, **211**, 97.

(268) Kober, E. M.; Caspar, J. V.; Lumpkin, R. S.; Meyer, T. J. *J. Phys. Chem.* 1986, **90**, 3722.

(269) Kober, E. M.; Meyer, T. J. *Inorg. Chem.* 1984, **23**, 3877.

(270) Sun, H.; Hoffman, M. Z. *J. Phys. Chem.* 1993, **97**, 5014.

(271) Dangelmaier, M.; Mulazami, Q. G.; Vescuri, M.; Claro, M.; Hwang, J. L.; Voth, G. A. *J. Am. Chem. Soc.* 1983, **105**, 1170.

(272) Konduri, R.; Ye, H. W.; MacDonnell, F. M.; Serrotti, S.; Campagna, S.; Rajeshwar, K. *Angew. Chem., Int. Ed.* 2002, **41**, 3185.

(273) Del'ave, P.; Forment, T. K.; Giannotti, C.; Whitten, D. G. *J. Am. Chem. Soc.* 1980, **102**, 5627.

(274) Del'ave, P.; Meyer, T. J. *J. Phys. Chem.* 1985, **89**, 4807.

(275) Loh, L. S.; Newton, G. A.; Voth, G. A.; Del'ave, P.; Sullivan, B. P.; Meyer, T. J. *J. Phys. Chem.* 1989, **93**, 77.

(276) Haga, M. A.; Ali, M. M.; Kozeki, S.; Fujimoto, K.; Yodohima, A.; Nozaki, K.; Ohni, T.; Nakajima, K.; Shinkai, D. J. *Inorg. Chem.* 1996, **35**, 3335.

(277) Iwang, H. J.; Lu, Y. *Proc. Natl. Acad. Sci. U.S.A.* 2004, **101**, 12842.

(278) Huynh, M. H.; Morris, D. E.; White, P. S.; Meyer, T. J. *Angew. Chem., Int. Ed.* 2002, **41**, 2330.

(279) Voth, G. A.; Sutin, N. A.; Meyer, T. J. *J. Phys. Chem.* 1986, **90**, 1281.

(280) Habie, C. T.; Crooks, R. M.; Valentine, J. R.; Giessner, R.; Wrighton, M. S. *J. Phys. Chem.* 1993, **97**, 6050.

(281) Samuel, G. J.; Meyer, T. J. *J. Am. Chem. Soc.* 1981, **103**, 307.

(282) Vining, W. J.; Meyer, T. J. *J. Electroanal. Chem.* 1987, **237**, 191.

(283) Marcus, R. A. *Annu. Rev. Phys. Chem.* 1966, **17**, 155.

(284) Marcus, R. A.; Stin, N. *Blockh. Biophys. Acta* 1985, **811**, 265.

(285) Sutin, N. S. *Prog. Inorg. Chem.* 1967, **6**, 391.

(286) Sutin, N. S. *Adv. Inorg. Chem.* 1986, **31**, 441.

(287) Newton, M. D.; Sutin, N. *Adv. Inorg. Chem.* 1984, **35**, 437.

(288) Sutin, N. *Acc. Chem. Res.* 1982, **15**, 275.

(289) Marcus, R. A. *Adv. Mod. Phys.* 1993, **65**, 599.

(290) Hush, N. S. *Coord. Chem. Rev.* 1985, **66**, 135.

(291) Barbera, P. F.; Meyer, T. J.; Rainier, M. A. *J. Phys. Chem.* 1996, **100**, 13148.

(292) Marcus, R. A. *Faraday Discuss.* 1960, **29**, 125.

(293) Chen, P. Y.; Meyer, T. J. *J. Chem. Rev.* 1998, **98**, 1439 and references therein.

(294) Meyer, T. J.; Taube, H. In *Electron Transfer Reactions in Congenerous Coordination Chemistry. The Synthesis, Reactions, Properties and Applications of Coordination Compounds*; Sir Wilkinson, G., Gillard, R. D., McCleverty, J. A., Eds.; Fergamon Press: Oxford, 1987; Vol. 1, p 331.

(295) Krushatik, L. I. *Bioclectrochem.* 1990, **21**, 249.

(296) Krushatik, L. I. *Bioelectrochem. Biophys. Acta* 1986, **849**, 162.

(297) Krushatik, L. I. *Electrochim. Acta* 2000, **46**, 1604, 13.

(298) Brunschwig, B. S.; Emerson, S.; Sutin, N. *J. Phys. Chem.* 1986, **90**, 3657.

(299) Creutz, C. *Prog. Inorg. Chem.* 1983, **30**, 1.

(300) Sutin, N.; Brunschwig, B. S.; Creutz, C.; Winkler, J. R. *Proc. Appl. Chem.* 1988, **60**, 1817.

(301) Sutin, N.; Creutz, C. *Proc. Appl. Chem.* 1988, **60**, 2717.

(302) Chandler, D.; Kuharski, R. *Faraday Discuss. Chem. Soc.* 1988, **35**, 229.

(303) Bader, J. S.; Kuharski, R. A.; Chandler, D. *J. Chem. Phys.* 1990, **93**, 2300.

(304) Kuharski, R. A.; Bader, J. S.; Chandler, D.; Sprlik, M.; Klein, M. L.; Impay, R. W. *J. Chem. Phys.* 1989, **90**, 3248.

(305) Brunschwig, B. S.; Logan, J.; Newton, M. D.; Sutin, J. *J. Am. Chem. Soc.* 1980, **102**, 3798.

(306) Temble, B. L.; Friedman, H. L.; Newton, M. D. *J. Chem. Phys.* 1982, **76**, 1490.

(307) Temble, B. L.; Newton, M. D. *Faraday Discuss. Chem. Soc.* 1982, **74**, 73.

(308) Matysushov, D. V.; Voth, G. A. *Inorg. Chem.* 1991, **30**, 1.

(309) Matysushov, D. V.; Voth, G. A. In *Review in Computational Chemistry*; Lipkowitz, K. B.; Boyd, D. B., Eds.; Wiley-VCH: New York, 2002; Chapter 4, p 147.

(310) Voth, P.; Zimmt, M. B.; Matysushov, D. V.; Voth, G. A. *J. Phys. Chem. B* 1999, **103**, 9130.

(311) Tomasi, J.; Parrico, M. *Chem. Rev.* 1994, **94**, 2027.

(312) Oh, O.; Boxer, S. G. *J. Am. Chem. Soc.* 1990, **112**, 8161.

(313) Oh, D. H.; Sano, M.; Boxer, S. G. *J. Am. Chem. Soc.* 1991, **113**, 6580.

(314) Hwang, J. P.; Hush, N. S. *J. Phys. Chem.* 1991, **95**, 9773.

(315) Weaver, M. J.; Tyma, P. D.; Nettles, S. M. *J. Electroanal. Chem.* 1988, **114**, 53.

(316) Guarr, T.; Buhks, E.; McLenden, G. *J. Am. Chem. Soc.* 1983, **105**, 3763.

(317) Casper, J. V.; Sullivan, B. P.; Kober, E. M.; Meyer, T. J. *J. Chem. Phys.* 1982, **77**, 91.

(318) Van Houten, J.; Watts, R. J. *J. Am. Chem. Soc.* 1975, **97**, 3843.

(319) Hong, M. L.; Gardasik, J. A.; Papazyan, A.; Manocelli, M. *J. Phys. Chem.* 1995, **99**, 1731.

(320) Kahlow, M. A.; Kang, T. J.; Barbara, P. F. *J. Phys. Chem.* 1987, **91**, 6452.

(321) Fleming, G. R.; Cho, M. *Annu. Rev. Phys. Chem.* 1996, **47**, 109.

(322) Ustun, I. *Charge-Transfer Processes in Condensed Media, Lecture Notes in Chemistry*; Springer-Verlag: New York, 1979; Vol. 10.

(323) Kohn, W. In *Local Density Functionals*; *Phys. Chem.* 1974, **76**, 2148.

(324) Jortner, J. *J. Chem. Phys.* 1976, **64**, 3440.

(325) Bixon, M.; Jortner, J. *Faraday Discuss.* Chem. Soc. 1982, **74**, 17.

(326) Marcus, R. A.; Jortner, J. *J. Am. Chem. Soc.* 1981, **103**, 741.

(327) Marcus, R. A. *J. Chem. Phys.* 1984, **81**, 4494.

(328) Bixon, M.; Jortner, J. *Adv. Chem. Phys.* 1999, **105**, 35.

(329) Ballhausen, C. *Molecular Electronic Structures of Transition Metal Complexes*; McGraw-Hill: New York, 1979.

(330) Eigen, M. *J. Phys. Chem. (M.F.)* 1954, **1**, 176.

(331) Pines, A. In *Topics in the Techniques of Organic Chemistry*, 2nd ed.; Pines, A.; Lewin, E. S.; Weisberger, A., Eds.; Wiley: New York, 1963; Vol. 8, Part 2, p 865.

(332) Fuoss, R. M. *J. Am. Chem. Soc.* 1958, **80**, 5059.

(333) Meyer, T. J. In *Progress in Inorganic Chemistry*; Lippard, S. J., Ed.; Wiley & Sons: New York, 1983; Vol. 30, p 389.

(334) Marcus, R. A. *J. Phys. Chem.* 1968, **72**, 89.

(335) Gutierrez, P. J. *J. Am. Chem. Soc.* 1997, **119**, 1151.

(336) Pellerine, M. J.; Brauman, J. I. *J. Am. Chem. Soc.* 1983, **105**, 2672.

(337) Reddish, J. F.; Balakrishnan, K. P.; Wong, C. L. *J. Am. Chem. Soc.* 1969, **91**, 10000.

(338) Krasov, M. M.; Ostrov, D.; Ivan, L. S.; Bindra, D. A.; King, G. W. *J. Am. Chem. Soc.* 1988, **110**, 324.

(339) Gutierrez, P. J. *J. Am. Chem. Soc.* 1996, **118**, 12886.

(340) Roth, J. P.; Yoder, J. C.; Woz, T.-J.; Meyer, J. M. *Science* 2001, **294**, 2524.

(341) Simber, J. A. M.; Greenberg, A.; Liebman, J. F. In *Emergencies of Organic Free Radicals*; Eds., Blaudek & Professional: New York, 1992.

(342) Gordis, B. M. *Radical Chemistry*; Ellis Horwood: New York, 1994.

(343) Fox, T.; Hazzard, J. T.; Edwards, S. L.; English, A. M.; Poelus, T. L.; Tollin, G. *J. Am. Chem. Soc.* 1990, **112**, 7626.

(344) Fenwick, C.; Marmor, S.; Govindaraju, K.; English, A. M.; Wishart, J. F.; Sun, J. *J. Am. Chem. Soc.* 1994, **116**, 3159.

(345) Fenwick, C. W.; English, A. M.; Wishart, J. F. *J. Am. Chem. Soc.* 1997, **119**, 4758.

(346) Sitter, A. J.; Shifflet, J. R.; Turner, J. *J. Biol. Chem.* 1988, **263**, 19333.

(347) Galloway, J. E.; Dunford, H. B. *J. Biol. Chem.* 1973, **247**, 3714.

(348) Dunford, H. B.; Stillman, J. S. *Coord. Chem. Rev.* 1976, **19**, 187.

(349) Gaibishe, M. *Biochim. Soc. Trans.* 2001, **29**, 93.

(350) Poad, A. E.; Sone, M.; Elenkov, E. A.; Cordin, D. S.; English, A. M.; Dawson, J. H. *Biospectroscopy* 1999, **5**, 542.

(351) Howes, B. D.; Rodriguez-Lopez, J. N.; Smith, A. T.; Smalevich, G. *Biochemistry* 1997, **36**, 1532.

(352) Boveris, A. *Fee. Proc.* 1972, **31**, 842.

(353) Fossell, L. G.; Garcia-Mollina, F.; Gilbert, M. A.; Vason, R.; Garcia-Ruiz, P. A.; Tudela, J.; Garcia-Caravaca, P.; Rodriguez-Lopez, J. N. *Biol. Chem.* 2005, **386**, 351.

(354) Monyer, D. K.; Naray-Szabo, G. *J. Phys. Chem. B* 1999, **103**, 227.

(355) Sauer, J. *J. Am. Chem. Soc.* 1997, **119**, 1036.

(356) The observed rate constant for eq 10,  $k_{10}$ , is the product of  $k_1$  and the protonation constant,  $K_A$  (eqs 57–59), with  $k_{10} = K_A k_1$ . The estimates for  $\Delta G^\circ$  were made by using the reaction rate theory expression,  $\Delta G^\circ = (k_B T)/k_1 \exp(-\Delta G^\circ/RT)$ ,  $k_B T = 6.7 \times 10^{12} \text{ eV}^{-1}$  at **25** °C, and  $K_A = 0.1 \text{ M}^{-1}$ . The latter is a lower limit, since it neglects the H-bond interaction.

(357) Roth, J. P.; Lovell, S.; Meyer, J. M. *J. Am. Chem. Soc.* 2000, **122**, 2036.

(358) Gross, N.; Linschitz, H.; Biczok, L. *Fullerenes Sci. Technol.* 1997, **5**, 343.

(359) Donaslie, K. D.; Hartshorn, C. M.; Meyer, T. J. *J. Chem. Rev.* 2001, **101**, 2653.

(360) Meyer, J. M. *Acc. Chem. Res.* 1998, **31**, 441.

(361) Meyer, J. M. In *Biomimetic Oxidations Catalyzed by Transition Metal Complexes*; Meunier, B., Ed.; Imperial College Press: London, 2000; pp 1–43.

(362) Meyer, J. M.; Hrovat, D. A.; Thomas, J. L.; Bortner, W. T. *J. Am. Chem. Soc.* 2002, **124**, 11142.

(363) Meyer, J. M. *J. Phys. Chem. B* 2002, **106**, 1745.

(364) Hatchett, E.; Sosulinov, A. V.; Hammes-Schiffer, S. *J. Am. Chem. Soc.* 2004, **126**, 5763.

(365) Lehner, N.; Solomos, E. I. *J. Biol. Inorg. Chem.* 2003, **8**, 294.

(366) Kaiser, J.; Klaiber, E. J.; Oh, N. Y.; Rohde, J. U.; Song, W. J.; Stuiba, A.; Kim, J.; Minick, E.; Nam, W.; Qu, J.; Jr. *J. Am. Chem. Soc.* 2004, 126, 472.

(367) Nethéim, J. C.; Lipscomb, J. D. *Biochemistry* 1996, 35, 10240.

(368) Gardner, K. A.; Mayer, J. M. *Science* 1995, 269, 1849.

(369) Gardner, K. A.; Kuehner, L. L.; Mayer, J. M. *Inorg. Chem.* 1997, 36, 2659.

(370) Mahaney, L. R.; Darogai, M. A. *J. Am. Chem. Soc.* 1975, 97, 4722.

(371) Hinkle, K. U.; Russell, G. A. In *Free Radicals*; Kochi, J. K., Ed.; 1973; p 205.

(372) Landolt-Bornstein. In *Radical Reduction Rates in Lipids* New Series; Fischer, H., Ed.; Wiley: New York, and Springer: New York, 1983; Vols. II/3 and II/18.

(373) Tedder, J. M. *Angew. Chem. Int. Ed.* 1982, 21, 401.

(374) Lam, W. Y.; Yu, S. M.; Yu, D. T. Y.; Lau, T. C.; Yip, W. P.; Che, C. M. *Inorg. Chem.* 2004, 43, 8011.

(375) Yu, D. T. Y.; Lam, W. F.; Lam, W. W. Y.; Lau, T. C. *Inorg. Chem.* 2003, 42, 1225.

(376) Lind, J.; Shen, X.; Erikson, T. E.; Merenyi, G. *J. Am. Chem. Soc.* 1996, 118, 472.

(377) Lide, D. R. *CRC Handbook*; CRC Press: Boca Raton, FL, 1996.

(378) Bordwell, F. G.; Cheng, J. P. *J. Am. Chem. Soc.* 1991, 113, 1736.

(379) Ternman, C.; Hoganas, C. W.; Di Valentini, M.; Lyckhuis-Simantirius, N.; Dorlet, P.; Westphal, K.; Chu, H. A.; McCracken, J.; Babcock, O. *J. Am. Chem. Soc.* 1991, 113, 1736.

(380) Baldwin, M. J.; Pescarolo, V. L. *J. Am. Chem. Soc.* 1996, 118, 11325.

(381) Caudle, M. T.; Pescarolo, V. L. *J. Am. Chem. Soc.* 1993, 115, 3415.

(382) Hariman, R. J. *J. Phys. Chem.* 1987, 91, 6.

(383) Ferrelin, K. N.; Iverson, T. M.; Maghlaoui, K.; Barber, J.; Iwata, S. *Science* 2004, 303, 1831.

(384) Agarwal, P. K.; Webb, S. P.; Hammes-Schiffer, S. *J. Am. Chem. Soc.* 2000, 122, 4803.

(385) Peltzman, J. *Crit. Rev. Biochem.* 1981, 10, 39.

(386) Peltzman, J. *Adv. Redox Chem.* *Adv. Biol.* 1987, 21, 349.

(387) Seck, W. K.; Meyer, T. J. *Inorg. Chem.* 1994, 33, 5205.

(388) Stultz, L. K.; Huyhn, M. H. V.; Binetruy, R. A.; Curry, M.; Meyer, T. J. *J. Am. Chem. Soc.* 2000, 122, 5984.

(389) Seck, W. K.; Dobson, J. C.; Meyer, T. J. *Inorg. Chem.* 1988, 27, 3.

(390) Hynes, J. T. *Nature* 1999, 397, 568.

(391) Ardo, K.; Hynes, J. T. *J. Phys. Chem. B* 1997, 101, 10464.

(392) Ardo, K.; Hynes, J. T. *J. Phys. Chem. A* 1999, 103, 1098.

(393) Gerber, J. L. P.; Dang, C.; Chandler, D.; Hutter, J.; Fariello, R. *J. Phys. Chem.* 1998, 102, 2143.

(394) Borgis, D.; Hynes, J. T. *J. Phys. Chem.* 1996, 100, 1118.

(395) Cukier, R. I.; Zhu, J. J. *Phys. Chem. S* 1997, 101, 7180.

(396) Bell, R. P. *The Tunnel Effect in Chemistry*; Chapman and Hall: London, 1980.

(397) Borgis, D.; Hynes, J. T. *Chem. Phys.* 1993, 176, 315.

(398) Christie, S. G. *Chem. Phys.* 1992, 168, 327.

(399) Warschel, A. *Acc. Chem. Res.* 2002, 35, 385.

(400) Krashatik, I. L. *Biochim. Biophys. Acta* 2000, 1458, 6.

(401) Krashatik, I. L.; Slobodkov, R. *Int. Rev. Phys. Chem.* 2001, 20, 591.

(402) Truhlar, D. G.; Gao, J. L.; Alhamra, C.; Garcia-Viloca, M.; Corchado, J.; Sanchez, M. L.; Villa, J. *Acc. Chem. Res.* 2002, 35, 341.

(403) Georgievskiy, Y.; Stucheburkova, A. A. *J. Chem. Phys.* 2000, 113, 10438.

(404) Kohan, A.; Kliman, J. *Acc. Chem. Res.* 1998, 31, 397 and references therein.

(405) Cukier, R. I. *J. Phys. Chem. B* 1999, 103, 10464.

(406) Soudakov, A.; Hammes-Schiffer, S. *J. Chem. Phys.* 1999, 111, 4672.

(407) Soudakov, A.; Hammes-Schiffer, S. *J. Chem. Phys.* 2000, 113, 2285.

(408) Rostov, I.; Hauxnes-Schiffer, S. *J. Chem. Phys.* 2001, 113, 285.

(409) Jordanova, N.; Deacone, H.; Hammes-Schiffer, S. *J. Am. Chem. Soc.* 2001, 123, 3723.

(410) Jordanova, N.; Hammes-Schiffer, S. *J. Am. Chem. Soc.* 2002, 124, 4848.

(411) Soudakov, A.; Hatch, E.; Hammes-Schiffer, S. *J. Chem. Phys.* 2005, 123, 14902.

(412) Villasi, G. *Chem. Phys.* 2004, 302, 309.

(413) Shin, S. I.; Cho, S. I. *Chem. Phys.* 2000, 259, 27.

(414) Pressé, S.; Silbey, R. *J. Chem. Phys.* 2005, 124, 164504.

(415) Bixon, M.; Jortner, J. *Electron transfer from isolated molecules to bionolecules: Advances in Chemical Physics*; p 106.

(416) Prigogine, I.; Rice, S. A., Eds.; John Wiley & Sons: New York, 1999, p 35.

(417) Wong, K. Y.; Sutat, P. N. *Prog. Inorg. Chem.* 1981, 28, 369.

(418) Bixon, M. J.; Yartsev, V. M.; Jacobson, C. S. *Phys. Rev. B* 1980, 21, 3437.

(419) Puppo, S. B. *J. Am. Chem. Soc.* 1990, 112, 4197.

(420) Warschel, A. *Computer Modeling of Chemical Reactions in Enzymes and Substrates*; John Wiley: New York, 1991.

(421) Henderson, T. M.; Cave, R. J. *J. Chem. Phys.* 1998, 109, 7414.

(422) Basilevsky, M. V.; Rostov, I. V.; Newton, M. D. *Chem. Phys.* 1998, 228, 189.

(423) Newton, M. D.; Basilevsky, M. V.; Rostov, I. V. *Chem. Phys.* 1998, 232, 201.

(424) Bell, R. P. *Chem. Soc. Rev.* 1974, 3, 513.

(425) Reinhardt, L. A.; Svedružić, D.; Chang, C. H.; Cleland, W. W.; Richards, N. G. J. *J. Am. Chem. Soc.* 2003, 125, 1244.

(426) Whitaker, M. M.; Whitaker, J. W. *Biochemistry* 2001, 40, 7140.

(427) Jortner, J. *Q. Rev. Biophys.* 1998, 31, 12513.

(428) Jortner, T.; Glickman, M. H.; Sun, S.; Kliman, J. P. *J. Am. Chem. Soc.* 1996, 118, 18219.

(429) Glickman, M. H.; Kliman, J. P. *Biochemistry* 1995, 34, 14077.

(430) Biegelsen, J.; Goepf-Mayr, M. *J. Chem. Phys.* 1947, 15, 261.

(431) Biegelsen, *J. Chem. Phys.* 1949, 17, 675.

(432) Leroy, J. R.; Murel, F.; Williams, F. *J. Am. Chem. Soc.* 1980, 102, 2325.

(433) Garcia-Garibay, M. A.; Jenks, W. S.; Pang, L. *J. Photochem. Photobiol. A* 1996, 96, 51.

(434) Garcia-Garibay, M. A.; Gamrikci, A.; Pang, L.; Jenks, W. S. *J. Am. Chem. Soc.* 1994, 116, 12095.

(435) Johnson, B. A.; Gamrikci, A.; Garcia-Garibay, M. A. *J. Phys. Chem.* 1996, 100, 4697.

(436) Albery, W. J.; Davies, M. H. *Trans. Faraday Soc.* 1969, 65, 1066.

(437) Albery, W. J.; Davies, M. H. *J. Chem. Soc., Faraday Trans. 1* 1972, 68, 167.

(438) Albery, W. J.; Davies, M. H. *Trans. Faraday Soc.* 1969, 65, 1059.

(439) Schowen, K. B.; Limbach, H. H.; Danzig, G. S.; Schewen, R. L. *Biochim. Biophys. Acta* 2000, 1458, 43.

(440) Sutin, S. N.; Benedict, H.; Golubey, N. S.; Denisov, G. S.; Kreyer, M. M.; Schowen, R. L.; Limbach, H. H. *Can. J. Chem.* 1999, 77, 943.

(441) Eliason, R.; Kreyer, M. M. *J. Am. Chem. Soc.* 1978, 100, 7037.

(442) Kreyer, M. M.; Liang, T.; Chang, K. C. *J. Am. Chem. Soc.* 1977, 99, 5207.

(443) Krueger, A. J.; More O'Ferrall, R. A.; Powell, M. F. In *Isotopes in Organic Chemistry*; Bunzel, E., Lee, C. C., Eds.; Elsevier: Amsterdam, 1987; Vol. 7, pp 177.

(444) Albery, W. J. In *Proton Transfer Reactions*; Caldin, E., Goki, V., Eds.; Wiley: New York, 1975; Chapter 9.

(445) Melander, L.; Saunders, W. H., Jr. In *Reaction Rates of Isotopic Molecules*; Wiley: New York, 1980; pp 284.

(446) Kreyer, M. M.; Tomlin, E. R. In *Isotopic Effects in Chemical Reactions*; Colgate, C. L., Bowman, N. S., Eds.; Van Nostrand: New York, 1970; pp 213.

(447) Laughlin, P. M.; Robertson, R. E. In *Solvent-Solvent Interactions*; Coetze, J. F.; Ritchie, C. D., Eds.; Marcel Dekker: New York, 1959; pp 401.

(448) Williams, D. L. H.; Buncel, E. In *Isotopes in Organic Chemistry*; Bunzel, E., Lee, C. C., Eds.; Elsevier: Amsterdam, 1980; Vol. 5, pp 147.

(449) McCarthy, D. G.; Hegarty, A. F. *J. Chem. Soc., Perkin Trans. 2* 1980, 4, 579.

(450) Wan, S. R.; Kreyer, M. M. *J. Org. Chem.* 1981, 46, 419.

(451) Covington, A. K.; Robinson, R. A.; Bates, R. G. *J. Phys. Chem.* 1966, 70, 3820.

(452) Goldblat, M.; Jones, W. M. *J. Chem. Phys.* 1969, 51, 1871.

(453) Chang, Y.; Kresge, A. J.; Offenrall, R. A. *M. J. Chem. Soc., Perkin Trans. 2* 1980, 17, 1833.

(454) Marcus, R. A. *Ann. Rev. Phys. Chem.* 1960, 29, 21.

(455) Miller, R. V.; Miller, J. R. *J. Chem. Phys.* 1979, 71, 4579.

(456) Clegg, G. J.; Miller, J. R. *Science* 1988, 240, 440.

(457) Miller, J. R.; Calcaterra, L. T.; Closs, O. J. *J. Am. Chem. Soc.* 1984, 106, 7795.

(458) Gould, I. R.; Ego, D.; Maites, S. L.; Farid, S. *J. Am. Chem. Soc.* 1987, 109, 3794.

(459) Gould, I. R.; Moise, J. E.; Armitage, B.; Farid, S.; Goodman, J. L.; Hermann, M. S. *J. Am. Chem. Soc.* 1989, 111, 1917.

(460) McLendon, G. *Acc. Chem. Res.* 1988, 21, 160.

(461) Chen, P.; Duesing, R.; Tapolsky, G.; Meyer, T. J. *J. Am. Chem. Soc.* 2002, 126, 7795.

(462) Claude, J. P.; Omberg, K. M.; Williams, D. S.; Meyer, T. J. *J. Phys. Chem. A* 2002, 106, 7795.

(463) Soudakov, A.; Hammes-Schiffer, S. *J. Am. Chem. Soc.* 1999, 121, 10598.

(464) Halperin, J.; Orgel, L. E. *Discuss. Faraday Soc.* 1968, 29, 32.

(465) McCormell, H. M. *M. J. Chem. Phys.* 1961, 35, 508.

(466) Beaton, D. N.; Hopfield, J. J. *J. Am. Chem. Soc.* 1984, 106, 1584.

(467) Beaton, D. N.; Onuchic, J. N.; Hopfield, J. J. *J. Chem. Phys.* 1985, 83, 5325.

(468) Beaton, D. N.; Betus, J. N.; Onuchic, J. N. *Science* 1991, 252, 1285.

(469) Jortner, J.; Ratner, M. A. *Molecular Electronics*; Blackwell: London, 1997.

(470) Anderson, N. A.; Xie, C.; Mohler, D. L.; Lian, T. Q. *J. Phys. Chem. B* 2003, 107, 423.

(471) Moser, C. C.; Keske, J. M.; Warneck, K.; Fand, R. S.; Dalton, P. L. *Nature* 1992, 355, 795.

(472) Mayo, S. L.; Ellis, W. R.; Crutchley, R. J.; Gray, H. R. *Science* 1986, 233, 948.

(473) Arkle, M. R.; Stemp, E. D. A.; Holmlin, R. E.; Barron, J. K.; Hornemann, A.; Olson, E. C.; Barbau, P. F. *Science* 1996, 272, 475.

(474) Bader, Y. A.; Burak, A. L.; Ramer, M. A. *J. Am. Chem. Soc.* 2001, 123, 2663.

(475) Chidsey, C. E. D. *Science* 1991, 251, 919.

(476) Newton, M. D. *Chem. Rev.* 1991, 91, 767.

(477) Jordan, K. D.; Paddison, M. N. *Chem. Rev.* 1992, 92, 395.

(478) Liang, C. X.; Newton, M. D. *J. Phys. Chem.* 1993, 97, 3199.

(479) Strauch, S.; McLendon, G.; McGuire, M.; Guarr, T. *J. Phys. Chem.* 1983, 87, 3579.

(480) Jeffrey, G. A.; Sasabe, W. *Hydrogen Bonding in Biological Structures*; Springer-Verlag: Berlin, 1991.

(481) Jeffrey, G. A. *An Introduction to Hydrogen Bonding*; Oxford University Press: New York, 1997.

(482) Schleinzer, S. *Hydrogen Bonding. Theoretical Perspectives*; Oxford University Press: New York, 1997.

(483) Bader, R. F. *Atom in Molecules: A Quantum Theory*; Oxford University Press: New York, 1990.

(484) Grimwood, S. J. *J. Phys. Org. Chem.* 2004, 17, 18.

(485) Epstein, L. M.; Shubina, E. S. *Coord. Chem. Rev.* 2002, 231, 165.

(486) Taylor, R. J.; Kenward, R. O. *J. Am. Chem. Soc.* 1982, 104, 5063.

(487) Steiner, T. *J. Am. Chem. Soc.* 1995, 117, 23.

(488) Steiner, T. *J. Am. Chem. Soc.* 2002, 124, 41.

(489) Lasse, J. *Appl. Spectrosc.* 1999, 53, 74.

(490) Brusseau, B. S.; Sutin, N. *Coord. Chem. Rev.* 1999, 187, 233.

(491) Sutin, N. *Adv. Chem.* 1999, 106, 7.

(492) Farrar, B. T.; Thorp, H. *Inorg. Chem.* 1999, 38, 2467.

(493) Westheimer, F. H.; Kirkwood, J. G. *J. Chem. Phys.* 1938, 6, 513.

(494) Celdin, E. B.; Dignall, S. P.; Mak, M. K. S.; Brooke, D. N. *Faraday Discuss.* 1998, 74, 215.

(495) Stern, C.; Jordaneva, N.; Hammett-Schiffer, S. *J. Am. Chem. Soc.* 2003, 125, 19429.

(496) Ceder, V.; Shafrir, R. *J. Chem. Phys.* 1999, 110, 5989.

(497) Kress, A. J. *Phys. Chem.* 1964, 68, 243.

(498) Gold, V. *Adv. Phys. Org. Chem.* 1969, 7, 259.

(499) Albany, W. J.; Davies, M. H. *Phys. Chem. Lab.* Oxford 167.

(500) Zundel, G. *Adv. Chem. Phys.* 2000, 111, 1.

(501) Eigen, M. *Angew. Chem., Int. Ed.* 1964, 1, 1.

(502) Marx, D.; Tuckerman, M. E.; Hutter, J.; Parrinello, M. *Nature* 1999, 397, 601.

(503) Vuillemenot, R.; Borges, D. *J. Chem. Phys.* 1999, 111, 4251.

(504) Lapid, H.; Agron, N.; Petersen, M. K.; Voth, G. A. *J. Chem. Phys.* 2002, 122, 14308.

(505) Mohammad, F.; Pines, D.; Dwyer, J.; Pines, E.; Nibbering, E. T. *J. Science* 2005, 310, 82.

(506) Jencics, W. P. *Carbohydrates in Chemistry and Enzymology*; McGraw-Hill: New York, 1959, p 172.

(507) In water, the equilibrium defining acidity is  $\text{H}_2 + \text{H}_2\text{O} \rightleftharpoons \text{H}_3\text{O}^+ + \text{A}^+$ , with  $\text{K}_a(\text{H}_2\text{O}) = (\text{a}_1/\text{a}_2)\text{a}_1^2/\text{a}_2^2 = (\text{a}_1/\text{a}_2)^2$  and  $\text{a}_1, \text{a}_2$ , etc. the activities of the components at equilibrium and  $\text{a}_1^0, \text{a}_2^0$ , etc. the activities of the components in their standard states. In dilute solution under ideal conditions,  $\text{K}_a(\text{H}_2\text{O}) = \text{H}_3\text{O}^+/\text{H}_2\text{O} = 1$ . In order to convert the activity of  $\text{H}_3\text{O}^+$  with  $\text{H}_2\text{O}$ , it is necessary to consider the concentration of water in water, 55.5 M at  $25^\circ\text{C}$ , with  $\text{K}_a(\text{H}_2\text{O}) = [\text{H}_3\text{O}^+]^2 = 55.5 \text{ M}$  and  $\text{pK}_a(\text{H}_2\text{O}) = -1.74$ . A related argument leads to  $\text{pK}_a(\text{H}_2\text{O}) = 15.7$  through the equilibrium  $\text{H}_2\text{O} \rightleftharpoons \text{H}_3\text{O}^+ + \text{OH}^-$  and  $\text{K}_a = 10^{-14}$ . We thank Professor R. L. Schowen for bringing this argument to our attention.

(508) Rani, M.; Magna, B.-Z.; Pines, E.; Nibbering, E. T. *J. Science* 2003, 301, 3479.

(509) Rani, M.; Pires, D.; Magna, B.-Z.; Pines, E.; Nibbering, E. T. J. *J. Chem. Phys.* 2004, 121, 9559.

(510) Krishnatic, L. *J. Biophys.* 1989, 34, 883.

(511) Westheimer, S. C.; Yang, I. V.; Arnett, P. A.; Thorp, H. H. *J. Phys. Chem. B* 2003, 107, 372.

(512) Westheimer, S. C.; Yang, I. V.; Thorp, H. H. *J. Am. Chem. Soc.* 2001, 123, 1236.

(513) Shafrir, V.; Dourandin, A.; Luneva, N. P.; Gencinov, N. E. *J. Phys. Chem. B* 2000, 104, 137.

(514) Kuzmin, V. A.; Dourandin, A.; Shafrir, V.; Gencinov, N. E. *J. Phys. Chem. Phys.* 2006, 2, 1531.

(515) Shafrir, V.; Dourandin, A.; Gencinov, N. E. *J. Phys. Chem. B* 2001, 105, 8431.

(516) Shafrir, V.; Dourandin, A.; Huang, W. D.; Luneva, N. P.; Gencinov, N. E. *Phys. Chem. Chem. Phys.* 2000, 2, 4399.

(517) Shafrir, V.; Ceder, A.; Gasparrini, D.; Dourandin, A.; Huang, W. D.; Gencinov, N. E. *J. Phys. Chem. B* 2001, 105, 389.

(518) Shafrir, V.; Gencinov, N. E. *Top. Curr. Chem.* 2000, 217, 129.

(519) Voth, G. A.; Hochstrasser, R. M. *J. Phys. Chem.* 1996, 100, 1034.

(520) Gutman, M.; Nachliel, E. *Biochim. Biophys. Acta* 1996, 1013, 391.

(521) Kuzmin, S.; Ishikawa, K.; Hirotsuka, K.; Tanaka, T. *J. Chem. Soc., Perkin Trans. 2* 1987, 6, 751.

(522) Burall, F. H. *J. Chem. Soc.* 1936, 173.

(523) Macrae, D. H.; Monley, A. *Can. J. Chem.* 1981, 59, 132.

(524) Koeniger, J.; Meyer, T. J.; Thorp, H. H. *J. Am. Chem. Soc.* 2006, 128, 11020.

(525) Gilberg, J.; Koeniger, L.; Meyer, T. J. *Inorg. Chem.* 1987, 26, 1126.

(526) Bach, R. D.; Welber, G. J.; Coddens, B. A. *J. Am. Chem. Soc.* 1984, 106, 6098.

(527) Hayes, M. H. V.; Meyer, T. J.; White, P. S. *J. Am. Chem. Soc.* 1999, 121, 4531.

(528) In this same report on the  $\text{N}-\text{H}$  resonance, a much lower  $\text{K}_a(\text{H}_2\text{O})/\text{M}_2\text{O}$  value of 41 was reported because of an improper accounting of the pH-dependent pathway.<sup>34</sup>

(529) Yoder, J. C.; Roth, J. A.; Gussenben, E. M.; Larsen, A. S.; Mayer, J. M. *J. Am. Chem. Soc.* 2003, 125, 2629.

(530) Soper, J. D.; Mayer, J. M. *J. Am. Chem. Soc.* 2003, 125, 12217.

(531) Maresco, M.; Ruettiger, W. F.; Bories, E.; McLendon, G. L.; Dismukes, G. C. *Proc. Natl. Acad. Sci. U.S.A.* 2003, 100, 3707.

(532) Carroll, T. J.; Bories, E.; Lin, M.; Dismukes, G. C. *Inorg. Chem.* 2003, 42, 2848.

(533) Riley, D. J.; Lourou, P. J.; Neumann, W. L.; Weiss, R. H. *J. Am. Chem. Soc.* 1997, 119, 6522.

(534) Swain, C. G.; Bader, R. F. W.; Thorton, E. R. *Tetrahedron* 1966, 16, 200.

(535) Osako, T.; Olikubo, K.; Taki, M.; Tachi, Y.; Fukuzumi, S.; Itoh, S. *J. Am. Chem. Soc.* 2003, 125, 11027.

(536) Shearer, J.; Zhong, C. X.; Zelkhanov, L. N.; Rinehgold, A. L.; Karlin, R. D. *J. Am. Chem. Soc.* 2005, 127, 5469.

(537) Simandi, T.; Mato, M.; Szegedi, I.; Simandi, L. I. *J. Chem. Soc., Dalton Trans.* 2005, 365.

(538) Partenopoulos, D. A.; McMorrow, D.; Kasha, M. *J. Phys. Chem.* 1997, 101, 2668.

(539) Partenopoulos, D. A.; Kasha, M. *Chem. Phys. Lett.* 1999, 173, 303.

(540) Kasha, M. *Mol. Electron. Devices* 1988, 107.

(541) Catalán, J.; Kasha, M. *J. Phys. Chem. A* 2000, 104, 10812.

(542) del Valle, J. C.; Domínguez, E.; Kasha, M. *J. Phys. Chem. A* 1999, 103, 2467.

(543) Catalán, J. del Valle, J. C.; Kasha, M. *Proc. Natl. Acad. Sci. U.S.A.* 1999, 96, 8338.

(544) del Valle, J. C.; Kasha, M.; Catalán, J. *Int. J. Quant. Chem.* 2006, 97, 118.

(545) Sekota, K.; Sekiya, H. *J. Phys. Chem. A* 2005, 109, 2722.

(546) Wu, F. Y.; Jiang, Y. B. *Chem. Phys. Lett.* 2002, 355, 438.

(547) Lou, K. H.; Hong, J. H. *J. Tetrahedron Lett.* 2000, 41, 5983.

(548) Jos, P.; Schärhammer, R.; Wipfl, G. *Chem.* 2000, 23, 4257.

(549) Böni, P. D.; Bernhard, P. V. J. *Chem. Soc., Dalton Trans.* 2001, 103.

(550) Schmidlein, F. P.; Berger, M. *Chem. Rev.* 1997, 97, 1609.

(551) Snowden, T. S.; Anslyn, E. V. *Curr. Opin. Chem. Biol.* 1999, 3, 740.

(552) Gole, P. A. *Coord. Chem. Rev.* 2006, 199, 181.

(553) Nishizawa, S.; Kato, Y.; Teramae, N. *J. Am. Chem. Soc.* 1999, 121, 9463.

(554) Peterson, M. J.; Robb, M. A.; Blancafort, L.; DeBellis, A. D. *J. Am. Chem. Soc.* 1998, 120, 2912.

(555) Gross, D.; Hahn, J.; Kiehn, M. *J. Phys. Chem.* 1990, 94, 1185.

(556) David, O.; Dodonec-Ladeau, C.; Jouvet, C. *J. R. Soc. Phys. Chem.* 2002, 21, 459.

(557) Dos, P. K.; Encinas, M. V.; Scaiano, J. C. *J. Am. Chem. Soc.* 1981, 103, 4154.

(558) Leigh, W. J.; Lathrop, E. C.; St. Pierre, M. J. *J. Am. Chem. Soc.* 1996, 118, 12339.

(559) Lathrop, E. C.; Leigh, W. J.; St. Pierre, M. J. *J. Am. Chem. Soc.* 1999, 121, 11984.

(560) Lathrop, E. C.; Beroes, T.; Linschitz, H. *J. Am. Chem. Soc.* 1997, 119, 11071.

(561) Shi, X. F.; Platz, M. S. *J. Phys. Chem. A* 2004, 108, 4385.

(562) Lucarini, M.; Pedrielli, P.; Pedulli, G. F. *J. Org. Chem.* 1996, 61, 5239.

(563) Mader, E. A.; Larsen, A. S.; Mayer, J. M. *J. Am. Chem. Soc.* 2004, 126, 8066.

(564) Milligan, J. R.; Aguilera, J. A.; Hough, O.; Ly, A.; Tran, N. Q.; Ward, J. F. *J. Am. Chem. Soc.* 2004, 126, 1682.

(565) Aguilera, J. A.; Chandrasekar, R.; Fanggi, M.; Klapper, M. H. *J. Am. Chem. Soc.* 1997, 119, 1414.

(566) Siegbahn, P. E. M.; Blumberg, M. R. A.; Crabbtree, R. H. *Chem. Rev.* 1997, 97, 289.

(567) Turcick, F.; Systrand, E. A. *J. Am. Chem. Soc.* 2003, 125, 3353.

(568) Carras, C.; Jordana-Soriano, N.; Haunies-Schiffer, S. *J. Phys. Chem. Chem.* 2002, 106, 8415.

(569) Olivella, S.; Anglada, J. M.; Sole, A.; Bofill, J. M. *Eur. J. Chem.* 2004, 10, 3404.

(570) Singh, N.; O'Malley, P. J.; Popelier, P. L. A. *Phys. Chem. Chem. Phys.* 2006, 7, 614.

(571) Luzhkov, V. B. *Chem. Phys.* 2005, 314, 211.

(572) DiLabio, G. A.; Ingold, K. U. *J. Am. Chem. Soc.* 2005, 127, 6693.

(573) Kroll, J. P.; Roberts, J. A.; Nocera, D. G. *J. Am. Chem. Soc.* 1997, 119, 9250.

(574) Roberts, J. A.; Kirby, J. P.; Wall, S. T.; Nocera, D. G. *Inorg. Chem. Acta* 1997, 263, 395.

(575) Turro, C.; Chang, C. K.; Leroy, G. E.; Cukier, R. L.; Nocera, D. G. *J. Am. Chem. Soc.* 1992, 114, 4013.

(576) Jorgenson, W. L.; Pranata, J. M. *Am. Chem. Soc.* 1990, 112, 2008.

(577) Miller, J. R.; Dein, J. V.; Huddleston, R. K. *J. Am. Chem. Soc.* 1984, 106, 5029.

(578) Parker, J. J.; Wierschke, S. G.; Jorgenson, W. L. *J. Am. Chem. Soc.* 1991, 113, 2810.

(579) Dennerli, N. H.; Hodgkiss, J. M.; Rosenthal, J.; Nocera, D. G. *J. Phys. Chem. B* 2004, 108, 6315.

(580) Massari, A. M.; McClain, B. L.; Finkelman, I. J.; Lee, A. P.; Reynolds, H. L.; Bren, K. L.; Fayer, M. D. *J. Phys. Chem. B* 2006, 110, 18853.

(581) Shukla, D.; Young, R. H.; Farid, S. *J. Phys. Chem. A* 2004, 108, 10286.

(582) Kroll, J. P.; Meyer, J. M. *Angew. Chem., Int. Ed.* 2005, 44, 1598.

(583) Rhine, J. J.; Meyer, J. M. *J. Am. Chem. Soc.* 2004, 126, 12716.

(584) Rhine, J. J.; Maricle, T. F.; Nagro, H.; DiPasquale, A. G.; Lano, O. P.; Lockwood, M. A.; Roitler, K.; Meyer, J. M. *J. Am. Chem. Soc.* 2006, 128, 6075.

(585) Thomas, P.; Jayaray, T. O.; Janet, H.; Hamman, S.; Saint-Aman, E.; Duboc, C.; Pierre, J.-L. *Angew. Chem., Int. Ed.* 2004, 43, 594.

(586) Kanamori, D.; Furukawa, A.; Okamura, T. A.; Yamamoto, H.; Ueyama, N. *Org. Biomol. Chem.* 2005, 3, 1453.

(587) Matsunaga, T.; Itoh, Y.; Ishii, Y.; Onomura, O.; Matsumura, Y. *J. Am. Chem. Soc.* 2001, 123, 3371.

(588) Bernas, L.; Bhatt, A. J.; Collison, D.; Davies, E. S.; Garner, C. D.; Melanes, E.; McMaster, J. L.; Whitaker, G.; Wilson, C.  *Dalton Trans.* 2003, 1975.

(589) Uri, S.; Atta, M.; Foncavage, M.; Ruthford, A. W. *J. Am. Chem. Soc.* 1995, 117, 10713.

(590) Soru, M.; Roush, M. P.; Coulter, E. D.; Dawson, J. H. *Chem. Rev.* 1996, 96, 2841.

(591) Ort, D. *de Montaigu, P. R. Cytochrome P450: Structure, Mechanism, and Inhibition*, 2nd edn, Plenum, New York, 1995.

(592) Ozaki, S.; Roush, M. P.; Matsui, T.; Watanabe, A. *Chem. Rev.* 2001, 34, 518.

(593) Evans, J.; Evers, K. E.; Grisham, M. B. *Peroxidases in Chemistry and Biology*; CRC Press: Boca Raton, FL, 1991; Vols. I and II.

(594) Dawson, J. H. *Science* 1988, 249, 433.

(595) Cheng, C. J.; Chung, L. L.; Nocera, D. G. *J. Am. Chem. Soc.* 2003, 125, 1866.

(596) Dinsley, J. L.; Bessman, A. J.; Maricle, D. R.; Rosenthal, J.; Soper, J. D.; Nocera, D. G. *J. Am. Chem. Soc.* 2005, 127, 6575.

(597) Ormanas, H. B.; Kolay, S.; Hammarström, C.; Kirchoff, D.; DeMattare, A. *J. Am. Chem. Soc., Chem. Commun.* 2004, 4, 668.

(598) Stecak, S.; Jovanovic, S. V. *J. Am. Chem. Soc.* 1997, 119, 617.

(599) Devadoss, C.; Fessenden, R. W. *J. Phys. Chem.* 1991, 95, 7253.

(600) Cape, J. L.; Bowman, M. K.; Kramer, D. M. *J. Am. Chem. Soc.* 2005, 127, 4208.

(601) Magnusson, A.; Berglund, K.; Horst, P.; Hammarström, L.; Åkermark, B.; Styrling, S.; Sun, L. *J. Am. Chem. Soc.* 1997, 119, 10720.

(602) Sun, L.; Hammarström, L.; Åkermark, B.; Styrling, S. *Chem. Soc. Rev.* 2001, 30, 36.

(603) Sjödin, M.; Glanser, R.; Poltys, T.; Pan, J.; Styrling, S.; Sun, L.; Sunström, V.; Hammarström, L. *J. Phys. Chem. Chem. Phys.* 2004, 6, 4851.

(604) Sjödin, M.; Styrling, S.; Wolpert, H.; Xu, Y.; Sun, L.; Hammarström, L. *J. Am. Chem. Soc.* 2005, 127, 1277.

(605) Sjödin, M.; Irbo, T.; Uss, J. E.; Lind, J.; Meréni, C.; Åkermark, B.; Hammarström, L. *J. Am. Chem. Soc.* 2006, 128, 13076.

(606) Hammarström, L. Personal communication.

(607) Creutz, C.; Sutin, N. *Proc. Natl. Acad. Sci. U.S.A.* 1975, 72, 2858.

(608) Hirst, J. K. *Coord. Chem. Rev.* 2005, 249, 313 and references therein.

(609) Reeca, S. V.; Nocera, D. G. *J. Am. Chem. Soc.* 2005, 127, 9448.

(610) Hirst, J. K.; Hwang, K. B.; Dutilboum, D.; Schoemayr, J.; Meyer, T. J. Unpublished results.

(611) Horthorf, C. M.; Maxwell, K. A.; White, P. S.; DeSimone, J. M.; Meyer, T. J. *Inorg. Chem.* 2001, 40, 601.

(612) Hordrox, R. M.; Finkelman, H. O. *J. Phys. Chem. B* 2004, 108, 1694.

(613) Che, C. M.; Wong, K. Y.; Ansoo, F. C. *J. Electroanal. Chem.* 1987, 225, 211.

(614) Liu, Y. K.; Wong, K. Y. *J. Electroanal. Chem.* 1994, 374, 255.

(615) Evans, J. K.; Kuwana, T. *Anal. Chem.* 1979, 51, 358.

(616) Engstrom, R. C. *Anal. Chem.* 1982, 54, 2310.

(617) Engstrom, R. C.; Strasser, V. A. *Anal. Chem.* 1984, 56, 136.

(618) Rice, M. E.; Galus, Z.; Adams, R. N. *J. Electroanal. Chem. Interfacial Electrochemistry* 1983, 143, 89.

(619) Abimlis, G. B.; Diamantis, A. A.; Murphy, W. R.; Linton, R. W.; Abimlis, G. B. *J. Electroanal. Chem.* 1985, 197, 1845.

(620) Bleed, W. J.; Jenkins, R. A. *Anal. Chem.* 1976, 48, 1240.

(621) Huck, H.; Schmidt, H. L. *Angew. Chem., Int. Ed.* 1981, 20, 402.

(622) Jagiełło, H.; Kuwana, T.; Jahnsson, G. *J. Am. Chem. Soc.* 1983, 105, 1805.

(623) Albery, W. J.; Bartlett, P. N. *J. Chem. Soc., Chem. Commun.* 1984, 225.

(624) Berne, F.; Tobalina, F.; Moreno, G.; Hernandez, L.; Lorenzo, E.; Abell, H. D. *Anal. Chem.* 1997, 69, 4065.

(625) Zare, H. R.; Golabi, S. M. *J. Electroanal. Chem.* 1999, 464, 14 and references therein.

(626) Ray, R. K.; McCreey, R. L. *J. Electroanal. Chem.* 1999, 469, 150.

(627) Diamantis, A. A.; Murphy, W. R.; Meyer, T. J. *Inorg. Chem.* 1984, 23, 3230.

(628) Hsyny, M. II; Meyer, T. J. Unpublished results.

(629) Preisendorf, M.; Pfeiffer, D.; Korinek, K. *J. Chem. Soc., Perkin Trans. 2* 1990, 1396.

(630) Siegbahn, P. E. M.; Blomberg, M. R. A. *Ann. Rev. Phys. Chem.* 1999, 50, 221.

(631) Siegbahn, P. E. M.; Blomberg, M. R. A. *Chem. Rev.* 2000, 100, 421.

(632) Siegbahn, P. E. M.; Blomberg, M. R. A. *J. Phys. Chem. B* 2001, 105, 9373.

(633) Barber, J. *Rev. Biophys.* 2003, 36, 71.

(634) Diner, B. A.; Bebbott, G. T. In *Advances in Photosynthesis: The Light Reactions*; Ort, D. R.; Yocom, C. F., Eds.; Kluwer Academic Publishers: Dordrecht, The Netherlands, 1996; p 401.

(635) Diner, B. A.; Rappaport, F. *Annu. Rev. Plant Biol.* 2002, 53, 551.

(636) Yachanda, V. K.; Sauer, K.; Klein, M. P. *Chem. Rev.* 1996, 96, 2927.

(637) Ruttiger, W.; Dianakis, G. C. *Chem. Rev.* 1997, 97, 1.

(638) Britz, R. D. In *Oxygenic Photosynthesis: The Light Reactions*; Ort, D. R.; Yocom, C. F., Eds.; Kluwer Academic Publishers: Dordrecht, The Netherlands, 1996; p 1.

(639) Barber, J. *Biophys. Biophys. Acta* 1998, 1365, 269.

(640) Perner-Hahn, J. E. *Metal Sites Proteins Models* 1998, 50, 1.

(641) Nugent, J. H. A., Eds. *Photosynthesis Water Oxidation Biochim. Biophys. Acta* 2001, 1563, 1.

(642) Ke, B. *Photosynthesis—Photochemistry and Photobiophysics*; Kluwer Academic Publishers: Dordrecht, The Netherlands, 2001.

(643) Siegbahn, P. E. M.; Cambre, R. H. *J. Am. Chem. Soc.* 1999, 121, 6447.

(644) Siegbahn, J. S.; Linburg, J.; Brudvig, O. W. *Biophys. Biophys. Acta* 2001, 1502, 229.

(645) Haunman, S.; Jungs, J.; Biel, B. R. J.; Evans, M. C. W. *Biophys. Biophys. Acta* 2004, 1655, 217.

(646) Pecoraro, V. L.; Baldwin, M. J.; Caudle, M. T.; Heish, W. Y.; Lew, N. A. *Pure Appl. Chem.* 1998, 76, 525.

(647) Ebenhoch, P. B. *Biophys. Biophys. Acta* 2004, 1655, 231.

(648) Ebenhoch, P. B. *Biophys. Biophys. Acta* 2002, 1602, 6, 227.

(650) Ebenhoch, P. B.; Brudvig, G. W. *Phys. Chem. Chem. Phys.* 2004, 6, 4754.

(651) Diner, B. A.; Bebbott, G. T. In *Oxygenic Photosynthesis: The Light Reactions*; Ort, D. R.; Yocom, C. F., Eds.; Kluwer Academic Publishers: Dordrecht, The Netherlands, 1996; p 213.

(652) Wu, H. T. *Ber. Bunsen-Ges. Phys. Chem.* 1996, 100, 1923.

(653) Debus, R. J. *Biophys. Biophys. Acta* 2002, 1102, 269.

(654) Gilchrist, M. L.; Ball, J. A.; Randall, D. W.; Britt, R. D. *Proc. Natl. Acad. Sci. U.S.A.* 1995, 92, 9545.

(655) Hogan, C. W.; Lydiard-Simmonds, N.; Tang, X. S.; Tomm, C.; Perner-Hahn, J. E.; Diner, B. A.; McCracken, J.; Styrling, S. *Photosynth. Res.* 1999, 49, 177.

(656) Goussain, C.; Bousse, A.; Rutherford, A. W. *Philos. Trans. R. Soc. London, Ser. B* 2002, 357, 1369.

(657) Sauer, K.; Yachanda, V. K. *Biophys. Biophys. Acta* 2004, 1655, 140.

(658) Hiller, W.; Messinger, J. In *The Catalytic Manganese Cluster in Photosystem II: The Water/Pastazopirone Oxido-Reductase of Photosynthesis*; Wydrzynska, T.; Sato, K., Eds.; Kluwer Academic Publishers: Dordrecht, The Netherlands, 2005; p 567.

(659) Barber, J. *Biophys. Biophys. Acta* 2004, 1655, 123.

(660) Zonai, A.; Wu, H. T.; Kern, J.; Fromme, P.; Krauss, N.; Saenger, W.; Ort, P. *Nature* 2001, 409, 739.

(661) Kamiya, N.; Shen, J. R. *Proc. Natl. Acad. Sci. U.S.A.* 2003, 100, 98.

(662) Loll, B.; Kern, J.; Saenger, W.; Zou, A.; Biesiadka, J. *Nature* 2005, 438, 1020.

(663) Korb, B.; Forbush, B.; McGloin, M. *Photochem. Photobiol.* 1970, 11, 457.

(664) Ioannidis, N.; Petroules, V. *Biochemistry* 2002, 41, 9580.

(665) Ioannidis, N.; Nugent, J. H. A.; Petroules, V. *Biochemistry* 2002, 41, 9589.

(666) Kouleugliotis, D.; Shen, J. R.; Ioannidis, N.; Petroules, V. *Biochemistry* 2003, 42, 2043.

(667) Renge, C.; Styring, S. *Biochemistry* 2003, 42, 8066.

(668) Nugent, J. H. A.; Mukundan, I. P.; Evans, M. C. W. *Biochemistry* 2003, 42, 5500.

(669) Clausen, J.; Junge, W. *Nature* 2004, 430, 480.

(670) Haumann, M.; Liechti, P.; Müller, C.; Bann, M.; Grabletz, M.; Dau, H. *Science* 2005, 308, 10650.

(671) Ono, T.-A.; Noguchi, T.; Inoue, Y.; Kasumoto, M.; Matsushita, T.; Ogawa, T. *Science* 2005, 308, 1334.

(672) Robles, J. A.; Lister, W. C.; Laflamme, M. J.; Circo, R. M.; Rompel, A.; Andrews, J. C.; Sauer, K.; Yachandra, V. K.; Klein, M. *Proc. Natl. Acad. Sci. U.S.A.* 1996, 93, 3335.

(673) Riggs, P. J.; Mel, R.; Yocom, C. E.; Pernerlehr, J. E. *J. Am. Chem. Soc.* 1992, 114, 10650.

(674) Yachandra, V. K. *Philos. Trans. R. Soc. London, Ser. B* 2002, 357, 1347.

(675) Yano, K.; Yamamoto, Y.; Ono, T.; Ishihara, S.; Sato, F. *Plant Physiol. (Rochelle)* 2005, 139, 1175.

(676) Yano, J.; Pushkar, Y.; Glazebrook, P.; Lewis, A.; Sauer, K.; Messinger, J.; Biegalski, U.; Yachandra, V. J. *Am. Chem. Soc.* 2005, 127, 14974.

(677) Renger, G. *Biochim. Biophys. Acta* 2001, 1503, 219.

(678) Lavergne, J.; Junge, W. *Photosynth. Res.* 1993, 38, 279.

(679) Latimer, M. J.; Das, H.; Liang, W. C.; Andrews, J. C.; Roelofs, A. J.; Circo, R. M.; Rompel, A.; Sauer, K.; Yachandra, V. K.; Klein, M. W. *Science* 1996, 271, 1700.

(680) Biegalski, U.; Dittmer, J.; Dörrner, W.; Meyer-Klinke, W.; Dau, H. *Biochemistry* 1998, 37, 17112.

(681) Schiller, H.; Dittmer, J.; Iazzolino, L.; Dornig, W.; Meyer-Klinke, W.; Sole, V. A.; Nolting, H.; Dau, H. *Biochemistry* 1998, 37, 7140.

(682) Robles, J. H.; Messinger, J.; Circo, R. M.; McFarlane, K. L.; Fernandez, C.; Pizarro, S. A.; Sauer, K.; Yachanda, V. K. *J. Am. Chem. Soc.* 2002, 124, 7459.

(683) Yano, J.; Kern, J.; Sauer, K.; Latimer, M. J.; Pushkar, Y.; Biesiadka, J.; Yachanda, V. K.; Sauer, K.; Messinger, J.; Zou, A.; Yachanda, V. K. *Science* 2005, 310, 873.

(684) Kulik, L. V.; Lubitz, W.; Messinger, J. *Biochemistry* 2005, 44, 9368.

(685) Haumann, M.; Junge, W. In *Oxygenic Photosynthesis: The Light Reactions*; Ort, D. R., Yocum, C. E., Eds.; 1996; pp 165.

(686) Dordrecht, J. W.; Haumann, M.; Ahlbirke, R. M. A.; Clausen, J. *Philos. Trans. R. Soc. London, Ser. B* 2002, 357, 1407.

(687) Schröder, E.; Witt, J. E. *Biochim. Biophys. Acta* 1999, 274, 30387.

(688) Feller, P.; Goussias, C.; Rutherford, A. W.; Us, A. *Proc. Natl. Acad. Sci. U.S.A.* 2004, 101, 8752.

(689) Diner, B. A.; Force, D. A.; Randal, D. W.; Britt, R. D. *Biochemistry* 1998, 37, 17931.

(690) Hays, A. M.; Vassiliev, L. P.; Golbeck, J. H.; Debus, R. J. *Biochemistry* 1999, 38, 11852 and references therein.

(691) Rappaport, F.; Gueorguieva-Kurn, M.; Nixon, P. J.; Diner, B. A.; Lavergne, J. *Biochemistry* 2002, 41, 8518.

(692) Westphal, K. L.; Lydtkin-Simithians, N.; Cukier, R. I.; Babcock, G. T. *Biochemistry* 2000, 39, 16220.

(693) Westphal, K. L.; Cukier, R. I.; Babcock, G. T. *Cur. Opin. Struct. Biol.* 2000, 10, 222.

(694)  $\Delta G^\circ$  was calculated from  $\Delta G^\circ = F(E^\circ(\text{Phe}^{+/-}) - E^\circ(\text{TyrOH}^{+/-})) - 0.035(k_1/192) - \mu\text{S}(\text{Phe}^{+/-})$  with  $\mu\text{S}(\text{Phe}^{+/-}) = -2$ . These values are only approximations to the membrane potentials and neglect  $\Delta G^\circ$  differences for the formation of the TyrOH<sup>•</sup>–H–His and TyrOH<sup>•</sup>–His H-bonded complexes.

(695) Kuhse, H.; Brügel, G. W. *J. Phys. Chem. B* 2002, 106, 8189.

(696) Spreviro, E. M.; Gacor, J. A.; McEvoy, J. P.; Brügel, G. W.; Brügel, V. S. *J. Chem. Theory Comput.* 2006, 2, 1119.

(697) Biesiadka, J.; Yano, J.; Iazzolino, K.-D.; Zou, A. *Phys. Chem. Chem. Phys.* 2004, 6, 4733.

(698) Perner-Hahn, J. E. *Bend* 1998, 90, 1.

(699) Robles, J. H.; Circo, R. M.; Yachanda, V. K. *Biochim. Biophys. Acta* 2001, 1503, 7.

(700) Debus, R. J.; Strickler, M. A.; Walker, L. M.; Hilde, W. *Biochemistry* 2005, 44, 1367.

(701) Yano, J.; Kern, J.; Iazzolino, K. D.; Latimer, M. J.; Bergmann, U.; Gacor, P.; Pushkar, Y.; Biesiadka, J.; Loll, B.; Sauer, K.; Messinger, J.; Zou, A.; Yachanda, V. K. *Proc. Natl. Acad. Sci. U.S.A.* 2005, 102, 12647.

(702) Circo, R. M.; Robles, J. H.; Messinger, J.; Fernandez, C.; Holman, K. M. L.; Sauer, K.; Yachanda, V. K. *Biochemistry* 2004, 43, 13271.

(703) Debus, B. A. *Biochim. Biophys. Acta* 2001, 1503, 147.

(704) Debus, B. A. *Biochim. Biophys. Acta* 2001, 1503, 164.

(705) Kuman, Y.; Mizutani, N.; Yamamoto, T.; Ishii, A.; Ono, T.-A. *J. Biol. Chem.* 2005, 280, 2078.

(706) Temm, C.; Skalicky, J. J.; Pifoud, D. L.; Wand, A. J.; Dutton, P. L. *Biochemistry* 1999, 38, 9493.

(707) Koppenol, W. H. *Generation and Thermodynamic Properties of Oxyradicals*. Printed from the CRC Critical Reviews in Membrane Lipid Oxidation, 1995; Vol. 1, pp 1.

(708) Debus, B. A. *Light to Biosphere: from Light to Biosphere*; Mathis, P., Ed.; Kluwer Academic Publishers: Dordrecht, The Netherlands, 1995; Vol. 2, p 269.

(709) Tonon, C.; Tang, X. S.; Waneen, K.; Hoganon, C. W.; Styring, S.; McCracken, J.; Diner, B. A.; Babcock, G. T. *J. Am. Chem. Soc.* 1995, 117, 1025.

(710) Gelacio, J. A.; Kirk, M. L.; Kampf, J. W.; Pecoraro, V. L. *Inorg. Chem.* 1997, 36, 1823.

(711) Brügel, G. W.; Brügel, G. W. *Philos. Trans. R. Soc. London, Ser. B* 2002, 357, 1304.

(712) Rich, P. R. In *Protein Electron Transfer*; Bendall, D. S., Ed.; BIOS Scientific Publishers, Oxford, 1997; pp 217.

(713) Although it seems reasonable to assume that the redox potentials for the  $S_1$  state transitions increase incrementally in the order  $E^\circ_{S_1} > E^\circ_{S_2} > E^\circ_{S_3}$ , this is not necessarily the case. If, for example,  $E^\circ_{S_1} > E^\circ_{S_2} > E^\circ_{S_3}$ , the  $S_1$  state would be unstable toward disproportionation, and  $S_1 \rightarrow S_2 \rightarrow S_3$  is the discussion in section 2.1. There would be no reversible consequences, since neighboring OECs are specifically isolated and there is no way for bimolecular disproportionation to occur.

(714) Binstead, R. A.; Chronister, C. W.; Ni, J. F.; Hartshorn, C. M.; Meyer, J. J. *J. Am. Chem. Soc.* 2000, 122, 8464.

(715) Yamada, H.; Siems, W. F.; Koike, T.; Hurst, J. K. *J. Am. Chem. Soc.* 2004, 126, 9785.

(716) Brügel, G. W. *J. Am. Chem. Soc.* 2001, 123, 423.

(717) Thorp, H. H.; Szwarczak, J. E.; Brügel, G. W.; Brügel, R. H. *J. Am. Chem. Soc.* 1989, 111, 9249.

(718) Baldwin, M. J.; Law, N. A.; Stennett, T. L.; Kampf, J. W.; Penner-Hahn, J. E.; Pecoraro, V. L. *Inorg. Chem. Chem. Phys.* 1998, 38, 4801.

(719) Poulsen, K. A.; Rompel, A.; McKenzie, C. J. *Angew. Chem. Int. Ed.* 2005, 44, 6915.

(720) Brügel, G. W.; Brügel, R. H. *Proc. Natl. Acad. Sci. U.S.A.* 1986, 83, 5586.

(721) Ochiai, A. G. *Bioelectrochroism*. Bioenergy, 1989, 21, 3.

(722) Ketschmann, H.; Schröder, E.; Witz, H. T. *Biochim. Biophys. Acta* 1994, 1274, 1.

(723) Renger, G. *Chem. Phys. Plant* 1997, 100, 828.

(724) Dasgupta, J.; van Willigen, R. T.; Dismukes, G. C. *Phys. Chem. Chem. Phys.* 2008, 6, 4793.

(725) Messinger, J.; Badger, M.; Wydrynski, T. *Proc. Natl. Acad. Sci. U.S.A.* 1995, 92, 3209.

(726) Dau, H.; Iazzolino, L.; Dittmer, J. *Biochim. Biophys. Acta* 2001, 1503, 126.

(727) Linberg, J.; Vretilas, J. S.; Likel-Sands, L.; Rheingold, A. L.; Brügel, R. H.; Brügel, G. W. *Science* 1999, 283, 524.

(728) Messinger, J. *Phys. Chem. Chem. Phys.* 2004, 6, 4764.

(729) Siegbahn, P. E. M. *Inorg. Chem.* 2000, 39, 2923.

(730) Meyer, T. J.; Huynh, M. H. V.; Thorp, H. H. *Angew. Chem. Int. Ed.* 2007, 46, 5284.

(731) Seyer, L. *Biochemistry*, 3rd ed.; Freeman: New York, 1988.

(732) Dau, H.; Iazzolino, L.; Dittmer, J. *Biochim. Biophys. Acta* 2001, 1503, 126.

(733) Haumann, M.; Junge, W. *Biochemistry* 1994, 33, 864.

(734) Iwata, S.; Barber, J. *Proc. Natl. Acad. Sci. U.S.A.* 2004, 14, 447.

(735) Barber, J.; Forreva, K.; Maglathou, K.; Iwata, S. *Proc. Natl. Acad. Sci. U.S.A.* 2004, 101, 4737.

(736) De La Rivas, J.; Barber, J. *Photosynth. Res.* 2004, 81, 329.

(737) Ishikita, H.; Saenger, W.; Loh, B.; Biesiadka, J.; Knapp, E.-W. *Biochemistry* 2006, 45, 2063.

(738) Junge, W.; Renger, G. *PEBS Lett.* 1988, 256, 425.

(739) Chirico, G. D. *Philos. Trans. R. Soc. London, Ser. B* 1999, 354, 2068.

(740) Schulte, M. J.; Rappaport, F.; Nugent, J. H. A.; Barnett, C. J.; Klug, D. R. *Biochemistry* 1998, 37, 3974.

(741) Junge, W.; Haumann, M.; Ahlbirke, R.; Mukundan, A.; Clausen, J. *Philos. Trans. R. Soc. London, Ser. B* 2002, 357, 14070.

(742) Hundert, M.; Hayes, A. M. A.; Debus, R. J.; Junge, W. *Biochemistry* 1998, 37, 14450.

(743) Bernaudou, J.; Münker, B. *Chem. Commun.* 1998, 20, 2167.

(744) Devioglou, A.; Meyer, T. J. *J. Am. Chem. Soc.* 1994, 116, 215.

(745) Diner, B. A.; Nixon, P. J.; Parchaus, J. W. *Curr. Opin. Struct. Biol.* 1991, 1, 546.

(746) Campbell, K. A.; Force, D. A.; Nixon, P. J.; Dale, F.; Diner, B. A.; Britt, R. D. *J. Am. Chem. Soc.* 2006, 122, 3754.

(747) Hillier, W.; Wydryzynski, T. *Biochim. Biophys. Acta* 2001, **1503**, 197.

(748) Shisler, M. A.; Walker, L. M.; Hillier, W.; Debus, R. J. *Biochemistry* 2005, **44**, 8571.

(749) Styring, S.; Foytnev, Y.; Mamedov, F.; Hillier, W.; Babcock, G. T. *Biochemistry* 2003, **42**, 6185.

(750) Rapaport, E.; Lavergne, J. *Biochemistry* 1991, **30**, 10004.

(751) Saphon, S.; Crofts, A. R. Z. *Naturforsch. Biosci.* 1977, **32C**, 617.

(752) Fowler, C. F. *Biochim. Biophys. Acta* 1977, **462**, 414.

(753) Förster, V.; Junge, W. *Photuchemie. Photochol.* 1985, **41**, 183.

(754) Waeker, U.; Haag, E.; Renger, G. *Curr. Res. Photochem.* 1990, **1**, 1.

(755) Lübbert, K.; Junge, W. *Curr. Res. Photochem.* 1990, 877.

(756) Chu, H.-A.; Hillier, W.; Debus, R. J. *Biochemistry* 2004, **43**, 3152.

(757) Glazel, P.; Bergmann, E. S.; Visser, H.; Robbie, J. H.; Gu, W.; De Groot, F. M. P.; Christou, G.; Pecoraro, V. L.; Cramer, S. P.; Yachandra, V. K. *J. Am. Chem. Soc.* 2004, **126**, 9946.

(758) Hillier, W.; Babcock, G. T. *Biochemistry* 2001, **40**, 1503.

(759) Noguchi, T.; Sugiyama, M. *Biochemistry* 2001, **40**, 1497.

(760) Kimura, Y.; Ono, T. A. *Biochemistry* 2001, **40**, 14061.

(761) Kimura, Y.; Ono, T. A. *FEBS Lett.* 1985, **187**, 224.

(762) Rapaport, E.; Baudier-Descor, M.; Lavergne, J. *Biochim. Biophys. Acta* 1994, **1184**, 178.

(763) Penner-Hahn, J. E.; Yocom, C. F. *Science* 2005, **310**, 582.

(764) Denissenko, A. S.; Kukuskin, A. K. *Biofizika* 2005, **50**, 833.

(765) Weng, T. C.; Hsieh, W. Y.; Ulfhake, E. S.; Gordon-Wylie, S. W.; Collins, T. J.; Pecoraro, V. L.; Penner-Hahn, J. E. *J. Am. Chem. Soc.* 2004, **126**, 8070.

(766) Bousso, A.; Rutherford, A. W.; Styring, S. *Biochemistry* 1990, **29**, 2490.

(767) Messinger, J.; Waeker, U.; Renger, G. *Biochemistry* 1991, **30**, 7852.

(768) Koike, H.; Hanusum, B.; Inoue, Y.; Renger, G. *Biochim. Biophys. Acta* 1978, **44**, 117.

(769) Renger, G.; Hanusum, B. *FEBS Lett.* 1992, **299**, 28.

(770) Renger, G. *Biochim. Biophys. Acta* 2004, **1555**, 195.

(771) Gregor, W. G.; Cinco, R. M.; Yu, H.; Yachandra, V. K.; Britt, R. D. *Biochemistry* 2005, **44**, 8817.

(772) Liang, W. C.; Roelofs, T. A.; Cinco, R. M.; Rompel, A.; Latimer, M. J.; Yu, W. O.; Sauer, K.; Klein, M. P.; Yachandra, V. K. *J. Am. Chem. Soc.* 2004, **122**, 3395.

(773) Pecoraro, S. A.; D'Amato, J. A.; McDermett, A. E.; Yachandra, V. K.; Cole, J. D.; Dzainer, S. L.; Britt, R. D.; Wiegandt, K.; Bossek, U.; Sauer, K.; Klein, M. P. *Biochemistry* 1998, **39**, 471.

(774) Cinco, R. M.; Hollan, K. L. M.; Robbie, J. H.; Yano, J.; Pizarro, S. A.; Belachochio, E.; Sauer, K.; Yachandra, V. K. *Biochemistry* 2002, **41**, 1928.

(775) Rompel, A.; Cinco, R. M.; Robbie, J. H.; Latimer, M. J.; McFarlane, K. L.; Hung, J.; Walters, M. A.; Yachandra, V. K. *J. Synchrotron Radiat.* 2004, **11**, 81.

(776) Messinger, J.; Robbie, J. H.; Bergmann, U.; Fernandez, C.; Glatzel, P.; Visser, H.; Cinco, R. M.; Motarjemi, L.; Belachochio, E.; Pizarro, S. A.; Cramer, S. P.; Sauer, K.; Klein, M. P.; Yachandra, V. K. *J. Am. Chem. Soc.* 2001, **123**, 7804.

(777) Dau, H.; Liebisch, P.; Haunmann, M. *Anal. Biochem.* **2003**, **376**, 562.

(778) Haunmann, M.; Bogershausen, O.; Cherepanov, D.; Ahlsbrink, R.; Junge, W. *Photochem. Photobiol. Sci.* 1997, **51**, 193.

(779) Korge, M.; Irgang, K.-D.; Renger, G. *Biochemistry* 1997, **36**, 8904.

(780) Haunmann, M.; Müller, C.; Liebisch, P.; Kuzoloski, L.; Dittmer, J.; Grönke, M.; Neusser, T.; Meyer-Klinke, W.; Dau, H. *Biochemistry* 2005, **44**, 8901.

(781) Messinger, J.; Robbie, J. H.; Yu, W. O.; Sauer, K.; Yachandra, V. K.; Klein, M. P. *J. Am. Chem. Soc.* 1997, **119**, 11349.

(782) Dau, H.; Liebisch, P.; Haunmann, M. *Phys. Chem. Chem. Phys.* 2004, **6**, 4781.

(783) Petroureas, V.; Koulougiotis, D.; Ioannidis, J. *Biochemistry* 2005, **44**, 6723.

(784) Messinger, J.; Robbie, J. H.; Bergmann, U.; Fernandez, C.; Glatzel, P.; Visser, H.; Cinco, R. M.; McFarlane, K. L.; Belachochio, E.; Pizarro, S. A.; Cramer, S. P.; Sauer, K.; Klein, M. P. *Biochemistry* 2005, **44**, 1372.

(785) Yachandra, V. K. *J. Am. Chem. Soc.* 2001, **123**, 7804.

(786) Andreasson, L. E.; Vass, I.; Styring, S. *Biochim. Biophys. Acta* 1995, **1230**, 155.

(787) Bousso, A.; Ziemannmann, J. L.; Rutherford, A. W. *Biochemistry* 1989, **28**, 8984.

(788) Nixon, P. J.; Diner, B. A. *Biochemistry* 1992, **31**, 942.

(789) Knoepfle, N.; Broeker, T. M.; Putman-Evans, C. *Biochemistry* 1999, **38**, 10000.

(790) Bousso, A.; Sugiyama, M.; Kirikoviy, D.; Rutherford, A. W. *Plant Cell Physiol.* 2005, **46**, 837.

(791) Lundborg, M.; Blomberg, M. R. A.; Siegbahn, P. E. M. *Inorg. Chem.* 2004, **43**, 264.

(792) Hillier, W.; Messinger, J.; Wydryzynski, T. *Biochemistry* 1998, **37**, 16909.

(793) Hillier, W.; Wydryzynski, T. *Biochemistry* 2000, **40**, 4399.

(794) Hendry, G.; Wydryzynski, T. *Biochemistry* 2002, **41**, 13228.

(795) Hillier, W.; Wydryzynski, T. *Phys. Chem. Chem. Phys.* 2004, **6**, 4882.

(796) Hesegawa, K.; Kimura, Y.; Ono, T. A. *Biochemistry* 2002, **41**, 13339.

(797) Kelley, P. M.; Izawa, S. *Biochim. Biophys. Acta* 1978, **502**, 198.

(798) Lindberg, K.; Andreasson, L. E. *Biochemistry* 1996, **35**, 14259.

(799) Yu, H.; Aznar, C. P.; Xu, X.; Britt, R. D. *Biochemistry* 2005, **44**, 12022.

(800) Rangwahid, R.; Pace, R. J. *Biochemistry* 1999, **38**, 1252.

(801) McGrath, J. P.; Renger, G. *Inorg. Chem.* 1999, **38**, 530.

(802) Pelizzetti, J. M.; Campbell, K. A.; Randall, D. W.; Evanschik, M. A.; Pecoraro, V. L.; Armstrong, W. H.; Britt, R. D. *J. Am. Chem. Soc.* 2000, **122**, 2026.

(803) Brötz, J. *Biochemistry* 2004, **43**, 3318.

(804) Grafton, A. K.; Wheeler, R. A. *J. Phys. Chem. B* 1999, **103**, 5380.

(805) Padlock, M. L.; Sagle, I.; Tehrani, A.; Beauty, J. T.; Feher, G.; Okamura, M. Y. *Biochemistry* 2003, **42**, 9626.

(806) Okamura, M. Y.; Madigan, M. T.; Bauer, C. E., Eds. *Anorganic Photochemistry*. Berlin: Kluwer Academic Publishers; Dordrecht: The Netherlands, 1995.

(807) Geage, M. S.; Paddock, M. L.; Bruce, J. M.; Feher, G.; Okamura, M. Y. *J. Am. Chem. Soc.* 1996, **118**, 9005.

(808) Okamura, M. Y.; Paddock, M. L.; Gniga, M. S.; Feher, G. *Biochim. Biophys. Acta* 2000, **1453**, 148.

(809) Graige, M. S.; Feher, G.; Okamura, M. Y. *Proc. Natl. Acad. Sci. USA* 1998, **95**, 11679.

(810) Graige, M. S.; Paddock, M. L.; Tehrani, A.; Beauty, J. T.; Feher, G.; Okamura, M. Y. *Biochemistry* 2001, **40**, 14513.

(811) Matsumoto, B. G. *J. Biol. Inorg. Chem.* 1998, **3**, 339.

(812) Stoeckbechov, A. A. *J. Theor. Comput. Chem.* 2003, **2**, 91.

(813) Granit, R. *Frontiers Biosci.* 2004, **9**, 581.

(814) Zaslavsky, D.; Genais, R. B. *Biochim. Biophys. Acta* 2000, **1458**, 164.

(815) Mills, D. A.; Ferguson-Miller, S. *FEBS Lett.* 2003, **545**, 47.

(816) Blomberg, M. R. A.; Siegbahn, P. E. M.; Babcock, G. T.; Wikstrom, M. J. *Inorg. Biochem.* 2000, **80**, 261.

(817) Blomberg, M. R. A.; Siegbahn, P. E. M.; Babcock, G. T.; Wikstrom, M. J. *J. Am. Chem. Soc.* 2000, **122**, 12948.

(818) Blomberg, M. R. A.; Siegbahn, P. E. M.; Wikstrom, M. *Inorg. Chem.* 2004, **43**, 5231.

(819) Yoshihaka, S.; Shinzawa-Itoh, K.; Nakashima, R.; Yoneda, T.; Yamashita, E.; Inoue, N.; Yao, M.; Fei, M. J.; Libeu, C. P.; Mizushima, T.; Yamaguchi, H.; Tomizaki, T.; Tsukihara, T. *Science* 1998, **280**, 1723.

(820) Ostermeier, C.; Harenga, A.; Ermler, U.; Michel, H. *Proc. Natl. Acad. Sci. USA* 1997, **94**, 10547.

(821) Wirsching, M.; Blomberg, M. R. A.; Siegbahn, P. E. M. *J. Am. Chem. Soc.* 1999, **121**, 10178.

(822) Firszt, B. C.; Poukos, T. L.; Kent, J. J. *J. Biol. Chem.* 1984, **259**, 13007.

(823) Choudhury, K.; Sundaramoorthy, M.; Mauro, J. M.; Poukos, T. L. *J. Biol. Chem.* 1992, **267**, 25656.

(824) Erman, J. E.; Vitello, L. B. *J. Am. Chem. Soc.* 1992, **114**, 6592.

(825) Rodriguez-Lopez, J. N.; Smith, A. T.; Thorneley, R. N. F. *J. Biol. Inorg. Chem.* 1996, **1**, 136.

(826) Shai, S.; Visser, S. P.; Ogliaro, F.; Schwarz, H.; Schröder, D. *Coord. Chem. Rev.* 2002, **26**, 536.

(827) Shai, S. *Coord. Chem. Rev.* 1994, **94**, 715.

(828) Wikstrom, P. C.; Wikstrom, J. S.; Shai, S. *J. Am. Chem. Soc.* 1997, **119**, 195.

(829) Klotz, I. M.; Kurtz, D. M. *Acc. Chem. Res.* 1984, **17**, 16.

(830) Brundell, T. C.; Solomon, E. I. *J. Am. Chem. Soc.* 1999, **121**, 8277.

(831) Brundell, T. C.; Solomon, E. I. *J. Am. Chem. Soc.* 1999, **121**, 8288.

(832) Stadlow, J. N.; Briggs, W. R., Eds. *Annual Review of Plant Physiology and Plant Molecular Biology*. Ann. Rev., Inc.: Palo Alto, CA, 1991; Vol. 42, p 145.

(833) Fordhethcison, A. W.; Grosser, M.; Young, R. N. *Annu. Rev. Biochem.* 1994, **63**, 363.

(834) Nishizuka, H.; Nagano, S. In *Lipoxygenases and Their Metabolites*; Nagano, S., Paoletti, A., Eds.; Plenum: New York, p 5.

(835) Braun, A. R. *J. Biol. Chem.* 1999, **274**, 23579.

(836) Samuelsson, B.; Dahlb, S. E.; Lindgren, J. A.; Rouzer, C. A.; Serhan, C. N. *Science* 1987, **237**, 1771.

(837) Kaup, M. J.; Rickett, K. W.; Klinman, J. P. *J. Am. Chem. Soc.* 2002, **124**, 3865.

(838) Gleckman, M. H.; Wiseman, J. S.; Klinman, J. P. *J. Am. Chem. Soc.* 1994, **116**, 793.

(839) Although the natural substrate for human lipoxygenase is arachidonic acid, it also reacts with linoleic acid. See: Lewis, E. R.; Johnson, E. H.; Holman, T. R. *J. Am. Chem. Soc.* 1999, **121**, 1395.

(840) Stubbe, J.; Neezen, D.; Yee, C. S.; Chang, M. C. Y. *Chem. Rev.* 2003, **103**, 2167.

(841) Ekblad, H.; Uhlin, U.; Farnsworth, M.; Logan, D. T.; Nordlund, P. *Prog Biophys Mol Biol* 2001, **77**, 177.

(842) Thielander, L.; Reichard, P. *Annu Rev Biochem* 1979, **48**, 133.

(843) Stubbe, J.; van der Donk, W. A. *Chem Rev* 1998, **98**, 705.

(844) Lieb, S.; Stubbe, J. In *Comprehensive Natural Products Chemistry*; Barton, S. D.; Nakashita, K.; Meth-Cohn, O.; Poulter, C. D., Eds.; Elsevier Science: New York, 1999; Vol. 5, pp 163.

(845) Ekblad, H.; Fenimore, M. *Struct. Funct. Des.* 1999, **7**, R257.

(846) Reichard, P. *Annu Rev Biochem* 1995, **64**, 1.

(847) Reichard, P. *Trends Biochem. Sci.* 1997, **22**, 81.

(848) Sevendjanymost, M. R.; Yee, C. S.; Recco, S. Y.; Nocera, D. G.; Stubbe, J. *J. Am. Chem. Soc.* 2006, **128**, 1562.

(849) McEvoy, J. P.; Brudvig, G. W. *Chem. Rev.* 2006, **106**, 4455.

(850) Recco, S. Y.; Hodgkin, J. M.; Stubbe, J.; Nocera, D. G. *Philos. Trans. R. Soc. London, Ser. B Biol.* 2004, **359**, 131.

(851) Soper, J. D.; Krylov, S. V.; Robak-Akimova, E. V.; Nocera, D. G. *J. Am. Chem. Soc.* 2007, **129**, 5069.

(852) Hatcher, E.; Sondackov, A. V.; Hammes-Schiffer, S. *J. Am. Chem. Soc.* 2007, **129**, 187.

(853) Hammes-Schiffer, S. *FASEB J.* 2007, **21**, A151.

(854) Costentin, C.; Robert, M.; Savcmt, I. M. *J. Am. Chem. Soc.* 2007, **129**, 5870.

(855) Costentin, J. J.; Brenaman, M. K.; Dayton, J. K.; Lebedeva, N. V.; Forbes, M. D. E.; Papanikolas, J. N.; Meyer, T. J. *J. Am. Chem. Soc.* 2007, **129**, 6958.

CR0500030